LEABHARLANN CHOLÁISTE NA TRÍONÓIDE, BAILE ÁTHA CLIATH | TRINITY COLLEGE LIBRARY DUBLIN
Ollscoil Átha Cliath | The University of Dublin

Terms and Conditions of Use of Digitised Theses from Trinity College Library Dublin

Copyright statement

All material supplied by Trinity College Library is protected by copyright (under the Copyright and Related Rights Act, 2000 as amended) and other relevant Intellectual Property Rights. By accessing and using a Digitised Thesis from Trinity College Library you acknowledge that all Intellectual Property Rights in any Works supplied are the sole and exclusive property of the copyright and/or other IPR holder. Specific copyright holders may not be explicitly identified. Use of materials from other sources within a thesis should not be construed as a claim over them.

A non-exclusive, non-transferable licence is hereby granted to those using or reproducing, in whole or in part, the material for valid purposes, providing the copyright owners are acknowledged using the normal conventions. Where specific permission to use material is required, this is identified and such permission must be sought from the copyright holder or agency cited.

Liability statement

By using a Digitised Thesis, I accept that Trinity College Dublin bears no legal responsibility for the accuracy, legality or comprehensiveness of materials contained within the thesis, and that Trinity College Dublin accepts no liability for indirect, consequential, or incidental, damages or losses arising from use of the thesis for whatever reason. Information located in a thesis may be subject to specific use constraints, details of which may not be explicitly described. It is the responsibility of potential and actual users to be aware of such constraints and to abide by them. By making use of material from a digitised thesis, you accept these copyright and disclaimer provisions. Where it is brought to the attention of Trinity College Library that there may be a breach of copyright or other restraint, it is the policy to withdraw or take down access to a thesis while the issue is being resolved.

Access Agreement

By using a Digitised Thesis from Trinity College Library you are bound by the following Terms & Conditions. Please read them carefully.

I have read and I understand the following statement: All material supplied via a Digitised Thesis from Trinity College Library is protected by copyright and other intellectual property rights, and duplication or sale of all or part of any of a thesis is not permitted, except that material may be duplicated by you for your research use or for educational purposes in electronic or print form providing the copyright owners are acknowledged using the normal conventions. You must obtain permission for any other use. Electronic or print copies may not be offered, whether for sale or otherwise to anyone. This copy has been supplied on the understanding that it is copyright material and that no quotation from the thesis may be published without proper acknowledgement.

Fragility Analysis of Steel and Concrete Wind Turbine Towers

A Thesis Submitted for the Degree of Doctor of Philosophy
to the University of Dublin, Trinity College

by

Aidan Quilligan

4th June 2013

TRINITY COLLEGE
1 9 JUN 2013
LIBRARY DUBLIN

Thesis 10115

Declaration

The author hereby declares that this thesis, in whole or in part, has not been submitted to any other university as an exercise for a degree. Except where reference has been provided in the text, this thesis is entirely the author's own work.

The author confirms that the library may, for academic purposes, lend or copy this thesis upon request.

Aidan Quilligan

June 2013

Summary

As the issues of global warming and a finite supply of fossil fuel based energy gain significance, the prospects and necessity for renewable energy concepts have become both socially and economically relevant. At the forefront of renewable energy development is the relatively mature concept of extracting electricity from the wind. Gaining prominence across the globe, wind turbines are striving to increase efficiency and extract greater amounts of energy from the available wind resources. The most recent state of the art developments see wind turbine capacities increasing to between 5 MW and 10 MW with the corresponding hub heights stretching beyond 100 m tall. This progression has called into question the capabilities of the current industry standard tubular steel towers to cater for these increasing hub heights. Relating to other similar applications such as bridge piers and prototype wind turbine concepts, prestressed concrete or hybrid (prestressed concrete/tubular steel) tower solutions can provide an efficient alternative to tubular steel towers at these greater heights. The focus of this thesis is on assessing the feasibility of prestressed concrete towers for onshore wind turbine applications and analysing the structural performance of both tubular steel and prestressed concrete configurations over a range of hub heights and loading conditions. This is achieved by means of a probabilistic analysis of the structural dynamic performance of various tower configurations subjected to the specified onshore loading conditions. The structural response is assessed through the use of a series of dedicated dynamic models which incorporate the relevant modelling capabilities. Firstly, a one dimensional linear dynamic model is derived which effectively models flapwise blade vibration and longitudinal tower motion. The flexible bodies are modelled by a modal approximation which represents their motion as a summation of specified modeshapes and corresponding temporal modal coordinates. The equations of motion are derived through the Lagrangian energy formulation which facilitates the accurate incorporation of coupling between the flexible bodies. Utilising this model an investigation of the relative structural performance of a series of steel and concrete towers is carried out. The three tower heights

investigated are 88 m, 103 m and 120 m with the structural input properties of the towers being modelled as probabilistic variables with specified probability density function, mean and coefficient of variance. By implementing the Monte Carlo method for the simulations and specifying appropriately defined limit states, it is possible to relate the probabilities of limit state exceedance to a loading intensity measure, such as mean hub height wind speed. Plots of these probabilities are known as fragility curves and, thus, provide a mechanism for illustrating relative tower performance over the range of heights. The results of this investigation imply that the prestressed concrete towers considered in this study offer an advantage over a corresponding set of steel towers for the range of heights considered. Due to a lack of openly available information on such towers at the time that these investigations were undertaken, some assumptions were made as to the relevant dimensions and properties. These chosen towers have since been validated against a series of similar towers and the discussion of results is considered in the context of this validation. Long term effects such as concrete shrinkage and creep are also considered, as well as the use of high strength concrete in the construction. The modelling framework is subsequently extended to incorporate two dimensional motion. Additional degrees of freedom are introduced to represent edgewise blade vibration, lateral tower motion, nacelle tilt, roll and yaw, as well as rotor shaft rotation and torsion. These capabilities are employed in further comparative studies of the aforementioned suite of towers. Considering seismic loading, it is shown that the chosen steel towers perform more effectively than the prestressed concrete towers, but as the hub height is increased the relative advantage is reduced. A similar conclusion can be drawn from a study of the effect of tower construction material on the resulting blade vibration response. Finally, the model is once again extended to facilitate the incorporation of soil structure interaction within the structural modelling framework. An investigation of the relative structural response of a wind turbine system for both a tubular steel and prestressed concrete tower highlighted the significance of soil structure interaction in estimating the response and showed that a significant reduction in the magnitude of the nacelle response can be achieved by employing a prestressed concrete tower.

Acknowledgements

I am very much indebted to so many people for their contributions to my work over the past number of years. First and foremost, I would like to express my gratitude to my supervisor, Dr. Alan O'Connor, for introducing me to this opportunity and providing the continued support and guidance necessary to succeed in the production of this thesis. I would also like to extend my appreciation to Dr. Vikram Pakrashi for his help and direction throughout my studies.

For their input and financial support throughout the last number of years I would like to sincerely thank the Irish Research Council and Banagher Precast Concrete Ltd. I would also like to acknowledge the the financial support provided by the Trinity Trust Travel Grant Award Scheme.

To everyone in the Department of Civil, Structural and Environmental Engineering, in Trinity College Dublin. I would like to extend my gratitude to the lecturers, administrative and technical staff for all their help and assistance.

I would also like to acknowledge the contribution to my education by Dr. Denis Kelleher and Prof. Michael J. Creed of University College Cork who were always available to give advice and answer questions during my undergraduate years and for helping me navigate to the postgraduate research field.

To all of my fellow postgrads in the department, you were a great help, a powerful inspiration and, most of all, a priceless distraction from the hard work. Whether we were cascading down ski slopes, jumping out of aeroplanes or just having a cup of tea and a chat, I enjoyed every minute. In particular I would like to thank Mick, Paraic, Simon, the postgrad tag rugby team and my Pearse Street officemates, Shane, Tara, Ciarán, Mairéad and Séan.

To all of my friends outside of Trinity College, especially Edel and all of my house-mates throughout my years in Dublin — Áine, Patrick, Tomás, Cian, Sarah, Brendan, Joe, Tom and Mike Mc. Anyone free for a few pucks, a game of FIFA or to climb a mountain tomorrow? I would like to thank you for the welcome distractions you provided from my work and for the inspiration and encouragement when the going got tough. Also, to my good friends Donnchadh and Elaine, John, Mike and Michelle, I will forever be grateful for your support and friendship throughout the dreaded summer of 2012.

To my Grandfather John and my Grandaunt Katherine. Your thoughts and, undoubtedly, countless prayers were thoroughly appreciated.

Finally, I would like to dedicate this thesis to my parents, Flan and Patricia, and my brother Gerard, for their unrelenting love, support and guidance throughout my entire life. You have been with me every step of the way. Thank You!

"The greater danger for most of us lies not in setting our aim too high and falling short; but in setting our aim too low, and achieving our mark."

MICHELANGELO

Contents

List of Figures

List of Tables

Glossary

Notation	Description	Page List
BEM	Blade Element Momentum Theory	26, 28, 29, 72, 99, 176
Bs	Blessington sand	185, 235
CFD	Computational Fluid Dynamics	27, 30, 33, 72
CG	centre of gravity	78, 82, 84, 85
CoV	Coefficient of Variation	92, 117, 133, 138, 143, 146, 171, 198, 204, 218, 228, 229
CPT	Cone Penetration Testing	173
DFT	Discrete Fourier Transform	89
DLC	design load case	23, 175, 176, 178, 179, 216
DNS	Direct Numerical Simulations	31
DOF	degree of freedom	54, 76, 97, 108, 109, 170, 227, 279
ECD	Extreme Coherent Gust With Direction Change	23, 176
EDC	Extreme Direction Change	23
EOG	Extreme Operating Gust	23, 176
ETM	Extreme Turbulence Model	23, 176
EWM	Extreme Wind Model	23, 176
EWS	Extreme Wind Shear	23, 176
FE	finite element	42–44, 46, 49, 61, 64, 104, 171, 172, 180, 183, 190, 229
FEM	Finite Element Method	27, 72, 75
GDW	Generalised Dynamic Wake Model	28, 99
GFRP	glass fibre reinforced polymer	42
GRG	Geotechnical Research Group	170–173, 181, 187
HAWT	horizontal axis wind turbine	1, 14, 15, 71
HS	Hardening Soil	170, 172, 185–188, 192, 193, 195, 196, 198, 200, 202–205, 207, 209–215, 218–221, 234

Notation	Description	Page List
HSS	Hardening Soil with small strain stiffness	170, 185–188, 195, 198, 200, 202–207, 209, 210, 212–216, 218–221, 234, 235
IDA	Incremental Dynamic Analysis	70
IM	intensity measure	70, 149
LES	Large Eddy Simulations	31
LSE	limit-state exceedance	67, 112, 113, 125, 127, 129–132, 136, 137, 139, 140, 159, 160, 162–164, 166, 202, 203, 205, 206, 209–212, 214–216, 218–221, 231, 233–235
MASW	Multi-Channel Analysis of Surface Waves	174
MBS	multi-body-systems	27, 75
MC	Mohr-Coloumb	170, 185–187, 195, 198, 200, 202–204, 206, 207, 209, 210, 212–214, 216, 218–221, 234, 235
MDOF	multi degree of freedom	44, 54, 63, 91
NREL	National Renewable Energy Laboratory	34, 65, 95, 114, 133, 142, 143, 145, 171, 175, 197, 228, 229, 276
NS	Navier-Stokes	27, 30, 31, 33
NTM	Normal Turbulence Model	23, 100, 176
NWP	Normal Wind Profile	23
O & M	operation and maintenance	22
ODE	ordinary differential equation	90, 94
PDF	Probability Density Function	117, 133, 138, 143, 146, 171, 198, 228, 229
PGA	Peak Ground Acceleration	149, 164
PGA	Peak Ground Velocity	149
PGD	Peak Ground Displacement	149
PSDA	Probabilistic Seismic Demand Analysis	6, 8, 70, 71, 74, 143, 145, 147, 149, 150
PSDF	Power Spectral Density Function	89, 91, 92
PSDM	Probabilistic Seismic Demand Model	70, 143, 147, 149, 153, 158, 160

Notation	Description	Page List
RANS	Reynolds Averaged Navier-Stokes	27
SDOF	single degree of freedom	24, 64, 65, 142, 150, 155
SFR	slip force ratio	46
SSI	soil structure interaction	64, 65, 84, 86, 104, 106–109, 169–172, 197, 200, 203, 204, 206–208, 210, 212, 213, 216, 218–221, 225, 229, 233, 234, 236
TLCD	tuned liquid column damper	21, 46
TMD	tuned mass damper	46
TWh	Terrawatt hours	11, 13
UCD	University College Dublin	170–172, 216, 229
UDL	uniformly disturbed load	184, 185
ULS	ultimate limit-state	23, 43, 45, 165, 228
VAWT	vertical axis wind turbine	14, 15
VFR	vibration reduction factor	46

List of Symbols

$[C]$	Damping matrix	
$[K]$	Stiffness matrix	
$[M]$	Mass matrix	
$\bar{V}$	Mean component of wind inflow velocity	(m/s)
$\bar{V}_k$	Mean wind velocity at node k	(m/s)
$\bar{V}_l$	Mean wind velocity at node l	(m/s)
$\bar{V}_{hub}$	Mean hub height wind velocity	(m/s)
$\ddot{u}_g(t)$	Earthquake ground motion acceleration	(m/s^2)
$\hat{V}_{kl}$	Mean wind speed of points k and l	(m/s)
$\{P(t)\}$	Generalised loading vector	
$\vec{p}_{cg,n}$	Position vector of the CG axis of blade n	
$\vec{u}_{nac}(t)$	Absolute nacelle position vector	
$\vec{u}_t(Z,t)$	Absolute tower position vector	
A	Transformed area of structure	(m^2)
C	Turbulence decay constant	
c	Blade chord length	(m)
C_D	Aerodynamic drag coefficient	
C_L	Aerodynamic lift coefficient	
$C_{D,t}$	Tower wind force drag coefficient	
$coh(k,l;f)$	Turbulent wind velocity coherence function	
E	Modulus of elasticity (Young's Modulus)	(Pa)
E_K	Kinetic energy	(Nm)
E_P	Potential energy	(Nm)
$E_{K,b}$	Kinetic energy of the blade	(Nm)
$E_{K,nac}$	Kinetic energy of the nacelle	(Nm)
$E_{K,t}$	Kinetic energy of the tower	(Nm)

$E_{P,C,bn}$	Potential energy centrifugal component for blade n	
$EI_{b,x}$	Bending stiffness of blade in x direction	(Nm^2)
$EI_{b,y}$	Bending stiffness of blade in y direction	(Nm^2)
$EI_{t,X}$	Bending stiffness of tower in X direction	(Nm^2)
$EI_{t,Y}$	Bending stiffness of tower in Y direction	(Nm^2)
f	Frequency	(Hz)
F_D	Aerodynamic drag force	(N)
F_L	Aerodynamic lift force	(N)
F_N	Aerodynamic force normal to plane of rotation	(N)
F_T	Aerodynamic force tangential to plane of rotation	(N)
g_{xy}	Coupling stiffness of the nacelle	
H	Tower height	(m)
$I_{f,X}$	Foundation mass moment of inertia (X axis)	$(kg.m^2)$
$I_{f,Y}$	Foundation mass moment of inertia (Y axis)	$(kg.m^2)$
I_{ref}	Reference turbulence intensity	
$J(t,t')$	Creep function	
k	Von-karman constant	
L_k	Velocity integral scale parameter for direction k	
L_s	Integral scale length parameter	
$m_{bn}(z)$	Mass per unit length of blade n	(kg/m)
$m_b(z)$	Mass per unit length of blade	(kg/m)
M_f	Foundation mass	(kg)
M_{nac}	Total mass of nacelle	(kg)
M_{top}	Total mass of nacelle and turbine components	(kg)
$m_t(Z)$	Mass per unit length of tower	(kg/m)
P_f	Fragility	
P_i	Generalised loading for mode i	
P_n	Generalised loading for mode n	
$q_{bn,i}(t)$	Modal coordinate for mode i of blade n	

$q_i(t)$	Modal coordinate as a function of time t	
$q_{t,j}(t)$	Modal coordinate for mode j of tower	
R	Blade length	(m)
S_C	Seismic capacity	
S_D	Seismic demand	
$S_{bn,i}$	Modal stiffness for mode i of blade n	
$S_{f,X}$	Foundation translation stiffness (X dir)	(N/m)
$S_{f,Y}$	Foundation translation stiffness (Y dir)	(N/m)
$S_{f\theta,X}$	Foundation rotational stiffness about X axis	(Nm/rad)
$S_{f\theta,Y}$	Foundation rotational stiffness about Y axis	(Nm/rad)
S_{FjFj}	Modal fluctuating drag force power spectrum	
$S_k(f)$	Velocity component spectrum for direction k	
$S_{V\_kk}(f)$	PSDF at node k	
$S_{V\_ll}(f)$	PSDF at node l	
S_{VkVl}	Velocity auto PSDF	
$S_{VV}(z_s, f)$	PSDF as a function of height z_s	
t	Time	(s)
$T_A(t)$	Transformation matrix from nacelle coordinates	
$T_B(t)$	Transformation matrix from drive-train coordinates	
$T_C(t)$	Transformation matrix from blade coordinates	
$u(z,t)$	Total displacement as a function of position z and time t	
$u_{b,nac}(z,t)$	Position of blade relative to the nacelle	
$u_{bn,x}(z,t)$	Blade position in x direction	
$u_{bn,y}(z,t)$	Blade position in y direction	
$u_b(z,t)$	Position of CG axis of the blade	
$u_{f,X}(t)$	Foundation position (X dir)	
$u_{f,Y}(t)$	Foundation position (Y dir)	
$u_{nac,X}(t)$	Nacelle position in X direction	
$u_{nac,Y}(t)$	Nacelle position in Y direction	

$u_{nacf,X}(Z,t)$	Nacelle position relative to foundation (X dir)	
$u_{nacf,Y}(Z,t)$	Nacelle position relative to foundation (Y dir)	
$u_{nac}(t)$	Position of the CG of the nacelle	
$u_{t,Y}(Z,t)$	Tower position in Y direction	
$u_{tf,X}(Z,t)$	Tower position relative to foundation (X dir)	
$u_{tf,Y}(Z,t)$	Tower position relative to foundation (Y dir)	
$u_t(Z,t)$	Position of CG axis of tower	
$V'(t)$	Turbulent component of wind inflow velocity	(m/s)
v_*	Friction velocity	(m/s)
V_0	Wind inflow velocity	(m/s)
V_{hub}	Hub height wind velocity	(m/s)
V_{rel}	Velocity of airflow relative to blade	(m/s)
x_i	General coordinate for DOF i	
Z	Variable position along height of tower	(m)
z	Variable position along length of blade	(m)
z_0	Roughness length	(m)
z_s	Elevation above the ground surface	(m)
$z_{sh}(t)$	Elevation relative to hub	(m)

Greek Symbols

α	Blade angle of attack	(rad)
β_C	Logarithmic standard deviation of seismic capacity	
β_D	Logarithmic standard deviation of seismic demand	
γ	Unit weight	(kg/m^3)
$\mathcal{L}$	The Lagrangian	
Ω	Blade rotational speed	(rad/s)
$\phi\,(t,t')$	Creep coefficient	
ϕ	Wind inflow angle	(rad)
$\phi_{bn,i}(z)$	Modeshape i for blade n	
$\phi_i(z)$	Modeshape i as a function of position z	

$\phi_{t,j}(Z)$	Modeshape j for tower	
ψ_n	Mean azimuth angle of blade n	(rad)
ρ	Air density	(kg/m^3)
σ_k	Standard deviation of velocity for direction k	
σ_B	Concrete compressive strength	(MPa)
$\theta_{f,X}(t)$	Foundation rotation about X axis	(rad)
$\theta_{f,Y}(t)$	Foundation rotation about Y axis	(rad)
$\theta_{nac,X}$	Nacelle rotation about X axis	(rad)
$\theta_{nac,Y}$	Nacelle rotation about Y axis	(rad)
$\theta_{nac,Z}$	Nacelle rotation about Z axis	(rad)
$\theta_{s,x}$	Rotor shaft torsion rotation about x axis	(rad)
ξ	Variable position along length of blade	(m)

Chapter 1 -

Introduction

With the looming consequences of the Kyoto Protocol (UN, 1998) and the obvious signs of climate change globally, renewable energy is now both a political and social issue of primary importance. At the forefront of this renewable energy push is wind energy with its primary use in electricity generation. As wind turbines are a relatively new and emerging technology, there is a significant body of research currently being undertaken by experts from a multitude of disciplines. These include mechanical, electronic, aeronautical and structural engineers, as well as economic and ecological experts, to name but a few. As wind energy strives to compete technically and economically with traditional fossil fuels, hydro and nuclear energy sources, numerous barriers have to be overcome and significant improvements have to be made.

Although various types of wind turbines have been tried and tested over the years, the wind energy industry appear to have settled on one particular design, the horizontal axis wind turbine (HAWT). This was determined as the most efficient, cost effective and straight forward solution and accounts for practically every megawatt of current global installed capacity. Figure 1.1(a) illustrates a basic HAWT configuration. An electric generator, located inside the nacelle, is driven by a rotor shaft connected to a set of aerofoil blades. While some designs have been known to operate with one or two blades, the current standard is predominantly a three blade design. The rotational kinetic energy of the rotor shaft is generated by successfully harnessing the aerodynamic lift force as the airflow interacts with the aerofoil profiles of the blades. This is the same principle which allows aircraft to fly. In order for the blades to be positioned within the airflow, the turbine must be elevated into the air by a support structure, known as a tower. The

height of the tower is dependent on the particular turbine design, although the advantages of an increased elevation off the ground surface is well documented, and is discussed in Chapter 2.

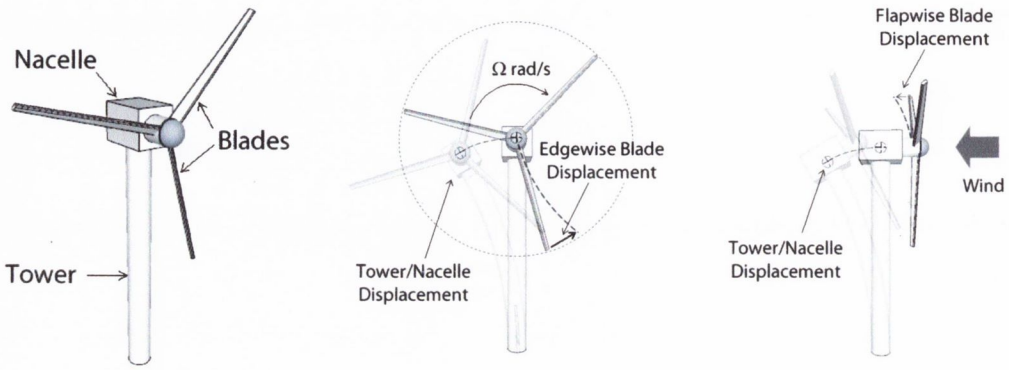

(a) Outline. (b) Front view. (c) Side view.

Figure 1.1: Outline of wind turbine components and dynamics (Quilligan *et al.*, 2012b).

By their very nature, wind turbines are machines which exhibit particularly complex dynamic behaviour. The continuous rotation of the blades while being subjected to turbulent aerodynamic loading induces a variable reaction from the system. This is further accentuated by the flexibility of the blades, tower and other components. As these machines evolve into the substantial structures which are prominent around the globe today, the magnitude of the dynamic response is increased. An underlying objective throughout this thesis is the modelling of this dynamic response. The primary dynamic effects observed in wind turbines are illustrated in Figure 1.1(b) and 1.1(c). Some of these are unique to wind turbines and may be unknown to the reader. The in-plane bending of wind turbine blades is observed in Figure 1.1(b). Throughout this thesis this motion will be referred to as "edgewise" vibration, although some authors may use the term "lead-lag" vibration. Out-of-plane blade bending can be seen in Figure 1.1(c). This will be referred to as "flapwise" vibration, although the term "pitching" vibration is sometimes used in the literature. As blades extend to considerable lengths, the effect of blade torsion is also an important consideration in blade design. The lateral and longitudinal vibration of the tower are also displayed in Figure 1.1. Further effects such as nacelle tilt, roll and yaw

will be outlined in Chapter 3.

So far, of all of the issues and components addressed in the literature, the tower has received relatively limited attention. In fact, until recently it was seen as sufficient to simply design the tower stiff enough so as to avoid any undesirable dynamic effects (Harte and Van Zijl, 2007). For smaller turbines this was not a problem, but as the scale of these structures increases the tower design has become more significant. It is upon this basis that the current thesis is established. The possibility of improving the dynamic characteristics of multi-megawatt wind turbine structures by employing prestressed concrete towers is investigated. It is widely accepted that with the growing size of wind turbine structures the tower is becoming a more critical component and companies such as ENERCON (2012) and ATS (2012) have established new and alternative designs employing prestressed concrete to cater for the larger multi-megawatt wind turbine machines. Despite this, while limited research has considered wind turbine towers, minimal examples exist which consider the concept of prestressed concrete or hybrid (prestressed concrete/steel) tower configurations. This thesis aims to improve on this deficiency by investigating the possible structural advantages of these alternative tower concepts over the current industry standard tubular steel designs. Specifically, the investigations will focus on tower heights in the range of 88 - 120 m, which are equivalent to the heights required for current and near future state of the art wind turbine designs. To the best of the author's knowledge, another study of this type has not been undertaken thus far.

1.1 Outline of Wind Turbine Tower Structures

The tower is the sole support element for the operating wind turbine components above. It is therefore an essential part of the overall structure and must be designed to survive all conditions whether the turbine is operational or not. It must also be designed so as not to interfere with the complex vibrations exhibited by the operational components. A poorly configured tower design could allow an unsafe proximity of the system operating frequencies and the tower natural frequency, thus leading to a dangerous resonance effect.

Various types of tower designs exist. The most popular concept is undoubtedly the tubular steel design. This is composed of one or more straight or tapered rolled steel tubular sections, bolted together through thick flanges at the end of each section. The advantage of this type of tower is the strong elegant solution which is achieved as well as the simple and fast on-site assembly process. Variations of this type of tower incorporate a less stiff tower which is augmented by the addition of steel guy wires or truss elements. These have generally only been employed in relatively small designs, if at all. Truss towers, similar to those which commonly support electricity transmission cables are another option. This solution can achieve a very stiff design with considerably less steel than the tubular design but opponents often cite the undesirable aesthetics, lengthy assembly process and susceptibility to corrosion as negatives of this option.

Concrete is a material which has previously been used in the construction of wind turbines and is gaining favour among designers once again. Utilising a steel reinforced or prestressed configuration, a considerably stiff tubular type solution can be achieved. The structure can be established through either in-situ pouring of the concrete or by assembling precast elements. The choice is dependent on the specific circumstances of each case. Proponents of concrete towers highlight the ability of a concrete configuration to achieve a stiffer solution for a greater range of heights than the alternative steel option (Harte and Van Zijl, 2007). It has also been suggested that despite the considerably greater mass of a concrete structure, the embodied energy and CO_2 may be less than a tubular steel tower over the design life of the respective structures (Cleary *et al.*, 2012). A variation of this option incorporates a hybrid design combining a concrete base section with a tubular steel upper section.

The focus of this thesis is on assessing the structural performance of both tubular steel and prestressed concrete towers for hub heights in the range of 88-120 m. This is of particular interest given the trend towards larger more powerful turbines, reaching higher into the atmosphere to attain greater and more stable wind speeds. A probabilistic representation of the relative performance of both configurations will be made for a series of loading conditions and measured responses with the aim of comparing the reliability of

the chosen series of wind turbine towers.

1.2 Objectives of Thesis

As modern wind turbines are a relatively new and evolving technology it has been noted that there exists significant gaps in the published research. One such area identified is in the investigation of the tower structure, in view of alternative tower materials to steel, in particular. The aim of this work is to assess the structural dynamic performance of both prestressed concrete and tubular steel wind turbine towers for heights from 88 m to 120 m. These heights represent the range at which the most advanced and tallest multi-megawatt turbines currently operate and over which the greatest structural challenges exist for modern wind turbines. More specifically, this comparison is achieved through the following objectives:

1. The development of a one dimensional dynamic model of a wind turbine which effectively simulates both the flapwise vibration of the blades, the longitudinal vibration of the tower as well as the accurate dynamic coupling of the various components. Initially, a thorough investigation will be conducted of the numerous existing methods employed in the modelling of wind turbine dynamics. On determining the most appropriate modelling techniques, these will be implemented in a numerical model which ensures accurate response estimation as well as efficient computation capabilities.

2. The assessment of the structural performances of both tubular steel and prestressed concrete towers under normal operating conditions for basic, one dimensional response. This will be achieved through the application of the one dimensional model established in Objective 1. A series of steel and concrete towers will be chosen, and the appropriate structural properties will be determined in order to represent the realistic tower construction.

3. Develop a more detailed structural model which further accounts for the complex

dynamic interactions within a two dimensional framework. The model derived in Objective 1 will be further extended to incorporate edgewise blade vibrations, lateral tower motion, nacelle tilt, roll and yaw as well as rotor shaft rotation. Again, this model must achieve accurate results with efficient computation capabilities.

4. As a continuation of Objective 2 the structural performance of the two tower construction materials will be assessed utilising the two dimensional model while subjecting the structures to various loading conditions. In the first instance seismic loading of wind turbine structures will be considered as this has become a more relevant issue with increasing wind turbine size and their greater prominence in seismically active regions. This will be accomplished by implementing the extended model developed in Objective 3, in combination with the probabilistic modelling technique, Probabilistic Seismic Demand Analysis (PSDA). This is a procedure which has not previously been adopted in the literature, and offers a tool for future seismic investigations of wind turbine systems.

5. While the previous objectives have, thus far, focussed on the effect of the tower construction material on the associated tower response, in this instance the effect of the tower construction material on the dynamic response of the blades will be addressed. This issue has not been addressed in the literature and may prove a beneficial exercise, given the detrimental effects of excessive vibration in wind turbine blades. In this investigation the recorded blade vibrations will be assessed in simulations of the dynamic response of a series of wind turbines with varying height and construction material.

6. The comparison made as part of Objective 2 will be extended to two dimensions, with the addition of a soil-structure interaction component. The effect of soil structure interaction has been shown, in some instances, to affect the dynamic response of structures. Given the considerable difference in structural mass between tubular steel and prestressed concrete tower designs, the effect of soil structure interaction may not be consistent between the two designs. By extending the model developed

in Objective 3 to account for a variable support condition at the tower base, the response of the suite of towers can be modelled under wind loading for a specified set of soil conditions. This will improve the realistic nature of the results of previous comparisons and possibly highlight relative differences in tower performance due to soil structure interaction effects.

1.3 Organisation of Thesis

This thesis is made up of seven chapters, outlined as follows:

Chapter 1 provides an introduction to the topic of wind turbine structures with particular emphasis on wind turbine tower development. The objectives of this work and an outline of this thesis are also presented.

Chapter 2 presents a state of the art review of current research in the area of wind turbine structures. Identified in the literature review are relevant publications on analysis and modelling techniques, as well as useful findings which provide a basis for the model development and determination of objectives for the current thesis.

Chapter 3 outlines the theoretical development of the numerical dynamic models formulated as part of the current project. The design, formulation and implementation of the models is discussed in the context of the aims of this research. Both a one and two dimensional model are derived in this section and their specific benefits to the research project demonstrated.

Chapter 4 demonstrates an assessment of the relative structural performance of a series of steel and prestressed concrete wind turbine towers for heights ranging from 88 m to 120 m, under normal operating conditions. Identified in this section are both the effect on nacelle and blade dynamic response as a result of implementing various tower configura-

tions. The optimum solution is identified at each representative hub-height for the range of operating wind speeds considered.

Chapter 5 considers the role of seismic response in the design of wind turbine structures. A method of considering the dynamic response to seismic events is outlined. The PSDA technique, commonly utilised in the context of bridge and steel moment frame structures, is applied to the results of the dynamic response analysis in order to quantify the fragility of the tower component in the wind turbine structure. This, once again, facilitates an assessment of the structural response of a series of steel and prestressed concrete towers for a range of hub-heights and seismic intensities.

Chapter 6 presents a comparison of the relative structural performance of the 88 m steel and prestressed concrete towers addressed in previous chapters with the additional effect of soil-structure interaction included in the analysis. An extension of the model derived in Chapter 3 is proposed to estimate the effect of soil-structure interaction on the overall response of the various towers. This effect is subsequently investigated in the context of the dynamic response of the suite of towers.

Chapter 7 concludes the thesis by outlining how the objectives detailed in Chapter 1 have been achieved. In addition, recommendations are made for future work to further develop an understanding of the viability of prestressed concrete wind turbine towers.

Chapter 2 -

Literature Review

2.1 Introduction

With the growing pressure both socially and politically for governments to address the impending global energy crisis as well as carbon emissions curtailment, renewable energy solutions have commanded noticeable attention in recent years. At the forefront of this movement is wind energy which is considered a relatively mature technology in comparison to other alternatives. While the first attempts at generating electricity from the wind can be traced back as far as the 19^{th} century, the start of the modern age of wind generated electricity is more precisely linked to the "oil price shock" of 1973 (Hau, 2006). From that point on, a renewed emphasis by numerous governments and bodies was placed on these technologies, which had for decades been forgotten. More recently, with stringent carbon emission targets laid down by agreements such as the Kyoto Protocol and ambitious objectives for the penetration of renewable energy in society, the roll out of wind energy has seen a considerable gain in momentum. As manufacturers and researchers addressed the problem of lowering the cost of wind generated electricity, a progression towards less conservative, large scale and optimised designs has been observed. An article by Quarton (1998) outlines the evolution of wind turbine design methods since 1980 and duly captures the magnitude in growth of scale, advancement in design concepts as well as the catalysts to this evolution. Since 1980 the generating capacity of a wind turbine machine has increased from 55 kW to the current maximum of 7,500 kW (ENERCON, 2010a), while numerous companies are currently working on developing a 10,000 kW machine.

As a consequence of this growth the wind energy industry has seen a correspond-

ing increase in the size of wind turbine components. Generators, gearboxes and control equipment have all had to follow this progression while wind turbine rotor diameters have increased from 15 m in 1980 (Quarton, 1998) to beyond 120 m (ENERCON, 2007). In order to meet the requirements of these growing structures, considerable research and development has had to be undertaken to produce the critical components for these structures. In the case of wind turbine blades, the materials utilised in their construction have had to consistently evolve. Some of the materials used over the years included steel, wood, fibre reinforced composites, wood-epoxy composites as well as carbon fibre. As the structural demands continue to increase, so too will the development of improved blade designs. A similar progression can be observed with the tower structure as various designs are considered in order to balance structural efficiency, cost, CO_2 emissions, ease of construction and transportation issues.

In the context of these issues the current chapter aims to provide an extensive review of the published material on the topics addressed in this thesis. Initially, a general overview of wind turbine technology is presented with a particular emphasis on design requirements and dynamic modelling methods. The well established field of blade dynamics and design is considered next, highlighting the vibration and fatigue issues which affect these components. Subsequently, the more specific subject of the wind turbine tower is considered. An in-depth review of steel, prestressed concrete and hybrid tower structures is provided which forms the basis for the research presented in this thesis. As wind turbines become more prevalent around the globe, the issue of seismic loading emerges. Due to the limited number of turbines in seismically active regions in the past, little consideration has been given to this issue in either design codes or published literature. Now however, with the increasing magnitude and density of these structures a greater focus on earthquake effects is necessary. This topic is discussed with a focus on design considerations and analysis techniques relevant to seismic loading. Finally, the issue of soil structure interaction and its influence on wind turbine dynamics is discussed. Modelling techniques, assumptions and results from published research are presented. Throughout this chapter an effort is made to provide a clear interpretation of the current state of the art in the areas addressed.

It is also intended to identify possible opportunities to progress the state of the art and improve on current solutions, techniques and methodologies.

2.2 Wind Energy

Wind energy is becoming ever more prominent around the globe with 237 GW of installed capacity at the end of 2011, an equivalent of providing for approximately 3 % of the global electricity demand (Gsänger and Pitteloud, 2012). For the first decade of the 21^{st} century there has been an average annual growth of 30 % and a long-term trend that sees the global installed capacity doubling every third year. Sesto and Casale (1998) attributes this to widespread concern about damage to the environment along with a fear of dwindling fossil fuel supplies and the inevitable price spikes as a result. As of the end of the last century, industrialised countries produced approximately 65 % of their electricity from fossil fuels. The author also predicts that by 2030, 50 % of the world's electricity will be generated and utilised by developing countries. If these nations were to emulate the industrialised west and become dependent on fossil fuels to the same extent, then irreparable damage to the environment as well as unsustainable energy prices would become a certainty.

2.2.1 Wind Energy Fundamentals

Wind, or the movement of air masses around the earth is a by-product of solar radiation from the sun. According to Frick *et al.* (2007), approximately 2.5 % of the total solar energy incident on the outer layer of the earth's atmosphere is transformed into wind energy. This equates to an overall wind power of approximately 4.3×10^{15} Watts or an equivalent annual energy resource of 3.8×10^{7} Terrawatt hours (TWh). In contrast, the annual OECD electricity consumption for 2009 was 10,308 TWh (IEA, 2010). Technically, there is more energy provided by the wind than could ever possibly be required. For the more specific case of Ireland, Clausen *et al.* (2004) suggests an estimated technical resource, or the amount of wind energy available, of 613 TWh per year compared to Ireland's annual electricity consumption of 27 TWh in 2003. Despite these impressive figures it is of course

unreasonable to believe that it is as straight forward as simply harvesting all of this free energy and forgetting about any energy worries. Like everything in this world, there are compromises to be made and these are discussed in the following section.

2.2.2 Barriers to the Development of Wind Energy

Richards *et al.* (2012) considers some of the barriers to renewable energy development through a case study of large-scale wind energy in Saskatchewan, Canada. Many of the foremost barriers to wind energy can be categorised as technological, economic, social, or political barriers. Technological barriers include issues such as the intermittent nature of wind, the lack of energy storage solutions and difficulties integrating wind energy with an electricity grid. If offshore wind energy is considered, the technological barriers extend further with higher costs, harsh environmental conditions and complex logistics. Economic barriers may be categorised as concerns relating to the cost of wind generated electricity compared to traditional sources and its integration within carbon pricing initiatives which in many jurisdictions are not fully established. Social barriers were generally not experienced in this case study due to an accepting public and sparsely populated rural environment. Despite this Haggett (2011) describes how widespread public resistance, associated planning difficulties and lengthy delays with windfarm development may be attributed to the consequential social disturbances in the form of visual, noise, harm to birdlife, local ecology and environment. Political barriers point towards the consideration and implementation of wind energy initiatives within public policy. It is suggested that the manner of leadership expressed by governments in relation to renewable energy policies can have a significant effect on the uptake of wind energy in a particular country or region.

In the context of the current thesis, the aforementioned barriers each have relevance to the topic of investigation. The possibility of utilising prestressed concrete towers may offer a solution to the technological barrier of increasing tower heights, as well as economic barriers by reducing the cost of the generated electricity through higher power machines operating in greater wind speeds at taller heights. On the other hand, both social and political barriers may impede the progression of this technology due to the opposition of

planning authorities and the general public to increasing tower heights. Another concern is the negative connotations associated with concrete in the public domain, although, as will be discussed further in this chapter, this perception may be unfounded. It is evident, as with any impartial analysis, that a balance of these opposing contributions is the only means of arriving at a satisfactory solution.

2.2.3 Realistic Expectations

In light of the many barriers which exist, it is necessary to consider the practicable annual resource of wind energy. This takes into consideration the total resource constrained by practical, social and economic factors. For Ireland, the practicable annual resource is estimated as 6.7 TWh (Clausen *et al.*, 2004). Although only 1 % of the total technical resource of 613 TWh, it still represents a significant proportion of the total electricity consumption (25 %).

It is clear that wind energy can provide at least part of a feasible solution to the current global energy constraints. By facilitating a clean and sustainable alternative to fossil fuel based energy production, it can be implemented in combination with other energy solutions to reduce the dependence on finite energy sources and curtail the extent of environmental damage through the release of CO_2 and other toxic gasses. Despite the prospects of wind energy, there are many barriers which must be overcome in order to improve the extent of its viability as an energy source. The only means of overcoming these barriers is through the amalgamation of extensive multidisciplinary research objectives which encompasses the complete framework of wind energy technology. This thesis focusses on a single facet of the research initiative by considering the technological constraints of the wind turbine tower structure.

2.3 Wind Turbines

The first examples of modern wind turbines emerged in the 1970s as a result of numerous governmental funding initiatives in the USA, Germany, Denmark and Sweden. This

resulted in a series of prototypes and experimental structures aimed at improving the understanding of wind generated electricity and the structures required for this purpose (Goodman Jr. and Vachon, 1982; Hydro-Québec, 1984; Energiministeriet, 1986).

During the 1980s these government backed initiatives focused mainly on constructing large scale multi-megawatt machines, as the general belief was that to make the industry financially viable and attractive to investors the turbine outputs would have to be of this scale. Two of the more notable projects included the NASA MOD series of turbines and the German Growian project. Hau (2006) suggested that these ambitious projects were, at the time, considered a disappointment once the governmental finances were withdrawn and the original expectations were not met, noting that they were over ambitious at too soon a stage. Despite this, a significant body of research had been conducted with all documentation publicly available, paving the way for future initiatives and the wide-spread implementation of the multi-megawatt turbines seen today.

At the same time as this ambitious research was taking place, a more understated approach was been adopted in Denmark. Concepts developed in the 1940s were being utilised to produce turbines in the 50-60 kW range for use by private owners and agricultural holdings (Hau, 2006). Coinciding with favourable tax incentives for wind farm developers in the state of California, the companies producing these turbines found a considerable market in exporting to the USA. By the end of 1985, about 40 % of all wind turbines in California had come from Denmark. Although these incentives eventually expired and the demand for wind turbines waned, many companies had refined their designs and gained a wealth of experience, further enhancing the prospects for the modern wind turbine industry.

During this initial phase of wind turbine development a principal topic was discussed. Two primary designs were proposed for a wind turbine configuration. The HAWT, most common today, and the vertical axis wind turbine (VAWT) seen in Figure 2.1. While the Growian and NASA MOD series turbines focussed on the horizontal design (NASA, 1979), other initiatives such as the Éole project (Hydro-Québec, 1984) considered the alternative vertical axis machines. Following the research conducted as part of these projects it was

determined that the VAWT concept, "did not offer an alternative which was economically equivalent to the horizontal-axis turbines" (Hau, 2006). The most common wind turbine

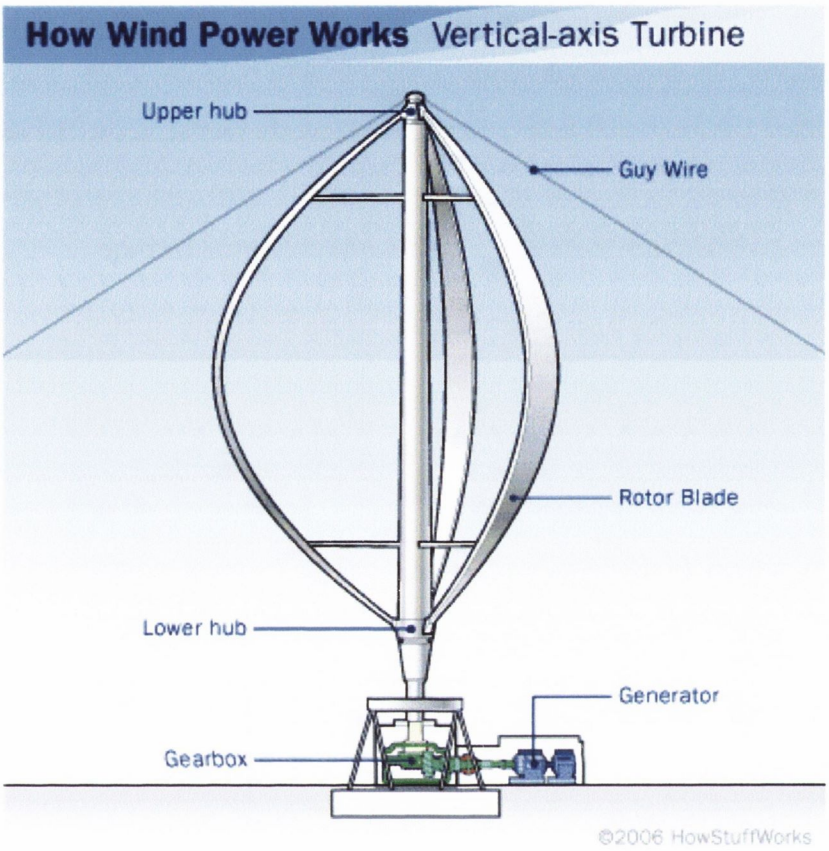

Figure 2.1: Darrieus design VAWT (Layton, 2012).

design seen in modern applications is the HAWT. The general assembly configuration of such turbines is depicted in Figure 2.2. There are three primary components of the structure. The support structure is made up of the foundation, which can vary in design based on its location and soil conditions as discussed in Section 2.6, and the tower which is generally constructed from rolled tubular steel sections or some of the alternative designs outlined in Section 2.5.1. The nacelle sits on top of the tower and contains much of the mechanical components for the turbine. These include the gearbox, mechanical shafts, the generator, braking systems and control systems. The rotor system is the most essential component for harnessing the energy of the moving air mass and transforming it into a useful form of energy. It is composed of the blades, hub and rotor shaft. The blades are

constructed with an aerofoil profile which allows them to efficiently capture the lift force as the wind passes over them and transfer this to the rotating hub. The root of the blades are anchored to the hub which houses the blade mechanical controls such as pitch actuators. The hub transfers the aerodynamic loads on the blade to the rotor shaft. The rotor shaft in turn transfers the rotational energy to the mechanical systems inside the nacelle. The

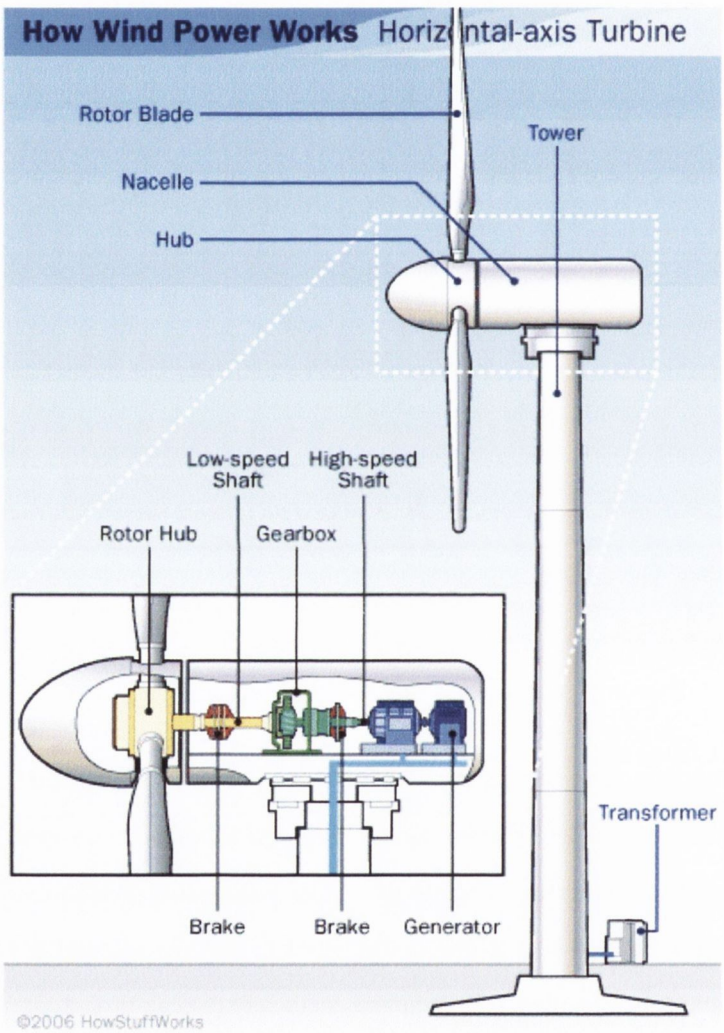

Figure 2.2: Standard design HAWT (Layton, 2012).

operation of wind turbines is based on harnessing the power of the wind. Equation 2.1 presents a mathematical expression for the quantification of the available wind power over

a certain area.

$$P = \frac{1}{2}\rho A U^3 \tag{2.1}$$

where P is the power of the wind, ρ is the air density, A is the area considered (i.e. the area swept by the rotor) and U is the mean wind velocity. The implication of this is that the power available from the wind is proportional to the cube of the wind speed, therefore highlighting the benefits of siting the wind turbines appropriately and extending the hub heights higher into the atmosphere where wind speeds are greater.

Wind shear is another feature which sees the wind speed increase with height from the surface. Figure 2.3 highlights the increased mean wind speeds experienced above various surface conditions. It is important to note from this graphic that higher wind

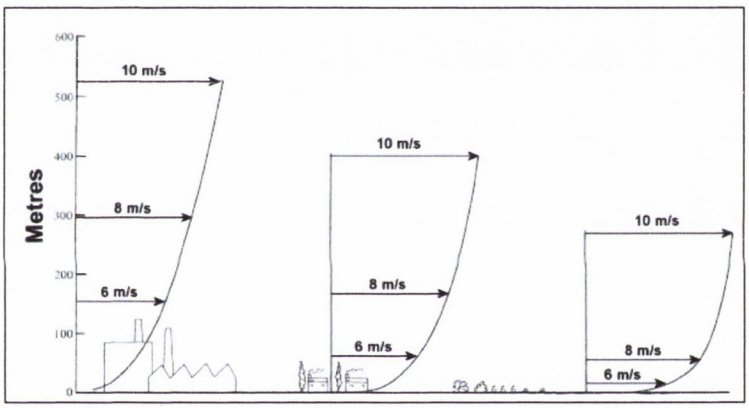

Figure 2.3: Wind shear profiles over various terrain conditions (WINDPOWER, 2012).

speeds can be achieved at lower heights where the surface condition is relatively smooth. The most desirable surface condition in terms of wind shear profiles would, therefore, be flat unvegetated land or water. In order to calculate the average wind speeds at a specific height, there are two mathematical formulae primarily employed. The power law, Equation 2.2, is generally used in the calculation of wind power, where $v(z)$ is the mean wind speed at height z above the surface, v_r is a reference wind speed at height z_r above the surface and α is the power law exponent, also known as the wind shear coefficient.

$$v(z)/v_r = \left(\frac{z}{z_r}\right)^{\alpha} \tag{2.2}$$

Rehman and Al-Abbadi (2005) presented a study of wind shear coefficients and their effect on power production calculations in Saudi Arabia. It was suggested that, while a value of 1/7 is commonly utilised for the wind shear coefficient, this may not always be accurate. In fact, this particular study demonstrated 6 % greater energy production than was estimated by the 1/7 factor. Another similar investigation was carried out by Gualtieri and Secci (2011) for three coastal sites in Southern Italy. Values for the underestimation of power production as a result of utilising the 1/7 factor were calculated at between 11 % and 26 %.

For engineering purposes the log law, Equation 2.3, is more common, where $v(z)$ is the mean wind speed at height z above the surface, v_* is the site specific friction velocity, k is the Von-karman constant and z_0 is the site specific roughness length.

$$v\left(z\right) = \frac{1}{k} v_* \ln \frac{z}{z_0} \tag{2.3}$$

The roughness length, z_0, is dependent on the site specific terrain surface characteristics and varies from 10^{-4} m over calm water to approximately 1 m in cities. It is determined as the height at which the wind speed theoretically becomes zero. Values of z_0 for various surface conditions may be found in Troen and Petersen (1989). This highlights the advantage of taller hub heights, particularly for inland sites where increasing the tower height can allow similar wind speed characteristics to coastal or offshore sites to be attained.

While Equation 2.1 determines the total available power from the wind, like any other energy conversion system, it is impossible for wind turbines to convert all of this energy into electrical power. A theory proposed by Albert Betz in 1926, known as Betz's law, proposes the maximum possible amount of energy to be derived from a wind turbine (Betz, 1926). The result, known as "Betz's limit", determines that for an ideal turbine the maximum efficiency which can be achieved, irrespective of the turbine design, is 0.593 or 59.3 %. In reality the actual maximum efficiencies or power coefficients of operational rotors are less than this value (0.29 (Kjellin *et al.*, 2011) and 0.37 (Lanzafame and Messina, 2010)), with the maximum values only being achieved at certain "rated" wind speeds.

2.3.1 Onshore

Onshore wind turbines account for the majority of wind generated electricity in the global energy market, accounting for 99.5 % of the current installed capacity at the end of 2011 (Gsänger and Pitteloud, 2012). Much of the expertise gained from the experimental turbines of the late 1970s and 1980s pertained to onshore applications with a general goal being to perfect the actual turbine components such as the blades (Yuncheng *et al.*, 1988; Chen and Zhong, 1988; Abramovich and Rosen, 1988; Bond and Clayton, 1989), generators (Seidel, 1978; Sambar *et al.*, 1980; Ula, 1987; Matsumiya *et al.*, 1990), as well as the overall experience of operating and maintaining wind turbines (Garside and Kyles, 1984; Stevenson *et al.*, 1989; Soria *et al.*, 1990; Neilsen, 1990).

Onshore wind turbines are typically constructed in rural locations away from large population centres. The ideal site combines the attributes of a secure accessible location, strong and consistent wind speeds as well as close proximity to the electrical grid for easy connection. Baban and Parry (2001) explained the criteria for locating wind farms. To facilitate the physical requirements of the turbines, the wind farms must be located on suitably elevated sites, avoiding summits, and facing the prevailing wind conditions with a minimum average wind speed of 5 km/h. So as not to affect the wind inflow, they must be at least 500 m from forested areas. In order to satisfy planning, health and safety regulations, they should be located some 2 km away from urban centres and at least 500 m away from single dwellings. To limit costs, the site should be located as close as possible to a main road but must maintain a safe distance so as to reduce visual intrusion. Another cost related constraint dictates a maximum distance of 10 km from the primary electrical grid. In Ireland the Department for the Environment, Heritage and Local Government has issued guidelines for wind energy development (DoELG, 2006). This document does not specify actual limits for the size, location and performance of wind turbines/farms, but instead places an emphasis on assessing the impact of a proposed development and balancing the negative aspects against the broader benefits on a national level. In terms of visual impact, it states, "sufficient distance should be maintained from farmsteads, houses and centres of population in order to ensure that wind energy developments do

not visually dominate them". In relation to noise, a daytime noise limit of 35 - 40 dB(A) is recommended and an night-time limit of 43 dB(A). It also states that, "in general, noise is unlikely to be a significant problem where the distance from the nearest turbine to any noise sensitive property is more than 500 metres". In order to assess the impact of a proposed development, the guidelines reflect on the mandatory requirement for an Environmental Impact Assessment for wind energy developments that exceed the threshold of more than five turbines, or have a total output greater than 5 megawatts.

Whilst it is clear that wind generated electricity is a positive and beneficial development, constructing wind farms is not quite as straight forward. The stated constraints result in a limited number of suitable sites being available for wind farm development. Coupled with this are the technological, economic, social and political barriers outlined in Section 2.2. Following over a decade of intensive wind farm development in countries such as Ireland and the UK, the opportunities for new wind farms are reducing and new concepts must be implemented in order to optimise the current installations. One such option to improve power production at inland sites is by increasing the hub height to benefit from greater average wind speeds. This, again, relates to the proposed investigation where an optimal structural solution for larger turbines and taller hub heights is sought.

2.3.2 Offshore

In an effort to overcome many of the barriers associated with onshore wind turbines, significant investigations have been conducted into the possibility of siting wind turbines offshore. There are some advantages in developing wind turbines offshore. It is noted by Hau (2006) that an energy yield of 30 - 40 % higher than that on land can be expected from offshore applications due to the higher and more consistent wind speeds. Ferguson (1998) highlights the improved turbulence characteristics offshore with typical values of about 8 % at a height of 60 - 70 m compared to a turbulence intensity over land within a range of 10 - 20 %. This has a major effect on the fatigue loading of the turbine structures. Due to the extensive sea and ocean environment on our planet, there are considerably more prospective sites, with an absence of the restrictions and regulations pertaining to

interaction with human settlements. This means that much larger turbines, in a greater concentration may be located out at sea without having the same social and environmental impact. In a study by Elgaard *et al.* (1988) into the prospects of offshore wind turbines, it is stated that one of the main reasons for initiating the study was the growing difficulty in finding suitable inland locations accepted by the authorities and the public in general. King *et al.* (2012) states that noise and visual impact are the most common negative effects related to onshore wind farms. While the visual impact would still exist out at sea, in many instances it would not have the same effect as at an onshore site and, when located away from the shoreline, the noise impact would not be of the same extent.

Considering the experience gained from the oil and gas industry in the construction of offshore platforms, it is not unreasonable to consider offshore wind turbines as a feasible solution. Since the first offshore based wind power plant was built in Sweden in 1990 (Larsson, 1994), there has been a steady progression in the development of offshore wind turbines. Zaaijer (2009) presents an extensive review of knowledge development for offshore wind energy technology. Highlighted within the review are advances made in understanding the wind speed distribution in an offshore context (Hansen and Larsen, 2003; Barthebnie *et al.*, 2004; Brand, 2007), hydrodymanic loading (Nielsen *et al.*, 2006; Henderson *et al.*, 2006), structural modelling techniques (Holierhoek, 2008; de Vries, 2009), as well as the integration of wind and wave loading for an assessment of the combined loading conditions (Nielsen *et al.*, 2006). Colwell and Basu (2009) considers the use of a tuned liquid column damper (TLCD) for the control of vibrations in offshore wind turbines.

It is obvious that the most affected element of the wind turbine structure, when offshore applications are considered, is the support structure. Instead of a relatively straightforward slab or piled foundation, the support structure must provide a secure platform for the tower and turbine, above the maximum water level for variable water depths. It must be capable of withstanding wind and wave loading as well as other occurrences such as sea ice and misplaced sea vessels. An extensive review of offshore wind turbine support structures is presented in Section 2.6.2.

Aside from the sub-structure, there are other aspects of siting wind turbines offshore

which must be considered. Due to the location of these machines in quite inaccessible locations out at sea as well as the aggressive environment in which they must operate, there are a number of routine procedures which prove more challenging for offshore turbines. Nielsen and Sørensen (2011) considers the contribution of operation and maintenance (O & M) costs of offshore wind turbines to the cost of energy. It is suggested that it may account for up to 30% of the overall cost of energy over the lifetime of a structure. Márquez *et al.* (2012) estimates that O & M accounts for 25-30 % of the overall energy generation cost or 75-90 % of the investment costs. It is obvious, therefore, that O & M is a significant issue for offshore wind turbines and Breton and Moe (2009) estimates the cost of repairs to be 5-10 times more expensive offshore.

Another issue relevant to offshore wind turbines is the difficulty in the assembly and erection of these large structures out at sea. For this purpose, specialised vessels must be employed which are expensive and often difficult to acquire. In fact Breton and Moe (2009) foresee a shortage of suitable vessels for construction and repair purposes as a result of the fast increasing development of offshore wind farms. Also, due to the unpredictable conditions at sea, the erection process becomes a slow and tedious procedure, balancing efficiency with safety and feasibility. In an effort to avoid much of these inherent delays, a new system has been developed which sees the complete wind turbine structure pre-assembled on shore and transported to its final location before being dropped into place (STRABAG, 2009). This methodology is only currently feasible for gravity based foundations, however, which are limited to relatively shallow depths.

Further aspects relevant to offshore wind turbines include the electrical transmission systems. Hau (2006) outlines how the greater distance over which the power must be transported, the higher costs of the electrical components and the necessity for greater redundancy in the electrical system, impacts on the implementation of an offshore wind farm.

While concrete towers and support systems may offer a feasible solution to offshore installations, it is evident from the preceding sections that the greatest gains to be made from increased tower heights are at inland sites. Coupled with this are the additional

technological and logistic constraints with offshore development which must be solved in order for offshore wind projects to achieve their full potential. It has therefore been decided to investigate the structural advantages of prestressed concrete towers for onshore sites, allowing the findings to be extended to offshore environments in the future.

2.3.3 Design Requirements

The primary loading component on wind turbines is the force of the wind impacting on the structure. For offshore wind turbines the hydrodynamic loading induced by waves is also a considerable component. Considering the wind conditions, the British and European standard of wind turbine design BS EN 61400-1 (2005) has specified three wind turbine classes dependent on the wind speed and turbulence parameters of the intended site. Having specified a wind turbine class it is necessary to analyse the structure for a set of design load case (DLC) events. The standard requires the use of a structural dynamics model to predict the design loads. Considered among the DLC events which must be analysed are environmental conditions represented by a Normal Wind Profile (NWP), Normal Turbulence Model (NTM), Extreme Wind Model (EWM), Extreme Turbulence Model (ETM), Extreme Coherent Gust With Direction Change (ECD), Extreme Wind Shear (EWS), Extreme Operating Gust (EOG) and Extreme Direction Change (EDC). The DLCs are configured to simulate a variety of situations including normal power production, power production with a fault occurrence, a start up event, normal shut down, emergency shut down, parked conditions, parked with a fault and transportation. Some of the faults which are common to wind turbines include a control system failure, electrical faults, and the loss of the electrical network connection. Within the load cases both ultimate and fatigue loads are examined.

While the turbine must be capable of resisting the most extreme wind conditions for the ultimate limit-state (ULS), it is often the fatigue loading of the turbine which dictates the design. Hau (2006) states that wind turbines are the perfect fatigue machines, owing to the considerable variability of the wind loads and the necessity for a highly elastic structure due to their size. Pedersen *et al.* (2012) notes that turbulence in the inflow

is the primary influence on fatigue damage accumulation in upwind turbines. Thomsen and Sørensen (1999) investigated the fatigue effects of a wind turbine operating in wakes. Since wind turbines are generally located in clusters or wind farms, this is an important consideration in the design. It was shown that the increased fatigue loading in the wind farm compared to free flow was between 5 and 15 %, depending on the wind farm layout. It was also found that the load increase caused by wake effects was the same for both offshore and onshore sites.

Another consideration in the design of wind turbines is the effect of seismic loading on the system. BS EN 61400-1 (2005) states that there are no earthquake resistance requirements for standard class turbines because such events are only design driving in a few regions of the world. In the cases where local codes necessitate the calculation of resistance to earthquake loading a simplified procedure is designated which estimates the seismic load through a single degree of freedom (SDOF) oscillator approach. While the reduction of the system to a single tower mode is considered a significantly non-conservative simplification, this is compensated for by adding a portion of the tower mass to the tower head mass as well as incorporating a conservative aerodynamic load. Similar simplified and conservative approaches are common to many other design codes and publications. For this reason, the issue of seismic loading on wind turbines has been identified as an area which requires further development and is, therefore, included as one of the primary objectives of this thesis within the context of comparing tower configurations.

Offshore wind turbines are subjected to additional loading conditions which must be considered in the design. BS EN 61400-3 (2009) defines a wind turbine as an offshore wind turbine if the support structure is subject to hydrodynamic loading. These additional marine induced effects such as loads due to waves, sea currents, tidal fluctuation in water level, sea ice, marine growth, seabed movement and scour must be considered in the design. Noting the unpredictable nature of waves, it is suggested that the features of a real sea are best reflected by describing a sea state by means of a stochastic wave model. Considerable research has been conducted on the topic of wave modelling for offshore wind turbines (Marino *et al.*, 2011a,b; Agarwal and Manuel, 2011; Jensen *et al.*, 2011; Chella *et al.*,

2012). BS EN 61400-3 (2009) and DNV-OS-J101 (2010) suggest the use of a spectral model for the simulation of the sea state. The Pierson-Moskowitz spectrum is applicable to a fully developed sea state while the JONSWAP spectrum pertains to a developing sea state for events such as a storm situation. The correlation of wind and wave conditions must also be addressed (Colwell and Basu, 2009). As these conditions are affected by local site factors such as fetch, water depth and bathymetry, the determination of parameters must be made from suitable long term measurements.

While for design purposes it is necessary to verify the turbine for all of the specified load cases, in the current investigation the tower structures will be compared under a selection of loading conditions. These include both wind and seismic considerations. Obviously, for an onshore simulation the requirement for hydrodynamic loading is removed, and whilst fatigue calculations may provide a useful comparison of tower designs, these effects are more concerned with the blades and other moving components. Nevertheless, a comprehensive comparison of fatigue may be a useful consideration for further work.

2.3.4 Dynamic Modelling

Wind turbines, by their nature, are dynamic machines. They necessitate the continuous movement of one component of the turbine (the rotor) relative to the rest of the structure. Also, the required flexibility of the blade and tower components which make up the turbine, coupled with the notoriously variable loading conditions of the wind, make it understandable that the induced system dynamics form a particularly complex problem which continues to be investigated even today. It is obvious that, in designing a wind turbine, consideration must be given to these dynamic forces and interactions so as to appropriately design the structure to withstand these conditions and operate effectively for the duration of its design life.

The behaviour of wind turbine structures as they respond to the aerodynamic loads is termed aeroelasticity. This implies that as the aerodynamic loads are applied to the structure there is an induced deflection which in turn induces a change in the aerodynamic loads, thus prompting an iterative loop of varying loads and deflections. As wind turbines

generally have low structural damping they can suffer from aeroelastic instabilities under certain conditions. The phenomena of aeroelastic stall and flutter in wind turbines are well documented (Friedmann, 1980; Janetzke and Kaza, 1983; Hansen, 2003, 2007; Baxevanou *et al.*, 2008). Both Hansen *et al.* (2006) and (Zhang and Huang, 2011) present extensive reviews of the state of the art in wind turbine aerodynamics and aeroelasticity. Detailed within the reviews are current aerodynamic and structural modelling techniques and a description of how the coupling between the two components can lead to aeroelastic instabilities.

Significant work has been performed to date on the dynamic modelling of wind turbine systems. Garrad (1983) summarises some of the modelling techniques applied to wind turbines in the early 1980s. While commercial finite element packages were not suitable, some designers opted to derive finite-element approaches from first principles, develop lumped parameter models, but most opted for a modal description of the structural dynamics. It is demonstrated that the concept of aeroelasticity was well understood but the author highlights the considerable effort required in deriving such a model with the formidable nature of the algebraic manipulation.

In analysing the dynamic behaviour of wind turbines the modelling framework must incorporate two components. An aerodynamic representation, and a structural model. Coupling of these two systems forms the basis of an aeroelastic model. In terms of the aerodynamic representation, the most commonly used methodology is Blade Element Momentum Theory (BEM), a combination of one dimensional momentum theory and blade element considerations (Hansen *et al.*, 2006; Hansen, 2008). Borrowed from the world of propeller design, it is a computationally efficient and fast solution which has proven to be remarkably reliable (Quarton, 1998). Certain modifications to the theory such as Prandtl's tip loss factor and the development of dynamic wake/inflow models (Snel and Schepers, 1995; Schepers and Snel, 1995), yaw/tilt models (Schepers and Snel, 1995; Bramwell *et al.*, 2001), and dynamic stall models (Theodorsen, 1935; Øye, 1991; Leishman and Beddoes, 1989; Hansen *et al.*, 2004), have led to the improvement and widespread use of this method.

The most accurate and reliable means of calculating aerodynamic effects on rotating wind turbine blades is through the use of Computational Fluid Dynamics (CFD) (Mann, 1998). This is a computationally intensive procedure which involves solving, or time averaging the Navier-Stokes (NS) equation to generate Reynolds Averaged Navier-Stokes (RANS) equations. While until recently CFD modelling was limited to simulating specific conditions for discrete events, the advances in computing power have allowed CFD modelling to be considered as an option for performing full aeroelastic computations of wind turbine rotors.

In terms of the structural modelling procedure, Lee *et al.* (2002) suggests that the methods employed currently may be classified into three approaches, the Finite Element Method (FEM), the modal approach and the multi-body-systems (MBS) approach. FEM is a popular approach across most engineering disciplines. Through the use of non-linear beam theory, the FEM approach allows for a complex deformation state of the wind turbine to be modelled. By employing a direct, time marching approach, a numerical solution of the differential equations of motion which represent the bending of the rotor blades as beam structures is produced. By the nature of the rigorous time marching approach, FEM is the most computationally expensive structural analysis method. The modal approach is generally considered the fastest and most efficient modelling solution. Although rigorous algebraic manipulation is required in the derivation of the equations of motion, it allows for a reliable representation of the dynamics of a wind turbine with relatively few degrees of freedom (Quarton, 1998). By implementing a modal representation of the flexible elements of the wind turbine, an energy formulation such as the Lagrangian approach is commonly employed to mechanically derive the equations of motion, once expressions for the kinetic and potential energy have been formed (Garrad, 1983). A limitation to this approach is found in the existence of periodic coefficients in the mass, stiffness and damping matrices because of the time dependent interaction of the dynamics of the rotor and tower. However, multi-blade coordinate transformations allow for the elimination of these coefficients under the assumption of isotropic blades (Hansen, 2003). The MBS approach consists of multiple rigid bodies connec-

ted by hinges. Adaptions of this system involve a coupling of the rigid bodies with a modal solution for the flexible bodies. The study by Lee *et al.* (2002) proposes a multi-body approach based on a previous paper by Hodges and Patil (2000), which details a multi-flexible-body formulation. This encompasses rigid-body subsystems (nacelle, hub) modelled as interconnected sets of rigid bodies using Kane's method and flexible-body subsystems (blades, tower) modelled using geometrically exact, non-linear beam finite elements.

An alternative methodology was proposed by Murtagh *et al.* (2004a, 2005b) which divided the major turbine components (blades, tower) into individual subsystems. The blade subsystems are solved individually using the mode acceleration approach (Nigam and Jennings, 1968) and coupling to the tower is accomplished by incorporating the output base shear of the blades into the solution of the tower subsystem. The total system response is subsequently calculated using a frequency based formulation which facilitates removal of the periodic dependencies. Although this method allows for efficient computation, because the blade and tower systems are solved in separate instances, this does not provide a true representation of the blade tower coupling effects.

The current commercial wind turbine design codes adopt variations of the methods discussed. Buhl Jr. and Manjock (2006) provides a comparison of aeroelastic codes used for the certification of wind turbines:

- AeroDyn (Laino, 2012) is a library of aerodynamic subroutines that can be linked with structural codes. To perform the calculations, AeroDyn has two options. A BEM model with the optional inclusion of tip and hub losses based on Prandtl's tip loss factor or a Generalised Dynamic Wake Model (GDW), which uses a method developed by Peters and He (1991). AeroDyn also has the option to include dynamic stall using the model proposed by Leishman and Beddoes (1989).

- ADAMS (ADAMS, 2012) is a multi-body dynamics simulator. It uses lumped masses connected by flexible fields similar to multidimensional spring dampers to model flexible structures. It is not a wind turbine specific code and, therefore, does not

have any aerodynamic modelling capabilities but it is now possible to couple ADAMS models with the AeroDyn subroutines discussed previously.

- DHAT (Buhl Jr. and Manjock, 2006) is a wind turbine specific code designed by Germanischer Lloyd and used for in-house calculations only (Passon and Kühn, 2005). It employs BEM for the aerodynamic modelling with the option of including models for dynamic and turbulent wake conditions, as well as dynamic stall. The flexible tower and blades are independently represented by a modal approximation while other components are modelled as rigid bodies connected by spring-damper systems.

- FAST (Jonkman, 2012) is a combined multi-body and modal-dynamics wind turbine design code. Flexibility in the blades and tower are characterized using a linear modal representation that assumes small deflections, while the rigid bodies include the base plate, nacelle, gears and hub. Similar to ADAMS, FAST employs the AeroDyn subroutines in the calculation of the rotor aerodynamics.

Besides those included in the study, a number of other prominent wind turbine design codes exist:

- BLADED (BLADED, 2012) is a comprehensive and widely used tool for the design of both onshore and offshore wind turbines. This is another example of the combined multi-body and modal-dynamics solution. Employing BEM with dynamic inflow and stall hysteresis models for the aerodynamic calculations, it employs a modal representation of the tower and blades as well as a multi-body framework for the rigid components.

- HAWC2 (HAWC2, 2012) is another popular design code which combines a Timoshenko beam finite element approach with a multi-body formulation to perform non-linear time domain dynamic simulations. It is particularly useful for its ability to accurately represent complex offshore support structures such as tripods and jackets. BEM forms the basis of the aerodynamic module with extensions to consider dy-

namic inflow, skew inflow, shear effect on induction, large blade deflections, tip loss and dynamic stall.

While the approaches discussed above relate to commercial wind turbine modelling solutions, many authors have chosen to employ elements of these models, often greatly simplified, in order to address a specific aspect of wind turbine dynamic response (Staino *et al.*, 2012; Pedersen *et al.*, 2012; Arrigan *et al.*, 2011; Colwell and Basu, 2009; Dueñas Osorio and Basu, 2008; Wang *et al.*, 2010; Murtagh *et al.*, 2005b; Hansen, 2003). This allows execution times to be considerably reduced and provides greater focus on the particular elements under consideration. In the current study, this is the method which is implemented. Both one and two dimensional models are derived using a combination of the modal representation and multi-rigid body approaches. These approaches offer the optimum balance of accuracy and computational efficiency. It is also possible to focus the model on a particular aspect of the system dynamics such as blade response, tower response or nacelle response. Many of the works listed in the preceding paragraphs provide the necessary methodologies to model the turbine in this way. Further details on the derivation of these models is provided in the next chapter.

Wind Field Modelling

An important component of dynamic modelling is accurate representation of the turbulent wind field. This is a topic which has been addressed in publications long before wind turbines became prominent with applications for bridges and building structures (Yang *et al.*, 1997; Suh *et al.*, 1997; Higson *et al.*, 1994). The emergence of wind turbines and the direct influence of accurate wind modelling on structural, aerodynamic and power production calculations has inspired considerable research on the topic.

In reality, the most accurate means of representing the aerodynamic influence of a turbulent wind field is to directly solve the NS equations, but as stated by Mann (1998), "the computational costs of this would be enormous". In recent times, however, with improvements in computing power a number of commercial finite element packages now perform this procedure through CFD. Despite this, it remains a relatively time consum-

ing process for the moment and is only valuable for optimising designs which are already reasonably accurate. It is noted by Hansen *et al.* (2006), however, that in the future, wind fields are expected to be generated numerically from Large Eddy Simulations (LES) or Direct Numerical Simulations (DNS) of the NS equations for the flow on a landscape similar to the actual siting of a specific wind turbine. This would offer the most accurate solution in terms of predicting structural loads as well as power production characteristics.

Without the availability of these computationally intensive techniques for the extensive design phase of a wind turbine, more efficient techniques have been derived which are based on turbulence spectra, often implemented in conjunction with a coherence model. Kaimal *et al.* (1972), specifically, made significant inroads into the concept of wind turbulence spectra and cospectra of the surface layer. The findings are still very much relevant today with the inclusion of the Kaimal Spectrum and Exponential Coherence Model in the European standard of wind turbine design, BS EN 61400-1 (2005). Connell (1982) and Madsen and Frandsen (1984) then addressed the issue of rotationally sampled turbulence, where the influence of the blade rotation in the turbulent wind field is considered. This has since been improved upon by Veers (1988) which considered the full spatial description of the random inflow turbulence field, instead of single-point-in-space statistics of the inflow (i.e. at hub height). The study also included across-wind and vertical turbulence characteristics. The most comprehensive model currently employed was derived by Mann (1998), in which the spectral tensor for atmospheric surface layer turbulence was developed through a linearisation of the NS equations. This is the primary turbulence model specified in BS EN 61400-1 (2005).

For its simplicity and computation speed, the Kaimal spectrum method is utilised in this instance for the provision of turbulent wind velocity time-histories in the generation of structural loads. Whilst other, more sophisticated methods could be implemented, in the context of a comparative study it provides a sufficient level of accuracy and the required computational efficiency.

2.4 Wind Turbine Blades

Being a primary component of wind energy converters, wind turbine blades have received considerable attention from designers and researches in the field of structural dynamics (Hansen, 2003; Chaviaropoulos *et al.*, 2003; Toft and Sørensen, 2011; Kong *et al.*, 2005; Maalawi and Negm, 2002). By their nature, as substantial elements rotating relative to a considerable support structure and intricate electricity generation equipment, wind turbine blades are subject to complex dynamic forces and interactions as part of the entire wind turbine system. This is further compounded by the unsteady aerodynamic forces imparted on the blades from a turbulent wind field. With the growth in scale of wind turbine units into the multi-megawatt domain, wind turbine blades have seen substantial progression to lengths exceeding 60 metres (ENERCON, 2007). As a result, the induced dynamic forces have increased in both magnitude and complexity. A principal goal of the wind turbine designer is to minimize the vibration of the wind turbine elements. This is particularly important for the blades where reduced vibration gives rise to lower stresses and hence improved fatigue resistance of the entire turbine system.

2.4.1 Blade Dynamics

There are a number of articles which deal specifically with the blade dynamics. Veers *et al.* (2003) presented an overview of the trends in the design, manufacture and evolution of wind turbine blades. This highlights in particular the changes in methods which have made the development of multi-megawatt turbines possible. Younsi *et al.* (2001) combined a CAD derived aerodynamic model and the theory of three-dimensional beams to evaluate the dynamic behaviour of a variable section blade. Another study by Baumgart (2002) developed a mathematical model for an elastic wind turbine blade and verified the results against an experimental modal analysis of a 19 m long blade. Encompassing edgewise, flapwise and torsional degrees of freedom, the elastic rod model solved as an eigenvalue problem matched the general modal characteristics of the blade

quite well. Chaviaropoulos *et al.* (2003) compared an aeroelastic NS analysis of individual blade sections subjected to combined pitch/flap or flap/lead-lag motion to alternative simplified aeroelastic methods. This CFD analysis was achieved through the coupling of existing NS codes with a routine that solves the dynamic elastic problem. The results showed good agreement although the linear model results obtained through eigenvalue analysis appeared to under-predict aerodynamic damping compared to the NS results.

2.4.2 Blade Design

Further examples which relate to the design of wind turbine blades include, Toft and Sørensen (2011) which provided a probabilistic framework for the design of wind turbine blades, and Kong *et al.* (2005) which focused on the structural design of composite blades. Maalawi and Negm (2002) considered the reduction of vibration in a blade design. This was achieved through the appropriate placing of system frequencies in the design. While in practice it may prove difficult to accurately tune the natural frequencies of specific wind turbine components, this highlights the possibility of vibration reduction and the positive implications for the whole system. A more recent effort at reducing blade vibrations was conducted by Staino *et al.* (2012). In this instance active controllers were considered as part of a blade design for the reduction of harmful edgewise vibrations with low aerodynamic damping. The control was based on a pair of actuators/active tendons mounted inside each blade, allowing a variable control force to be applied in the edgewise direction. A mathematical model of a wind turbine with the addition of the active tendons was proposed. Numerical simulations carried out on a standard 5 MW wind turbine showed that the use of the proposed control scheme significantly improved the blade response with a 65 % reduction in maximum blade displacement.

2.4.3 Blade-Tower Interaction

An issue which has been proven to have a significant influence on the fatigue damage of wind turbine blades is the effect of tower shadow. This is a periodic process which sees a reduction in the aerodynamic loading on the blade as it passes in front of (or behind for downwind rotors) the tower during each revolution of the rotor. Hansen *et al.* (2006) states that the effect of the tower on the rotor of an upwind turbine is comparable to other unsteady effects, such as incoming turbulence or time variations of the rotor. Pedersen *et al.* (2012) presented a study on the effect of the stress reversals during blade passages through the stagnating and deflected mean wind field in front of the tower. The significant contribution of tower shadow to fatigue accumulation in wind turbine blades was outlined. It was demonstrated that the expected damage accumulation per unit of time in the turbine blades are reduced significantly for a tripod type lattice tower design when compared to the damage in a comparable tubular mono-tower design. Kim *et al.* (2011) studied the influence of blade-tower interaction by carrying out numerical simulations for uniform, yawed, wind shear flow conditions, and various tower cases using the non-linear vortex correction method. It was shown that the root region of the rotor was more affected by blade-tower interaction and showed a greater change in aerodynamic loading compared to the tip region. It was also highlighted that the blade-tower interaction did not significantly affect the total fatigue load of the rotor blade at relatively high winds and more unstable atmospheric conditions, although the relatively weak atmospheric turbulence conditions in offshore environments may increase its influence. The helicoidal vortex model was applied to the simulation of tower shadow for downwind turbines by Chattot (2008), and compared with the National Renewable Energy Laboratory (NREL) S-Sequence experimental data (Hand *et al.*, 2001). The results were shown to have good agreement when corrections were made for the coned rotor shape in the S Sequence experiment.

The literature discussed has highlighted the adverse effects of blade vibrations. Although the presence of the tower and the effects of blade-tower interaction are unavoidable for this type of device, other approaches may be taken in order to limit blade vibrations.

This has prompted consideration of the influence of tower construction material on the magnitude of blade vibrations as part of the current study. This is investigated in Chapter 4.

2.5 Wind Turbine Towers

For both onshore and offshore wind turbines the tower is an essential component of the structure. Hau (2006) estimates that for an onshore installation the tower accounts for 16 % of the overall component costs for a medium sized 750 kW wind turbine and 21 % for a large 1,500 kW turbine. Another report by Engström *et al.* (2010) estimates that for a 3 MW turbine on a 100 m tall tubular steel tower the cost of the tower amounts to 17 % of the total installed cost, a substantial proportion of the wind turbine cost. With the trends discussed in Section 2.1 for the growth in wind turbine magnitudes towards the 5-10 MW range and the associated increase in size and hub heights, it is clear that the tower solution has to evolve to meet these requirements.

2.5.1 Tower Solutions

Truss Towers

Over the years, numerous different tower solutions have been devised. According to Hau (2006), a three dimensional truss tower, often called a lattice tower is the simplest method of achieving a stiff construction for a high tower. Lattice towers, as seen in Figure 2.4, were a preferred design for the first experimental turbines such as the NASA MOD-1 turbine (Puthoff *et al.*, 1980). Today, the lattice tower has again become an alternative to the steel tubular tower in the case of the very high towers required for large turbines sited at inland locations (Dehm, 2007). The advantages of a lattice tower construction is that a very stiff structure can be assembled quite efficiently and cheaply from standard steel stock sections. It has been suggested that a 40 % saving on mass my be achieved over a tubular steel design with a consequential cost saving, although Frederick and Savino (1986) suggests that only at small heights does the truss tower appear to have a weight

advantage with respect to other steel towers. While issues such as the complex assembly process, reliability concerns with the considerable number of steel connections, and the susceptibility of the weaker diagonal members to wind excitation have been cited for the lack of use of these types of towers (Harte and Van Zijl, 2007), Hau (2006) states that the main argument against lattice towers is in relation to their "ugliness".

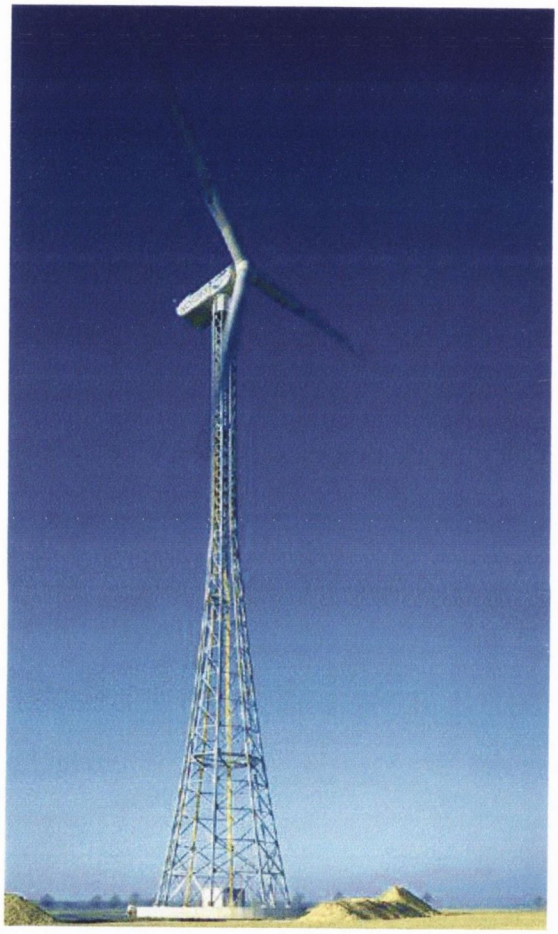

Figure 2.4: Wind turbine with lattice tower (OTDS, 2012).

Steel Tubular Towers

Steel tubular towers have undoubtedly been the most widely used tower solution for modern wind turbines. The preference for this type of tower is partly attributed to the relatively low steel prices which existed in the lead-up to the middle of the last decade (Hau,

2006), although other benefits exist. With the tower divided into cylindrical or conical tubular lengths of up to 30 m, this allows for rapid on-site assembly by simply bolting the sections together. The tower sections are rolled from sheets of high grade steel with a thickness of between 10 mm and 50 mm, depending on the tower requirements, and joined together using high-quality welding techniques. The tubular lengths may be subsequently transported to site with specialised transportation systems. While tubular steel towers offer a straightforward and elegant solution, there are some drawbacks to this system. Hau (2006) highlights the serious manufacturing difficulties with steel tower sections for tower heights beyond 90 m. It is noted that manufacturing steel tubular towers with a diameter of up to about 4 m is a conventional technology that does not make any great demands on the equipment of the manufacturers. At heights of more than 90 m, the tower base diameter becomes greater than 4.5 m and the required thickness of the steel exceeds 40 mm, requiring the development of specialised equipment. An additional constraint is that the transportation of the lower tower sections by road is no longer feasible in many cases. In Ireland, for example, road traffic regulations specify that the maximum overall height of a vehicle may not exceed 4.65 m (Dempsey, 2008) which is unavoidable for tower heights in excess of 90 m. Similar restrictions exist for most other countries. According to Burton *et al.* (2011), however, some companies have developed a solution to this particular problem through the use of bolted friction joints which allow the tubular steel sections to be split up into more manageable components and subsequently reassembled on site. Engström *et al.* (2010) also notes that bolted friction joint technology was previously in use in the 1980s for very small turbines and that it is only recently beginning to reappear in the industry. Variations of the tubular steel design incorporate a slender tower supported by steel guy cables or, in some instances, steel trusses. These are generally only applied to small wind turbines of the proportions for private domestic use.

Concrete Towers

Another tower design which has been implemented over the years incorporates a concrete construction. While this type of tower was prominent in the test turbines of the 1980s

(Frederick and Savino, 1986), like truss towers they have also been generally overlooked in favour of tubular steel towers until recently. Concrete towers can either be designed as simply reinforced, prestressed or a combination of both. With concrete towers becoming prominent in the construction of very large turbines, prestressing has been the preferred option due to the significant height and high dynamic loads associated with these large structures. The construction methods can also vary, with two primary construction solutions.

The emergence of slip-forming and other related technologies for cast-in-situ reinforced and prestressed concrete structures (Zayed *et al.*, 2008) such as bridge piers and building cores has provided a viable solution for cast-in-situ concrete wind turbine towers. Issues with this method include the dependency on appropriate weather conditions for pouring concrete, the slow curing of the concrete and the required infrastructure for the mixing, delivery and pouring of the concrete which may prove uneconomical for small wind farms (Hau, 2006).

Another option is precast or prefabricated concrete components which may be assembled on site. Figure 2.5 provides a possible configuration for a prestressed, precast concrete tower. Relatively small cylindrical or conical concrete sections are constructed in a factory and delivered to site. The larger sections towards the base of the tower may be sub-divided for transportation. The sections are subsequently assembled on-site and the tensioning cables are introduced to form the stable tower structure. This method has the benefit of allowing the concrete sections to be poured and cured in a controlled factory environment. Difficulties with transportation are overcome by the possibility of breaking the structure into manageable pieces and the assembly process, while more complex than a tubular steel tower, is relatively efficient compared to other options such as lattice towers. A variation of this solution is a hybrid tower which employs both a prestressed concrete solution in combination with a tubular steel solution. This is particularly useful for exceptionally tall towers where the lower portion of the tower can be constructed from prestressed concrete with a standard tubular steel section forming the upper tower section. Examples of this include the E-126 turbine by Enercon (ENERCON, 2007), and

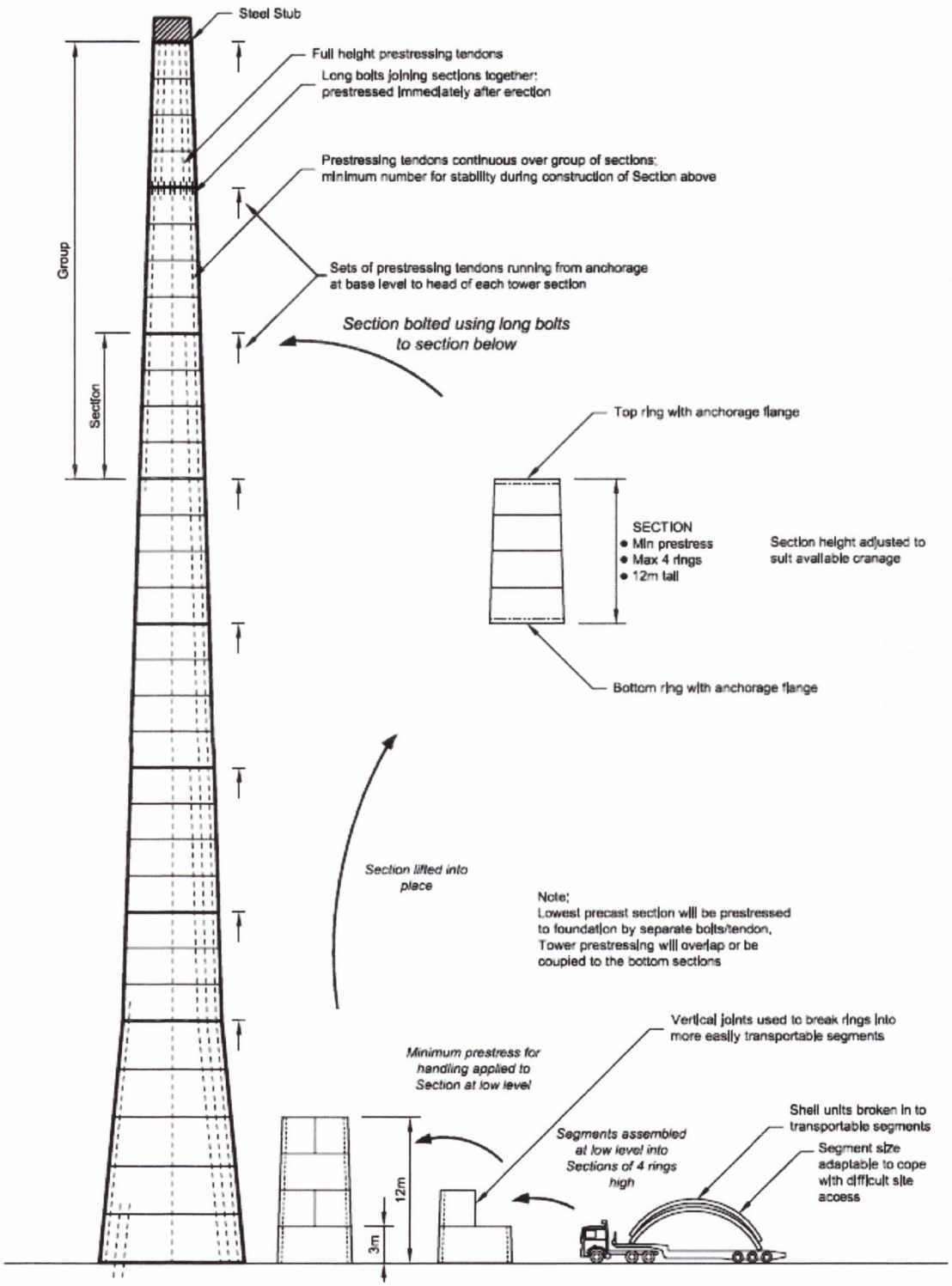

Figure 2.5: Precast concrete wind turbine tower - example construction sequence (Trickle-bank *et al.*, 2007).

a wind farm in Castledockrell, Co. Wexford (Ireland), which consists of eighteen 2.3 MW E-70 Enercon turbines supported on 60 m precast prestressed concrete towers extended to 84 m with the addition of a steel tubular section (ENERCON, 2010b). Seidel (2003) also presents a comparison of the various merits of both a hybrid and tubular steel tower design.

A primary component of these large prestressed concrete towers is the addition of prestressing tendons or cables. These serve to induce a compressive force in the concrete, thus reducing or even eliminating the existence of tension in the material, an effect which causes cracking of the concrete. The existence of cracks can lead to corrosion of the reinforcement and prestressing tendons as well as non-linear dynamic behaviour as the cracks open and close under dynamic loading. The prestressing tendons can be applied both internally and externally to the concrete section. It is suggested by Tricklebank *et al.* (2007) that fixing the tendons externally to the concrete, inside the tower is a straightforward process. This is particularly useful in that the tendons may be easily accessed for inspection and repair in future. It also facilitates a more straightforward decommissioning of the structure at the end of its service life where the different material components can be separated and prepared for recycling. Seidel (2003) provides a discussion of the three options for prestressed concrete towers. Post-tensioning with grout filled sheaths involves the placement of the steel tensioning cables within protective sheaths which are themselves placed inside the cast concrete section. This procedure helps prevent corrosion and through the bond formed with the surrounding concrete, allows a combined load carrying behaviour of concrete and tendons. While in a perfect case this is a very efficient solution, in reality a perfect bond is not always fully guaranteed and high stresses can be experienced at the anchorage points of the cables. Post-tensioning where the sheaths are left unfilled overcomes the stress issues at the anchorage points but increases uncertainty for corrosion protection. Externally post-tensioned towers such as previously discussed facilitate a corrosion safe environment, allows for visual inspection and even replacement of tendons as well as providing a greater tolerance for dynamic loading which is particularly beneficial for these types of structures.

There are additional economic and environmental advantages with such a solution. In the case of Ireland, in particular, where there is no significant steel industry, the construction of concrete towers would eliminate the requirement for importing steel towers from countries such as Britain, Portugal, Brazil and China. This would both reduce the environmental impact of the product as well as benefiting the local construction industry and economy. Furthermore, an increase in the durability of concrete structures is achievable through the use of cement replacement materials which are themselves recycled, thus improving the design life as well as reducing the environmental impact of the structure. The advantages of this type of structural solution, particularly for the large hub heights in question, have prompted the current study to investigate the structural performance relative to a traditional tubular steel design. Further studies to quantify the monetary and environmental comparisons of these solutions have also been recently conducted. Engström *et al.* (2010) compared a number of different tower types for both a 3 and 5 MW wind turbine at heights of 80 - 175 m. From an economic perspective a comparison was made through the specific investment cost, the investment for the tower divided by the annual energy production (Cost / MW hr / y). Unfortunately, this method does not account for the varying design service life which would be expected for the different towers. It does, however, provide a useful initial comparison. For the 3 MW turbine, wood and steel lattice towers offer the cheapest solution. A hybrid design offers the next cheapest solution followed by friction jointed steel and slip-formed concrete. The welded steel design offers a similar cost as the friction jointed design up to the 125 m height, after which it becomes the most expensive option. A height limit for the timber tower is put at 125 m while the welded and lattice steel towers are not extended beyond 150 m. For the 5 MW turbine, the welded steel design does not extend beyond 100 m. Up to 150 m the friction jointed steel tower offers the cheapest option, followed by the hybrid solution and then the slip-formed concrete tower. At the 175 m height, the hybrid design becomes the cheapest, then the slip-formed concrete while the steel tower is the most expensive. Again, it should be emphasised that these values do not take into account the varying service lives which would be expected of the different solutions. As the concrete designs would be expected

to last from 40 to 60 years as compared to 20 to 30 years for the steel towers, this would reduce the whole life cost of the concrete designs. Cleary *et al.* (2012) showed that over a 40 year service life, concrete towers equated to 4 % lower life cycle emissions compared to an equivalent tubular steel tower for an onshore application and 9 % less in the offshore case.

The feasibility of an alternative tower design composed of glass fibre reinforced polymer (GFRP) was also considered in an analysis by Polyzois *et al.* (2009). An experimental investigation involved the testing of two jointed scaled towers. With a total height of 4.88 m, the specimens were tested as cantilevers under static and dynamic loading. A finite element (FE) analysis was subsequently carried out to analyse the structural response of towers of this type. Both the experimental and analytical results were shown to have close agreement. The merits of this solution have not yet been proven, although it may offer a possible alternative in the future.

2.5.2 Analysis and Design

One of the primary considerations in the design of wind turbine towers is the consideration of the natural frequency of the tower relative to the other system frequencies, notably the first multiple of the rotational frequency of the blades, 1Ω, and the higher multiples, 2Ω and 3Ω. van der Tempel and Molenaar (2002) described the influence on dynamic response of the turbine for frequencies of excitation within a narrow region around the system's natural frequencies, such as the tower frequencies. In this region, the elastic spring force and inertia force almost cancel, producing a response that is a number of times larger than it would be statically. This is a phenomenon known as resonance and can prove extremely detrimental to the structural stability and fatigue life of a turbine if the natural frequencies coincide with the frequencies of excitation. Harte and Van Zijl (2007) stated that, for small turbines it is easy to design the towers stiff enough in order to shift the eigenfrequencies beyond the excitation levels; a so-called "stiff-stiff" construction. Today, the tower heights required for multi-megawatt turbines merely allow a balance of the eigenfrequencies between the frequency ranges of excitation, a "soft-stiff" construction.

Hau (2006) also comments on this design issue, noting that in a tower of stiff design, the natural tower frequency is not encountered during the start-up or shut-down procedures, thus eliminating the resonance hazard. Conversely, the risk of resonance does exist in the "soft" tower in which the first tower natural frequency lies below the 1Ω rotational frequency of the blades. The term "soft-stiff" relates to balancing the natural frequencies between the multiples of the blade rotational frequency, 1Ω and 3Ω. Despite the risks, the economic saving achievable from the more flexible, soft designs has made this type of tower a requirement from an economic perspective.

Despite the fact that the tower is considered a relatively non-complex component of the structure, with the increasing size of wind turbines, greater interest has been shown to its design and optimisation. Negm and Maalawi (2000) considered the design and optimisation of a typical tubular steel wind turbine tower structure. The developed optimisation models were successfully applied to an existing 100 kW wind turbine achieving a reduction of vibration level by direct maximization of the system natural frequencies. Bazeos *et al.* (2002) presented the results of a structural analysis of a 38 m high tubular steel wind turbine tower. With the aid of a refined FE model and other simplified models recommended by appropriate design standards, the structure was analysed for static and seismic loads representing the effects of gravity, the operational and survival aerodynamic conditions, and possible site dependent seismic excitation. It was shown that simplified analytical models can predict relatively accurate results for the local buckling and seismic response of the structure, if they are applied appropriately. Another similar investigation was conducted by Lavassas *et al.* (2003), in which two FE models were employed in the analysis of a 44 m tubular steel tower for a 1 MW wind turbine. It was shown that in the analysed case the extreme wind was the dominant load combination for the design of the structure, whereas the seismic design could become critical only for the case of constructing the towers in a seismically hazardous area, on a medium or soft soil. It was also highlighted that although the simplified linear static model was sufficient for the calculation of the basic response and the eigenvalues of the structure, the more complex model was necessary to take account of local stresses for the ULS calculations. Although these

static models offer a quantification of the performance of a structure, they do not take account of the detailed dynamic interactions between the turbine components. In order for the proposed study to be implemented with consideration for the complete turbine dynamics, a more sophisticated modelling procedure must be developed.

Focusing on wind turbine response analysis, a study by Murtagh *et al.* (2004b) utilised a lumped mass model to establish the modal characteristics of a lattice tower with a mass at the top, representative of a utilities tower or wind turbine tower. It was concluded, following comparison of the results against a detailed FE analysis, that the proposed approximate methods yielded accurate estimates of the first three natural frequencies and mode shapes of any arbitrary lattice tower with mass at the top. A further investigation by Murtagh *et al.* (2005b) considered the along-wind forced vibration response of a wind turbine tower. The effects of blade-tower coupling were included in the analysis by solving the response of individual rotating multi degree of freedom (MDOF) blade representations subject to rotationally sampled wind loading. The computed base shear time-histories of the blades were subsequently applied to the tower top, allowing the entire system to be solved in the frequency domain by employing the mode acceleration approach. Comparison against an analysis neglecting the blade/tower interaction illustrated the considerable influence of the blades on the tower response, particularly if the fundamental frequencies of the tower and turbine blades are close together. Chen *et al.* (2009) employed the same formulation in a study of the response analysis of an idealised wind turbine with 30 m blades and an 80 m tower. The analysis showed a 300 % increase in the maximum tower displacement response once blade-tower coupling was taken into account. A dynamic response analyses of a pitch-regulated 2 MW wind turbine was carried out by Ishii and Ishihara (2010), for the estimation of maximum wind loads acting on support structures. Analysing the structure using the wind turbine design code BLADED (2012), the average and maximum tower base moment was calculated for 11 different mean wind speeds, varying from 5 m/s to 25 m/s at 2 m/s intervals, and 3 different turbulence intensities. Simplified formulas were subsequently proposed for estimating the expected maximum base moment and the results showed good agreement with those obtained from field measurement data.

These more comprehensive examples of dynamic modelling techniques offer a greater relevance in the case of the current investigation. Adoption of similar methods can provide an appropriate platform for the development of a dynamic model.

2.5.3 Vibration and Fatigue

As discussed in Section 2.3.3, due to the dynamic nature of wind turbines, fatigue loading is at the forefront of the design considerations. Mikitarenko and Perelmuter (1998) examined the definition of service life for high-rise steel tower installations depending on the fatigue damage accumulated in members or sections. Employing the linear summation theory of fatigue damage, a formulation for the estimation of structural durability of tower structures was developed. Application of this formulation to a series of broadcasting towers consisting of tubular steel, lattice and hybrid reinforced concrete/steel towers resulted in critical resonance wind velocities being calculated in the range of 7-20 m/s. It should be noted that this is within the normal operating range of most modern wind turbines. The calculations also highlighted that the durability in some initial designs was insufficient (only 5 years in one instance) necessitating the addition of dampers and an increase in metal thickness. Petrov (1998) presented a similar investigation of the dynamic response and life prediction of steel structures under wind loading. Utilising a damage accumulation model, a methodology for the estimation of the expected fatigue lifetime was proposed. This procedure was applied to a 64.8 m tall monument structure, consisting of 2 m diameter tubular steel elements. Consequently, the critical velocity for fatigue damage was estimated as 14 m/s, and the fatigue lifetime was calculated as 46.23 years. A more recent study carried out by Repetto and Solari (2010) considered the fatigue collapse of two slender structures due to wind-induced vibrations. While both structures satisfied the national and international structural codes from the ULS point of view, they both exhibited premature collapses due to wind-induced fatigue damage. For the case of a 10 m anemometric pole, the collapse was associated with a particularly windy condition for the site. It was highlighted that the safety factor adopted in the structural design accounted for this from the ULS point of view, but it was inadequate for the case of fatigue. The

analysis also highlighted the contribution of lateral turbulence to the collapse, a condition currently disregarded in structural standards. The second case study considered a 30 m antenna tower, the damage and collapse of which were mainly linked with the aerodynamic effects generated by resonant vortex shedding actions of a top cover cylinder.

As a consequence of the highlighted fatigue issues relating to wind induced vibrations of tall towers and other vibration sources in wind turbines there has been a response in the literature with proposals for vibration suppression solutions for wind turbine structures. Qu *et al.* (2001) investigated the effectiveness of friction dampers when applied to large truss towers. Combining both a dynamic lumped mass model and a 3D static FE model for a so-called "bi-model method", it was shown that by appropriately tuning the slip force ratio (SFR) of the friction dampers, a displacement, velocity and acceleration vibration reduction factor (VFR) of 67 %, 70 % and 54 % respectively, could be achieved for a 339 m telecommunications tower. The use of a tuned mass damper (TMD), was considered by Murtagh *et al.* (2008) for the mitigation of vibrations due to the along-wind forced vibration response of a simplified wind turbine model. Employing a numerical representation of the TMD device, reductions in vibration magnitudes of between 20 % and 22 % were achieved. The restrictions of a passive control device in a time-variant system were highlighted and it was recommended that in reality, an active control strategy would probably be more appropriate for use in actual wind turbines. A more specific case of a TLCD installed in offshore wind turbines was examined by Colwell and Basu (2009). Through numerical simulations it was shown that vibration reductions of up to 55 % of the peak response could be achieved for an offshore turbine subjected to correlated wind and wave loading. It was also observed through a rain-flow calculation of fatigue life, that a significant increase in fatigue life could be achieved through the addition of a TLCD. The suppression of the vibrations of a wind turbine tower using co-located feedback to achieve strong stability was addressed by Zhao and Weiss (2011). Employing a combination of force control (controlling the turbine blade pitch angle) and torque control (an electrically driven mass located in the nacelle), it was mathematically proven that strong stabilisation of the wind turbine tower model could be achieved.

An issue identified throughout the literature was the limited space available in the nacelle for incorporation of damping devices. This in fact calls into question the feasibility of using these devices in commercial wind turbines. The possibility of reducing vibrations through an efficient design, therefore proves to be a more attractive option. This thesis will investigate the comparable vibration magnitudes for both a steel and concrete design, thus highlighting the optimal solution in terms of vibration suppression.

2.5.4 In-Service Testing

While efficient methods of analysing and simulating the dynamic behaviour of wind turbines have been discussed in the preceding sections, in-service testing of the operating structure is still an essential component for the verification of structural stability. A remote-sensing technique based on microwave interferometry was applied to the dynamic testing of wind turbine towers by Pieraccini *et al.* (2008), as part of an experimental campaign on a wind farm in Sardinia, Italy. Although the rotating blades caused interference with the equipment, this procedure was shown to accurately identify locations along the tower susceptible to vibrations, such as at welded connections, as well as vibrations induced by aerodynamic interaction of the nacelle and blades with the wind. It also accurately identified the tower natural frequency. Wireless sensor technologies were applied by Swartz *et al.* (2010) as part of a dynamic analysis of two operational wind turbine structures in Germany. Implementing a system of wireless accelerometers facilitating the collection of vibration data throughout the height of the tower, it was shown to accurately identify system frequencies and responses after some post-processing.

Implementation of a physical assessment of wind turbine structures with varying tower structures could add an interesting perspective to the proposed study. Particularly taking into consideration the possibility of non-linear response and long term effects in the structure, it would contribute a functioning comparison of the structural performance. While this possibility was pursued as part of the current research, the opportunity for such an experiment was not available within the time constraints. This would, however, prove an interesting undertaking as part of future research initiatives.

2.5.5 Prestressed Concrete Towers

As discussed in Section 2.5.1 concrete tower solutions have recently regained popularity, particularly in the construction of tall towers for large scale multi-megawatt wind turbines. The flexibility of concrete solutions in terms of construction, assembly and transportation make them a viable alternative to the industry standard steel towers for these multi-megawatt installations. A report by Tricklebank *et al.* (2007) outlined many of the benefits of concrete towers for both onshore and offshore applications. These include the durable, low maintenance solution achievable with concrete, the flexibility of mix design and prestressing configurations which allow the structure to be finely tuned to a particular strength and stiffness, and the ability to tailor the design and construction method to avoid height and size limitations faced by other solutions. It was also noted that due to concrete's inherent damping properties, it can offer superior dynamic performance, a greater resistance to fatigue and a longer lifespan relative to other alternatives. The resulting impact on the environment was also addressed with estimates proposed by independent consulting engineers showing that for a typical 70 m onshore tower, reductions in embodied energy and CO_2 of 40 % and 60 % respectively could be achieved compared to a standard tubular steel design (Tricklebank *et al.*, 2007). These findings highlight the benefits to be gained from concrete in the future. In another study by Harte and Van Zijl (2007) it was suggested that for heights beyond 85 m, steel tubular towers are incapable of providing the stiffness required for the structural stability of towers of this height. In this study on the structural challenges faced by wind turbines and solar chimney towers, it was stated that for turbine capacities beyond 2 MW, reinforced and prestressed concrete towers are required. Despite this, issues such as material non-linearities, like cracking and crushing of concrete, were highlighted as possible influences that may impact on the dynamic behaviour and the long-term durability of reinforced or prestressed concrete towers and require further investigation. The role of concrete as a construction material, particularly for the construction of towers was considered in the context of a developing wind energy industry in India by Singh (2007). In order to meet ambitious targets for wind energy capacity, larger, more powerful turbines are required which will challenge the capabilities of standard

technology. The advantages of utilising prestressed concrete towers in combination with other concrete components were outlined.

In terms of the technical aspects of concrete wind turbine towers, some of the studies conducted on this topic are discussed. Silva *et al.* (2008) presented an optimisation of reinforced concrete wind turbine towers. An FE based dynamic model was developed. Taking geometrical properties and steel reinforcement area as the design variables, a cost function was established against the constraints of specified stresses, displacements and frequencies of vibration. Minimisation of the cost function was subsequently performed for a series of tower heights between 65 m and 100 m. An assessment of the dynamic performance of an 80 m prototype reinforced concrete wind turbine tower was performed by Rodríguez *et al.* (2010). Artificial cracking was induced in the tower through the application of a high load at the tower top by a steel cable. The findings of the investigation showed that cracking did have an effect on the dynamic characteristics of the tower, although for normal loading situations the induced cracks remained in compression and the natural frequency of the tower was unaltered. It was suggested that if very high loading was to occur, the extent of the cracking may prove to affect the tower dynamics at operational loading levels. Paredes *et al.* (2011) developed and applied a numerical procedure for the analysis of precast reinforced concrete wind turbine towers subjected to cyclic loads. Through the combination of serial/parallel mixing theory, a compression-tension damage model and an elasto-plastic constitutive law, a procedure was proposed for the analysis of non-linear dynamic effects in structures of this type.

An important aspect of the analysis of prestressed concrete towers is to take appropriate consideration of the influence of the prestressing forces applied. The effect of prestress force on the dynamic performance of prestressed concrete elements is a topic which has been widely debated. Over the years there have effectively been two main arguments. The first indicates that as the prestress force in a member is increased the natural frequency of the member decreases due to an action of "compression softening" (Chan and Yung, 2000; Dall'Asta and Leoni, 1999; Raju and Rao, 1986; Tse *et al.*, 1978). A number of authors dispute this theory, however, explaining that this effect only applies to members

with an externally applied force, which is not the case in the context of prestressing (Deák, 1996; Jain and Goel, 1996; Bažant and Cedolin, 1987). Zhang and Li (2007), Kim (2004), Jain and Goel (1996) and Saiidi *et al.* (1994) each endorse a contrary argument through the derivation of mathematical representations as well as physical dynamic testing. The argument notes that increasing the prestress force induces a closure of micro-cracks in the member, thus increasing the bending stiffness and therefore the natural frequency. Based on the argument by Saiidi *et al.* (1994), Dall'Asta and Dezi (1996) present an equation for the n^{th} natural frequency of a prestressed concrete beam element:

$$\omega_n^2 = \frac{n^4\pi^4}{mL^4}\left[\left(E_b - \frac{N}{A_b}\right)I_b + \left(E_c - \frac{N}{A_b}\right)I_c\right] \tag{2.4}$$

where m is the mass of the concrete beam, E_b and E_c represent the modulus of elasticity of the beam and prestress tendon respectively, N is the prestress force and A_b is the cross-sectional area of the beam. The same article, however, states that the magnitude of the N/A_b term is negligible compared to the E_b term for practical ranges of prestress and the I_c term is also negligible compared to the I_b term. Consequently, the authors conclude that the inclusion of prestressing has a negligible effect on the natural frequency of the beam element and Equation 2.4 can effectively be reduced to:

$$\omega_n^2 \approx \frac{n^4\pi^4}{mL^4}E_bI_b \tag{2.5}$$

Maintaining this argument, Hamed and Frostig (2006) also states that, "it has been mathematically rigorously proven that the magnitude of the prestressed force does not affect the natural frequencies of bonded or unbonded prestressed beams". Consequently, it is considered appropriate to discount the prestress force from the tower model and employ linear elastic beam theory in the analysis.

As discussed previously, the long term effects in concrete can also have an effect on the structural dynamics. While the non-linear dynamic action induced by concrete cracking can be particularly difficult to model, other effects such as creep and shrinkage have been well accounted for in previous literature (Zeng and Han, 2011; Shen *et al.*, 2009; Reid

and Qin, 1990; Mayfield, 1982). These processes have the ability to alter the structural performance of prestressed concrete wind turbine towers over time by the introduction of tensile stresses which may lead to a reduction in the rigidity of the structure. Taking the approach outlined by Mayfield (1982) and utilising the formula:

$$J(t,t') = \frac{1+\phi(t,t')}{E(t')} \tag{2.6}$$

where $J(t,t')$ is a creep function, $\phi(t,t')$ is a creep coefficient and $E(t')$ is the modulus of elasticity at age t', it is possible to get an estimate of the reduced modulus of elasticity of the concrete after loading for time t. These effects will be accounted for throughout the analyses carried out in this thesis.

2.6 Wind Turbine Foundations

DNV (2001) presents an extensive overview of the various types of wind turbine foundations along with guidelines as to the relevant considerations for their design. With the foundation providing the sole link between the wind turbine structure and the ground surface at the site, it plays a crucial role in the stability of the wind turbine structure. Transferring the entire range of loads outlined in Figure 2.6, it must be accurately designed to sufficiently stabilise the structure while not overcompensating and incurring unnecessary costs. The stiffness of the tower/soil interface is very much dependant on both the soil type and the foundation design. It is obvious, therefore, that this interface will directly affect the bending stiffness of the tower and all of the system natural frequencies as a result.

A study by Bhattacharya and Adhikari (2011) highlights the strong relationship between system natural frequencies and the stiffness of the foundation which reinforces the requirement to consider soil/structure interaction in the design of wind turbines. The inherent diversity of soil conditions across this planet coupled with the variation of wind turbine units currently in operation has necessitated numerous different concepts to provide a stable foundation for the wind turbine structure. These concepts are discussed in the following sections.

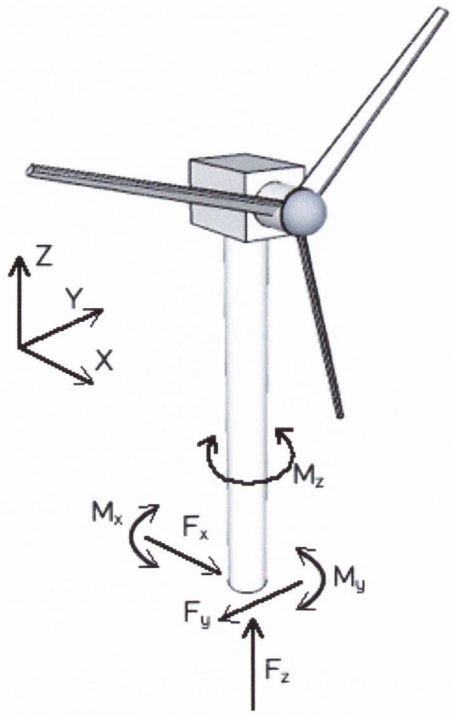

Figure 2.6: Outline of wind turbine foundation loads.

2.6.1 Onshore Foundations

There are two primary foundation types for onshore wind turbines as seen in Figure 2.7. These include a solid slab foundation, sometimes called a "raft", or "mat" foundation as well as a piled foundation. The choice of foundation is very much dependent on the soil type and the loads which need to be supported. A slab foundation is a reinforced concrete mat generally formed in a circular or polygonal shape and primarily dimensioned based on the overturning moment of the whole structure. It operates by spreading the loads transmitted through the tower out over a large area of soil so that the structure can remain stable. This type of solution is suitable for strong soil conditions which have an appropriate bearing capacity such as sands and gravels as well as some medium to hard clays. In most cases it is the least expensive solution and, therefore, the most desirable. A piled foundation design is composed of a base plate for the tower which is supported by a series of driven or drilled piles. The piles act by transferring the loads through the upper, non-bearing layers of soil down to more stable soil or even bedrock at a greater

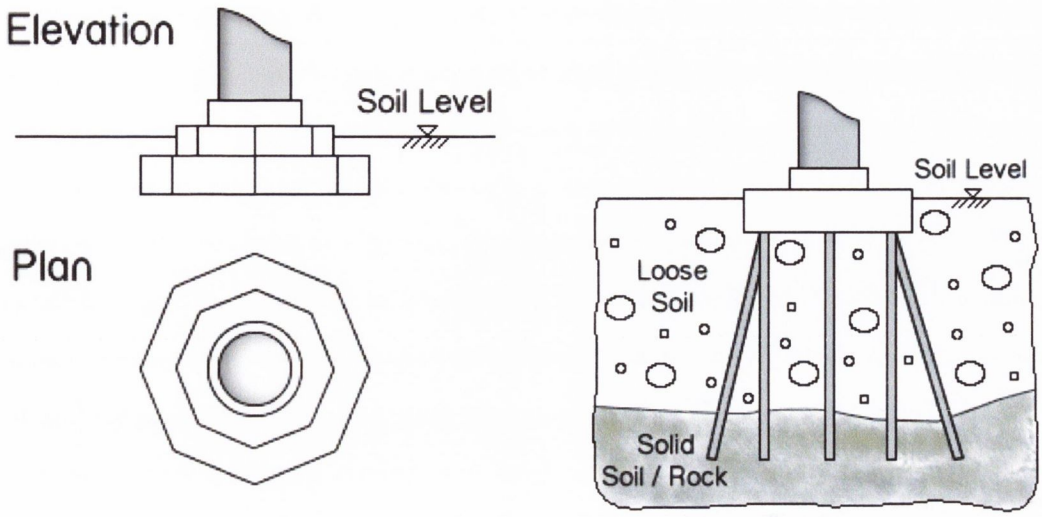

(a) Reinforced concrete slab foundation.

(b) Piled foundation.

Figure 2.7: Onshore wind turbine foundation configurations.

depth. This more expensive foundation design is often required when soft soils, which do not have sufficient bearing capacity, are present at the surface. An issue relevant to both designs is the connection between the tower and foundation through which all of the loads must be transferred. For steel towers this connection is established by including a steel circular plate, anchored to the foundation reinforcement and cast into the concrete slab or base plate. Hau (2006) states that integration of the foundation section, "requires some experience", with a maximum tolerance in the horizontal placement of the foundation section flange of ± 2 mm before tower tilt becomes an issue. With tower base diameters of up to 4 m now common, this becomes a difficult task. For concrete towers the base of the tower or a transition piece is generally cast into the foundation but the issue of tower tilt is ever prominent.

As offshore wind turbine foundations provide a greater challenge to the designer but also a greater reward in terms of cost savings for improved concepts, the vast majority of research on wind turbine foundations relates to offshore applications. A number of publications relevant to onshore foundations, however, have been assessed and are discussed in the following paragraphs. Harte *et al.* (2012) investigates the along-wind (i.e. motion in the plane of the primary wind direction) forced vibration response of an onshore wind tur-

bine including the dynamic interaction effects between the foundation and the underlying soil. The author proposes a MDOF dynamic representation of the along-wind motion of the wind turbine which incorporates the rotor blade system, the nacelle, the tower and a two degree of freedom (DOF) approximation of the foundation, the movement of which is related to the surrounding soil by means of complex impedance functions generated using the cone model (Wolf and Deeks, 2004). The derived model facilitates the estimation of the natural frequencies of a standard turbine as well as a series of frequency domain simulations subjecting the turbine to both steady-state and turbulent wind loading for a variety of soil conditions. It was found from the analysis that with decreasing shear wave velocity (i.e. softer soils) the total nacelle displacement was seen to increase and the fundamental modal frequency of the turbine system decreased. At the lower range of shear wave velocities (i.e. very soft soils) the fundamental frequency of the turbine was seen to occur within the range of the rotational speed of the rotor, an issue which could result in damaging resonance behaviour for the turbine system. It was also shown that the peak shear and moment values at the base of the tower varied minimally across the range of soils, although a marked difference in the frequency at which these peaks occurred was evident. For stiffer soils, the peak shear/moment values occurred more often, inferring a direct implication for fatigue in the tower.

He *et al.* (2009) used a finite element model of a wind turbine with additional spring and dashpot elements introduced at the base in order to represent the effects of the soil on the dynamic response when subjected to seismic excitation. The investigation considers a 1 MW wind turbine on a 44 m tall tower which tapers linearly from base to top. The proposed foundation is assumed to be a 10 metre square pad which is 1.8 m deep. The results produced from the analysis showed a 26 % increase in tower tip response when soil structure interaction was considered.

A design report for the NASA MOD-2 test turbine (NASA, 1979) gives a brief description of the foundation design employed in an early concept. In this case a buried, octagonal shaped, reinforced concrete footing was employed. While no details are given of the sizing of the footing, it is stated that the foundation cost depends primarily on the

volume of concrete which is a function of the overturning moment due to seismic loads. This moment is a function of the tower height, tower bending frequency and the mass on top of the tower. The additional mass of a concrete tower structure compared to a tubular steel design may have a significant effect on the characteristics of this overturning moment and will, therefore, be included in the study. Hau (2006) specifies the highest assumed wind speed acting on the turbine at stand-still as the defining factor for a foundation in most cases, although, it also states that maximum operating loads should be checked in addition. Another study of interest by Murtagh *et al.* (2005a) considers the along-wind forced vibration response of a wind turbine tower including dynamic interaction with the underlying soil. Within the study the foundation of the structure is modelled as a circular footing, whose movement is related to the surrounding elastic soil by means of a complex translational impedance function. The study concluded that soil-structure interaction has the effect of decreasing the natural frequency of the structure (lengthening the natural period) and also adds damping to the system. These findings match those of a more recent study by AlHamaydeh and Hussain (2011) which presents a synopsis of a series of wind turbine tower/foundation designs constructed in a number of remote Alaskan villages. What was discovered in this particular case was that the foundation design was driven by the natural frequency of the soil-foundation-structure system rather than by strength or serviceability considerations. Due to the difficulty and cost of casting concrete elements in this extreme environment, an all steel foundation solution was considered. It was discovered, however, that this significantly "softened" the system, or reduced the natural frequency, therefore risking unfavourable interaction with the blade rotational frequency and resulting in violent, near-resonant vibrations. In order to avoid immediate or fatigue driven damage an optimised reinforced concrete piled mat system was devised. The authors state that, "had a fixed-base-tower assumption been adopted, significantly under-designed systems would have been incorporated".

As has been previously stated, there is currently more to gain and fewer barriers in relation to the implementation of concrete towers in onshore environments as compared to offshore. It is, therefore, an objective of this study to consider the prestressed concrete

solution primarily for onshore installations. Despite this, there is considerable effort being expended on researching offshore installations, support structures in particular, and many lessons may be learned from the literature.

2.6.2 Offshore Foundations

The offshore environment provides a totally different set of conditions to deal with compared to onshore designs. The obvious interaction of the foundation with the sea and sea-bed makes it the most affected element of the offshore design. In addition to the turbine loads from above the foundation, offshore foundations also have to cater for difficult sea bed topographies, variable water depths, high-pressure underwater environments, wave loading, currents as well as collisions from floating objects such as boats and in some cases, floating ice. They are further required to provide a stable platform, safely beyond the wave crests, for the turbine above. A paper by Byrne *et al.* (2002) acknowledges how these issues accumulate to make foundations a more substantial component of the cost of offshore wind energy than the onshore alternative. It also notes how UK Department of Trade and Industry funding initiatives from 2002 placed a high priority on innovative foundation concepts and offshore installation techniques in order to reduce the cost of offshore wind energy. This resulted from the opinion that offshore wind was the best possibility for reducing carbon emissions on the scale required for a country the size of Britain. The offshore priority was also true for many other renewable energy funding initiatives such as the European Union funded DOWNWIND FP6 project (DOWNWIND, 2012), the aim of which was to understand the impact of deep water windfarms, prove the deep water windfarm concept and share experiences across the industry. ORECCA FP7 (ORECCA, 2012) was a similar project which focused on offshore renewable energy conversion platforms for wind, wave and other ocean energy resources and HYPERWIND FP7 (HYPERWIND, 2012) was tasked with creating and testing cost effective approaches to floating offshore wind turbines.

The combination of these research initiatives as well as past experience, particularly in the offshore oil and gas industry where more than 10,000 offshore platforms have been

constructed since 1947 (Chakrabarti *et al.*, 2005), has provided the wind industry with five main solutions to placing wind turbines out at sea. These are illustrated in Figure 2.8. Some of the concepts are discussed in Byrne and Houlsby (2003) along with the modelling procedures applied in their design.

For water depths up to 15 m, gravity based foundations may be employed, as shown in Figure 2.8(a). These are simply mass concrete structures which sit on the sea bed and stabilise the structure above by means of their self weight. Krogh *et al.* (2011) detailed the construction and installation of gravity based foundations at the Red Sand 2 offshore windfarm in the Baltic Sea, Thomsen *et al.* (2007) demonstrated the experience gained in the construction of two pioneering gravity based foundation designs at the Nysted windfarm in Denmark and Thornton Bank in Belgium, while Henderson and Zaaijer (2002) considered the difficulties in analysing hydrodynamic loading of gravity based foundations.

The most common type of offshore foundation utilised at this time is the monopile, Figure 2.8(b). A monopile is a single tubular steel pile which is driven into the seabed and extends above the water surface. With the inclusion of a transition piece these foundation solutions can support turbines in water depths of up to 30 m. Gjerse (2005) described the development of offshore monopile foundations for major British offshore sites, Gill and Fraser (2002) outlined some of the challenges faced in designing monopile foundations for Arctic conditions, while Andersen *et al.* (2011, 2012) considered the uncertainties in the natural frequency of offshore wind turbine systems supported on monopile foundations by employing a probabilistic approach.

A similar solution developed for greater depths is the jacket or tripod solution, Figure 2.8(c) and 2.8(d). These are three or four legged structures made from tubular steel which extend into the sea bed and allow wind turbine construction in depths of up to 50 m. The experience gained by REpower in the construction of two prototype jacket substructures at depths of 30 m and 45 m was presented by Seidel (2007). Zhang *et al.* (2010) also outlined a fundamental analysis of the structural frequencies of an offshore wind turbine with a jacket type substructure.

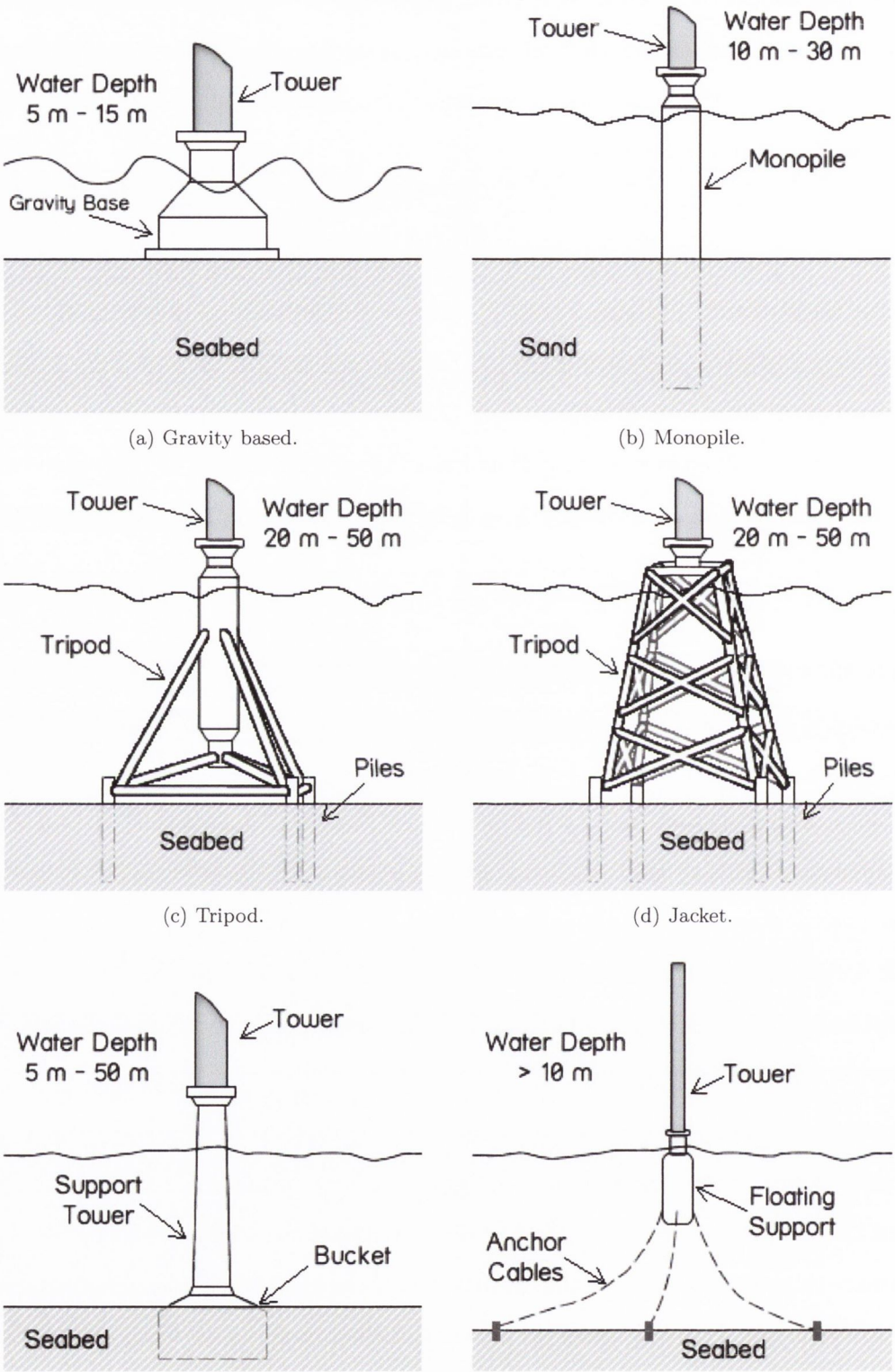

(a) Gravity based.

(b) Monopile.

(c) Tripod.

(d) Jacket.

(e) Suction bucket.

(f) Floating support structure.

Figure 2.8: Offshore wind turbine foundation configurations.

Another possibility currently being investigated is a suction bucket foundation, Figure 2.8(e). This includes a lower steel caisson referred to as the bucket and a vertical tower that extends above the water level. The suction caisson consists of a skirted section and a lid, which is reinforced by a series of stiffeners. The bucket is installed by applying a suction pressure to the top of the lid, which generates a differential pressure between the inside and outside of the bucket, effectively sucking the foundation into the seabed. These structures are being considered for depths between 5 m and 50 m, highlighting their versatility. A primary advantage of this type of solution is its simplicity in terms of installation as compared to monopile or jacket structures. Some of the relevant publications on this technology include a feasibility study for the design of a suction caisson foundation for the Dutch Offshore Wind Energy Converter project (Zaaijer *et al.*, 2002) and a study which tests monopod and tetrapod suction caisson foundations in a soft clay site (Houlsby *et al.*, 2005).

A new concept which is aiming to remove the constraints of water depth from the equation is the notion of floating offshore wind turbines. One possible configuration is illustrated in Figure 2.8(f). While considerable research has been conducted on this topic to date, its relevance is beyond the scope of this thesis.

The prospect of extending concrete tower structures to offshore development poses many possibilities as well as difficulties. In fact, many large offshore structures, such as bridges, already incorporate concrete solutions. Despite this, the advantage of extending tower heights is not as beneficial for offshore installations as it is for onshore. Furthermore, the current offshore construction and installation techniques all relate to tubular steel towers. Therefore, the concept of considering the prestressed concrete tower solution primarily for onshore installations as part of the proposed thesis is further endorsed.

2.6.3 Structural Modelling

Although it is not unusual to consider the base of a wind turbine as a fully fixed support in a dynamic model (Hau, 2006), it has been shown that in certain soil conditions the consideration of soil structure interaction can have the effect of lowering the natural frequencies

of the entire system (Murtagh *et al.*, 2005a). Miscalculation of these system frequencies can prove detrimental to a design by the induction of dynamic amplification resulting in large-amplitude stress variations in the structure if the natural frequencies approach or coincide with the frequencies related to excitation from wind and waves or the rotational frequencies of the blades (Andersen *et al.*, 2012). In fact, following a series of scaled model experiments as well as an analytical study, Bhattacharya and Adhikari (2011) conclude that due to the sensitivity of the natural frequency to the foundation flexibility, "it may not be appropriate to consider that the wind turbine is fixed at the base". In order to consider the dynamic interaction of the wind turbine structure with the underlying soil and to effectively account for the influence of the soil-structure interaction on the overall dynamics of the system, a number of methodologies have been developed which facilitate the inclusion of a soil model in a dynamic representation of a wind turbine.

Novak and Hifnawy (1988) investigates the effect of soil-structure interaction on structural response to wind. In particular, emphasis is placed on shallow foundation types such as mat or raft foundations. It describes a methodology for describing the soil stiffness and damping properties through frequency dependent impedance functions. Novak and Hifnawy (1983) describes how, for shallow foundations, the stiffness and damping constants can be evaluated using elastic half-space theory. This same theory is employed in many modern finite element packages in order to estimate soil behaviour. While it was already stated that the soil stiffness and damping constants are frequency dependent (i.e. they depend on the frequency of loading) Novak and Hifnawy (1983) states that it is usually possible to choose constant values of which are representative for the region of the dominant frequency.

Zaaijer (2006) presents a discussion of a number of options for the case of a monopile type foundation. These include assuming an apparent fixity length, formulating a representative stiffness matrix and also the implementation of a system of uncoupled springs. For the case of the apparent fixity length model, the clamping effect of the soil is simulated by an apparent extension of the pile to an effective depth below the soil surface at which point it is anchored by a fully fixed support. Through experience in the design of other offshore piled structures in the past, depending on the soil conditions, effective fixity lengths

of between 3.3 and 8 times the pile diameter, have been proposed by Barltrop *et al.* (1991) and Kühn *et al.* (1997). In order to formulate a representative stiffness matrix at the soil surface for the foundation-soil system two methods may be used. In the first approach the unknown elements of the stiffness matrix are obtained from static analyses of a reference FE model. This method may be applied to the other foundation types such as gravity based and tripod/jacket structures. In the second approach Randolph's elastic continuum model is used (Randolph, 1981). The stiffness matrix elements are established from an expression relating the pile-head flexibility to a linear fit of the soil shear modulus at the site. For the tripod and lattice solutions the vertical degree of freedom is constrained, as this method provides no value for the axial pile stiffness. For the method of uncoupled springs the coupled stiffness of the pile head is represented by independent springs for each relevant degree of freedom. For a pile these include both lateral translation and the rotation. For the tripod and lattice tower an additional spring is established for the vertical degree of freedom. To obtain the stiffness of the spring elements both the force and displacement methods are applied, using a reference FE model. The linear spring stiffness of the uncoupled springs can be determined from the stiffness matrix. The inherent non-linear behaviour of soil-structure interaction will result in small deviations in the results from those given by an FE analysis, but this is ignored in this case.

Further examples include Ma and Chen (2010) which utilises a Mohr-Coulomb model in order to describe the non-linear soil behaviour as part of a complete finite element model for an offshore wind turbine supported on a monopile foundation. The Mohr-Coulomb model simply allows the shear strength of a soil to be defined for different effective stresses, hence encapsulating the inherent non-linear behaviour of the soil. For the case of gravity based foundations, a publication by Zhao and Maißer (2006) details the incorporation of an uncoupled spring-damper representation of the soil-foundation interaction in a multibody model of a wind turbine system. The cone model (Wolf and Deeks, 2004) is employed by Harte *et al.* (2012) in a study of the along-wind forced vibration response of an onshore wind turbine. Utilising a frequency based approach, the support structure is modelled as a rigid circular foundation resting on a homogeneous elastic half space whose movement is

related to the surrounding soil by means of complex impedance functions obtained from the cone model. Van Buren (2011) modelled two offshore wind turbine support structures in the dynamic wind turbine analysis program HAWC2 (2012), which utilises a system of uncoupled non-linear soil springs to represent the stiffness of the soil. A four-legged, full height lattice tower with piled foundations, and a traditional monotower with a monopile foundation were considered. The investigation showed that including a representation of the foundation can provide a significant difference in the results of a dynamic analysis of a wind turbine. It also highlighted that the monotower experiences much higher forces and moments which requires thicker cross sections and more robust foundations as well as the fact that the lattice tower provides a better solution for deep water applications.

This thesis proposes to compare the structural response of tubular steel and prestressed concrete towers. In initial investigations it is, therefore, seen appropriate to assume a fully fixed support condition for the tower as the literature has shown that only in the case of softer soils does the issue of soil structure interaction noticeably affect the response (Moghaddasi *et al.*, 2011; Luco, 1986). However, due to the considerable variation in structural mass for both tower solutions, any possible relative differences related to soil structure interaction are investigated in Chapter 6.

2.7 Wind Turbines and Earthquakes

In the early stages of wind energy development the focus mainly came from countries in north-western Europe where seismicity is relatively low. Furthermore, the risk to humans as a result of the structural failure of a wind turbine is not considered serious due to the fact that wind turbines are primarily located in remote areas, away from significant populations. However, with the increasing size of wind turbine structures, their growing prominence around the world as well as the considerable investment required for their installation and maintenance, the design and response of wind turbine structures subject to seismic excitation has become a topic of heightened importance. Witcher (2005) states that the approach taken for such analysis is generally based on codified methods which have

been developed for the assessment of seismic loads acting on buildings. These improvised methods are not capable of accurately accounting for the complex dynamics present in an operational wind turbine, nor the aeroelastic interaction of the dynamic motion of the wind turbine structure with either the wind loading acting on the rotor blades or the response of the turbine controller. It is obvious that detailed investigations of the seismic response of wind turbine structures need to be carried out in order to achieve improved structural designs, greater structural reliability, as well as reducing the turbine downtime required for repairs. As the global popularity of wind energy escalates, the necessity for this research is becoming more evident. As it stands the two current leading countries, in terms of installed capacity, are China (24.5 % of global installed capacity) and the USA (19.7 %) WWEA (2011), both countries which have regions that are susceptible to seismic activity.

2.7.1 Seismic Analysis of Wind Turbines

Although there is a sparsity of research which considers the effect of seismic loading on wind turbines, this topic has recently begun to gain popularity with the emergence of some examples in the literature which aim to broaden our understanding of the subject. Many of these examples examine simplified representations of the structures and dynamical systems which aim to simulate the dynamic response to within a reasonable degree of accuracy.

Bazeos *et al.* (2002), which considered the design of a 38 m prototype steel wind turbine tower, suggested that tall steel towers are usually designed considering the effect of wind loads as the only source of environmental dynamic disturbances. The effect of earthquakes as a possible source of damage or loss of serviceability is often neglected, even in high-risk seismic areas. As a result, a seismic analysis was incorporated as part of the tower design in question. The study considered both a refined finite element model as well as a simplified MDOF oscillator to carry out the analysis. It is important to note, however, that these models consider the tower in isolation, without accounting for the complex dynamic system which is supported by the tower. The study concluded that the computationally intensive finite element model produced minimal improvements over the simplified model and the induced stresses as a result of seismic loading were not critical in comparison to

those for survival wind conditions. Lavassas *et al.* (2003) conducted a similar analysis for a 44 m steel tower. Two finite element models, of varying complexity, were established to model the tower. One model included a representation of the soil structure interaction (SSI) in order to determine the implications of this on the response. It was shown that due to the stiff (rocky) soil conditions and sufficiently stiff tower shell, the overall participation of non-linearities and the soil-structure interaction into the total strain state of the tower was calculated as less than 2 %, thus not affecting the overall structural response of the tower. Akin to the previous investigation, it was found that the extreme wind was the dominant load combination for the design of the structure, whereas the seismic design could only become critical in a more seismically hazardous area which was underlain by medium or soft soil. Once again, the dynamics of the components supported by the tower were not considered. The FE approach was further adopted by Nuta *et al.* (2011) in an assessment of the seismic risk of tubular steel wind turbine towers in the Canadian environment. A methodology for the seismic risk assessment of tubular steel wind turbine towers was developed which included a non-linear incremental dynamic analysis, resulting in the development of fragility curves. It was concluded from the results of the incremental analysis that the seismic risk for the wind turbine tower that was investigated is very small for the Canadian locations assessed. This was attributed to the long fundamental period of the tower and the short predominant period of most earthquakes

A multi-body framework incorporating SSI was adopted by Hänler *et al.* (2006) to model an entire wind turbine configuration subject to earthquake loading. Both the multi-body model and a simplified lumped mass model were compared through an analysis of a typical wind turbine with an 80 m diameter rotor and 60 m tall tower. The findings showed that simplified SDOF oscillators derived from lumped mass models were not effective in estimating the turbine eigenfrequencies, nor the seismic loads on wind turbine systems. Zhao and Maißer (2006) also utilised a multi-body formulation for wind turbine towers to investigate the seismic response properties in the time domain. In this instance the model was limited to the tower only, with consideration for the soil interaction. The analysis was carried out on a 1.5 MW wind turbine supported by a 65 m tower. The find-

ings suggest that in areas of relatively flexible soil the influence of SSI may be significant. Furthermore, it is suggested that while it is important to design wind turbines to resist earthquake loading, it is neither economical nor practical to design wind turbines to resist strong earthquakes, given their rare occurrence. A further instance of a multi-body model is provided in Witcher (2005) in which a multi-body based wind turbine design code, GH Bladed (BLADED, 2012), was considered for the calculation of seismic loads on wind turbines. A comparison was made between the codified frequency based approaches standard to building design and a dedicated aeroelastic time domain approach provided by the multi-body design code. Highlighted within the study was the inability of the frequency domain approaches to account for aerodynamic damping which in some situations can have a significant influence on results.

The modal approach was implemented in a study by Ritschel *et al.* (2003) which compared an analysis from a modal based design code to the simplified SDOF oscillator method outlined previously. It was shown that the SDOF oscillator produced relatively conservative results near the tower base while at the tower top it produced slightly lower results due to the absence of a tilt mode in the SDOF oscillator model. Overall, it was concluded that the envelope of the two approaches should yield a reliable measure for the tower loads. Finally, Prowell *et al.* (2009, 2010) conducts both a numerical time domain simulation of wind turbines subject to seismic loading as well as a full scale shake table test on a 23 m high wind turbine. The FAST design code (Jonkman and Buhl, 2005), which models the turbine with a combination of a modal and multi-body dynamics formulation, generated a series of time domain simulations for the NREL 5 MW reference wind turbine (Jonkman *et al.*, 2009) subject to a variety of earthquake events. The FAST simulation highlighted the importance of considering seismic loading for large scale wind turbines as the induced moment demand at the tower base often exceeds that calculated for ultimate wind loading. It also suggests that a slight improvement in the resulting loads may be achieved by triggering an emergency shut-down upon the initiation of strong shaking in the nacelle. The shake table experiment carried out on the 23 m high wind turbine was aimed at exploring the response of a parked turbine due to base excitation. It concluded

that for small scale wind turbines, such as the experimental turbine, the seismic response is primarily governed by the first mode of tower vibration. However, it is noted that for modern large scale wind turbines subject to high frequency seismic excitation higher modes of vibration may contribute significantly to the seismic response. It was also indicated that the level of damping has a considerable effect on response, suggesting the need to gain a more comprehensive insight into tower damping characteristics, particularly for higher order modes.

Although in a number of the instances discussed the seismic response did not influence the design, with the growing diversity of locations where wind turbines are present and the increasing size of the structures, the risk from seismic excitation is heightened and a greater understanding of the dynamic effects is necessary. As another means of comparing the relative structural performance of prestressed concrete and steel towers, this study will consider the effects of seismic loading on these structures.

2.8 Probabilistic Basis for Structural Analysis

Due to the difficulty in specifying deterministic values for variables relating to structural analysis as well as the inherent uncertainty associated with earthquake events, an often more suitable method of assessing a structure is through structural reliability analysis. This is a performance based analysis technique which evaluates the risk of various levels of damage or destruction to a structure by appropriately accounting for the uncertainties affecting the parameters characterizing the physical state of the structure and its environment (load fluctuations, variability of material properties, etc.). A primary facet of reliability based analysis is the development of fragility curves. Fragility curves describe the probability of a structure exceeding a prescribed limit-state given an input hazard intensity parameter and have, therefore, proved useful in, for example, earthquake loss assessment. Ellingwood *et al.* (2007) uses the theorem of total probability to outline the

concept of seismic risk as follows:

$$P\left[Loss > c\right] = \sum_{s}\sum_{LS}\sum_{d} P\left[Loss > c|DS = d\right] \times P\left[DS = d|LS\right] \times P\left[LS|IM = s\right] \times P\left[IM = s\right] \tag{2.7}$$

where IM is the seismic intensity, measured in terms of ground motion (peak ground acceleration, velocity) or spectral intensities (spectral acceleration, velocity or displacement), $P\left[LS|IM = s\right]$ is the probability of reaching a structural limit-state LS, given the occurrence of $IM = s$, $P\left[DS = d|LS\right]$ is the probability of an arbitrary damage state $DS = d$, given limit-state LS, and $P\left[Loss > c|DS = d\right]$ is the probability that the loss exceeds c, given that $DS = d$. $P\left[LS|SI = s\right]$ is known as the fragility term or fragility function and it is in calculating this that fragility curves serve their purpose. Fragility curves are not only confined to seismic analysis but can be successfully implemented in various other structural analysis applications. Dueñas Osorio and Basu (2008) developed wind-induced acceleration fragility curves in combination with an annual distribution of the wind hazard in order to predict the risk of malfunction of acceleration-sensitive equipment in wind turbines. As a result, these tools may be utilised to provide a probabilistic representation of the relative structural response of various tower configurations for a series of loading situations and limit-states.

2.8.1 Fragility Curve Development

The fragility function represents the ability of an engineered system or component to withstand a specified event. Figure 2.9 illustrates the continuous form of a set of fragility curves and their interpretation at a particular ground motion intensity. The hazard intensity measure is displayed on the horizontal axis while the vertical axis represents the probability of limit-state exceedance (LSE) on a scale of zero to one.

Padgett (2007) outlined some of the various types of fragility curves with examples of their implementation to bridge structures in relation to seismic analyses. Expert based fragility curves are formed from the expert opinions of structural engineers as to the par-

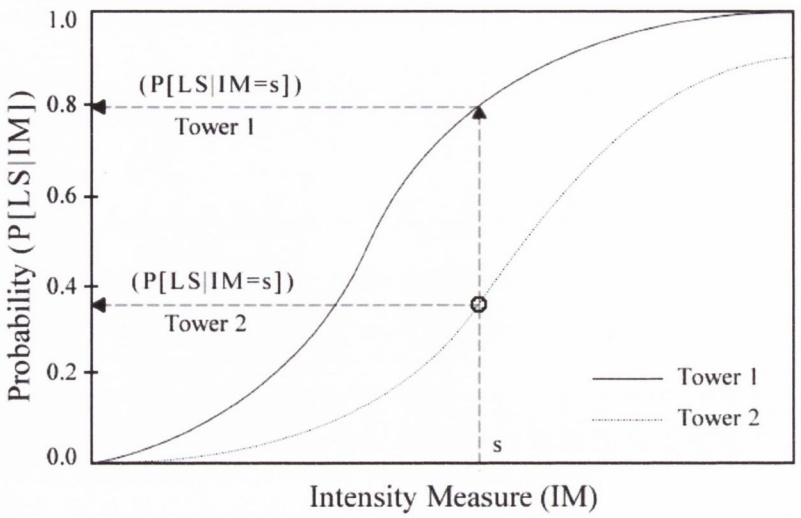

Figure 2.9: Sample fragility curve.

ticular damage state that would be attained by a structure for different levels of ground shaking using the Modified Mercalli Intensity scale (ATC, 1985, 1991). Empirical fragility curves predict the expected level of damage to a structure given a specific ground motion intensity based on past damage to bridges from earthquake events. These fragility curves are developed from a combination of damage data in post-earthquake inspection reports and spatial distributions of ground motion information. With increasing availability of information on the damage sustained by structures during earthquake events the use of empirical fragility curves has become more common (Basoz *et al.*, 1999; Basoz and Kiremidjian, 1999; Shinozuka *et al.*, 2000b, 2003; Yamazaki *et al.*, 1999).

The most common type of fragility curves, and those applicable to the current study are analytical fragility curves. These are formed on the basis of relating the level of damage (structural capacity) to the magnitude of the intensity measure (structural demand) through a probabilistic representation of the relevant parameters. One method of representing fragility is by determining the probability that the structural demand, D, exceeds the structural capacity, C, as shown in Equation 2.8.

$$P_f = P\left[\frac{D}{C} \geq 1\right] \tag{2.8}$$

Hwang and Jaw (1990) showed that fragility can also be modelled by a lognormal cumulative distribution function where the structural demand and capacity are assumed to be lognormally or normally distributed and Melchers (1987) presented a closed form solution for the estimation of fragility as follows:

$$P_f = \Phi\left(\frac{\ln S_D/S_C}{\sqrt{\beta_D^2 + \beta_C^2}}\right) \tag{2.9}$$

where Φ is the standard normal probability integral, S_C is the median value of the structural capacity, β_C is the associated logarithmic standard deviation of structural capacity, S_D is the seismic demand, and β_D is the associated logarithmic standard deviation for the demand. This approach along with a brute force approach (i.e. Monte Carlo), detailed in the relevant chapters, are utilised as tools for comparing the relative structural responses of the various tower configurations.

Following on from the fragility curve formulation it is necessary to define the structural demand and capacity for input into Equation 2.9. Numerous methods have been implemented for this particular purpose and Padgett and DesRoches (2008) outlined their application to bridge structures. The elastic spectral method determines the seismic demand through elastic spectral analysis with the capacities taken from design manual literature (Jernigan and Hwang, 2002; Hwang *et al.*, 2000). Non-linear static methods define a capacity spectrum through non-linear static pushover analysis, and a demand spectrum through reduction of the elastic response spectrum (Mander and Basoz, 1999; Shinozuka *et al.*, 2000a; Dutta and Mander, 1998).

The most reliable and widely used methodology for determining seismic demand is non-linear time-history analysis (Elnashai *et al.*, 2004; Karim and Yamazaki, 2003; Mackie and Stojadinović, 2004, 2001; Kunnath *et al.*, 2006). In this method a suite of ground motions is selected which is representative of seismicity of the region in question. Padgett (2007) suggests that in regions with recorded strong ground motion, such as Japan, Greece, or California, the recorded earthquake ground motion records are utilised. In regions where the availability of strong ground motion records is limited, synthetic ground motions are

often adopted.

Upon specifying a suite of representative ground motions, the next step is to appoint a base model of the structure in question. The structural properties of this base model are subsequently probabilistically sampled to account for inherent uncertainties in the model. For the particular purpose of relating the seismic demand to the appointed intensity measure Shome (1999) developed the procedure of PSDA and Cornell *et al.* (2002) outlined its application to steel moment frame buildings. A Probabilistic Seismic Demand Model (PSDM) provides a mathematical relationship between the ground motion intensity measure (IM) and the structural response, often termed the demand (S_D). The assumption that an estimate of the median of the seismic demand, $\hat{S}_D$, may be described by a power law, $\hat{S}_D = a \times IM^b$, where a and b are unknown coefficients, provides the basis for the PSDM. By transforming the power law relationship to lognormal space the parameter estimation may be simplified to a linear regression as follows:

$$\ln \hat{S}_D = b \ln IM + \ln a \tag{2.10}$$

Mackie and Stojadinović (2005) outlined three methods for deriving PSDMs. These include the Cloud, Incremental Dynamic, and Stripe methods. A Stripe analysis involves scaling all ground motions to the same intensity level to find a probability distribution of S_D for a single IM level. A collection of Stripe analyses at different IM levels is termed an Incremental Dynamic Analysis (IDA). Alternatively, PSDA can be performed using a Cloud approach. The cloud describes the selection of earthquakes with variable IM. All three methods can be used to determine the median (or mean) relationship between S_D and IM, and an associated measure of uncertainty.

Following on from specifying the structural demand for the model, it is then necessary to define the structural limit-state capacities. These offer a quantitative measure of capacity which corresponds to a damage state definition. This is often based on expert judgement, experimental data (Jin and Astaneh, 1998; Rihal, 1982), or analytical methods (Eidinger and Goettel, 1998; Behr and Worrell, 1998). Once the parameters have been

determined the fragility function or fragility curves may be derived from Equation 2.9.

The approaches outlined in the current section are utilised as a tool for comparing the relative structural response of various tower configurations. In the case of the seismic response PSDA is applied to quantify the associated risk to the wind turbine components for a specified level of seismic intensity. To the best of the author's knowledge, this is the first instance of the application of this method to wind turbine structures.

2.9 Conclusion

Highlighted throughout this literature review was the impending progression of wind energy concepts, in particular HAWTs for onshore and offshore installations. The most noticeable trend in the literature was the increasing size of wind turbine structures in order to generate greater amounts of energy at a cheaper cost. This increased size requirement has necessitated the extension of tower heights and it is evident that the current industry standard concepts are reaching their limit as a feasible solution. Tubular steel wind turbine towers provide a fast and efficient solution for installations at current tower heights but at heights beyond 85 m and turbine units above 2 MW they can no longer provide a sufficiently stiff structure. Fabrication and transportation issues were also highlighted for these towers. It has, therefore, been proposed to investigate the possibilities of an alternative tower solution with the re-emergence of prestressed concrete as a possible tower construction method. Although some examples were found in the literature concerning prestressed concrete towers, many of these focussed on promoting the observable advantages of this type of solution. Further examples considered the technical aspects of prestressed concrete tower structures. These focused on particular aspects of the structural design, however, none have developed the issue of structural performance. Therefore, it was decided to concentrate on modelling the structural performance of these towers and comparing the results to those of industry standard tubular steel designs.

Discussed in the literature review were the conceptual and technical aspects of electricity generation from the wind. The continuing depletion of fossil fuel resources and the

unnerving realities of over-dependence, fuel price surges and environmental issues were initially highlighted. The role of wind energy in a renewable-based solution to these issues and its capabilities from both a local and global perspective were cited. While it is easy to classify wind energy as an ideal solution, it was seen that there are many technical, social, economic and political barriers and difficulties. These lead to a more realistic estimation of the future capabilities of wind energy and specify the areas where continued research can improve the prospects and feasibility of this renewable energy solution. One particular technical barrier identified was the requirement for increased tower heights to support larger more powerful turbines within a faster and more stable airflow. Prestressed concrete or hybrid tower configurations have been proposed as a possible solution to the inadequacies of other options at the required heights.

In assessing the design and dynamic modelling requirements of wind turbine structures, it was noted that these structures necessitate a unique perception of the structural dynamics. This is primarily due to the inherently dynamic nature of wind turbine structural behaviour coupled with the stochastic loading considerations relating to the wind, and waves in the case of offshore turbines. In this regard, the concept of aeroelasticity was outlined. Although the notably accurate modelling concepts of BEM, CFD, FEM, multi-body and modal representations were extensively described, it was determined that a simplified modelling framework, incorporating the specific design elements relevant to the study would prove a more efficient solution for modelling the wind turbine structural dynamics as part of this study. The specific scope of the model was determined based on computational efficiency, relative accuracy and level of detail required of the analysis. A similar perspective was taken on the topic of wind field modelling. In this instance spectral methods were adopted by virtue of their simplicity and computational efficiency. Further approaches such as rotationally sampled turbulence and spectral tensors were also considered but not deemed necessary to achieve the objectives of this thesis.

Considering wind turbine blades and the related dynamics, the requirement for increased blade lengths for the design of multi-megawatt turbines was once again highlighted. The issue of blade vibration and its consequences for a blade design was considered, par-

ticularly from the perspective of fatigue effects. In response to this, it was proposed that a reduction in vibration could be achieve through accurate placement of system natural frequencies. Another example proved the possibility of controlling edgewise blade vibrations with a pair of active tendons mounted inside the blade, controlled by actuators. In view of the positive implications of reduced blade vibrations, it has been proposed to investigate the effect of tower construction material on the resulting magnitude of blade response, thus identifying the relative merits of alternative tower solutions in terms of minimisation of blade vibrations.

Since the focus of this thesis is primarily on wind turbine towers, an extensive description of the various tower designs and the associated advantages and disadvantages was provided. In terms of the taller hub heights required for modern multi-megawatt turbines, the two solutions identified as the most appropriate were steel truss towers and prestressed concrete or hybrid towers. The concepts of "stiff" and "soft" towers were discussed, along with the assertions that tubular steel towers can no longer provide the required stiffness for tower heights beyond 85 m and turbines larger than 2 MW. A thorough review of literature pertaining to vibration and fatigue issues for towers was performed. This was followed by a discussion of vibration suppression techniques. While numerous approaches to increasing structural damping were considered, the difficulty of locating damping devices within the space restrictions of a nacelle in a wind turbine structure was a common argument. The possibility of achieving reduced vibrations with a prestressed concrete tower was subsequently identified as a primary objective of this thesis. As previous literature has alluded to the fact that a prestressed concrete tower can provide improved vibration response as compared to tubular steel towers, this fact will be investigated as part of this thesis.

While it is not uncommon to model the base support of a wind turbine tower as fully fixed, it was shown by a number of authors that such an assumption can have the effect of overestimating the system natural frequencies in the presence of certain soil conditions. While the assumption of a fully fixed support proves sufficient for a comparative study, such as that which is proposed here, the possibility of a differential response of the various tower

solutions when soil structure interaction is included is also a proposed objective of this study. This is of particular interest considering the substantial variation in structural mass between tubular steel and prestressed concrete towers. Numerous modelling techniques for the incorporation of soil structure interaction were also discussed. These are revisited later in the thesis when it is necessary to incorporate soil effects into the structural model.

An area in the literature which has been identified as significantly under-researched was the consideration of seismic effects on wind turbines, in particular wind turbine towers. It was evident from the literature that in most cases the consequences of an earthquake event on a wind turbine is determined from highly idealised codified methods which were shown to significantly miscalculate the response. Although numerous studies determined that seismic effects were not the determining factor in the design, it was evident that within certain areas and with certain soil conditions seismic effects could prove significant. A methodology for the incorporation of earthquake loading in the structural modelling procedure has, therefore, been proposed. Utilising this methodology, it is possible to compare the dynamic response of both the steel and prestressed concrete towers when subjected to seismic loading.

In order to provide a comparison of the computed dynamic response of the various tower configurations, a probabilistic framework has been proposed. The development and possible applications of fragility curves is extensively discussed in the literature review as a result. In the context of the seismic response, a methodology, known as probabilistic seismic demand analysis (PSDA), commonly employed in the analysis of bridge structures is proposed.

Considering the proposed objectives of this thesis, as listed in Section 1.3, it is felt that the current chapter provides a clear and extensive review of the relevant topics. Many of the concepts and methodologies discussed in this chapter will be further established throughout this thesis as they are applied to the proposed investigations.

Chapter 3 -

Wind Turbine Modelling

3.1 Introduction

A wind turbine is made up of numerous flexible and rigid bodies which interact dynamically through the rotation of the rotor and the vibration of the whole system. This is further influenced by the variable loading of the wind, ground motions and, in the case of offshore turbines, the sea. As discussed in Section 2.3.4, there are various methods for representing wind turbine dynamics. These include FEM, MBS formulations, modal representations as well as combinations of these techniques. In modelling the dynamics of a wind turbine the most important aspect is the accurate coupling of the various components in order to effectively capture the complex dynamic interactions inherent to these systems.

A common approach used by researchers in the simulation of wind turbine dynamics is to formulate the equations of motion by the Lagrangian approach. This allows straightforward coupling of the numerous flexible bodies (blades, tower, rotor shaft, etc.) and rigid bodies (i.e. nacelle, generator, yaw and pitch mechanisms) in two or even three dimensional space. For the most part the dynamics are represented by a modal approximation of the flexible bodies while rigid bodies may also be included. Examples of this are provided by Garrad (1983), Arrigan *et al.* (2011) and Hansen (2003). The Euler-Lagrange equation, as derived from Hamilton's Principle may be expressed as follows:

$$\frac{d}{dt}\left(\frac{d\mathcal{L}}{d\dot{x}_i}\right) - \frac{d\mathcal{L}}{dx_i} = P_i \tag{3.1}$$

where $\mathcal{L} = E_K - E_P$ is the Lagrangian given the kinetic energy E_K and the potential

energy E_P of the system, x_i is the general coordinate for DOF i, $\dot{x}_i$ is the first temporal derivative of the general coordinate and P_i is the generalised loading. This approach allows all elements of coupling to be accurately referenced in the system of differential equations describing the dynamics.

This chapter outlines two dynamic models of a wind turbine system which are employed in the investigations carried out in this thesis. These are formulated utilising the aforementioned Lagrangian approach, incorporating a modal representation of the flexible tower and blades. The first is a one dimensional model that captures the dynamic response in the along-wind direction of the rotating blades (flapwise) and tower (longitudinal or fore-aft) only. This type of model has been employed previously in order to identify specific dynamic effects and carry out initial investigations (Arrigan *et al.*, 2011; Murtagh *et al.*, 2005b). The second model extends the modelling capabilities to two dimensions with the addition of edgewise blade vibration and lateral tower motion. This model also incorporates rigid body dynamics for the nacelle with yaw, tilt and roll included as well as the rotational dynamics of the rotor shaft. An extension of this model for the inclusion of soil-structure interaction is also described. Validation of the proposed models is provided through a comparison with a verified aeroelastic wind turbine analysis code.

3.2 One Dimensional Model

The proposed flapwise system is illustrated in Figure 3.1. The model includes two coordinate frames of reference, a local co-rotating system for each blade (x, y, z) and a global system for the combined elements which includes the tower and nacelle (X, Y, Z). At the root of each blade exists the origin of the local blade system. In Figure 3.1 the orientation of the local axes, but not the origin, are shown at the tip of the blade. Wind loading is solely considered in the global X-direction as this is the extent of the model capabilities. It should also be noted, however, that assuming there is no yaw misalignment and the turbine is located on relatively flat terrain, then significantly less loading occurs in the other directions (BS EN 61400-1, 2005). As already stated, in this particular model only

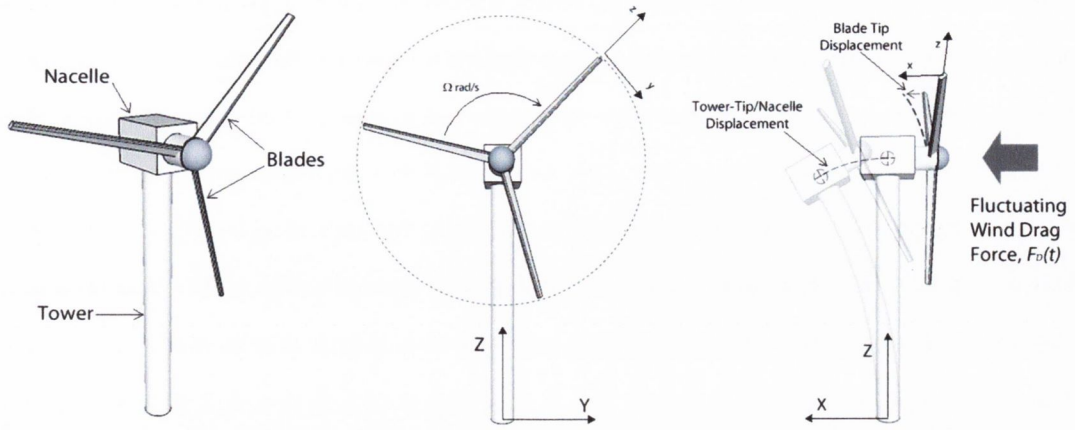

Figure 3.1: Sketch of flapwise model & coordinate axes (Quilligan *et al.*, 2012b).

motion in the direction of the x-axis is considered. Axial and rotational vibrations of the tower are neglected as the most important vibration interaction occurs between the exciting rotor forces and the tower bending frequencies Hau (2006).

Assuming a modal representation of the flexible tower and blades, their flapwise motion, $u(z,t)$, as a function of position z and time t in the proposed model may subsequently be considered as a summation of the products of calculated modeshapes $\phi_i(z)$ and the corresponding temporal modal coordinate $q_i(t)$ for each particular mode i in the general form, as follows:

$$u(z,t) = \sum_{i=1}^{I} [\phi_i(z) \times q_i(t)] \tag{3.2}$$

In order to represent the motion in this manner a set of shape functions must first be derived for both the tower and blades. This is achieved by an eigenvalue analysis of the individual flexible components. The mass of the element is lumped at specific nodes. A method based on virtual work, detailed in Appendix A, is employed to generate the stiffness matrix of the elements. It is then possible to carry out an eigenvalue analysis of the free vibration condition which produces the shape functions or approximated modeshapes. Once computed, it is then possible to approximate these shapes with a polynomial expression. In the case of the blades, however, a more comprehensive solution is required due to the rotation of the elements about a central hub. This has the effect of increasing

the bending stiffness of the blades, an effect known as centrifugal stiffening. The consequences of centrifugal stiffening have been proven in previous literature to be significant and it is therefore included in this model (Ozgumus and Kaya, 2006; Naguleswaran, 1997, 1994). In order to model this effect a geometric stiffness matrix is added to the original stiffness matrix. This is assembled using the formula for centrifugal stiffness outlined by Hansen (2003). The resulting mass and stiffness matrices may then be implemented in an eigenvalue analysis using the "eig()" function in Matlab (Math Works, 2010).

Having specified the modal components of the flexible elements, the next step is to calculate the kinetic energy of these elements for input into Equation 3.1. Considering just the tower, the total kinetic energy, $E_{K,t}$ may be expressed as:

$$E_{K,t} = \frac{1}{2}\int_0^H m_t(Z) \times \dot{u}_t^2(Z,t)dZ \tag{3.3}$$

where H is the total height of the tower, $m_t(Z)$ is the mass of the tower as a function of height Z and $\dot{u}_t(Z,t)$ is the first temporal derivative of the position of the tower centre of gravity (CG) axis as a function of height Z and time t. Following on from this, the kinetic energy of the motion of the nacelle may be described as:

$$E_{K,nac} = \frac{1}{2}M_{nac} \times \dot{u}_{nac}^2(t) \tag{3.4}$$

where M_{nac} is the total mass of the nacelle and $\dot{u}_{nac}$ is the first temporal derivative of the position vector for the nacelle. In the case of the blade it is possible to represent the overall motion of the CG axis of the blade as a sum of the motion of the blade relative to the nacelle, $u_{b,nac}$, and the nacelle motion, u_{nac}, as follows:

$$u_b(z,t) = u_{b,nac}(z,t) + u_{nac}(t) \tag{3.5}$$

This leads to a description of the total kinetic energy of a blade.

$$E_{K,b} = \frac{1}{2}\int_0^R m_b(z) \times \dot{u}_b^2(z,t)dz \tag{3.6}$$

where R is the total length of the blade, $m_b(z)$ is the mass of the blade as a function of its length z and $\dot{u}_b(z,t)$ is the first temporal derivative of the blade position as a function of its length z and time t.

Combining the elements of Equation 3.3 to 3.6 and having expanded the modal representation of the motion of the flexible components, the total kinetic energy of the system can be shown to be:

$$\begin{aligned} E_K = \frac{1}{2}\sum_{n=1}^{3}\Bigg\{ & \int_0^R m_{bn}(z)\left[\sum_{i=1}^{I}\left[\phi_{bn,i}(z)\times\dot{q}_{bn,i}(t)\right]\right]^2 \mathrm{d}z + 2\sum_{j=1}^{J}\left[\phi_{t,j}(H)\times\dot{q}_{t,j}(t)\right] \\ & \times\int_0^R m_{bn}(z)\left[\sum_{i=1}^{I}\left[\phi_{bn,i}(z)\times\dot{q}_{bn,i}(t)\right]\right]\mathrm{d}z + \left[\sum_{j=1}^{J}\left[\phi_{t,j}(H)\times\dot{q}_{t,j}(t)\right]\right]^2 \\ & \times\int_0^R m_{bn}(z)\mathrm{d}z\Bigg\} + \frac{1}{2}M_{nac}\left[\sum_{j=1}^{J}\left[\phi_{t,j}(H)\times\dot{q}_{t,j}(t)\right]\right]^2 \\ & + \frac{1}{2}\int_0^H m_t(Z)\left[\sum_{j=1}^{J}\left[\phi_{t,j}(Z)\times\dot{q}_{t,j}(t)\right]\right]^2 \mathrm{d}Z \end{aligned} \tag{3.7}$$

where the subscript n represents the blade number and $\phi_{t,j}(H)$ is the value of the j^{th} modeshape of the tower at the top of the tower. Likewise, the total potential energy of the elements of the system can be evaluated as:

$$E_P = \frac{1}{2}\sum_{n=1}^{3}\left\{\sum_{i=1}^{I}\left[S_{bn,i}\times q_{bn,i}^2(t)\right] + E_{P,C,bn}\right\} + \frac{1}{2}\sum_{j=1}^{J}\left[S_{t,j}\times q_{t,j}^2(t)\right] \tag{3.8}$$

where $S_{bn,i} = EI_{bn}(z)\phi''_{bn,i}$ is the modal stiffness of blade n for mode i with EI_{bn} representing the bending stiffness of blade n as a function of z, $S_{t,j} = EI_t(Z)\phi''_{t,j}$ is the modal stiffness of the tower for mode j with EI_t representing the bending stiffness of the tower as a function of Z and $E_{P,C,bn}$ represents the additional potential energy in blade n due to centrifugal stiffening effects. The formula specified by Hansen (2003), and used by Arrigan *et al.* (2011), for the centrifugal tension distribution throughout a rotating cantilever beam results in the potential energy term due to centrifugal body forces being approximated,

for flapwise motion, as:

$$E_{P,C,bn} = \frac{1}{2}\Omega^2 \int_0^R \left(\sum_{i=1}^{I} \left[q_{bn,i} \times \frac{d(\phi_{bn,i}(z))}{dz} \right] \right)^2 \times \int_z^R m_{bn}(\xi) d\xi dz \tag{3.9}$$

where Ω is the blade rotational frequency (rad/s) and ξ is an alternative variable representing the position along the blade.

Evaluating the expressions for the potential and kinetic energy of the system, Equation 3.7 and 3.8, and substituting them into the Lagrangian formulation from 3.1 gives rise to a set of coupled equations of motion of the following form:

$$[M]\{\ddot{u}(t)\} + [C]\{\dot{u}(t)\} + [K]\{u(t)\} = [P(t)] \tag{3.10}$$

when damping for the system is formulated as stiffness proportional damping and is specified based on the particular tower and blades being modelled. An illustration of the format of these matrices is presented in Appendix B. An example of the implementation of this model is presented in Section 3.5.2.

3.3 Two Dimensional Model

Having considered only the flapwise blade motion and longitudinal tower vibration, the one dimensional model outlined in Section 3.2 ignored significant elements of the system dynamics. The two dimensional model extends upon the modal representation of the flexible blade and tower components to include the additional effects of edgewise blade vibration and lateral tower motion. It also takes account of nacelle tilt, roll and yaw as well as rotor shaft rotation as described in Figure 3.2. In a similar manner to the one dimensional model, the two dimensional model is formulated from the Lagrangian formulation outlined in Equation (3.1) by directly minimising the total energy functions of the dynamical system. As illustrated in Figure 3.2 the model includes two coordinate frames of reference, a local co-rotating system for each blade (x, y, z) and a global ground-fixed system for the combined elements which includes the tower and nacelle (X, Y, Z).

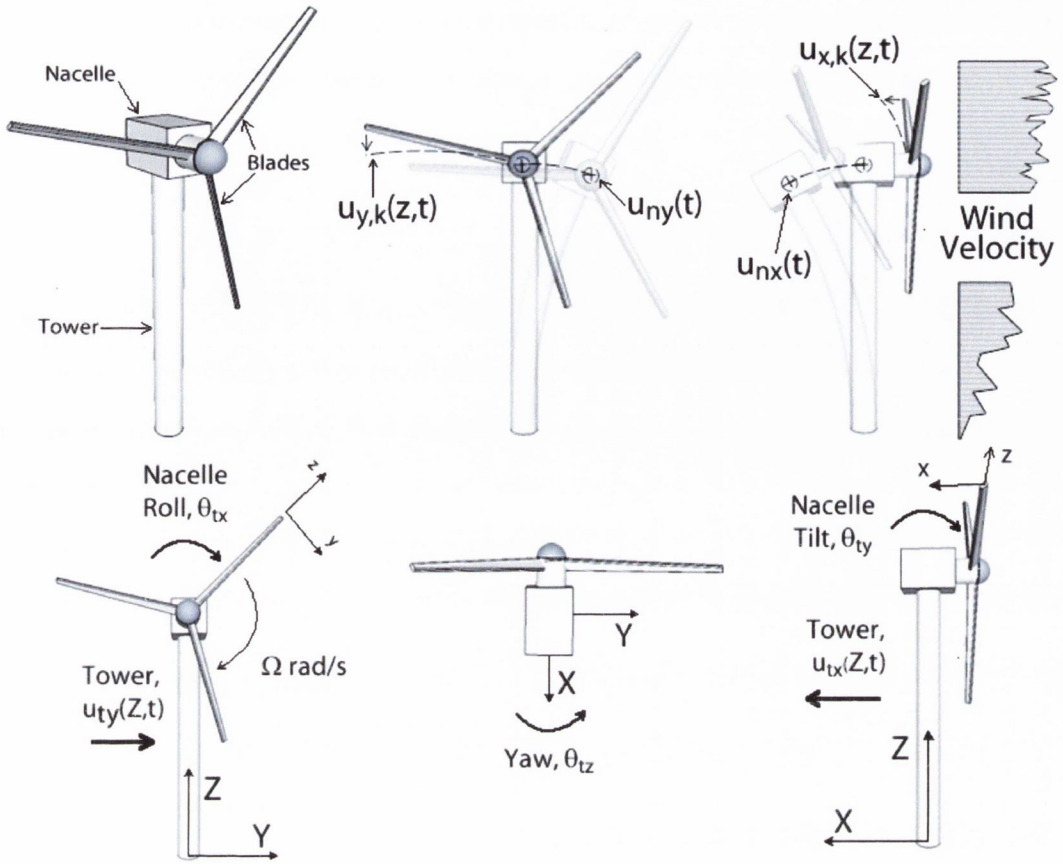

Figure 3.2: Two dimensional model outline.

At the root of each blade exists the origin of the local blade system. In Figure 3.2 the orientation of the blade local axes, but not the origin, are shown at the tip of the blade. Flapwise blade vibration and longitudinal tower vibration occur in the local "x" and global "X" directions respectively while edgewise blade vibration and lateral tower vibration correspond to the "y" and "Y" axes respectively. Wind inflow is solely considered in the global X-direction for the same reasons as outlined in Section 3.2.

Once again a modal representation of the flexible tower and blade motion is formulated in the form of Equation (3.2). Modeshapes are approximated from a free vibration analysis of the individual flexible components where a lumped mass model is applied to establish the mass matrix and virtual work is utilised in the derivation of the associated stiffness matrix.

The next step is to focus on the motion of the elements within the overall dynamic

system. As shown by Hansen (2003), the position vector of an arbitrary point at radius z on the CG axis of the blade n with respect to the origin of the ground fixed frame is:

$$\vec{p}_{cg,n} = \begin{Bmatrix} u_{nac,X}(t) \\ u_{nac,Y}(t) \\ H \end{Bmatrix} + T_A(t) \left[\begin{Bmatrix} -L_s \\ 0 \\ 0 \end{Bmatrix} + \quad T_B(t)\, T_C(t) \begin{Bmatrix} u_{bn,x}(z,t) \\ u_{bn,y}(z,t) \\ z \end{Bmatrix} \right] \tag{3.11}$$

where $u_{nac,X}(t)$ and $u_{nac,Y}(t)$ is the position of the centre of the nacelle with respect to the ground fixed frame in the X and Y directions respectively, H is the vertical height of the tower, L_s is the length of the rotor shaft, while $u_{x,n}(z,t)$ and $u_{y,n}(z,t)$ are the position of the CG axis of blade n in the x and y directions respectively with respect to the local blade axis. The transformation matrices are defined as:

$$\begin{aligned} T_A = & \begin{bmatrix} 1 & 0 & 0 \\ 0 & cos\,\theta_{nac,Y} & -sin\,\theta_{nac,Y} \\ 0 & sin\,\theta_{nac,Y} & cos\,\theta_{nac,Y} \end{bmatrix} \times \begin{bmatrix} cos\,\theta_{nac,Z} & -sin\,\theta_{nac,Z} & 0 \\ sin\,\theta_{nac,Z} & cos\,\theta_{nac,Z} & 0 \\ 0 & 0 & 1 \end{bmatrix} \\ & \times \begin{bmatrix} cos\,\theta_{nac,X} & 0 & sin\,\theta_{nac,X} \\ 0 & 1 & 0 \\ -sin\,\theta_{nac,X} & 0 & cos\,\theta_{nac,X} \end{bmatrix} \end{aligned} \tag{3.12}$$

$$T_B = \begin{bmatrix} cos\,\theta_{s,x} & 0 & sin\,\theta_{s,x} \\ 0 & 1 & 0 \\ -sin\,\theta_{s,x} & 0 & cos\,\theta_{s,x} \end{bmatrix} \tag{3.13}$$

$$T_C = \begin{bmatrix} cos\,\psi_n & 0 & sin\,\psi_n \\ 0 & 1 & 0 \\ -sin\,\psi_n & 0 & cos\,\psi_n \end{bmatrix} \tag{3.14}$$

where T_A, T_B and T_C correspond to the transformation from nacelle coordinates, drive-train coordinates and blade coordinates respectively. $\theta_{nac,X}$, $\theta_{nac,Y}$, $\theta_{nac,Z}$ and $\theta_{s,x}$ as shown in Figure 3.2 signify nacelle roll, tilt, yaw and drive-train shaft torsion while $\psi_n =$

$\Omega t + \frac{2\pi}{3}(n-1)$ is the mean azimuth angle to blade n.

The total kinetic energy of the system may consequently be described as:

$$\begin{aligned} E_K = & \frac{1}{2}\int_0^H m_t(Z)\left[\dot{u}_{t,X}^2(Z,t) + \dot{u}_{t,Y}^2(Z,t)\right] dZ + \frac{1}{2} I_x \dot{\theta}_{nac,X}^2 \\ & + \frac{1}{2} I_y \dot{\theta}_{nac,Y}^2 + \frac{1}{2} I_z \dot{\theta}_{nac,Z}^2 + \frac{1}{2} M_{nac}\left[\dot{u}_{nac,X}^2(t) + \dot{u}_{nac,Y}^2(t)\right] \\ & + \frac{1}{2}\sum_{n=1}^{3}\left\{\int_0^R m_{bn}(z) \times |\dot{p}_{cg,n}|^2 \, dz\right\} \end{aligned} \tag{3.15}$$

where $m_t(Z)$ is the tower mass as a function of its height, $\dot{u}_{t,X}(Z,t)$ and $\dot{u}_{t,Y}(Z,t)$ are the first temporal derivatives of the position of the centre of gravity axis of the tower with respect to the ground fixed frame in both the X and Y directions, I_x, I_y and I_z are the mass moments of inertia of the nacelle about the X, Y and Z axes and M_{nac} is the total mass of the nacelle and hub components excluding the blades. Likewise, the total potential energy of the elements of the system can be evaluated as:

$$\begin{aligned} E_P = & \frac{1}{2}\int_0^H \left[EI_{t,X}(u''_{t,X})^2 + EI_{t,Y}(u''_{t,Y})^2\right] dZ + \frac{1}{2} G_x \theta_{nac,X}^2 \\ & + \frac{1}{2} G_y \theta_{nac,Y}^2 + \frac{1}{2} G_z \theta_{nac,Z}^2 - g_{xy}\,\theta_{nac,Y}\,u_{nac,X}(t) + g_{xy}\,\theta_{nac,X}\,u_{nac,Y}(t) \\ & + \frac{1}{2} G_s \theta_{s,x}^2 + \frac{1}{2}\sum_{n=1}^{3}\left\{\int_0^R \left[EI_{b,x}(u''_{x,n})^2 + EI_{b,y}(u''_{y,n})^2\right] dz + E_{P,C,bn}\right\} \end{aligned} \tag{3.16}$$

where $EI_{t,X}$ and $EI_{t,Y}$ represent the tower bending stiffness as a function of Z, $u''_{t,X}$ and $u''_{t,Y}$ are the second spatial derivatives with respect to Z of the tower position, G_x, G_y and G_z are the roll, tilt and yaw stiffnesses of the nacelle support, g_{xy} is the coupling stiffness of the nacelle support, G_s is the torsional stiffness of the drive-train, $EI_{b,x}$ and $EI_{b,y}$ signify the blade bending stiffness as a function of z, while $u''_{x,k}$ and $u''_{y,k}$ are the second spatial derivatives with respect to z of the blade position. $E_{P,C,bn}$ represents the centrifugal stiffening effects. Extending on Equation (3.9) and utilising the formula specified by Hansen (2003) for the centrifugal tension distribution throughout a rotating cantilever beam results in the potential energy term due to centrifugal body forces being

approximated as:

$$E_{P,C,bn} = \frac{1}{2}\Omega^2 \sum_{n=1}^{3} \left\{ \int_0^R \left[(u'_{bn,x})^2 + (u'_{bn,y})^2 \right] \times \int_x^R m_{bn}(\xi) d\xi dz \right\} \tag{3.17}$$

where Ω is the blade rotational frequency in (rad/s), R is the total length of the blade, $u'_{x,n}$ and $u'_{y,n}$ are the first spatial derivatives of the position of the CG axis of blade n and $m_{bn}(\xi)$ is the mass per unit length of the blade (kg/m).

Evaluating the expressions for the potential and kinetic energy of the system, Equation (3.15)-(3.16), and then substituting them into the Lagrangian formulation from Equation (3.1) produces a non-linear dynamic model of the system. Linearisation of the model results in a set of linear equations of motion for the vibration of the system in the following form:

$$[M]\{\ddot{u}(t)\} + [C]\{\dot{u}(t)\} + [K]\{u(t)\} = \{P(t)\} \tag{3.18}$$

where C represents the system gyroscopic forces as well as the damping which may be specified as stiffness proportional damping specific to the wind turbine being studied.

3.3.1 Inclusion of Soil Structure Interaction

In all aspects of the models outlined thus far it has been assumed that the connection between the structure and underlying soil can be implemented as a fully fixed support. As discussed in Section 2.6.3 this is an acceptable procedure in preliminary design and it has been shown to have minimal effect on the system response for many strong soils. Despite this, it has been proven in certain situations that SSI can have a significant effect on the system response with the exclusion of this effect having the consequence of significantly overestimated natural frequencies. For this reason as well as the possibility of identifying relative differential SSI effects for steel and concrete towers, the current section outlines a framework for incorporation of SSI in the preceding structural models.

The extension for the inclusion of SSI effects is limited to the two dimensional model only. Following the same Lagrangian framework previously outlined, four additional degrees of freedom are established to represent the effect of SSI on the overall response of the

system. These are illustrated in Figure 3.3 and include lateral and longitudinal motion as well as rotation of the foundation about both horizontal axes. Considering the additional

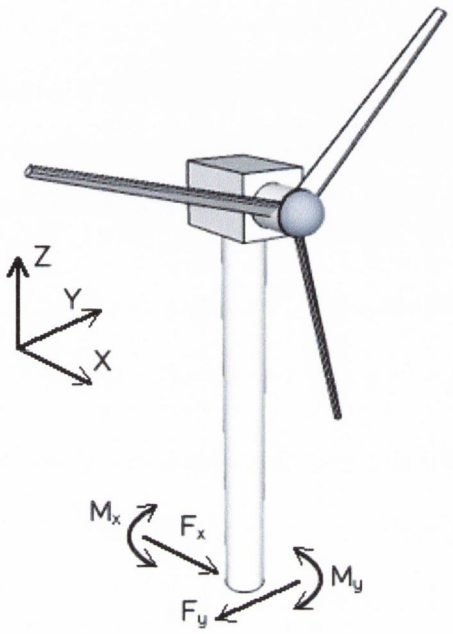

Figure 3.3: Additional foundation degrees of freedom.

degrees of freedom established in Figure 3.3 it is necessary to redefine the expression for the motion of the tower and nacelle as follows:

$$\vec{u}_t(Z,t) = \begin{Bmatrix} u_{tf,X}(Z,t) \\ u_{tf,Y}(Z,t) \\ Z \end{Bmatrix} + \begin{Bmatrix} u_{f,X}(t) + Z \times \theta_{f,Y}(t) \\ u_{f,Y}(t) + Z \times \theta_{f,X}(t) \\ 0 \end{Bmatrix} \tag{3.19}$$

where $u_{tf,X}(Z,t)$ and $u_{tf,Y}(Z,t)$ are the position of the tower CG axis relative to the foundation in the X and Y directions respectively, $u_{f,X}(t)$ and $u_{f,Y}(t)$ represent the motion of the foundation in the X and Y directions respectively, while $\theta_{f,X}(t)$ and $\theta_{f,Y}(t)$ signify

the rotation of the foundation about the X and Y axes.

$$\vec{u}_{nac}(t) = \begin{Bmatrix} u_{nacf,X}(t) \\ u_{nacf,Y}(t) \\ Z \end{Bmatrix} + \begin{Bmatrix} u_{f,X}(t) + H \times \theta_{f,Y}(t) \\ u_{f,Y}(t) + H \times \theta_{f,X}(t) \\ 0 \end{Bmatrix} \tag{3.20}$$

where $u_{nacf,X}(Z,t)$ and $u_{nacf,Y}(Z,t)$ correspond to the position of the nacelle relative to the foundation in the X and Y directions respectively. This leads to a definition of the kinetic energy added to the system as a result of the SSI effects.

$$E_{K,SSI} = \frac{1}{2}\left\{M_f\left[\dot{u}^2_{f,X}(t) + \dot{u}^2_{f,Y}(t)\right] + I_{f,X}\dot{\theta}^2_{f,X}(t) + I_{f,Y}\dot{\theta}^2_{f,Y}(t)\right\} \tag{3.21}$$

with M_f signifying the total mass of the foundation, while $I_{f,X}$ and $I_{f,Y}$ are the respective mass moments of inertia of the foundation about the X and Y axes. It should also be noted that the values for absolute tower and nacelle motion derived in Equations (3.19) and (3.20) must be implemented in the overall derivation of the kinetic energy. In a similar manner the additional potential energy may be described as follows:

$$\begin{aligned} E_{P,SSI} = \frac{1}{2}\Big\{&S_{f,X} \times u^2_{f,X}(t) + S_{f,Y} \times u^2_{f,Y}(t) \\ &+ S_{f\theta,X} \times \theta^2_{f,X}(t) + S_{f\theta,Y} \times \theta^2_{f,Y}(t)\Big\} \end{aligned} \tag{3.22}$$

where $S_{f,X}$ and $S_{f,Y}$ are the translational stiffnesses of the foundation in the X and Y directions respectively, while $S_{f\theta,X}$ and $S_{f\theta,Y}$ are the rotational stiffnesses of the foundation about the X and Y axes.

Once formulated, the results of Equation (3.21) and (3.22) can be incorporated in the expansion of Equation (3.1) resulting in a set of dynamic equations of motion equivalent to Equation (3.18). Following on from this it is necessary to define the time dependent generalised loading vector $\{P(t)\}$ for both the one and two dimensional models.

3.4 Structural Loading

As an obvious consequence of their function, the primary source of loading on a wind turbine relates to the wind. The most apparent source is the wind inflow acting upon the structure as it passes through the rotor. This is a highly variable loading which has a dependency on site specific conditions, mean wind speed as well as overall climatic factors. Due to the considerable variability of wind loading from one time point to another, whether being measured in seconds or even years, it has been shown that stochastic methods are the most appropriate means of simulating wind loading on a structure. Another environmental condition which has been demonstrated as relevant to wind turbines is seismic loading. This has become more pertinent with the growing prominence of wind turbines in seismic regions across the globe. In the case of offshore turbines, wave and hydrodynamic loading are coupled with the wind loads. Further conditions which require consideration in the structural design of wind turbines includes impact loads from vehicles, airborne objects or even ships, ice loads in certain regions as well as loads induced during transport and assembly. Due to the focus on onshore turbines this thesis will be limited to the effects of wind and earthquake loading as a means of comparing the structural response of the various tower configurations.

3.4.1 Blade Loading

Due to the aerofoil design of the blades, as the wind passes through a turbine it imparts both a lift and drag force upon the blades. Employing the same aerodynamic principles applied to aircraft wings, the lift force provides the driving force for the turbine. According to Hansen (2008) the values for the lift and drag forces on such an aerofoil are given by:

$$F_L = \frac{1}{2}\rho c V_{rel}^2 C_L \tag{3.23}$$

$$F_D = \frac{1}{2}\rho c V_{rel}^2 C_D \tag{3.24}$$

where ρ is the air density, c is the aerofoil chord length, while C_L and C_D are aerodynamic lift and drag coefficients which are a function of α, the local angle of attack of the blade element. V_{rel} is the airflow velocity relative to the blade and is derived as:

$$V_{rel} = \sqrt{V_0^2 + z^2\Omega^2} \tag{3.25}$$

where V_0 is the wind inflow velocity. Due to the increasing blade velocity along its span, V_{rel} is also a function of the position along the blade, z. Figure 3.4 presents an outline of the forces acting upon a blade element twisted, either by design or through active pitch control, at an angle θ to the plane of rotation of the blades. In calculating the forces on a

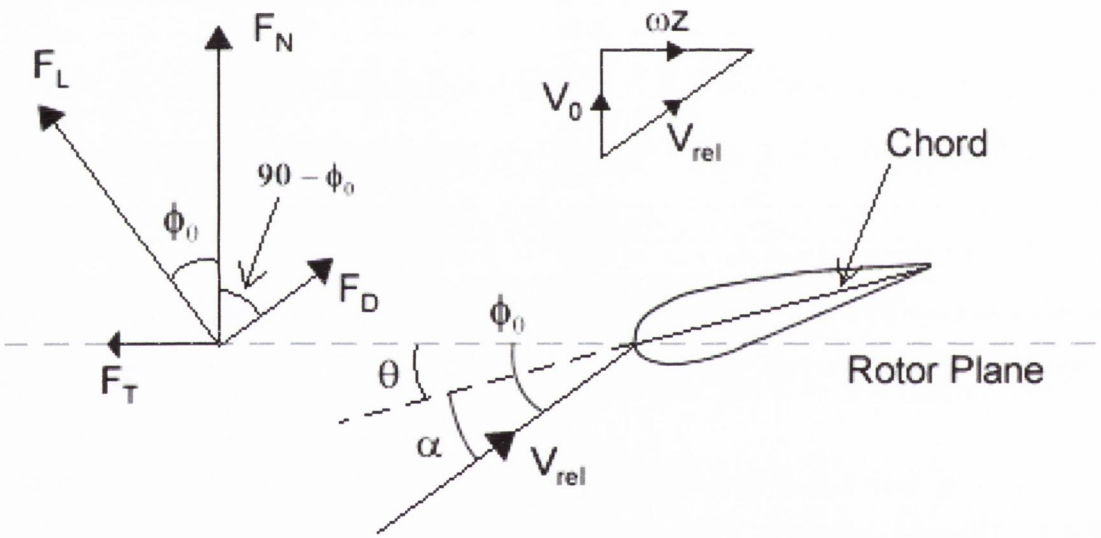

Figure 3.4: Wind forces acting on aerofoil.

wind turbine the interest is primarily focused on the forces acting normal and tangential to the plane of rotation. These are derived as follows (Hansen, 2008):

$$F_N(z,t) = F_L cos(\phi_0) + F_D sin(\phi_0) \tag{3.26}$$

$$F_T(z,t) = F_L sin(\phi_0) - F_D cos(\phi_0) \tag{3.27}$$

where $\phi_0 = \arctan(V_0/(z\Omega))$ is the relative inflow angle of the wind as shown in Figure 3.4.

Using the formulae derived in Equations (3.26) and (3.27) it is possible to establish the generalised blade loading associated with an arbitrary mode n as follows (Clough and Penzien, 1993):

$$P_n(t) = \int_0^R \phi_n(z)\, F(z,t)\, dz \tag{3.28}$$

3.4.2 Wind Modelling

The wind inflow, $V_0 = \bar{V} + V'(t)$ is modelled as a stochastic wind model with a fluctuating component $V'(t)$, as well as a mean component, $\bar{V}$, which includes the effects of wind shear. As the blades rotate about the hub their vertical position above the ground varies periodically. This is significant for large turbines where rotor diameters can extend beyond 100 m and a significant height difference exists between the bottom and top of the rotor arc. The effect of wind shear is accounted for in this case by the log law:

$$\bar{V}(Z) = \frac{1}{k} v_* \ln \frac{z_s}{z_0} \tag{3.29}$$

in which z_s is the height above the ground surface, $\bar{V}(z_s)$ is the mean wind velocity at height z_s, v_* is the friction velocity, k is the Von-Karman constant and z_0 is the roughness length. The periodic height of a point along the rotating blade n relative to the hub is determined by:

$$z_{sh}(t) = z \cos\left(\Omega t + \frac{2\pi}{3}(n-1)\right) \tag{3.30}$$

The fluctuating, or turbulent, wind velocity time-histories, $V'(t)$, are generated using the Discrete Fourier Transform (DFT) method, as detailed by Murtagh *et al.* (2004c). Fourier coefficients are established from a specific Power Spectral Density Function (PSDF) as normally distributed random numbers with zero mean and standard deviation σ_i, where σ_i is equal to the area under the PSDF between the frequency limits f_i and $f_i + df$. The

Kaimal spectrum as specified in Annex B of BS EN 61400-1 (2005) is used in this analysis and it may be represented as follows:

$$\frac{fS_k(f)}{\sigma_k^2} = \frac{4fL_k/V_{hub}}{(1+6fL_k/V_{hub})^{5/3}} \tag{3.31}$$

where $S_k(f)$ is the frequency dependent single sided velocity component spectrum, f is the frequency in Hertz, k is an index referring to the velocity component direction (1 = longitudinal, 2 = transverse, 3 = vertical), σ_k is the velocity component standard deviation and L_k is the velocity component integral scale parameter.

Figure 3.5 presents a sample of a generated wind velocity time-history with a prescribed mean value of zero and standard deviation of 2.29 m/s. This is a typical value for mean wind speeds of 18 m/s with low turbulence characteristics (BS EN 61400-1, 2005). A time step of 0.001 s was employed as this is the time step required by the ordinary differential equation (ODE) solvers to assure convergence of the solution to the two dimensional model. The calculated mean and standard deviation of the resulting time series were 1.5×10^{-16} m/s and 2.25 m/s respectively. This demonstrates the notable accuracy of the method over a short simulation time of 100 s.

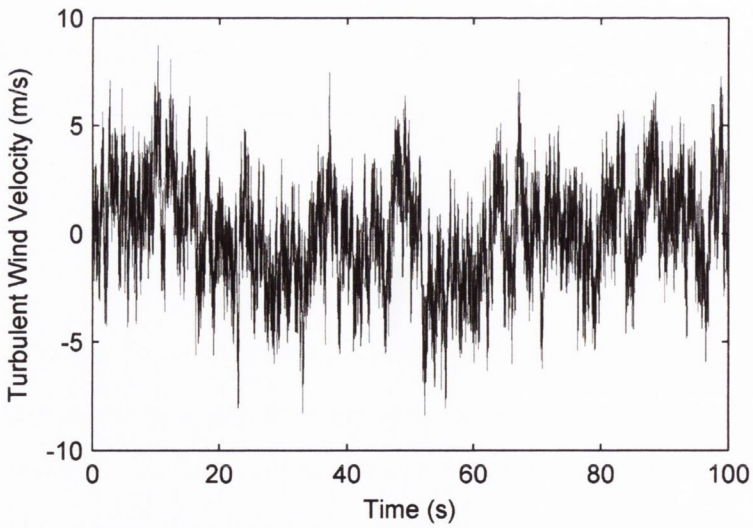

Figure 3.5: Mean-removed wind velocity time-history

BS EN 61400-1 (2005) assumes that the longitudinal turbulence standard deviation σ_1 is invariant with height. This is deemed a valid assumption, having been also implemented by the design standard DNV-OS-J101 (2010) and was demonstrated to have sufficient accuracy by Bowen (2008). The code also suggests that a coherence model be specified to correlate the turbulence effects across the entire rotor. In this instance uniform turbulence is assumed for the blades as the complexity of a coherence model is not necessary for the proposed study.

3.4.3 Tower Wind Loading

The loading on the tower is calculated in a similar fashion to the blades except the coherence of the fluctuating drag force component was taken account of by implementing a formulation proposed by Nigam and Narayanan (1994) and successfully implemented by Murtagh *et al.* (2005b) and Colwell and Basu (2009). This identifies the modal fluctuating drag force power spectrum, $S_{FjFj}(f)$, for a continuous line-like structure, which is discretised into a MDOF dynamic system. It may be formulated as:

$$S_{FjFj}(f) = A\left(C_{D,t}\rho\right)^2 \sum_{k=1}^{K}\sum_{l=1}^{L} S_{VkVl}(f)\bar{v}_k\bar{v}_l\phi_{t,j}(k)\phi_{t,j}(l) \tag{3.32}$$

where A is the transformed area of the structure, k and l are discrete nodes, $\bar{V}_k$ and $\bar{V}_l$ are the mean wind velocities at nodes k and l, while $\phi_{t,j}(k)$ and $\phi_{t,j}(l)$ are the components of the j^{th} modeshape which correspond to nodes k and l respectively. $S_{VkVl(f)}$ is the velocity auto PSDF when $k = l$ and the cross PSDF when $k \neq l$ and may be defined as:

$$S_{VkVl}(f) = \sqrt{S_{V\_kk}(f)S_{V\_ll}(f)}coh(k,l;f) \tag{3.33}$$

where $S_{V\_kk}(f)$ and $S_{V\_ll}(f)$ are the PSDFs at nodes k and l and may be calculated from the following expression proposed by Kaimal *et al.* (1972):

$$\frac{fS_{VV}\left(z_s,f\right)}{v_*^2} = \frac{200n}{\left(1+50n\right)^{5/3}} \tag{3.34}$$

where $S_{vv}(z_s, f)$ is the PSDF as a function of height and frequency and n is given by:

$$n = \frac{f z_s}{\bar{V}(z_s)} \tag{3.35}$$

where $\bar{V}(z_s)$ is the mean wind velocity at height z_s. Equation (3.34) is similar to Equation (3.31) except for the addition of the elevation variable z_s and v_* which is given by Equation (3.29). The coherence function $coh(k, l; f)$ is represented as:

$$coh(k, l; f) = \exp\left[-\frac{|k - l|}{L_s}\right] \tag{3.36}$$

where $|k - l|$ is the spatial separation of the nodes and L_s is a length scale parameter given by:

$$L_s = \frac{\hat{V}_{kl}}{fC} \tag{3.37}$$

with $\hat{V}_{kl}$ being the average of the two mean wind speeds at k and l and C is a decay constant. The modal fluctuating drag force power spectrum may then be used to generate the modal fluctuating drag force time-history for all relevant modes. This is added to the mean component which is calculated as follows:

$$\bar{F}_D(t) = \frac{1}{2} C_{D,t} \rho A \bar{V}^2 \tag{3.38}$$

with the mean modal force then determined by multiplying the result by the relevant modeshapes. Figure 3.6 presents an example of a computed modal drag force time-history for the first mode of vibration. The time-history has a mean value of approximately 6 kN which is equal to the mean modal drag force and it exhibits a Coefficient of Variation (CoV) of approximately 5 % of the mean which is close to the CoV of the wind velocity at the hub (6 % of mean wind speed). The generated time-histories account for the entire tower loading and allow for straightforward implementation in the generalised form of Equations (3.10) and (3.18).

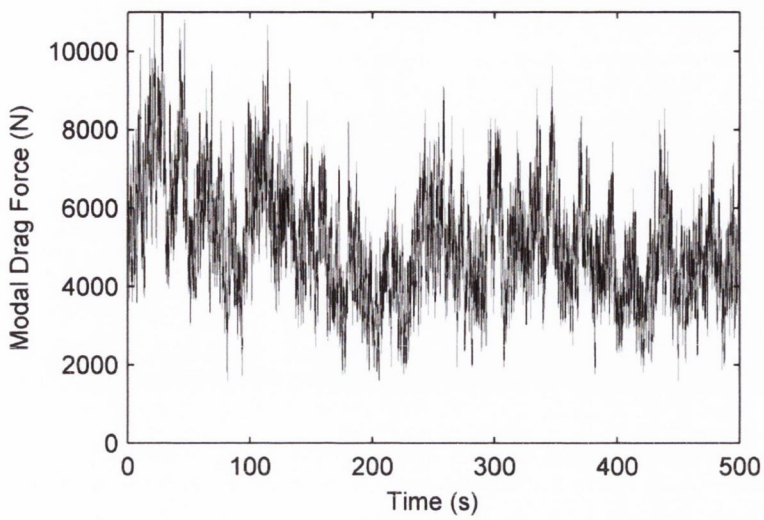

Figure 3.6: Tower modal drag force time-history for first mode.

3.4.4 Earthquake Loading

Until recently the effect of seismic loading on wind turbines was not considered an important aspect of the structural design. With the growing prevalence of wind turbine structures around the globe coupled with their increasing size and associated investment cost, the seismic response of wind turbines has certainly become an important factor. This has consequences for the protection of investments, minimisation of down-time necessary for repairs and maximisation of energy output. This section proposes a method of incorporating the ground motion effects with the dynamic modelling framework outlined in the preceding sections.

The earthquake loading is established from ground motion acceleration time-histories such as illustrated in Figure 3.7 for an earthquake of size 1.1 g. These are either taken from actual recorded earthquake events or synthetically generated from a specified response spectrum. Adapting the procedure outlined by Clough and Penzien (1993) the effective

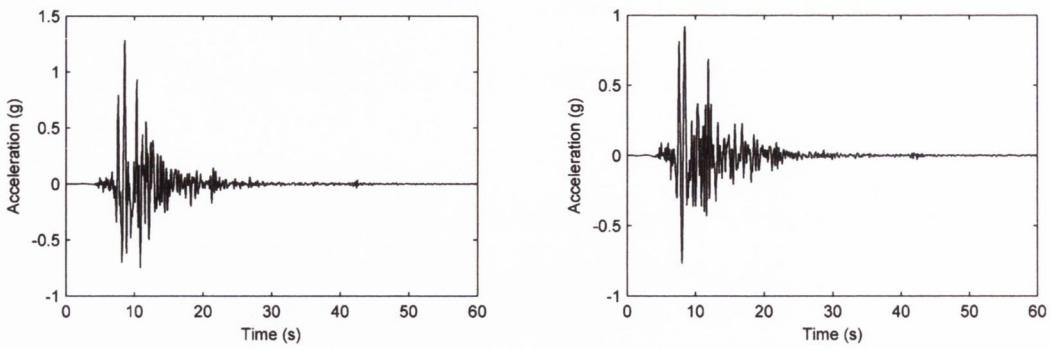

(a) X component.

(b) Y component.

Figure 3.7: Sample earthquake ground motion acceleration time-history.

generalized loading of the tower for an arbitrary mode j can be computed as:

$$P_{t,j} = -\ddot{u}_g(t) \left[\int_0^H m_t(Z)\, \phi_{t,j}(Z)\, dz + M_{top}\, \phi_{t,j}(H) \right] \tag{3.39}$$

where $\ddot{u}_g(t)$ is the recorded or generated earthquake ground motion acceleration and M_{top} is the total mass of the components supported by the tower (blades, nacelle, hub, etc.). Once computed for each mode the generalized earthquake loading may be added to the wind loading components specified in Sections 3.4.1 and 3.4.3.

3.5 Numerical Examples

The dynamic systems outlined in Equations (3.10) and (3.18) may be solved once the equations have been formatted in a state-space formulation with the mass, damping, and stiffness matrices as well as the force vector represented in generalised form. The resulting linear dynamic response is subsequently computed using a Runge-Kutta ODE solver.

A series of numerical examples have been carried out to demonstrate the effectiveness of the dynamic modelling systems. These include both the one and two dimensional model as well as examples incorporating earthquake loading and soil structure interaction. The results of these simulations are discussed in the following sections.

3.5.1 Definition of Test Turbine

For the implementation of the current analytical study a representative multi-megawatt wind turbine has been chosen. The turbine in question is the NREL offshore baseline 5 MW wind turbine which has an equivalent tubular steel tower for onshore installations (Jonkman *et al.*, 2009). The key properties of the turbine are listed in Table 3.1 with further details of structural and aerodynamic properties specified in Appendix C. This

Property	Value
Rating	5 MW
Rotor Diameter	126 m
Hub Diameter	3 m
Hub Height	90 m
Cut-in Wind Speed	3 m/s
Rated Wind Speed	11.4 m/s
Cut-out Wind Speed	25 m/s
Cut-in Rotor Speed	6.9 rpm
Rated Rotor Speed	12.1 rpm
Nacelle Mass	240,000 kg
Rotor Mass	110,000 kg
Blade Material	Glass-fibre
Blade Length	61.5 m
Blade Mass	17,740 kg
Blade CM (From Blade Root)	20.475 m
Blade Damping Ratio (All Modes)	0.48 %

Table 3.1: Key properties of NREL baseline 5 MW wind turbine (Jonkman *et al.*, 2009).

turbine is utilised in all of the simulations carried out as part of the peer reviewed publications included in Appendix D and which are outlined in this thesis. The standard 88 m tubular steel tower, fitted with the nacelle unit, is considered for simulations at the 90 m hub height. A suite of additional towers comprised of prestressed concrete and tubular steel towers of heights from 88 m to 120 m are introduced in due course for the purposes of the comparative analysis.

3.5.2 One Dimensional Model

Figure 3.8 shows a 200 second displacement time-history of the nacelle and blade-tip for a typical simulation with the 88 m steel tower subject to a mean hub height wind speed

of 11.4 m/s, i.e. the rated turbine wind speed. 200 seconds was chosen for the simulation length as this ensures that a steady state response is achieved and it allows sufficient computation time to demonstrate the characteristics of the response. It is clear from both plots that the response shows an initial spike in magnitude but the system shortly settles down to a steady state response. The nacelle displacement response can be seen to oscillate about a mean positive displacement of approximately 0.075 m and after an initial maximum displacement of almost 0.2 m, beyond the 25 second mark the displacement magnitudes are reduced and more consistent. The same can be said for the blade response in Figure 3.8(b). Therefore, in order to base any comparisons on the standard operating response levels, the first 25 seconds of the simulations will be neglected.

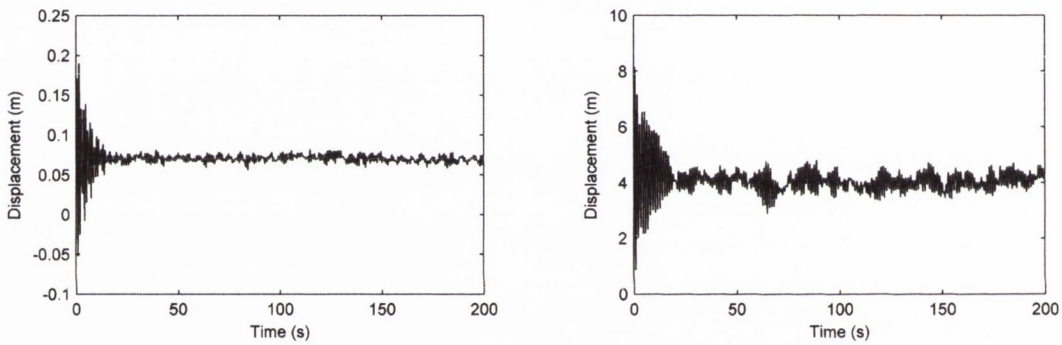

(a) Nacelle displacement.

(b) Blade-tip displacement.

Figure 3.8: Nacelle and blade-tip one dimensional displacement time-history response for 200 second simulation.

The frequency content of the displacement time-history response is assessed to identify the important frequencies at which the tower responds. Figure 3.9 displays a plot of the frequency content following a Fourier Transform of the two displacement time-histories shown in Figure 3.8. These frequency plots are useful in that they allow validation of the performance of the model with respect to the incorporation of the system coupling. They also allow identification of the natural frequencies of the vibrating structural elements. Considering Figure 3.9(a), two main peaks in energy are evident in the plot. The first is at 0.2 Hz which corresponds to the rotational speed of the turbine at rated conditions (0.202 Hz). The next frequency of interest occurs at 0.38 Hz, close to the specified natural

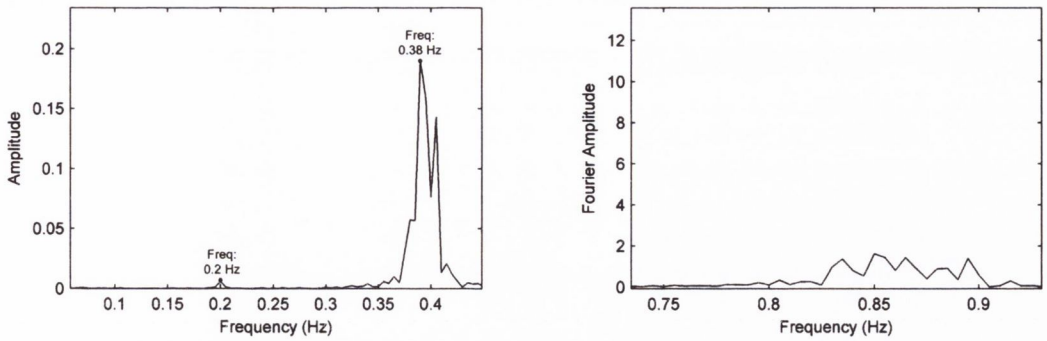

(a) Nacelle frequency response.

(b) Blade frequency response.

Figure 3.9: Frequency content of nacelle and blade one dimensional displacement response.

frequency of the tower (0.33 Hz). The reason for the difference can be attributed to the fact that the one dimensional model does not consider a significant number of the dynamic DOFs. The coupling of nacelle tilt in the system, in particular, would have a considerable effect on the computed natural frequency, effectively lowering the result as will be shown in the two dimensional examples. The frequency response of the blade in Figure 3.9(b) is less clear. Aside from a small peak at the blade rotational frequency (0.2 Hz), the most notable concentration of energy is between 0.77 Hz and 0.93 Hz. This energy concentration coincides with the first natural frequencies of flapwise vibration for the blade, 0.79 Hz and 0.97 Hz. Again, the slight difference in results can be attributed to the limited DOFs associated with the one dimensional model. This confirms that the system is operating correctly as the natural frequencies agree closely with those calculated previously and the coupling of the system is evident as the tower can be seen to exhibit a response coinciding with the rotational speed of the blades.

3.5.3 Two Dimensional Model

The two dimensional structural model and loading systems outlined in the preceding sections output both an eigenvalue analysis of the system modes as well a time-history response of the system to the loading. Table 3.2 exhibits the system natural frequencies for the test turbine with the standard 88 m tubular steel tower configuration. The system natural frequencies produced by the derived model are shown to agree with those com-

Mode	**FAST** (Hz)	**Calculated** (Hz)
1^{st} Tower Longitudinal	0.33	0.33
1^{st} Tower Lateral	0.32	0.32
1^{st} Blade Asymmetric Flapwise Yaw	0.56	0.57
1^{st} Drivetrain Torsion	0.74	0.74
1^{st} Blade Asymmetric Flapwise Pitch	0.88	0.79
1^{st} Blade Collective Flap	0.90	0.97
1^{st} Blade Asymmetric Edgewise Pitch	1.29	1.28
1^{st} Blade Asymmetric Edgewise Yaw	1.68	1.69

Table 3.2: Comparison of specified and computed natural frequencies.

puted by the wind turbine analysis package, FAST (Jonkman, 2012). This verifies that the proposed model sufficiently models the relevant dynamic characteristics of the wind turbine.

Figure 3.10 illustrates a sample displacement response of the nacelle during a 200 second sample simulation at the rated wind speed of 11.4 m/s and the rated rotor speed of 12.1 rpm. The plots include the displacement response for both the along-wind (X) and across-wind (Y) directions as well as the corresponding time-history responses for a simulation carried out using the design code FAST.

In order to gain a realistic perspective of the comparative results, it is first necessary to understand the modelling capabilities of the FAST design code. The primary operating mode of FAST allows the time-marching of the non-linear equations of motion describing the aeroelastic behaviour of a wind turbine structural model. The concept of aeroelasticity, which has long been understood within the aerospace industry, describes how the interaction of structural and aerodynamic effects leads to a non-linear dynamic response. A more detailed description of this phenomenon has already been provided in Section 2.3.4. As a verified design code for use in detailed wind turbine design, FAST is formulated so as to accurately capture this effect. In the case of the one and two dimensional dynamic models derived in the current chapter, aeroelasticity has not be included. Within the context of the objectives of this thesis, the inclusion of aeroelasticity was not deemed necessary. As the focus of the objectives was on the comparative tower response, a high level of detail for the blade model was not required. As long as

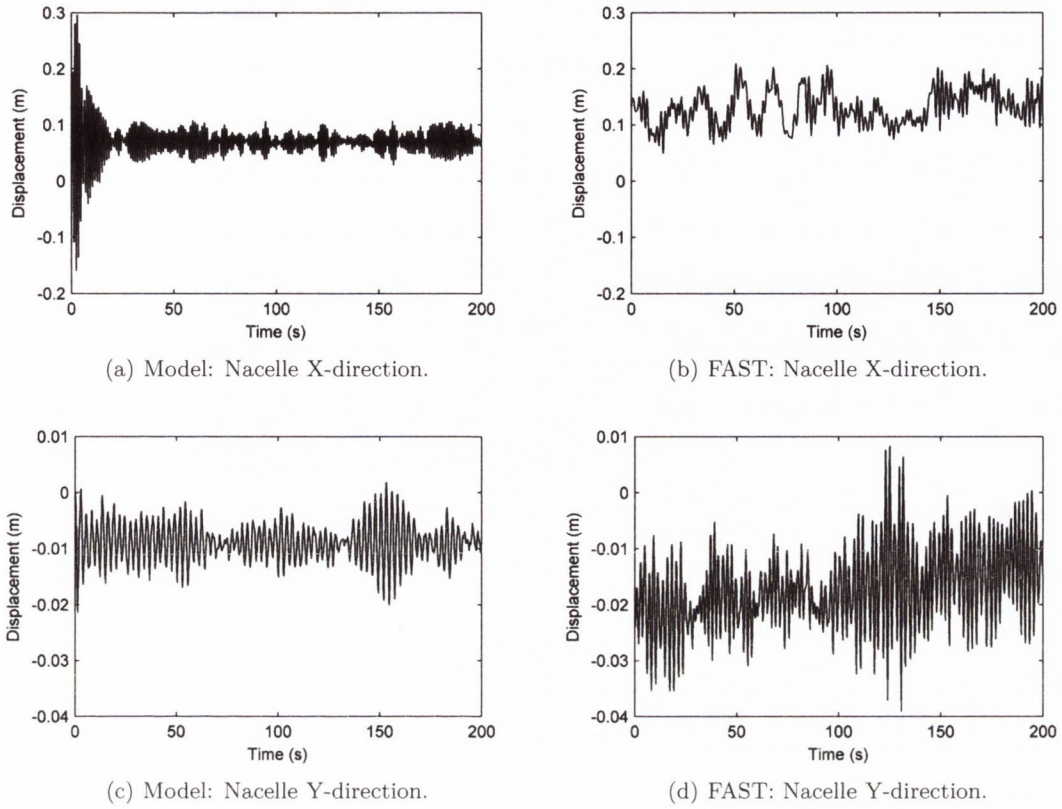

(a) Model: Nacelle X-direction.

(b) FAST: Nacelle X-direction.

(c) Model: Nacelle Y-direction.

(d) FAST: Nacelle Y-direction.

Figure 3.10: Sample two dimensional nacelle displacement time-history response.

the blade model captured the general characteristics of the dynamics and could be applied to both the steel and concrete towers in an equal fashion, then any further model complexity was not required. Previous studies considering wind turbine dynamics have also seen this as an appropriate consideration (Staino *et al.*, 2012; Arrigan *et al.*, 2011; Colwell and Basu, 2009; Murtagh *et al.*, 2005b). Many of these studies even focussed primarily on blade dynamics. In terms of the aerodynamic loading of the system, there are also some differences in the modelling capabilities of the derived models and FAST. FAST utilises the aerodynamic subroutine, AeroDyn (Laino, 2012), to compute the aerodynamic loads on the rotor. By interfacing with the structural model to provide updated velocities and positions, AeroDyn computes the aerodynamic loads on individual blade elements. The subroutine uses either BEM or GDW to incorporate the wake effects into the aerodynamic calculations. It also has the capabilities of including blade tip-loss, hub-

loss, skewed wake, tower shadow as well as dynamic stall using a Baddoes-Leishman stall model. All of these effects have already been discussed in Section 2.3.4. For the purposes of a detailed dynamic analysis as part of a wind turbine design procedure all of these complex aerodynamic considerations are required. However, in the case of the current thesis and the peer reviewed publications in Appendix D, the same level of detail is not deemed necessary. Simplified blade element theory is utilised and the effects of tip losses, wake effects and aerodynamic stall are not included. Incorporation of these effects in the derived models would have required considerable effort that would have altered the focus from the primary objectives of the thesis. Finally, on the topic of wind modelling, there are a number of differences which must be highlighted. The FAST-AeroDyn interface utilises a stochastic, full-field, turbulent wind simulator called TurbSim (Kelley and Jonkman, 2012) to generate the representative turbulent wind inflow. This provides a numerical simulation of a full-field flow that contains coherent turbulence structures that reflect the proper spatiotemporal turbulent velocity field relationships. The primary difference between the FAST wind modelling and that utilised in the derived models relates to the generation of coherent turbulence structures. The derived models utilise a stochastic turbulence generation procedure which creates random variations in the wind velocity independently at each location and at each time step based on the turbulence spectrum. This does not take account of the spatiotemporal characteristics of turbulent structures in which the wind gusts or turbulence at a single point is related to the wind velocity at spatial points around it as well as the wind velocity at the previous and future time steps. While this procedure is not completely representative of the actual turbulent behaviour of the wind inflow, it does introduce stochastic characteristics to the aerodynamic loading which is a requirement of any probabilistic analysis routine.

The simulation highlighted in Figure 3.10 was implemented for the rated wind speed of the turbine, employing the BS EN 61400-1 (2005) specified NTM. Although the FAST model incorporates considerably more sophisticated structural, aerodynamic and wind modelling procedures than those employed in the derived model, there still exists a no-

ticeable degree of accuracy between the two models. Considering Figure 3.10(a) and 3.10(b), the mean displacement is seen to be 0.08 m and 0.129 m respectively. The range of displacements for the derived model, excluding the first 25 seconds, is between 0.028 m and 0.108 m with the FAST model exhibiting slightly larger displacements. A difference evident in the plots is the existence of coherent turbulence structures in Figure 3.10(b). A clear pattern of displacements about the mean related to the spatiotemporal characteristics of the gusts is present whereas in Figure 3.10(a) there is simply a random variation about the mean. This can be attributed to the more sophisticated turbulence generation procedure employed by the verified design code. For the case of the lateral tower motion, the nacelle displacements illustrated in Figure 3.10(c) and 3.10(d) again display similar characteristics. Excluding the first 25 seconds, the derived model has a mean response of -0.009 m, which compares to a larger -0.018 m mean response for the FAST model. The presence of coherent turbulence structures are not evident in this instance but the magnitude of the variation of the displacement from the mean is greater for the FAST model. This can be related to the inclusion of lateral and vertical turbulence in the verified design code which was not considered in the derived models.

Figure 3.11 presents another set of comparable plots for the blade response. Again reasonable agreement is established in the results. Focussing on the flapwise blade displacement, Figure 3.11(a) and 3.11(b), there are respective mean displacements of 3.904 m and 4.199 m. The FAST model exhibits larger deviations from the mean value of up to 3.038 m whereas the derived model deviates by a maximum of 1.235 m, excluding the initial 25 seconds. The presence of coherent turbulence structures is once again evident with a distinct pattern in Figure 3.11(b) whereas the more simple random deviations from the mean are present in Figure 3.11(a). The accuracy of the edgewise blade vibration response is not quite as evident. While both exhibit negative displacements, the derived model has a mean value of -0.117 m which compares to -0.395 m for the FAST model. The deviations from the mean value are also noticeably larger for the FAST model. The effects of lateral and vertical turbulence are most certainly

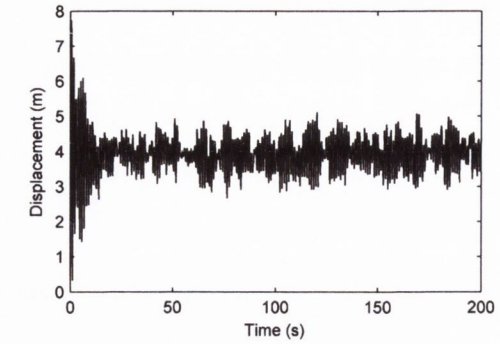

(a) Model: Blade X-direction.

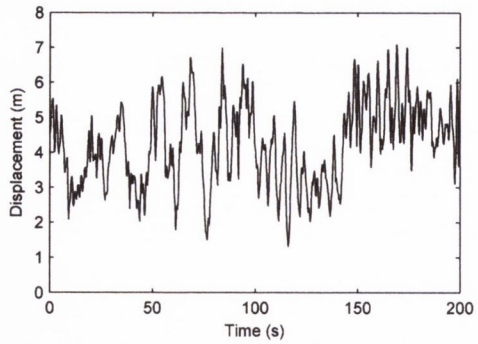

(b) FAST: Blade X-direction.

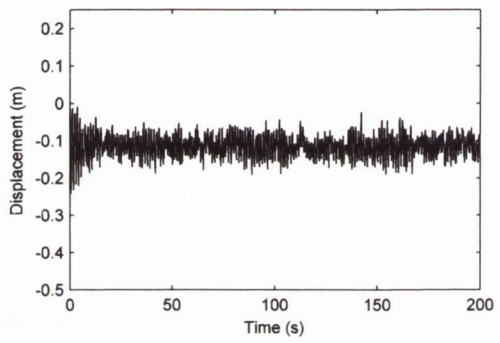

(c) Model: Blade Y-direction.

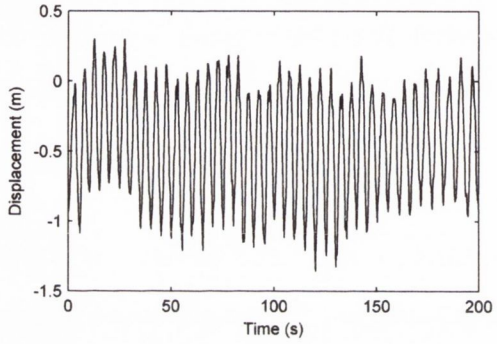

(d) FAST: Blade Y-direction.

Figure 3.11: Sample two dimensional blade-tip displacement time-history response.

at least partly responsible for the difference in response. Another contributor to the variation in values is the level of detail in the generator and drivetrain representations. While the derived model incorporates the drivetrain torsional flexibility and rotational inertia, the FAST model includes a much more detailed consideration of these effects which also takes into account the generator torque and gearbox efficiency. The connection of the generator and drivetrain to the rotor ensures a coupling of these responses with the edgewise blade vibrations and therefore implies that they will affect their mutual responses. Despite the differences in responses, the derived model is shown to have considerable accuracy compared to a verified wind turbine model, particularly for the tower response and this is the most vital aspect for the proposed investigations.

When the frequency content of the time-histories outlined in Figures 3.10 and 3.11 is

analysed the dominant frequencies can be seen to match up with the calculated natural frequencies in Table 3.2. This is illustrated in Figure 3.12 where the frequency content of the tower and blade responses in the X direction are plotted. For the case of the tower,

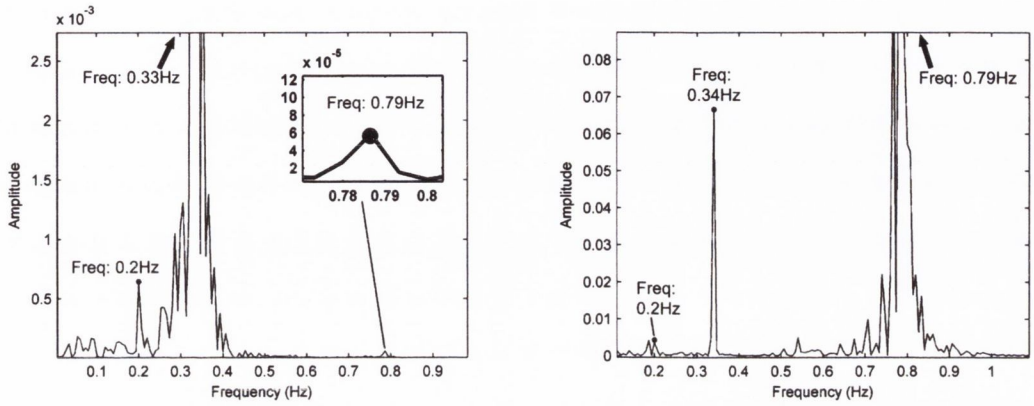

(a) Tower (X direction).

(b) Blade (X-direction).

Figure 3.12: Frequency content of two dimensional tower and blade displacement response.

Figure 3.12(a), the dominant frequencies are seen to be 0.2 Hz, the rotational frequency of the rotor, and 0.33 Hz, the first longitudinal natural frequency of the tower. The actual peak of the later frequency is not visible within the scale of the plot due to the disproportionate amount of energy centred under this peak. Another isolated peak is visible at 0.79 Hz, which corresponds to the first blade asymmetric flapwise pitch frequency. The flapwise blade frequencies in Figure 3.12(b) exhibit peaks at 0.2 Hz, 0.34 Hz, close to the longitudinal tower frequency (0.33 Hz), and a range of peaks between 0.5 and 1.0 Hz which encompass the three flapwise natural frequencies of the blades. The most prominent peak in this range is at 0.79 Hz, the first blade asymmetric flapwise pitch frequency. Again, due to the amount of energy corresponding to this frequency its peak is beyond the scale of the plot.

3.5.4 Seismic Loading

Figure 3.13 illustrates a sample displacement response for the nacelle during a simulated earthquake event. The particular earthquake applied during the simulation is that illustrated in Figure 3.7 which has a resultant maximum acceleration of 1.1 g. The beginning

of the acceleration time-history is delayed until 60 seconds into the simulation. It then takes approximately 5 seconds for the increased accelerations to commence. Prior to the earthquake event initiation, between 25 and 60 seconds into the simulation, the nacelle can be seen to exhibit controlled vibration within the range of about 0.15 m in the longitudinal direction and with considerably lower magnitudes in the lateral direction. This is a result of the wind loading on the structure caused by a mean hub-height wind inflow at the rated turbine wind speed. Once the earthquake commences the displacements grow significantly with maximum displacements of approximately 0.7 m from the neutral position. As the earthquake recedes the system damping brings the displacements back to normal operating levels by about the 100 second mark.

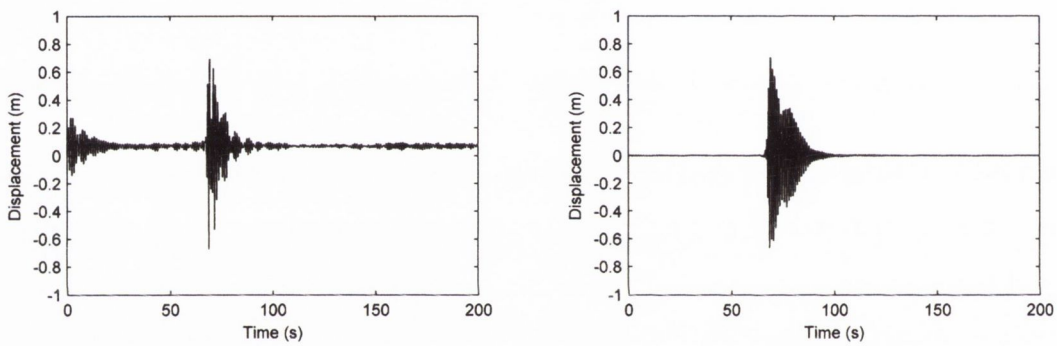

(a) Longitudinal response.

(b) Lateral response.

Figure 3.13: Sample seismic displacement response of nacelle in both lateral and longitudinal directions.

3.5.5 Inclusion of SSI

In order to simulate the effects of SSI on the overall system dynamics, it is first necessary to specify a foundation design and identify appropriate values for the structural properties of the soil structure interface. The considered foundation is a reinforced concrete slab of dimensions 14 m by 14 m in plan and having a depth of 2 m. The essential structural input properties derived from an FE analysis of the foundation on a stiff sand are summarised in Table 3.3. A further discussion of this particular foundation design is presented in Chapter 6.

Property	Value	Units
Foundation Mass	9.6×10^5	(kg)
Rotational Stiffness (about X-axis)	339	(GNm/rad)
Mass Moment of Inertia (about X-axis)	16×10^6	$(kg.m^2)$
Rotational Stiffness (about Y-axis)	339	(GNm/rad)
Mass Moment of Inertia (about Y-axis)	16×10^6	$(kg.m^2)$
Lateral Stiffness (X-direction)	839	(MN/m)
Lateral Stiffness (Y-direction)	839	(MN/m)

Table 3.3: Key properties of sample foundation.

Figure 3.14 illustrates a sample displacement response for both the nacelle and blade-tip during a 200 second sample simulation at the rated wind speed of 11.4 m/s and the rated rotor speed of 12.1 rpm, including the soil stiffness properties detailed in Table 3.3. In Figures 3.14(a), 3.14(b) and 3.14(c), an initial spike in displacement is evident at the beginning of the simulation. After approximately 25 seconds, the system has reached a

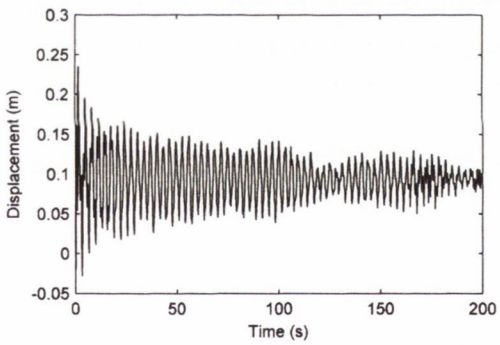

(a) Longitudinal tower response.

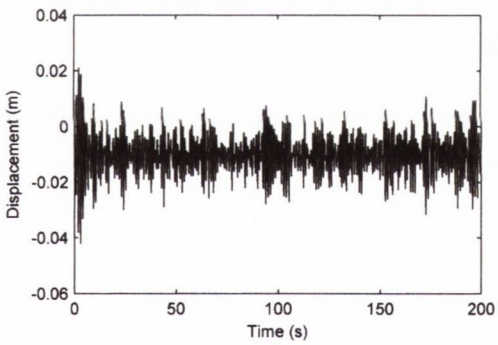

(b) Lateral tower response.

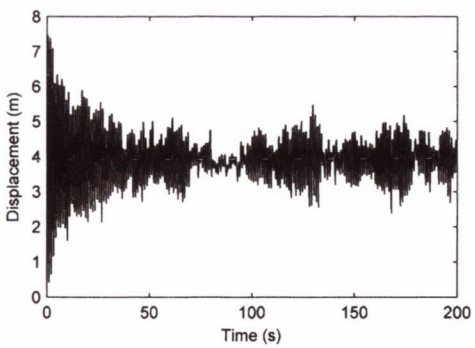

(c) Flapwise blade response.

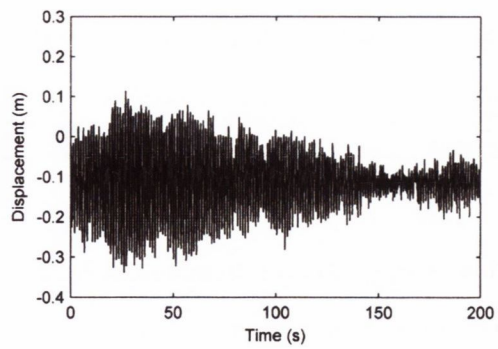

(d) Edgewise blade response.

Figure 3.14: Sample two dimensional time-history response with SSI effects.

steady state. The plots include the displacement response for both the along-wind (X) and across-wind (Y) directions. In Figure 3.14(a) the longitudinal tower response is shown, with a mean value of 0.093 m, slightly larger than the 0.08 m mean value achieved for a simulation without the inclusion of SSI (Figure 3.10(a)). Harte *et al.* (2012) achieved similar results with the longitudinal tower response increasing as the soil stiffness decreased. While the mean values are close, there is a noticeable difference in the characteristics of the response. Excluding the first 25 seconds, the response shown in Figure 3.14(a) varies over a range of 0.03 m to 0.15 m, whereas for the standard response, in Figure 3.10(a), the range is 0.028 m to 0.108 m. Again, this is not a significant difference, but for the case of the SSI simulation, the response is consistently fluctuating within this range but the standard response exhibits generally lower displacements with only a limited number of displacements coming close to the maximum range. Figure 3.14(b) illustrates a sample displacement response for the tower in the lateral direction. The mean value of the response is -0.011 m which compares to a mean for the standard response -0.009 m. Again, although minimal difference exists between the mean response values, the range of displacements throughout the simulation is larger. For the SSI simulation, the response varies between -0.03 m and 0.01 m, excluding the initial 25 seconds. In the case of the standard response, the range varies between -0.02 m and 0.002 m.

With respect to the blade response, Figures 3.14(c) and 3.14(d), a similar trend is evident. With mean values of 3.896 m and -0.116 m for the flapwise and edgewise vibrations including SSI respectively, there is minimal deviation from the mean values of the standard responses of 3.904 m and -0.117 m (Figures 3.11(a) and 3.11(c)). What is evident is the greater range of magnitudes displayed in the SSI response and the consistency of blade displacements between these magnitudes.

Figure 3.15 presents the frequency content of the time-histories outlined in Figures 3.14(a) and 3.14(c). Focussing on Figure 3.15(a) which displays the frequency content of the tower response, three main peaks are evident. Similar to the other frequency response plots, the first peak, at 0.2 Hz, coincides with the rotational speed of the blades. The second peak indicates that the tower natural frequency has reduced from 0.33 Hz to

0.315 Hz and the third peak shows an increase in the blade flapwise natural frequency from 0.79 Hz to 0.9 Hz. This is reflected in Figure 3.15(b) which illustrates a single dominant peak at 0.9 Hz for the frequency content of the blade flapwise response.

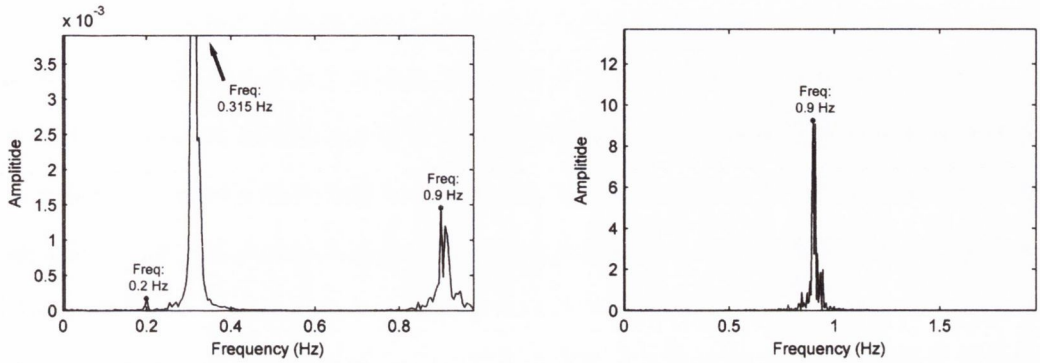

(a) Tower (X-direction).

(b) Blade (X-direction).

Figure 3.15: Frequency content of two dimensional tower and blade displacement response incorporating SSI.

It should be noted that the soil properties used in these simulations are for a relatively dense sand which relates to significantly high horizontal and rotational stiffness values. This would have the effect of limiting the influence of the SSI on the resulting response.

3.6 Conclusion

Following on from the extensive discussion of wind turbine dynamic analysis techniques in Section 2.3.4, the current chapter presented a description of the dynamic modelling framework employed in this thesis. This included a description of the underlying theory and assumptions made, an outline of the derivation of the dynamic equations of motion as well as a series of examples demonstrating the implementation of the modelling framework and verifying the validity of the output results.

Both a one and two dimensional model were developed using a Lagrangian formulation. This facilitated the derivation of the dynamic equations of motion through the quantification of both the kinetic and potential energy of the dynamical system and the subsequent application of the Euler-Lagrange equation. This particular formulation ensured that all elements of dynamic coupling inherent to the system would be systematically incorpor-

ated in the equations of motion once they have been included in the initial specification of potential and kinetic energy.

The one dimensional model considered the motion of the system in the along-wind dimension only. This includes the flapwise vibration of the blades and the longitudinal motion of the tower. A modal representation of the flexible bodies was implemented where the motion of the components is described by the summation of a set of predefined modeshapes and corresponding temporal modal coordinates. The effect of blade rotation on its resulting stiffness, known as centrifugal stiffening, was also accounted for within the potential energy definition. The two dimensional model expanded on the initial model by incorporating a number of additional DOFs. These included edgewise blade vibration, lateral tower motion, nacelle tilt, roll and yaw as well as rotor shaft torsion. The resulting model was therefore capable of capturing the dynamic response of a wind turbine in both the along-wind and across wind dimensions. Extensions to this model were developed in order to include the effects of soil structure interaction (SSI) on the overall system dynamics. This was achieved through the addition of four DOFs which include foundation translation in both the X and Y directions as well as foundation rotation about axes in either direction.

The subsequent sections focused on the structural loading of the system. This included a detailed description of the aerodynamic loading characteristics of a rotating aerofoil element as well as a description of a method to construct turbulent wind loading time-histories. A specific procedure for the generation of coherent modal wind loading on the tower element was also proposed. The next step was to extend the loading capabilities of the model to include seismic ground motions. Utilising recorded or synthesised ground motion acceleration time-histories, a methodology for calculating the resulting generalised loading on the wind turbine system was identified.

Following the derivation of the series of dynamic models, a number of sample simulations were conducted to verify the modelling procedure and assess the accuracy of the resulting responses. In order to facilitate these simulations, a standard multi-megawatt wind turbine was prescribed. Firstly, a 200 second simulation was presented for the one dimensional model employing a wind loading of 11.4 m/s, the rated wind speed for the

turbine. The displacement response time-histories for both the nacelle and blade-tip were plotted. The initial large deflections at the beginning of the simulation were highlighted and a suggestion to eliminate the first 25 seconds from any further analysis was proposed in order to ensure all comparisons are made with steady state responses. Upon examining the frequency content of the time-histories it was possible to identify the natural frequencies of the tower and blades as well as the rotational speed of the turbine. Considering the extent of the one dimensional model, these were noted to be sufficiently close to the verified values. Another example was presented for the two dimensional model, again for the prescribed rated wind speed for the turbine. The results illustrated included both the X and Y nacelle displacements as well as the flapwise and edgewise blade displacement response. These were compared against the response time-histories from an equivalent simulation using the verified wind turbine design code FAST. The results showed close agreement considering the significantly greater complexity of the FAST aerodynamic loading and wind generation procedures as well as its additional computational capabilities. The next example demonstrated the system response with the inclusion of an earthquake event. This highlighted the capability of the model to incorporate a seismic event with the standard operating conditions. Finally, a sample simulation was conducted with the two dimensional model incorporating the additional SSI DOFs. Soil stiffness values were assigned based on a foundation design detailed in Chapter 6. Plots of the lateral and longitudinal tower vibration as well as the flapwise and edgewise blade response were included. These showed the similarity in mean response values as compared to the previous simulations which assumed a fixed support at the tower base. However, there was a noticeable difference observed in the magnitude and consistency of the vibrations with the SSI model responses tending to deviate more from the mean position and there was a higher frequency of large vibrations. In assessing the frequency content of these displacement response time-histories, it was observed that the natural frequency of the tower, 0.315 HZ, was reduced from its value for a tower with fixed base, 0.33 Hz. It was also shown that the flapwise blade natural frequency was increased from 0.79 Hz to 0.9 Hz.

This chapter outlined the modelling procedure to be employed in the relevant analyses

as part of this thesis. The proposed models incorporate a significant degree of dynamic complexity and were shown to perform well compared to a certified wind turbine design code. The following chapters will detail the implementation of these models in a series of analyses which compare the dynamic performance of prestressed concrete wind turbine towers with their tubular steel counterparts.

Chapter 4 -

Fragility Comparison of Wind Turbine Tower Structures

4.1 Introduction

As discussed in Chapter 2, wind turbine tower design has received greater attention in recent years as the trend for larger multi-megawatt turbines and taller hub heights dominates the state of the art in the industry. Enercon currently possess the world's largest wind turbine, the E-126 (ENERCON, 2010a), which is rated at 7.5 MW and sits at a hub height of 135 m. This progress towards larger turbines supported by taller towers has highlighted a number of downsides to the traditional tubular steel solution. Hau (2006) highlighted the serious manufacturing difficulties with steel tower sections for tower heights beyond 90 m, while Harte and Van Zijl (2007) stated that steel tubular towers are no longer able to balance the vibration excitation beyond a height of 85 m. A further constraint is that the transportation of the lower tower sections by road is no longer feasible in many cases. In Ireland, for example, road traffic regulations specify that the maximum overall height of a vehicle may not exceed 4.65 m (Dempsey, 2008), which is unavoidable for the steel sections required for tower heights of 90 m and above. Similar restrictions exist for most other European countries. Another aspect of steel towers at these ever increasing heights is their suitability from an economic and structural performance perspective. In view of similar structural engineering applications such as suspension and cable-stayed bridge towers it is evident that prestressed concrete and/or hybrid assemblies present an alternative, and often more optimal structural solution for heights exceeding 100 m (Virlogeux, 2006). In

fact, the Enercon E-126 incorporates a hybrid solution of prestressed concrete and traditional tubular steel. Additional authors such as Tricklebank *et al.* (2007) and Singh (2007) have focussed on concrete's ability to overcome the obstacles facing steel towers. These include its versatility in terms of construction method and transportation, the ability to easily tune its structural properties to particular requirements through optimising the mix design and pre-stressing characteristics as well as the longer service life achievable with concrete allowing the possibility of supporting multiple turbines throughout its design life.

The primary objective of this thesis is to investigate structural performance of prestressed concrete and tubular steel towers for a range of heights representative of current and future multi-megawatt applications. In light of this, the current chapter, building on the theoretical formulations developed in Chapter 3, initialises this analysis through two studies. In the first instance, the one dimensional model outlined in Section 3.2 is employed to consider onshore turbine installations, i.e. excluding hydrodynamic effects, evaluated under varying degrees of turbulent wind loading for a series of typical hub heights. The standard turbine specified in Section 3.5.1 is applied in each simulation. A probabilistic approach is established in characterising the structural input properties of the towers, the environmental parameters and in assessing, in a realistic sense, the resulting response. Following the identification of a displacement-based limit-state, the performance of the various tower configurations is illustrated by means of fragility curves. These illustrate the probabilistic characteristics of LSE as a function of the loading conditions, which in this case is the turbulent wind loading.

The second study investigates the effect of the choice of tower construction material on the resulting dynamic response of the blades. This is a particularly relevant issue given the susceptibility of wind turbine blades to fatigue damage from the high level of vibrations present in a wind turbine system. The previously developed modelling framework in Chapter 3 allows for the output of blade response time histories, thus providing the necessary tools to carry out the study. The effect of tower construction material on wind turbine blade response has not previously been addressed in the literature, to the best of

the author's knowledge. If it can be shown that a reduction in the magnitude of blade response is achievable by using alternative tower configurations, this study could prove of great benefit to the future design of wind turbine systems. The investigation effectively examines the comparative response of wind turbine blades which are connected to the nacelle units supported by either tubular steel or prestressed concrete towers. The two dimensional model derived in Section 3.3 is utilised to compute dynamic time-history responses. These are generated at a variation of hub heights and for a series of mean hub height wind speeds up to the turbine cut-out wind speed. Once again a probabilistic framework is established for the characterisation of the structural and environmental properties. The construction of fragility curves with a pre-defined limit-state is also employed as a means of illustrating the probabilities of LSE and consequently facilitating a comparison of structural performance. The implementation of these proposed studies as well as a description of the results and conclusions are presented in the following sections.

4.2 One Dimensional Tower Comparison

Following on from the peer reviewed publication of the paper detailed in Appendix D, this section describes an investigation into the performance of tubular steel and prestressed concrete tower solutions for a selection of heights and wind speeds by means of a flapwise numerical model. For each case, elements of the baseline 5 MW wind turbine, outlined in section 3.5.1, are used to model the components supported by the tower. The one-dimensional dynamic model is employed to compute the structural response. The analysis is performed for a range of typical tower heights from 88 - 120 m. Both steel and concrete towers are specified for each height. A displacement based limit-state was chosen as this reflects the stability of the tower structure and its ability to resist the prescribed loading conditions. This facilitated a comparison of the relative performance of the chosen suite of tower solutions using fragility curves which relate the probability of LSE for the towers to the incident wind loading conditions.

4.2.1 Steel Towers

Three tower heights are considered. The NREL 5 MW baseline onshore wind turbine tower (Jonkman *et al.*, 2009) is specified for the 88 m tower height, with a resulting hub-height of 90 m. The 103 m tower for the Vestas V-90 3 MW wind turbine (Vestas, 2004, 2005) is scaled up to accommodate the additional mass of the 5 MW turbine unit, for an overall hub height of 105 m. Due to a lack of specification for the Vestas tower a number of properties and dimensions are assumed based on the available material, as detailed in Appendix E.1. A third tower of 120 m, which is close to the current maximum height of state of the art prototype multi-megawatt wind turbines, is considered with a resulting hub height of 122 m. The properties of this tower are estimated from a scaling of the properties of the other two towers as no material was sourced for steel towers of this height. In all cases the tower diameter and steel thickness is assumed to taper linearly from bottom to top. Details of the key tower properties are outlined in Table 4.1. Further information on the tower proper-

Property	**88 m Tower**	**103 m Tower**	**120 m Tower**
Height	87.6 m	103 m	120 m
Base Diameter	6 m	7.2 m	8.43 m
Base Steel Thickness	0.035 m	0.041 m	0.048 m
Top Diameter	3.87 m	3.87 m	3.87 m
Top Steel Thickness	0.025 m	0.025 m	0.025 m
Young's Modulus	Table 4.4	Table 4.4	Table 4.4
Steel Density	Table 4.4	Table 4.4	Table 4.4
Total Mass	356,620 kg	535,850 kg	798,640 kg
Location of CM (Above Base)	35.967 m	39.2 m	43.042 m
Tower Damping Ratio (All Modes)	1%	1%	1%

Table 4.1: Key properties of steel towers

ties as well as any assumptions made are provided in Appendix E. It should be noted that for each tower, the base diameter significantly exceeds 4.5 m and would, therefore, make them unsuitable for transport by road and notably difficult to manufacture. This, however, could possibly be overcome by employing a friction jointed tubular steel solution. Also, following the emergence of a similar suite of tower structures in a publication by Engström *et al.* (2010), Appendix E.3 provides a validation of the studied towers

against these similar towers. It also addresses the possible affects on the analyses produced in this thesis as a result of the assumptions made in specifying the tower properties.

4.2.2 Concrete Towers

There is a lack of information in the literature relating to details of concrete wind turbine towers. This is due to the relatively recent emergence of prestressed concrete towers as an alternative to the more familiar steel towers. Therefore, in order to address heights equivalent to the steel tower heights it was decided to use the same base and top diameters as well as concrete thicknesses for the two larger towers as for the 88 m tower, for which some basic properties were acquired. It is obvious that in reality this would not be the case and larger towers would utilise more optimised structures, but in this instance any interpolation of tower properties to taller hub heights could not be verified by published material at the time the analysis was undertaken. As a consequence of this decision, any results which are generated from simulations of these towers must be interpreted in the context of the tower properties. In reality, it would be expected that a stiffer structure would be employed, thus increasing the structure's flexural resistance. Since this investigation was carried out, a source of information on prestressed concrete towers of a similar size became available (Engström *et al.*, 2010). Akin to the steel towers, Appendix E.3 provides a validation of the studied towers against these similar towers which were designed as part of a cost comparison of various tower configurations. It also addresses the possible influences of the assumptions made in establishing the tower properties on the analysis results.

The studied towers are assumed to have a circular cross-section the diameter of which tapers linearly from bottom to top, as with the steel towers. The concrete thickness is assumed to be constant throughout the height of the structure. The assumption is also made that the concrete structure is designed to Class 1 prestressed specifications. This means that it is not necessary to account for the effects of concrete cracking and the resulting non-linear response. Details of the key concrete tower properties are outlined in

Table 4.2. As well as for the steel towers, further information on the tower properties and assumptions made are provided in Appendix E. For the purposes of this study the concrete

Property	88 m Tower	103 m Tower	120 m Tower
Height	87.6 m	103 m	120 m
Base Diameter	8.2 m	8.2 m	8.2 m
Top Diameter	4.8 m	4.8 m	4.8 m
Concrete Thickness	0.25 m	0.25 m	0.25 m
Young's Modulus	Table 4.4	Table 4.4	Table 4.4
Steel Density	Table 4.4	Table 4.4	Table 4.4
Total Mass	1,053,500 kg	1,258,500 kg	1,466,300 kg
Location of CM (Above Base)	37.95 m	44.34 m	51.66 m
Tower Damping Ratio (All Modes)	1%	1%	1%

Table 4.2: Key properties of concrete towers

towers considered represent a baseline to more realistic towers as shown in Appendix E.3. This, in itself, will provide a means of comparing performance to the specified steel towers.

An important aspect of the analysis of the towers described above is to take appropriate consideration of the influence of the prestressing forces applied. The effect of prestress force on the dynamic performance of prestressed concrete elements is a topic which has been widely debated. A detailed discussion of this debate is provided in Section 2.5.5. A primary conclusion of this discussion is that for practical ranges of prestress force, the impact on the member's stiffness properties is negligible. Consequently, it is considered appropriate to discount the prestress force from the tower model and employ linear elastic beam theory in the analysis.

4.2.3 Model Implementation

Six mean hub-height wind speed values have been chosen as outlined in Table 4.3. The values specified lie within the normal operational range of multi-megawatt wind turbines, with 25 m/s being the usual cut-out wind speed (Jonkman *et al.*, 2009; Vestas, 2005, 2004). This allows for an analysis of structural performance within the context of normal wind turbine operation. The lower limiting value of 16 m/s was chosen following a series of preliminary simulations which indicated that, below this wind speed, the maximum turbine response did not approach the prescribed limit states and, therefore, would not affect the

eventual results. In modelling the wind turbulence for the blades, the longitudinal wind

Mean Hub-Height Wind Speed, $\bar{V}$(m/s)		16	18	20	22	24	25
σ_1 (m/s)	**Low Turbulence**	2.11	2.29	2.47	2.65	2.83	2.92
	Medium Turbulence	2.46	2.67	2.88	3.09	3.30	3.41
	High Turbulence	2.82	3.06	3.30	3.54	3.78	3.90

Table 4.3: Turbulence standard deviation at mean hub-height wind speeds

speed standard deviation as required by Equation (3.31), is given by a formula in BS EN 61400-1 (2005), as:

$$\sigma_1 = I_{ref}\left(0.75\bar{V}_{hub} + b\right) \tag{4.1}$$

which accounts for a reference turbulence intensity I_{ref} and the mean wind speed at the hub height $\bar{V}_{hub}$. The reference turbulence intensity is specified based on whether the wind environment has low, medium or high turbulence characteristics. b is simply a constant equal to $5.6\,m/s$. In the case of the tower, the turbulence standard deviation is based on the friction velocity v_* which is a site specific parameter calculated from Equation (3.29). As friction velocity is dependent on the mean wind speed at the hub-height, which is a variable in this study, only the values for σ_1 are specified for the varying mean hub-height wind speeds in Table 4.3.

The variables employed in the simulations, as characterised in Table 4.4, are considered random variables with specified Probability Density Function (PDF) and CoV, excluding model uncertainty. Sample distributions of the modulus of elasticity (lognormally distributed) and density of concrete (normally distributed) are presented in Figure 4.1. The values assigned to these variables are taken from previous research and design standards as referenced in Table 4.4. These values are subsequently implemented as part of a Monte Carlo simulation in order to generate batches of variables within the required statistical distributions. Following on from this, the batches are used for individual simulations, therefore providing discrete responses. Once combined with the other responses, the results form the probabilistic characteristics of the structural system and can be illustrated with the aid of fragility curves. A value of 1.2 is specified for the drag coefficient C_d of both towers based on their cylindrical shape (Simiu and Scanlan, 1996).

Tower Material	Variable	Dimension	PDF	Mean (μ)	C.O.V (%)	Ref.
Steel	E_s (Young's Modulus)	(GPa)	LN	210	3	(Jonkman *et al.*, 2009; Vrouwenvelder, 1997)
	ρ_s (Density)	(kg/m^3)	N	8500	1	(Jonkman *et al.*, 2009; Vrouwenvelder, 1997)
	t_s (Thickness)	(mm)	N	varies	2	(Vrouwenvelder, 1997)
Concrete	E_c (Young's Modulus)	(GPa)	LN	26	23	(Kong and Evans, 1987)
	ρ_c (Density)	(kg/m^3)	N	2450	4	(Vrouwenvelder, 1997)
	t_c (Thickness)	(mm)	N	varies	2	(Vrouwenvelder, 1997)
General	ρ_{air} (Air Density)	(kg/m^3)	-	1.225	-	(BS EN 61400-1, 2005)
	k (Von-karman Constant)	-	-	0.35	-	(Businger *et al.*, 1971)
	z_0 (Roughness Length)	-	-	0.05	-	(Hau, 2006)

Table 4.4: Model input variables

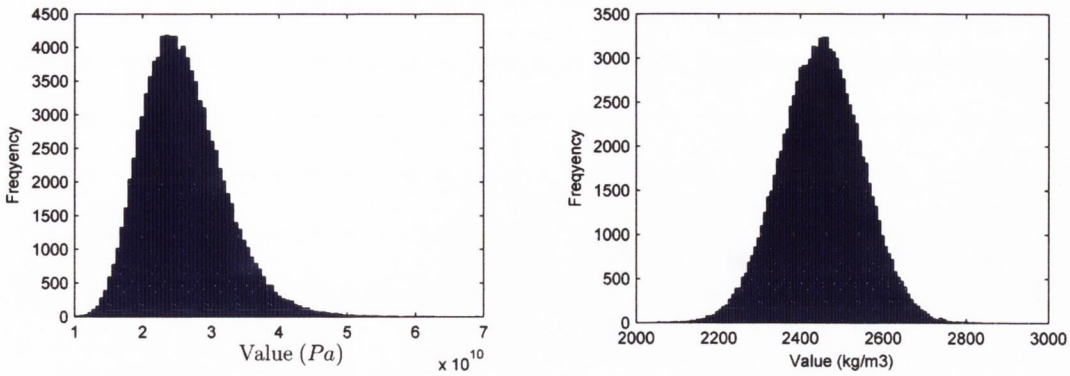

(a) Concrete modulus of elasticity.

(b) Concrete density.

Figure 4.1: Sample model input variable distributions.

4.2.4 Relative Comparison of Maximum Tip Displacements

Following on from the batches of variables generated as part of the Monte Carlo modelling, the dynamic wind turbine simulations were carried out for each wind turbine at each of the wind speeds. Figure 4.2 presents the results from a series of simulations, chosen at random, for the various tower configurations at the turbine cut-out wind speed of 25 m/s. Although these are random simulations picked from the analyses, it is evident in each of the plots that the concrete towers have consistently lower displacements than their steel counterparts. It is also noticeable that with increasing height the difference in the responses reduces. This is understandable, given that the 103 m and 120 m concrete towers have the specifications of an 88 m tower.

It is a statistical representation of the maximum nacelle displacements experienced during the simulations, such as those illustrated in Figure 4.2, which forms the basis for the results presented in this section. Figure 4.3 presents the percentage variation in maximum tip displacements between the six towers modelled for varying wind speeds, where in the legend 'S' indicates the steel towers which are represented by solid lines and likewise 'C' is for concrete which have dotted lines. The points on the graph are the 95^{th} percentile of the maximum displacement magnitudes at each wind speed. Only medium turbulence is considered in this instance. The plot shows a distinct difference between the maximum

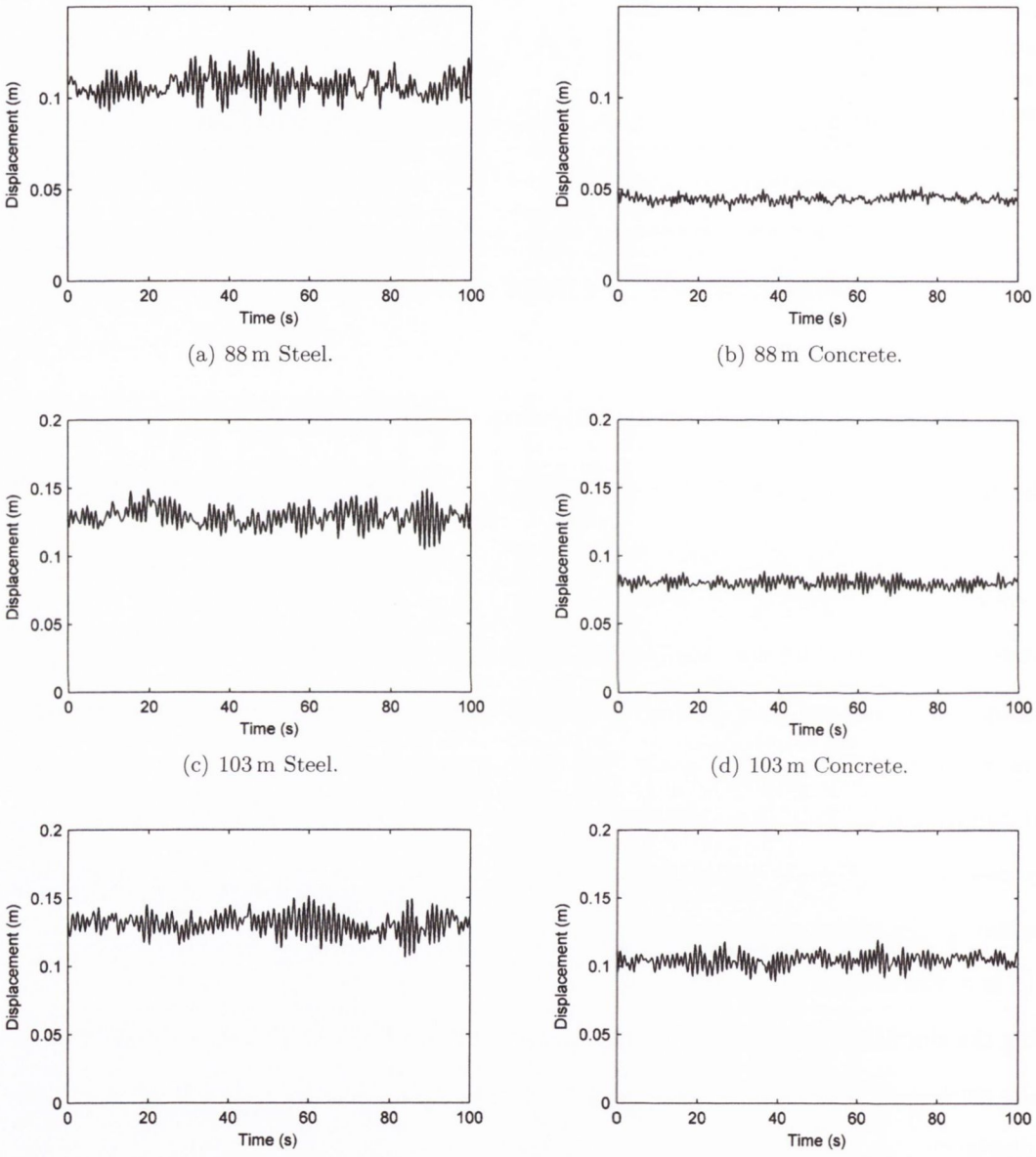

(a) 88 m Steel.

(b) 88 m Concrete.

(c) 103 m Steel.

(d) 103 m Concrete.

(e) 120 m Steel.

(f) 120 m Concrete.

Figure 4.2: Sample nacelle displacement response for 25 m/s wind speed.

displacements of the concrete and steel towers. As outlined previously, the 103 m and 120 m concrete towers are baseline estimates of realistic towers. This was re-emphasised in Appendix E.3 where the 103 m and 120 m concrete towers were shown to offer lower resistance to wind excitation than a suite of similar, designed towers. Furthermore, the corresponding 103 m and 120 m steel towers were shown to offer greater resistance to wind excitation than a comparable set of designed towers. Despite this, the 120 m concrete tower exhibits only 85 % of the magnitude of the maximum displacement of the 120 m steel tower. This significant difference in magnitude is observed equally for the 88 m and 103 m towers with a consistent 15 % to 20 % difference in maximum displacement magnitude. This implies that the concrete towers outperform the steel towers in terms of maximum displacement amplitudes for the wind speeds considered.

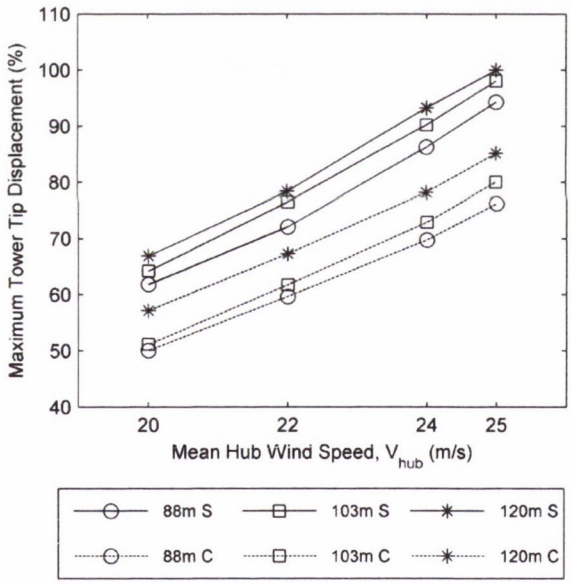

Figure 4.3: Maximum nacelle displacements as a percentage of the overall maximum displacement for varying hub-heights and wind speeds with medium turbulence (Quilligan *et al.*, 2012b).

For each of the towers, an almost linear increase, or possibly power-law relationship is observed for the displacement magnitude with increasing height. In the case of the steel towers, however, the rate of increase appears greater with increasing wind speed. This

suggests that, as the mean wind speed approaches the cut-out wind speed, the difference in performance between the two tower configurations is increased.

4.2.5 Long Term Effects In Concrete

Prestressed concrete structures are subject to a number of effects which can alter their structural performance over time. Creep and shrinkage are two processes which must be considered in the long term design of prestressed concrete, and consequently in the consideration of prestressed concrete wind turbine towers. Both of these effects have the ability to induce tensile stresses which may lead to cracking of the concrete and a reduction in the overall strength of the structure. Numerous efforts have been made by authors such as Cluley and Shepherd (1996) and Mazloom (2008) to quantify the effects of creep and shrinkage on the strength of prestressed concrete structures. Taking the approach outlined by Mayfield (1982) and utilising the formula:

$$J\left(t,t'\right)=\frac{1+\phi\left(t,t'\right)}{E\left(t'\right)} \tag{4.2}$$

where $J\left(t,t'\right)$ is a creep function, $\phi\left(t,t'\right)$ is a creep coefficient and $E\left(t'\right)$ is the modulus of elasticity at age t', it is possible to get an estimate of the reduced modulus of elasticity of the concrete after loading for time t. Considering that $J\left(t,t'\right)$ is the strain at time t due to a unit constant stress that has been acting since time t' it can be shown that $1/J\left(t,t'\right)$ is an approximation of the modulus of elasticity at time t. The creep coefficient, $\phi\left(t,t'\right)$, is assumed to be 1.0, which according to BS 8110-2 (1985) is a conservative assumption for outdoor exposure in Ireland or the UK with a loading age of one year or greater. Setting the modulus of elasticity, $E\left(t'\right)$, to be $26\,MPa$ (as per Table 4.4) yields a value for the adjusted modulus of elasticity of $E\left(t'\right)/2$ or $13\,MPa$. Accounting for the effects of shrinkage and creep in this manner, a simulation will be undertaken to provide comparison to the standard results.

4.2.6 High Strength Concrete

As concrete wind turbine towers are considered to be high performance structures it would not be expected that normal grade concrete would be employed in their production. It would be advisable that a high grade of concrete such as C50/60 (as specified in BS EN 206-1 (2000), with a characteristic compressive strength of 60 N/mm^2) or higher would be specified. This, in turn, would also have an influence on the modulus of elasticity (Young's Modulus) of the concrete as these two properties are known to be related. Noguchi *et al.* (2009) proposed an equation for the modulus of elasticity of concrete with a specific relevance to high-strength concrete. This was formulated from over 3000 sets of experimental data and expresses the modulus of elasticity as:

$$E = k_1 k_2 \cdot 3.35 \times 10^4 \left(\gamma/2400\right)^2 \left(\sigma_B/60\right)^{1/3} \tag{4.3}$$

where E is the modulus of elasticity expressed in MPa, k_1 and k_2 are correction factors corresponding to aggregate coarseness and the addition of mineral admixtures respectively, γ is the unit weight of the concrete expressed in kg/m^3 and σ_B is the concrete compressive strength expressed in MPa.

Taking, for example, a high-strength concrete with a mean unit weight of 2450 kg/m^3, as per Table 4.4, and characteristic compressive strength of 60 MPa will result in a modulus of elasticity of 34.91 GPa if both correction factors are set to 1.0. This is a 34 % increase on the previous mean value for Young's modulus specified for concrete. For comparison, a simulation will be carried out using the modulus of elasticity calculated above with the same distribution characteristics as specified in Table 4.4.

Furthermore, it would be expected that concrete wind turbine towers would be designed as Class 1 prestressed concrete structures which do not allow tensile forces to arise in the concrete under service loading. This would avoid any reduction in the strength of the structure in bending due to cracking of the concrete in both the short and long term. Creep and shrinkage may still affect the concrete, however, so an additional simulation will be undertaken using an adjusted modulus of elasticity, as per Section 4.2.5, for the

high strength concrete specified in the current section.

4.3 Performance Analysis Using Fragility Curves

As discussed in Section 2.8, fragility curves are most commonly used in seismic analysis as they provide an effective means of relating seismic hazard intensity to the probability of reaching or exceeding predefined limit-states and are, therefore, a critical tool in earthquake loss assessment. In this study it is intended to employ fragility curves, which relate wind hazard intensity to a tower limit-state, as a method for comparing the relative structural performance of the wind turbine towers considered. A displacement based fragility curve generation procedure is utilised, based upon a limit-state related to nacelle (tower-tip) displacement. The choice of displacement limit-state reflects the stability of the tower structure and its ability to resist the prescribed loading conditions. Mean hub-height wind speed has been chosen as the fragility hazard parameter as it is quite straightforward and it dictates the underlying turbulent parameters of the wind speed. The fragility term employed in this analysis is represented as:

$$P\left[d_{tip} > LS|\bar{V}_{hub} = \bar{V}\right] \tag{4.4}$$

where d_{tip} is the maximum nacelle displacement, LS is the tower limit-state and $\bar{V}_{hub}$ is the mean hub-height wind speed.

The tower limit-state for each tower height has been defined as the minimum extreme displacement of the nacelle for either the steel or concrete tower (whichever is the lesser) at the maximum mean hub-height wind velocity, 25 m/s.

4.4 One Dimensional Results

The output of the analysis outlined in the previous sections is in the form of tip displacements for the particular tower being examined. These results are presented in three formats. A comparison of the maximum nacelle displacements with respect to the varying

hub heights was presented in Section 4.2.4. In this section a comparison of the tip displacements resulting from various turbulence levels are illustrated along with the presentation of a set of fragility curves, to describe the relative performance of concrete and steel towers at each particular hub-height.

4.4.1 Comparison of maximum nacelle displacements for varying turbulence levels.

Figure 4.4 outlines the variation in maximum displacements of each tower studied for the three turbulence levels at the six mean hub-height wind speeds. In each case, 'Low', 'Med' and 'High' represent the displacements of the particular tower in conditions of low, medium or high turbulence respectively. All three turbulence levels are investigated in order to certify that variation in turbulence levels affects both the steel and concrete towers proportionately. The displacements are characterised as a percentage of the maximum displacements for that particular tower height. It is evident that there is a consistent increase in maximum tip displacements with increasing turbulence for both steel and concrete towers, as would be expected, but as the tower height increases the separation of the magnitudes appears less defined as can be seen in Figure 4.4(c), 4.4(e) and 4.4(f). There is no clear pattern which effects either of the two tower materials in solitude. In what follows, the comparison of the performance of the two materials is presented for one turbulence level only.

4.4.2 Fragility Curves

Figures 4.5 to 4.7 present sets of fragility curves which outline the relative performance of the two tower materials at the three heights specified. Only the case of medium turbulence is considered as the effect of turbulence has already been addressed in Section 4.4.1. In each graph the probability of exceeding the limit-state is defined on the y-axis as described in Section 4.3 while the x-axis defines the mean hub-height wind speed. The probabilities of LSE were calculated from a set of 100 independent simulations at each of the specified wind speeds.

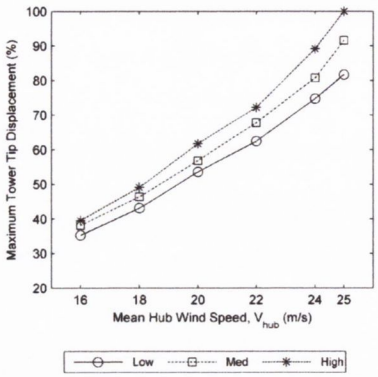

(a) 88 m Steel.

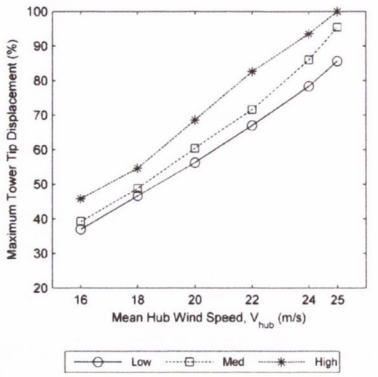

(b) 88 m Concrete.

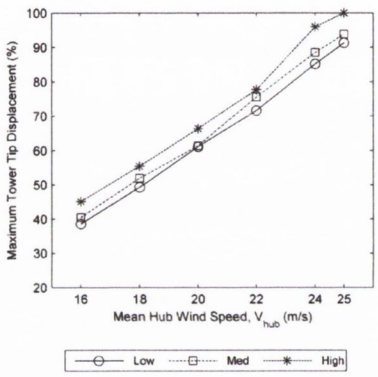

(c) 103 m Steel.

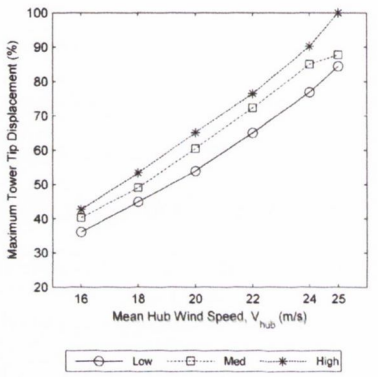

(d) 103 m Concrete.

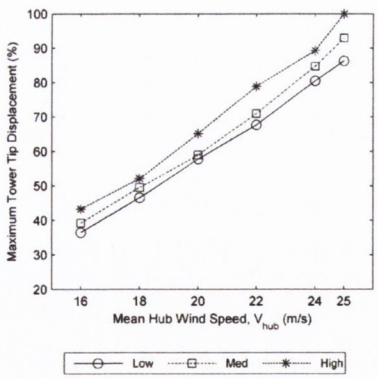

(e) 120 m Steel.

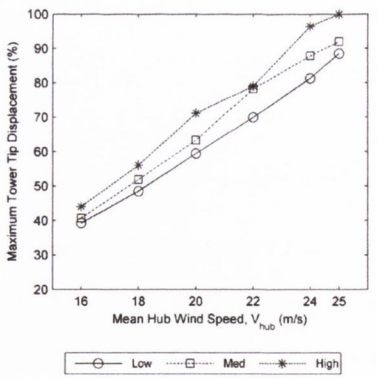

(f) 120 m Concrete.

Figure 4.4: Maximum nacelle displacements for steel and concrete towers with varying turbulence level (Quilligan *et al.*, 2012b).

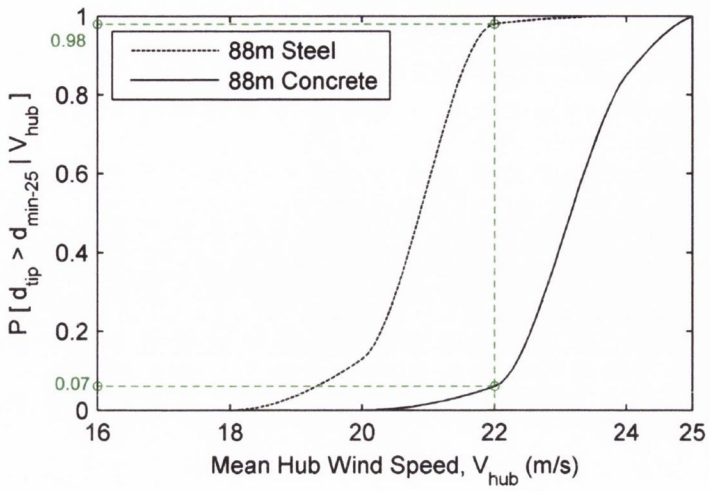

Figure 4.5: Fragility curves for 88 m steel and concrete towers (Quilligan *et al.*, 2012b).

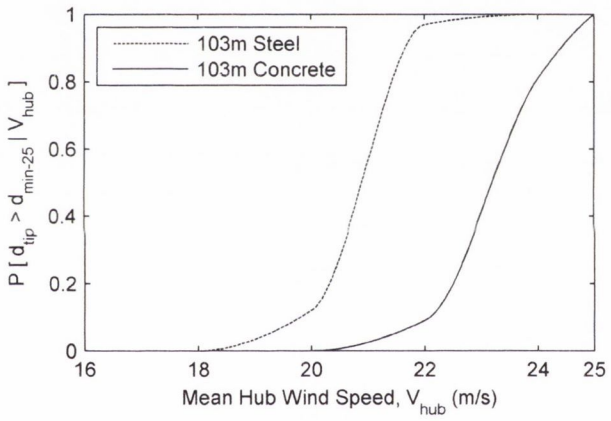

Figure 4.6: Fragility curves for 103 m steel and concrete towers (Quilligan *et al.*, 2012b).

A consistent disparity is evident between the results for the two tower materials in all three figures indicating the superior structural performance of the specified concrete towers as opposed to their steel counterparts for the considered limit-state, e.g. in Figure 4.5 at a mean hub-height wind speed of 22 m/s the probability of LSE is 7 % for the concrete tower and 98 % for the steel tower. Despite the fact that the diameter and material thickness properties for the two taller concrete towers are the same as the 88 m tower, Figures 4.5 to 4.7 demonstrate the considerably lower probabilities of LSE of the concrete towers for all three hub heights. This is seen to be most significant at higher wind speeds.

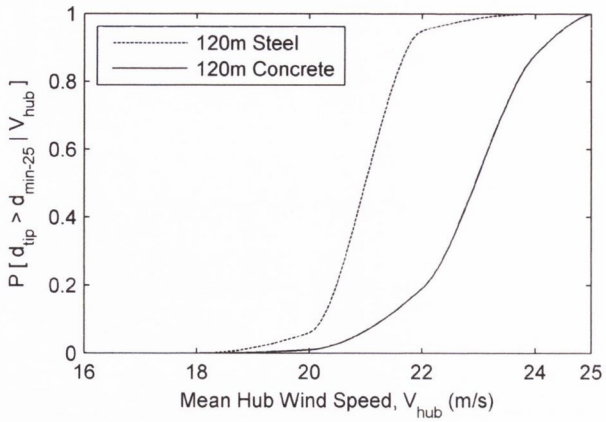

Figure 4.7: Fragility curves for 120 m steel and concrete towers (Quilligan *et al.*, 2012b).

Figure 4.7 does show a reduction in the disparity between the two tower materials but this is to be expected given that the 120 m tall concrete tower is specified with the properties of a typical 88 m tower whereas the 120 m steel tower is scaled from the 103 m and 88 m towers. These results echo the findings of Section 4.2.4 where a clear distinction is established between the maximum displacements of the steel and concrete towers. It can be seen that the 120 m concrete tower, which again offers a baseline to a realistic tower of this height, exhibits between 5% and 10% lower displacements than the 88 m steel tower over the range of wind speeds considered.

Figure 4.8 is the same as Figure 4.7 but with the addition of a third curve. This curve

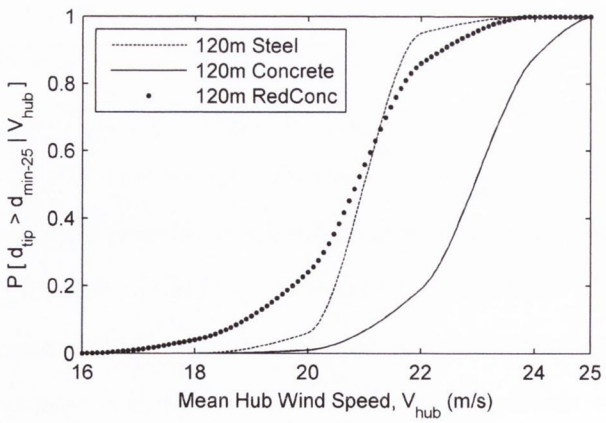

Figure 4.8: Fragility curves for 120 m steel and concrete towers with a concrete tower modelled with long term effects (Quilligan *et al.*, 2012b).

represents the probability of LSE for a 120 m concrete tower which incorporates a reduction in strength due to long term effects, creep and shrinkage. This is identified as "RedConc" in the accompanying legend. The properties of the concrete are for standard grade and not high strength concrete. There is a clear decrease in performance from the original concrete tower. It can be seen that the aged tower behaves in a similar fashion to the steel tower with slightly inferior performance up to $21\,m/s$ mean wind speed but improved performance beyond this speed. This can be related back to Figure 4.3 where the performance of the concrete tower improved relative to the steel tower with increasing wind speed.

Figure 4.9 presents a set of fragility curves for a 120 m tower constructed from a high strength concrete compared to the standard 120 m steel and concrete towers. An additional curve has been added for a standard high strength concrete prestressed structure along with a curve representing the same tower incorporating long term effects. These are

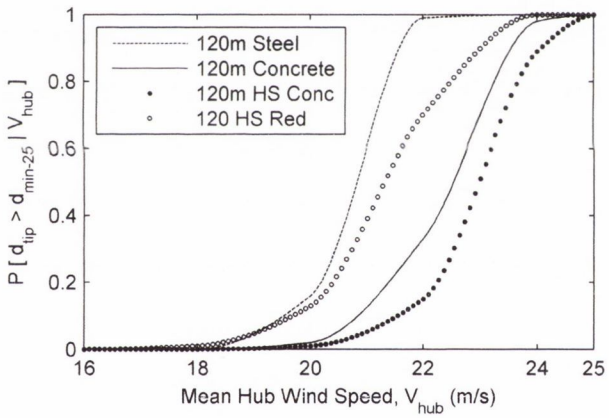

Figure 4.9: Fragility curves for 120 m steel and concrete towers with a high strength concrete tower (Quilligan *et al.*, 2012b).

referred to as "120 m HS Conc" and "120 m HS Red" respectively in the accompanying legend. As expected, the high strength concrete tower displays a clear improvement in performance over the original concrete tower as well as the reference steel tower. When long term effects are taken into account the performance is below the standard concrete tower but it still maintains improved performance over the steel tower, with increasing benefit as the mean hub-height wind speed increases. Again, it is critical to note that the specified

concrete tower offers less resistance to wind excitation than a more realistic tower and if an optimum design was specified the results for the concrete tower performance would be expected to improve considerably.

4.5 Conclusion of One Dimensional Tower Comparison

As alternative tower configurations are being sought for large scale multi-megawatt wind turbines, the first part of this chapter set out to assess the relative structural performance of tubular steel and prestressed concrete wind turbine towers for heights ranging from 88 m to 120 m. Utilising the one dimensional model outlined in Chapter 3, a suite of towers were investigated to determine the comparative structural responses under various conditions of turbulent wind loading. In all cases a representative 5 MW wind turbine was supported by the towers while in an operational state. A probabilistic representation of the tower structural properties as well as the environmental conditions was employed in the classification of the study parameters. Consequently, the resulting responses were illustrated with the use of fragility curves, a method of characterising the reliability of a structure, or structural component, for a prescribed limit-state or limit-states.

Maximum nacelle displacements were utilised in comparing relative structural performance of the various towers. The effect of increasing the level of turbulence on the towers was investigated. Varying the turbulence level was seen to have a noticeable effect on the magnitudes of maximum tip displacements. However, this was observed to effect both tower types equally with no evident pattern exclusive to either material.

Fragility curves were employed to directly compare the performance of the two tower materials. The limit-state was defined as the lowest maximum tip displacement for either tower at each specific height. For all cases it was seen that the steel towers exhibited significantly higher probabilities of limit-state exceedance (LSE). Despite the fact that the prestressed concrete towers defined offered less resistance to wind excitation than a suite of comparable optimised designs, they outperformed the steel alternatives in terms of the probability LSE. A basic model of long term effects in prestressed concrete, such

as creep and shrinkage, was developed in order to simulate prestressed concrete tower performance in the long term. When these effects were taken into account for a 120 m tall tower it was observed that the steel and concrete tower showed minimal difference in performance with steel exhibiting superior results at lower wind speeds but a reversal of performance was observed at higher wind speeds. As details on concrete specification for these structures were unavailable it was decided to specify regular strength concrete for the simulations. However, it would be expected that a high strength concrete would be prescribed for these high performance structures. The simulation of a high strength concrete in a 120 m tall tower was observed to induce a distinct improvement over regular strength concrete and, therefore, the steel option as would be expected. The inclusion of long term effects in the simulation reduced this improvement but the prestressed concrete tower remained significantly ahead of the steel option in terms of reduced probability of LSE. An interesting undertaking for future work would be to consider the effects of creep and shrinkage on prestressed concrete structures in a more detailed manner. It was suggested that a conservative estimate of the creep coefficient was chosen in this instance. By varying the creep coefficient based on external conditions and structural specifications, a variation of resulting long term concrete strengths may be achievable.

As discussed in Chapter 3, the one dimensional model used in this study only captures the flapwise vibration of the blades and longitudinal tower motion. These, however, represent the most significant vibrational characteristics of a wind turbine with the magnitudes of the other components, such as edgewise blade vibration and lateral tower motion, shown to be considerably less in Section 3.5. Numerous authors have employed such a model in previous studies of wind turbine dynamics to highlight particular vibrational characteristics, and in this instance it provides an accurate and efficient tool for an initial comparison of the performance of tubular steel and prestressed concrete tower performance. By including additional vibrational effects with the use of a two dimensional model the results may be altered somewhat, but in capturing the most significant vibrational characteristics of the system, as is achieved by the one dimensional model, an accurate initial estimate of the relative tower performance is achieved.

4.6 Tower Comparison With Blade Fragilities

Being a primary component of wind energy converters, wind turbine blades have received considerable attention from designers and researches in the field of structural dynamics (Toft and Sørensen, 2011; Kong *et al.*, 2005; Hansen, 2003; Chaviaropoulos *et al.*, 2003; Maalawi and Negm, 2002). By their nature, as substantial elements rotating relative to a considerable support structure and intricate electricity generation equipment, wind turbine blades are subject to complex dynamic forces and interactions as part of the entire wind turbine system. This is further compounded by the unsteady aerodynamic forces imparted on the blades from a turbulent wind field. With the growth in scale of wind turbine units into the multi-megawatt domain, wind turbine blades have seen substantial progression to lengths exceeding 60 metres (ENERCON, 2007). As a result, the induced dynamic forces have increased in both magnitude and complexity. A principal goal of the wind turbine designer is to minimize the vibration of the wind turbine elements. This is particularly important for the blades where reduced vibration gives rise to lower stresses and hence improved fatigue resistance of the entire turbine system.

This study addresses the influence of the choice of tower construction material on the resulting dynamic response of the blades. The investigation effectively examines the comparative response of wind turbine blades which are connected to the nacelle units supported by either steel or prestressed concrete towers. This is carried out for the same range of tower heights as considered in Section 4.2. In order to study the proposed dynamics the two dimensional structural model is employed in the computation of the dynamic structural response. The model incorporates dynamic coupling between the blades, rotor shaft and tower, thus allowing accurate simulation of the dynamic interactions between the elements. The same series of towers prescribed in Sections 4.2.1 and 4.2.2 are implemented in the current study. The results are presented through a series of fragility curves which quantify the probability of LSE of the blade tip displacements for each configuration.

Outlined in the following sections is a description of the investigation carried out and the presentation of the results produced by the study. The results are subsequently dis-

cussed in the context of the influence of relative blade response on the serviceability of the wind turbine structure.

4.6.1 Model Implementation

The study considers the same suite of towers utilised for the one dimensional study in Section 4.2, i.e. both steel and concrete towers at heights of 88 m, 103 m and 120 m. In order to achieve realistic results the specified structural input properties take account of the inherent variability of their values. These are specified in Table 4.4 where the variables are given a mean value along with a CoV and a PDF. The Monte Carlo modelling technique is once again implemented in order to generate batches of variables within the required statistical distributions. These batches form the input for the subsequent simulations. In all cases the towers are assumed to support the NREL baseline 5 MW nacelle and rotor (Jonkman *et al.*, 2009) which was previously described in Section 3.5.1.

The blades of the specified 5 MW turbine are 61.5 m in length and are considered to be constructed from fibreglass. The blade root is located at the edge of the 3 m diameter hub. The total mass of each blade equates to 17,740 kg with a centre of mass acting at 20.475 m from the blade root. From a modelling perspective the blades are broken into nodes with equivalent mass density, stiffness and aerodynamic properties. These properties necessary for input to the model may be found in Appendix C.

The analyses necessary for this particular investigation requires batches of discrete response time history calculations for each wind turbine at each of the predefined mean hub-height wind speeds. Figure 4.10 presents the results from a series of simulations, chosen at random, for the 88 m steel and concrete tower configurations at the cut-out wind speed. Both sets of results appear to be quite similar. For the steel tower the mean flapwise displacement is 4.837 m and once the steady state response is reached, the displacements range between 4.272 m and 5.439 m. This compares to a mean value of 4.840 m for the concrete tower and a steady state response range of 4.399 to 5.292 m. Similarly, for the case of edgewise vibrations, the steel and concrete towers exhibit the same mean blade displacement of 0.181 m with respective ranges of displacement values

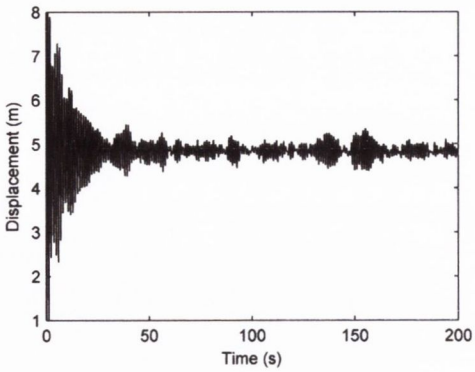

(a) 88 m Steel - Flapwise.

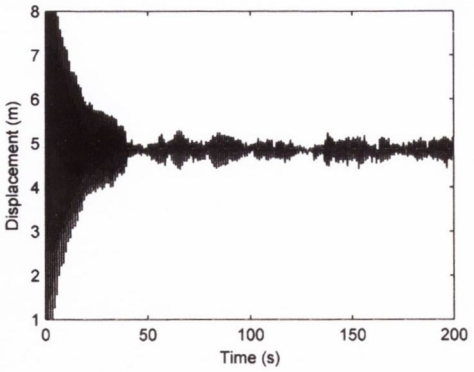

(b) 88 m Concrete - Flapwise.

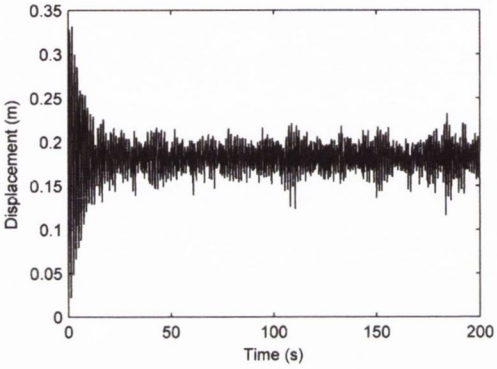

(c) 88 m Steel - Edgewise.

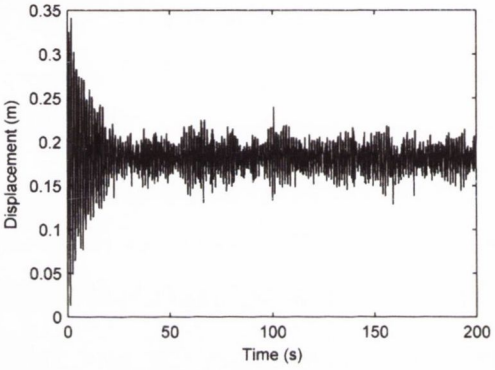

(d) 88 m Concrete - Edgewise.

Figure 4.10: Sample blade-tip displacement response for 25 m/s wind speed.

of 0.116 to 0.233 m for the steel tower and 0.129 to 0.239 m for the concrete tower. While these are random responses chosen from the system, it is clear that there exists minimal difference in performance between the two tower materials at the lower height of 88 m.

4.6.2 Results

Blade-tip displacement is chosen as the variable with which to perform a relative comparison of the results for various tower configurations. For each simulation the maximum blade-tip displacement, which is a resultant combination of the coinciding flapwise and edgewise displacements, is recorded to form a set of maximum displacements for each configuration. Figure 4.11 presents the 95^{th} fractile of the maximum resultant blade displacement values calculated for each tower. What is noticeable from the three plots is that

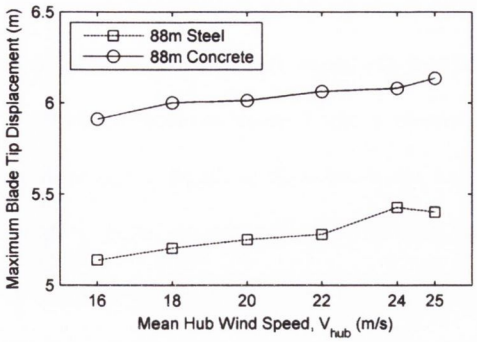

(a) 88 m steel and concrete towers.

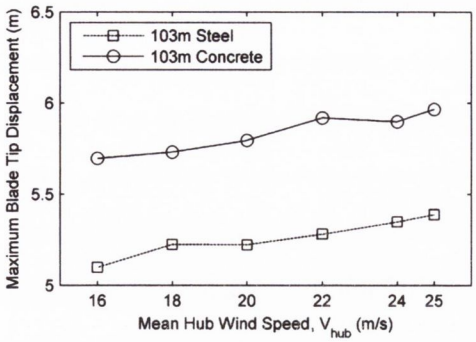

(b) 103 m steel and concrete towers.

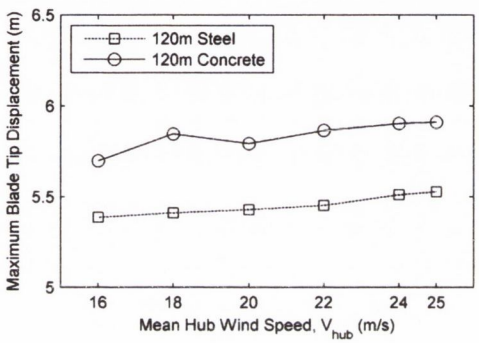

(c) 120 m steel and concrete towers.

Figure 4.11: Maximum blade-tip displacements.

in each case the range of displacement magnitudes is similar, varying from 5.1 m to 5.5 m for the steel towers and 5.8 m to 6.1 m for the prestressed concrete towers. What is also evident, however, is that with increasing height the maximum displacements of the blade tips on the steel towers increase minimally where as the reverse is true for the prestressed concrete towers with the displacements decreasing as tower height increases. The steel towers show a 3.1% increase in mean maximum blade tip-displacement for the series of wind speeds over the height range while the mean maximum displacement of the concrete towers reduces by 3.3% over the same interval. This is most likely due to the fact that the natural frequency values for the steel towers increase with height, thus bringing them closer to the blade natural frequencies and inducing increased response as a result. The opposite trend is seen with the concrete towers, where the natural frequencies decrease with height. What is also evident from the plots is that the prestressed concrete towers

display consistently higher maximum blade-tip displacements than the steel towers. Although the gap decreases with increasing height, there remains an obvious difference in maximum displacements. The natural frequency values for the towers cannot account for this, however, as both sets of towers possess a similar range of values despite the varying trends (0.33 - 0.44 Hz for steel and 0.47 - 0.25 Hz for concrete). The tower height, therefore, does have an influence on the maximum blade-tip displacements for the range of mean hub-height wind speeds and the series of towers considered. Had the suite of towers proposed by Engström *et al.* (2010) been employed in this study, the results may have been altered somewhat. Given that both the steel and concrete towers exhibit decreasing natural frequency values with increasing height, it would be expected that a decrease in blade response with increasing hub height would be experienced in both instances. Also, given that the frequency values for the concrete towers are significantly higher than the comparable steel towers, this may result in a further increased advantage for the steel towers.

Fragility curves are developed to compare the relative performance of the various tower configurations by characterising the frequency of LSE by the blades for the range of tower configurations. A displacement based fragility curve generation procedure is utilised, based upon a limit-state related to blade-tip displacement, d_{tip}. For the case of each hub height specified, the limit-state is chosen as the lowest maximum displacement for all of the simulations carried out at the particular height for the 25 m/s mean hub-height wind speed, d_{min-25}, including both tower options. Figure 4.12 presents a series of such curves for each of the tower heights considered. Figure 4.12(a) illustrates two curves corresponding to the 88 m steel and concrete towers. In this instance the curve representative of the concrete tower is seen to exhibit a distinctly higher probability of LSE across the range of wind speeds studied. As a result, it can be said that for a tower height of 88 m, the magnitude of blade displacement vibrations are noticeably larger for a support tower constructed from prestressed concrete. This ties in with results from Figure 4.11(a) where the maximum blade displacements for the concrete tower consistently exceeded those of the steel tower. Figure 4.12(b) highlights the probabilities of LSE for the 103 m towers. Noticeably lower

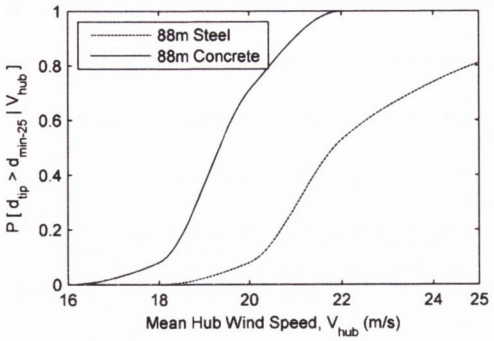

(a) 88 m steel and concrete towers.

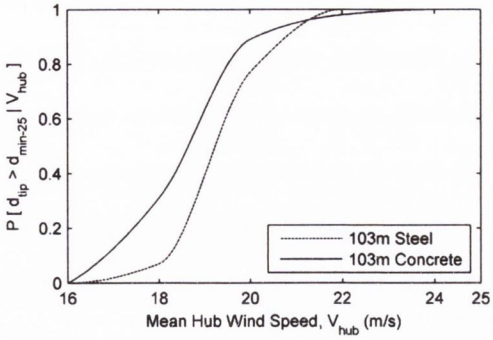

(b) 103 m steel and concrete towers.

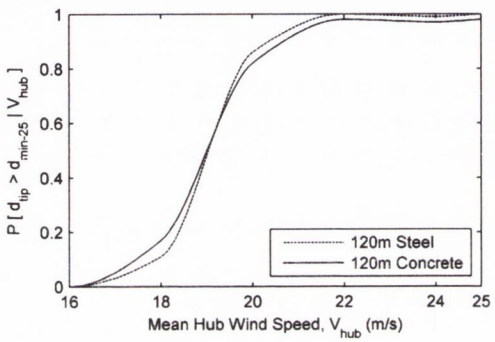

(c) 120 m steel and concrete towers.

Figure 4.12: Blade fragilities.

displacement magnitudes are identified in the blades for the steel configuration at wind speeds of 18 m/s and 20 m/s, with the performance converging as the 22 m/s wind speed is approached. At 22 m/s the concrete tower outperforms the steel tower, although only by 2%. A similar scenario is illustrated in Figure 4.12(c) for the 120 m tower height. In this case the steel tower demonstrates minimally less LSE up until approximately 19 m/s where the curves are seen to converge. From this point on, the concrete tower outperforms the steel tower by a margin of between 2% and 4%. Overall, a pattern is evident in the results which suggests that, although the probability of LSE is noticeably less for a steel tower at a height of 88 m, with increasing height the concrete configuration becomes more competitive. This is particularly true for the upper range of wind speeds where the concrete towers were shown to slightly outperform the steel towers in Figures 4.12(b) and 4.12(c). The results in these two figures may seem unusual when contrasted with Figure 4.11(b)

and Figure 4.11(c) where the maximum blade-tip displacements were significantly larger for the prestressed concrete towers. This is a direct result of the higher CoV specified for concrete as compared to steel in Table 4.4, therefore allowing for a greater variability in the results for the concrete towers and higher maximum displacements as a consequence. As already discussed, however, had more optimised tower designs been employed at 103 m and 120 m, an improved level of performance may have been experienced by the steel towers, while the blade response relating to the concrete towers would have been expected to dis-improve.

4.7 Conclusion of Tower Comparison With Blade Fragilities

In an extension of the previous study comparing the relative structural performance of tubular steel and prestressed concrete wind turbine towers for heights ranging from 88 m to 120 m, the second part of this chapter set out to investigate the influence of the choice of tower construction material on the dynamic response of the wind turbine blades. Once again, prestressed concrete towers were considered as an alternative to the industry standard steel option. Both configurations were analysed at the proposed heights of 88 m, 103 m and 120 m, using the previously defined two dimensional structural model to calculate the structural response of the wind turbine system to stochastically generated turbulent wind loading. Akin to the first study, in all cases a standard 5 MW wind turbine was supported by the towers. Turbulent wind loading was simulated for a series of mean hub-height wind speeds varying from 16 m/s to 25 m/s, the cut-out wind speed for the turbine. This range was chosen as it is at the upper level of operating wind speeds for the turbine and it is at these wind speeds that the wind turbine experiences the largest responses during operation. The Monte Carlo method was employed to generate batches of input variables for each of the tower configurations with specified PDF, mean and CoV.

Utilising the two dimensional dynamic structural model, simulations were carried out for each batch of input variables, thus providing dynamic displacement time history responses for each of the blades and the tower. For the range of mean hub-height wind

speeds considered, in each case the maximum blade-tip displacement was noted. This was a resultant displacement, being a combination of the flapwise and edgewise response at each time-step. The 95^{th} fractile of the maximum displacements was identified to allow for a relative comparison to be made. In keeping with the probabilistic framework applied in the first study, further comparison was made through the development of fragility curves by classifying the frequency of limit-state exceedance (LSE) for the specified range of mean hub height wind speeds.

Overall, this study highlighted that the tower construction material does in fact have an influence on the magnitude of vibrations in the wind turbine blades. By focussing on the chosen suite of steel and prestressed concrete as the two options in the current investigation, it was shown that at lower heights the steel towers exhibit more favourable performance in terms of the magnitude of the blade-tip displacements and the frequency of LSE. As the hub-height was increased the relative advantage of the steel option was seen to diminish. Although the steel tower maintained lower magnitudes of maximum tip displacements at 103 m and 120 m, the gap in performance was reduced. In terms of the probability of LSE, the prestressed concrete towers improved relative to the steel towers and at 103 m, in fact, performed slightly better above 22 m/s mean hub-height wind speed. This improvement extended to the 120 m towers with a minimal difference in performance across the range of wind speeds. The steel tower outperformed the prestressed concrete by 6% at the 18 m/s wind speed while a reversal in performance was observed beyond 19 m/s with the concrete tower showing slightly superior performance for the greater wind speeds. While the difference in performance was seen to reduce with increasing height, it was suggested that this was most likely due to the differing trends in natural frequency values over the height range. On reviewing another suite of similar towers, it was seen that both the steel and concrete towers exhibited decreasing natural frequency values with increasing height. This would most likely serve to increase the advantage of the steel towers over the corresponding prestressed concrete towers.

Tubular steel wind turbine towers have been the predominant solution used in the wind industry thus far. The results in this chapter suggest that for the particular towers chosen

for this study, the tubular steel option offers both reduced magnitudes of maximum blade displacements as well as frequency of LSE. It was also highlighted that, had more optimised tower designs been chosen, the difference in performance could have been further increased. This may prove useful in the design of wind turbine structures and may form a catalyst for further research where improved structural performance and vibration reduction is of primary importance.

Chapter 5 -

Seismic Response of Wind Turbine Towers

5.1 Introduction

The considerable growth in the wind energy industry in recent years has given rise to an increasing prevalence of wind turbine structures in areas of high seismic activity. Coupled with this is the fact that wind turbine structures are becoming consistently larger, utilising more advanced materials in order to balance the flexibility, cost, CO_2 emissions, ease of construction and transportation issues. Prestressed concrete and hybrid tower solutions are primary examples of this as they provide a necessary substitute for tubular steel at heights exceeding 85 m (Harte and Van Zijl, 2007). Although these larger turbines reduce the cost per unit of electricity generated, the capital cost of such structures is significant and any damage will result in considerable repair costs and an associated loss of income due to downtime. Consequently, the requirement for a greater understanding of the dynamic response of wind turbines during earthquake events is essential in order to improve reliability, reduce operational downtime due to repairs and ensure the safety of surrounding properties and their inhabitants. It is also a necessary requirement to facilitate the accurate tuning of structural damping systems. Colwell and Basu (2009) presents an investigation into the use of tuned mass dampers to reduce excessive nacelle vibrations in wind turbine systems subject to both wind and wave loading. As wind turbine structures grow in size the use of sophisticated structural damping systems may become necessary in order to limit the consequences of seismic events.

Seismic structural response is a well researched topic, with particular attention focussed on buildings, bridge structures, nuclear power stations, as well as various other structures of significant importance where the consequences of failure have grave safety related and economic consequences. Wind turbine development has now reached a stage where the implications of structural failure poses considerable physical and economic risk. On reviewing the literature, it was evident that there is an imminent requirement to expand on the understanding of seismic effects on wind turbines. Some examples of investigations of earthquake loading of wind turbine systems can be found (Lavassas *et al.*, 2003; Bazeos *et al.*, 2002; Arasu *et al.*, 2011), but these studies are limited to small scale wind turbines and simplified structural models. More detailed studies by Hänler *et al.* (2006) and Ritschel *et al.* (2003) which incorporated multi-body dynamic formulations to describe the structural system highlighted the inadequacies of simplified SDOF oscillators in estimating the seismic response. Zhao and Maißer (2006) extended the multi-body formulation to consider the effects of soil structure interaction on the seismic response of a 1.5 MW wind turbine supported on a 65 m tower, while Prowell *et al.* (2010) conducted a numerical time domain simulation, utilising the FAST design code (Jonkman and Buhl, 2005) for the NREL 5 MW reference wind turbine (Jonkman *et al.*, 2009), as well as a full scale shake table test on a 23 m high wind turbine (Prowell *et al.*, 2009). A more detailed discussion of the relevant literature is provided in Section 2.7. What was evident from these studies, however, was the fact that the current procedures for estimating wind turbine loads and responses to earthquake events are inadequate and there is a requirement for further work to be carried out in this area.

This chapter maintains the overall objective of the thesis by continuing the assessment of the structural performance of both tubular steel and prestressed concrete wind turbine towers. In this instance, however, the scope of the study is extended to incorporate seismic loading in the comparison. Akin to the previous analyses in Chapter 4, the investigation is conducted for a series of three steel and three prestressed concrete towers at heights of 88 m, 103 m and 120 m. The analysis employs a probabilistic framework for the seismic assessment of the wind turbine structures by modelling the tower structural properties and

environmental variables probabilistically, with specified PDF and CoV, excluding model uncertainty, thus providing batches of input properties for each tower configuration using the Monte Carlo method. The dynamic response of the various wind turbine configurations is computed using the two dimensional model outlined in Chapter 3. The model is extended to cater for two dimensional earthquake excitation as demonstrated in Section 3.4.4. Once again each tower is modelled as the support structure to the NREL baseline 5 MW wind turbine which is specified in Section 3.5.1. In each simulation the specified turbine is subjected to a combination of stochastically generated wind loading and recorded earthquake ground motion acceleration time-histories. Utilising a suite of 100 evenly distributed earthquake ground motion records of varying magnitude and epicentral distances, a PSDA is carried out on each tower in order to compare the resulting structural responses to the earthquake intensity. This procedure has previously been successfully employed in the study of steel moment resisting frame buildings (Cornell *et al.*, 2002), as well as bridge structures (Mackie and Stojadinović, 2001; Padgett *et al.*, 2008). This produces a mathematical model termed a PSDM. From the resulting PSDA a fragility analysis of the various structures may be undertaken. It is the resulting fragility curves which permit an assessment of the structural performance of the steel and prestressed concrete towers at varying heights. The following sections describe the implementation of the proposed methodology and the results of the aforementioned analyses.

5.2 Model Application

The investigation in the current chapter stems from that carried out in Chapter 4. The focus is on assessing the structural performance of a suite of tubular steel and prestressed concrete wind turbine towers for a series of hub heights representative of current industry standard multi-megawatt wind turbines. The modelling requirements for the incorporation of seismic loading have been discussed in Chapter 3 and a detailed description of the derived dynamic model was presented in Section 3.4.4. The primary considerations of this modelling framework are presented in Figure 5.1.

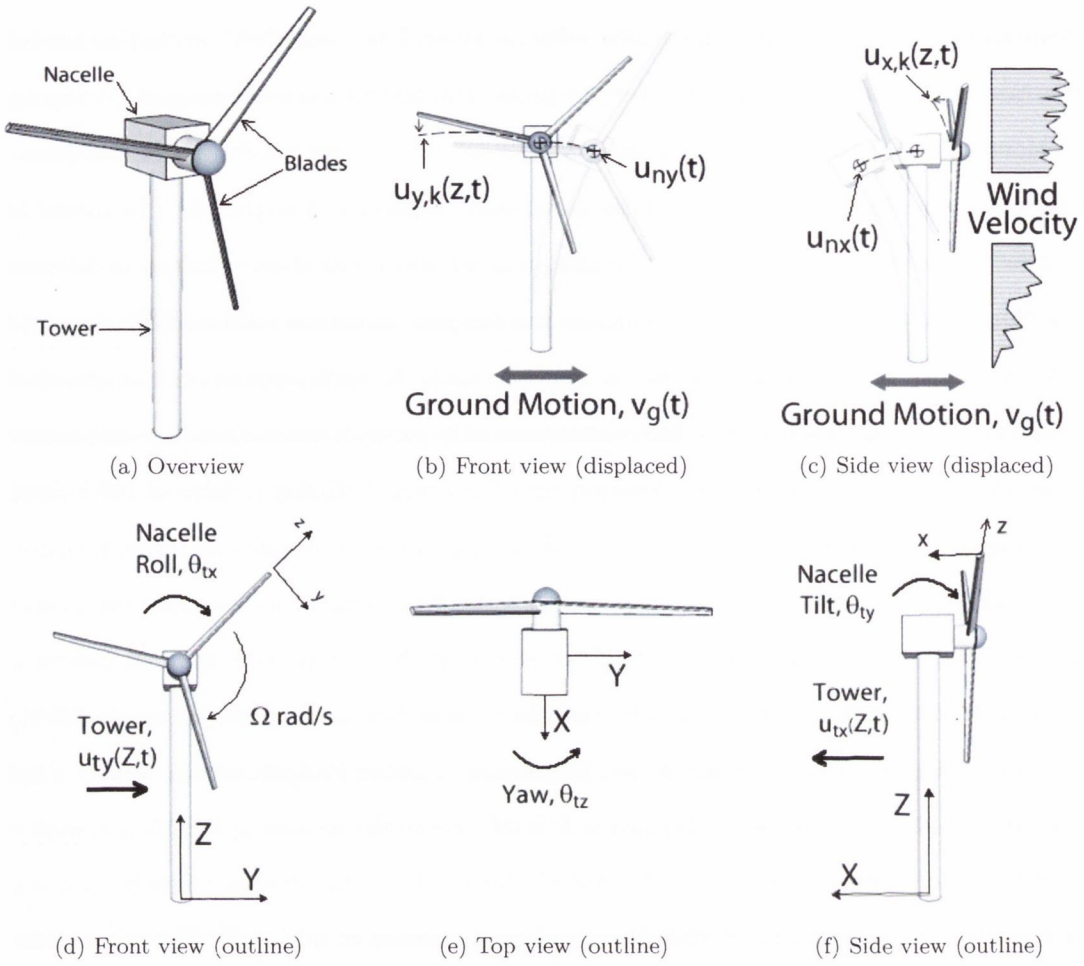

(a) Overview (b) Front view (displaced) (c) Side view (displaced)

(d) Front view (outline) (e) Top view (outline) (f) Side view (outline)

Figure 5.1: Representation of seismic modelling considerations.

In structural design, reliability based analysis offers an advantage over deterministic methods in that it can be employed to quantify the risk of various levels of damage or destruction to a structure or structural element as opposed to a deterministic calculation of structural capacity, the inherent uncertainty of which must be accommodated through conservative safety factors. With reliability based analysis an attempt is made to quantify the uncertainty, thereby facilitating a better understanding of the inherent risk as well as an often more efficient design (O'Connor and Enevoldsen, 2008). Given the considerable uncertainty associated with seismic design it is understandable that reliability based analysis and probabilistic methods offer an efficient design framework for structural engineers. As discussed in previous chapters, fragility curves form an essential component

of structural reliability analysis and offer an effective means of illustrating the associated structural risk as a function of an input design parameter. Generally this parameter is representative of the magnitude or intensity of loading. A number of methods of generating fragility curves have been outlined in Section 2.8.1 and the analyses of Chapter 4 utilised the Monte Carlo method to generate batches of input variables which were simulated using stochastic loading at each loading intensity. For the case of seismic loading where the variability of loading conditions varies drastically, the computational requirement for employing this method would be enormous. The more efficient methodology of PSDA, which has previously been successfully applied to other structural applications, is therefore called upon in the current chapter to facilitate the fragility curve generation.

5.2.1 Model Input Properties

The hub heights considered are 90 m, 105 m, and 122 m which, given the addition of the nacelle unit, are achieved by implementing a tower that is 2.4 m less in height. A description of the three steel towers has already been provided in Section 4.2.1, with the associated structural input properties specified in Table 4.1. The corresponding prestressed concrete towers are detailed in Section 4.2.2 and Table 4.2. Table 5.1 details the first natural bending frequencies of the suite of towers used in this study. The relevance of these values will be further discussed in Section 5.2.4. In all cases the towers support a representative multi-megawatt wind turbine, the NREL 5 MW baseline wind turbine. This turbine has already been thoroughly discussed in Section 3.5.1 with the relevant properties specified in Table 3.1 and further details provided in Appendix C. It should, once again, be noted that due to a lack of publicly available literature concerning the structural properties of prestressed concrete wind turbine towers at the time this analysis was undertaken, the properties of the 103 m and 120 m concrete towers are established by increasing the height of the 88 m tower, for which verified properties could be established. Although this is not a realistic representation of these towers, it does provide a baseline to the actual towers which would be specified and therefore offers a benchmark by which to compare with the steel towers. A validation of the studied towers against a suite of

recently discovered, similar towers is provided in Appendix E.3. Also discussed in the appendix are some of the possible influences on results which may be expected due to the specific choices of tower properties. The results of this chapter are discussed in the context of these influences.

Tower	Height	Units	Nat. Freq.
Concrete	88 m	(Hz)	0.47
	103 m	(Hz)	0.35
	120 m	(Hz)	0.25
Steel	88 m	(Hz)	0.33
	103 m	(Hz)	0.37
	120 m	(Hz)	0.44

Table 5.1: First natural tower bending frequencies of steel and concrete wind turbine towers.

It has been stated that a probabilistic representation of the six tower configurations is employed by modelling the tower structural properties and environmental variables as stochastic variables. The structural input variables such as the material modulus of elasticity (E), density (ρ), material thickness (t), and the environmental variables such as air density (ρ_{air}) are each given a specified PDF with a corresponding mean (μ) and CoV. These values have been previously defined in Table 4.4. This results in the generation of batches of input variables, randomly modelled with the appropriate statistical variation.

5.2.2 Long Term Effects on Concrete Strength

A discussion has already been provided in Section 4.2.5 on the effects of creep and shrinkage on the long term strength of prestressed concrete structures. Both of these effects have the ability to induce tensile stresses which may lead to cracking of the concrete and a reduction in the overall strength of the structure. Equation (4.2), which estimates the creep function for a concrete element was used to calculate a reduced value for the modulus of elasticity of the concrete. Taking a conservative estimate for the creep coefficient, it was shown that the long term modulus of elasticity could be estimated as half of its initial value following a 28 day curing period. Given the mean value specified in Table 4.4, an adjusted modulus of elasticity of 13 MPa was established. Accounting for the effects of shrinkage and creep

in this manner, a simulation will be undertaken to provide comparison to the standard results.

5.2.3 Influence of Rate of Application of Load on Concrete Strength

Another phenomenon observed in concrete structures is the influence of the rate of application of load on the concrete strength. As the proposed towers are subjected to earthquakes as the primary loading, and this generally takes the form of a high rate of load application ($> 1\,\text{Hz}$), it was deemed appropriate to conduct some simulations with a consideration for this effect. Neville (1996) outlines how a loading rate six orders of magnitude greater than in a static test (which may be the case with earthquake loading) induces a 50 % increase in compressive strength and an 80 % increase in tensile strength. It is suggested that this may be explained by the inertial resistance of concrete to microcracking. It is also suggested that at low rates of loading the effect of creep, which is addressed in Section 5.2.2, may be dominant. Bearing in mind the evidence in Neville (1996), it was decided to investigate the effect of a 50% increase in the concrete modulus of elasticity for the series of simulations considering the effect of the rate of load application. This resulted in a mean modulus of elasticity of 39 GPa.

5.2.4 Probabilistic Seismic Demand Model

Section 2.8.1 has already discussed the use of fragility curves in representing seismic risk as well as the merits of forming the capacity/demand relationship using PSDA. In summary, a PSDM provides a mathematical relationship between the ground motion intensity measure (IM) and the structural response, often termed the demand, under the assumption suggested by Cornell *et al.* (2002) that an estimate of the median of the seismic demand $\hat{S}_D$ plotted against the corresponding IM may be represented by a power law as shown in Equation (5.1):

$$\hat{S}_D = a \times IM^b \tag{5.1}$$

where a and b are unknown coefficients. By transforming the relationship into lognormal space the parameter estimation may be simplified to a linear regression as follows:

$$\ln \hat{S}_D = b \ln IM + \ln(a) \tag{5.2}$$

Figure 5.2 demonstrates a sample regression of this form. From this regression it is possible to achieve an estimate of $\hat{S}_D$ along with the statistical variation about this value. Under the assumption, as per Mackie and Stojadinović (2005) and Shinozuka *et al.* (2000a), that the demand may be probabilistically modelled using a lognormal distribution, it is possible, in the transformed space, to model the residual as normally distributed with zero mean and a specified standard deviation, σ, as shown in Figure 5.2. An estimate of the

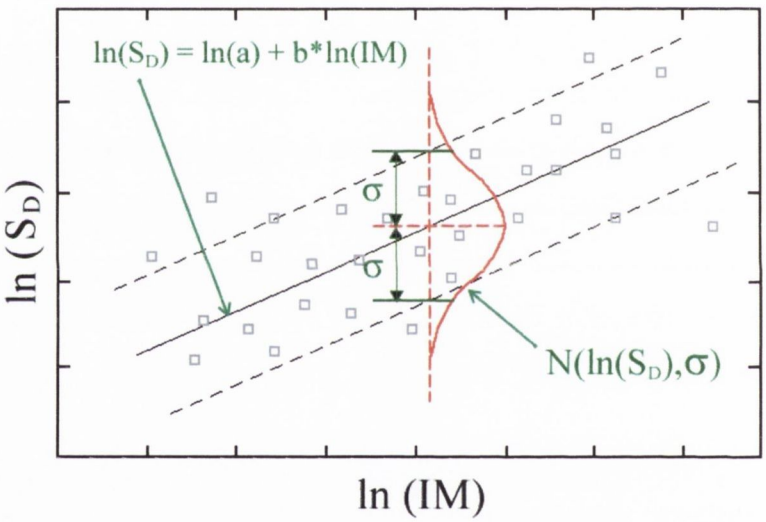

Figure 5.2: Sample linear least squares fit regression of seismic demand in lognormal space.

lognormal standard deviation of the model error, also termed dispersion $\beta_{D|IM}$ may be formulated as:

$$\beta_{D|IM} \equiv \sqrt{\frac{\sum_{i=1}^{n} \left\{ \ln\left(S_{D,i}\right) - \ln\left(\hat{S}_D\right) \right\}^2}{n-2}} \tag{5.3}$$

where $S_{D,i}$ is the seismic demand at realisation i and n is the total number of realisations. Having derived the appropriate parameters it is subsequently possible to model the relationship between the seismic demand and the input seismic intensity measure as

follows:

$$P\left[D \geq d|IM\right] = 1 - \Phi\left(\frac{\ln(d) - \ln(S_D)}{\beta_{D|IM}}\right) \tag{5.4}$$

where d is a specified demand threshold. This can be further simplified for ease of substitution of the regression variables as:

$$P\left[D \geq d|IM\right] = \Phi\left(\frac{\ln(IM) - \frac{\ln(d)-\ln(a)}{b}}{\frac{\beta_{D|IM}}{b}}\right) \tag{5.5}$$

Following on from the theoretical concepts there is a decision to be made about which IM to utilise in representing the seismic ground motion. The available options include Peak Ground Displacement (PGD), Peak Ground Velocity (PGA), Peak Ground Acceleration (PGA) as well as spectral representations including spectral acceleration. Mackie and Stojadinović (2003) identified and compared 23 different potential IMs for the development of PSDMs for multi-frame highway bridges. It was found that the spectral parameters at the fundamental period of the bridge (i.e. spectral acceleration and displacement) tended to be the most appropriate because of their tendency to reduce uncertainty in the demand model. This was based on a structure specific assessment, however, and the challenges of utilising these parameters in the analysis of portfolios of structures was highlighted. Padgett *et al.* (2008) proposed, that for a study of this type which includes a portfolio of structures, the most appropriate IM is PGA. It has, therefore, been decided to utilise the PGA parameter in the current study where a comparison between a suite of structures is implemented.

There are also a variety of techniques available for the development of a PSDA. Mackie and Stojadinović (2005) outlined three methods which included the cloud, incremental dynamic, and stripe methods. The relative merits of each of these methods has previously been discussed in Section 2.8.1. In the analysis presented here the cloud method is utilised in which a selection of earthquakes with variable magnitudes of IM are described by the cloud. In this study a suite of 100 recorded ground motions are taken from Shafieezadeh *et al.* (2011). These are representative of the seismicity of California, a region with a high density of wind turbine structures. 80 of the ground motions were assembled from the

PEER Strong Motion Database (PEER, 2012) with an even selection of recorded time-histories from four bins that include combinations of low and high magnitudes (5.8 - 6.9) as well as large and small epicentral distances (10 km - 60 km). The remaining 20 ground motions were sourced from the SAC project database (SAC, 2012). These consist of 10 pairs each with intensities of 2% and 10% probability of exceedance in 50 years respectively. Of the 100 earthquake ground motion time-histories, the smallest was of magnitude 0.03 g and the x and y component accelerations are plotted in Figure 5.3. The largest magnitude

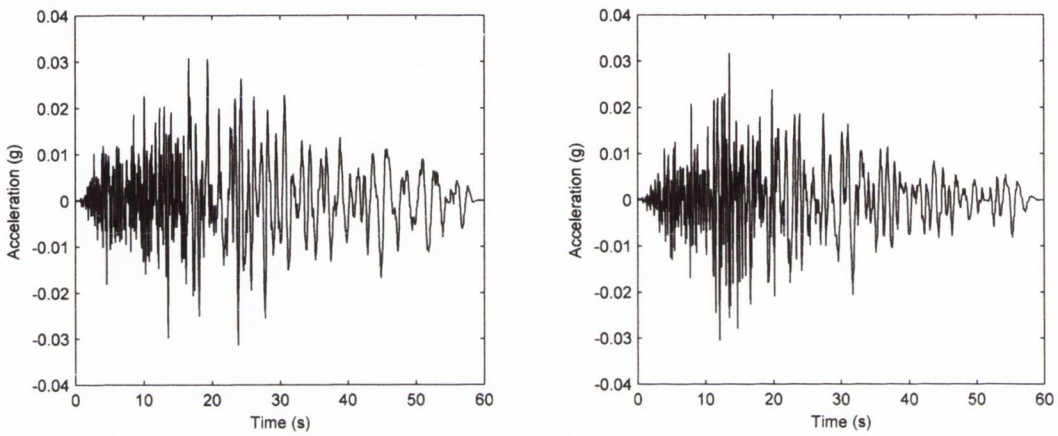

(a) X component.

(b) Y component.

Figure 5.3: X and Y component acceleration ground motion time-histories for 0.03 g earthquake.

earthquake was 1.09 g and the respective component time-histories are presented in Figure 5.4. There was considerable variation in magnitude and epicentral distances between the whole suite of ground motions. Figure 5.5, however, presents an illustration of the individual and mean spectral components of the studied earthquakes for a SDOF oscillator.

The PSDA undertaken for this study will involve matching each of the earthquake ground motion time-histories with the batches of input variables described in Section 5.2.1, carrying out the simulations and assessing the output response. For each simulation, the wind turbine will be initially set at rated operating conditions and subjected to wind loading at the rated wind inflow speed, 11.4 m/s. Due to the complex dynamic effects induced by an emergency shut-down alone, the possibility of shutting down the turbine

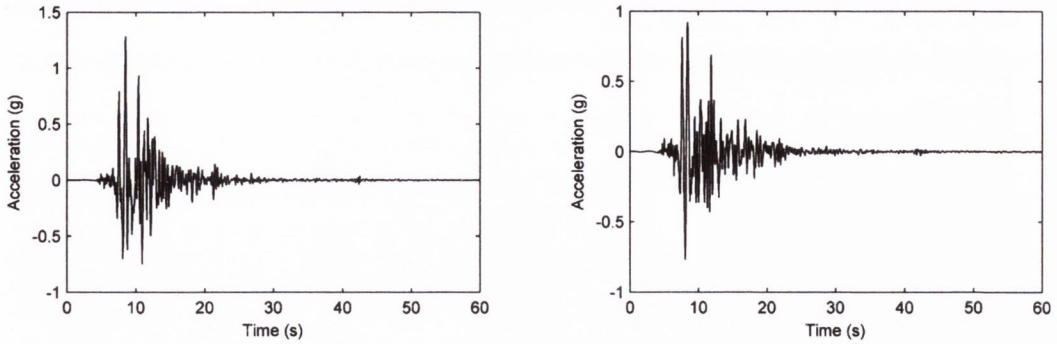

(a) X component. (b) Y component.

Figure 5.4: X and Y component acceleration ground motion time-histories for 1.09 g earthquake.

upon initiation of the earthquake event will not be considered. The wind loading will be considered to act on the turbine throughout the earthquake event and for the remainder of the simulation once the earthquake recedes. In reality, this would not be the case as when the onset of large accelerations is detected, the wind turbine would initiate an emer-

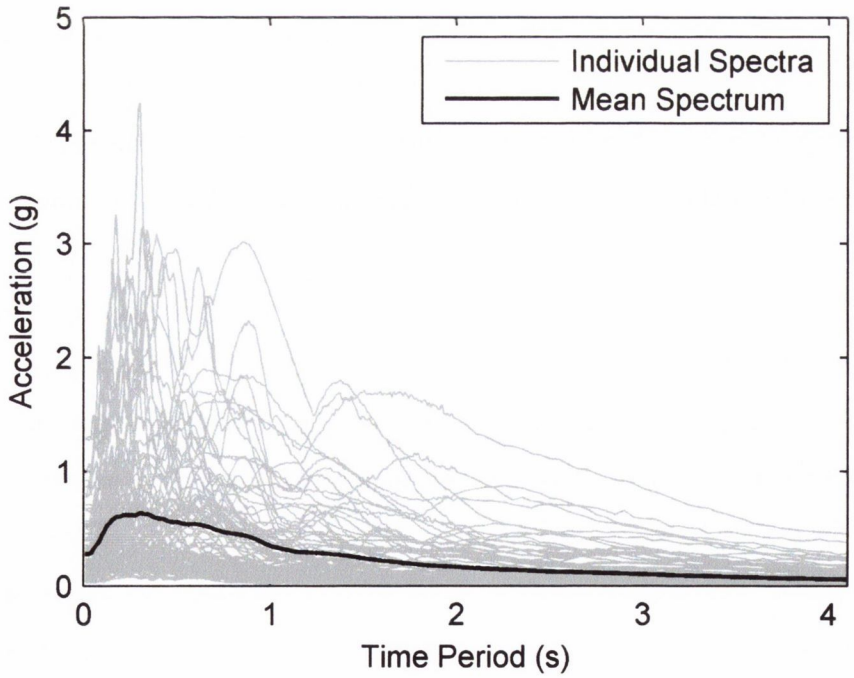

Figure 5.5: Individual and mean spectral components of specified earthquakes for a SDOF oscillator.

gency procedure. However, for the purposes of this comparative analysis of various tower configurations, it is not unreasonable to discount this point.

The response variable used in this study is the maximum resultant nacelle acceleration, which may be computed as $|\ddot{u}_{nac}| = \sqrt{\ddot{u}_{nac,x}^2 + \ddot{u}_{nac,y}^2}$. The justification for using this response variable is that a series of acceleration based limit-state capacities, presented in Section 5.2.5, have been chosen for the fragility analysis. This is a particularly suitable parameter choice given the presence of sensitive control equipment and components in the nacelle, which are susceptible to disruption and damage from excessive accelerations. Figure 5.6 illustrates a sample 200 second acceleration response for the nacelle during simulated earthquake events utilising the ground motion acceleration time-histories depicted in Figure 5.3 and Figure 5.4. In both cases the earthquake initiation is delayed until 60 seconds into the simulation in order to ensure the system has fully stabilised before the earthquake loading is applied as well as to illustrate the steady state response of the turbine subjected to wind loading. Immediately, the contrast in response between the two earthquake ground motion records is noticeable. For the 0.03 g ground motion, the response is depicted in Figure 5.6(a) and Figure 5.6(b). In analysing the longitudinal acceleration response, Figure 5.6(a), it is difficult to identify any change in the accelerations during the earthquake event. A very slight increase in response is noticeable between 75 and 110 seconds although this is difficult to decipher from the steady state response which is less than 0.2 g. At the beginning of the simulation an initial jump in response to 0.8 g is observed but is seen to revert to a steady state response after approximately 25 seconds, corresponding with wind loading at the standard rated wind speed. This is also true of for the larger record in Figure 5.6(c). As a result the first 25 seconds of each simulation will not be considered in any further analysis. Considering the lateral nacelle acceleration response in Figure 5.6(b) the change in response during the earthquake event is more noticeable. With a clear steady state of the order of 0.01 g, the lateral accelerations are seen to extend beyond 0.1 g with an evident jump in response between 65 and 115 seconds. The larger 1.09 g ground motion induces a more considerable departure from the standard response with accelerations of up to 3.4 g in the longitudinal direction and

2.8 g in the lateral direction. In both cases it is seen that the system damping forces the tower response to return to the original wind induced response as the earthquake ground motion recedes.

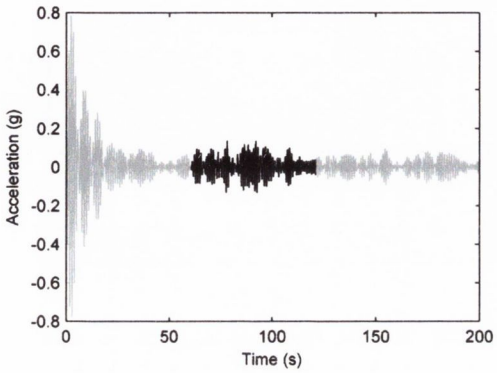

(a) Longitudinal component, 0.03 g.

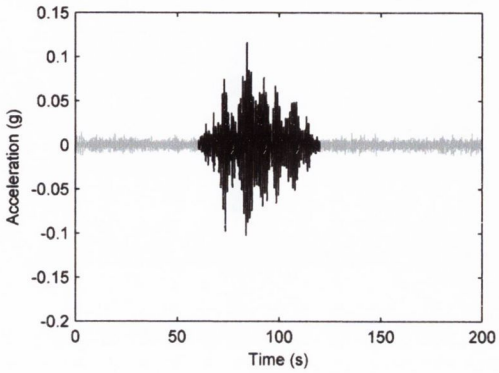

(b) Lateral component, 0.03 g.

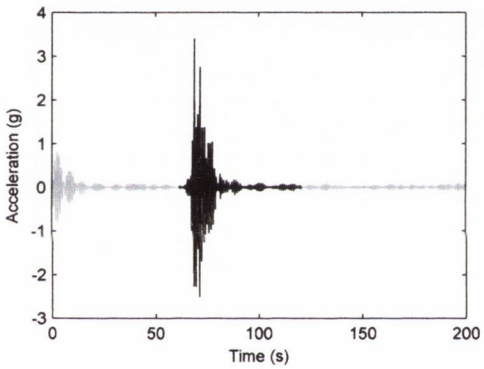

(c) Longitudinal component, 1.09 g.

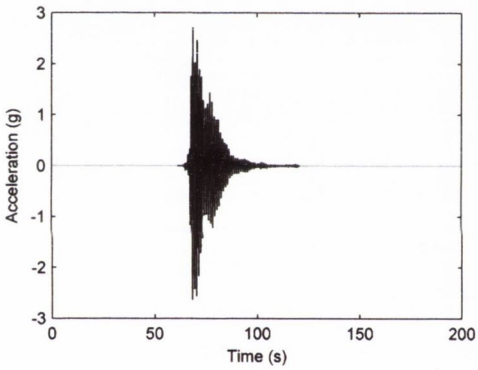

(d) Lateral component, 1.09 g.

Figure 5.6: Nacelle acceleration response for 88 m steel tower to earthquake excitation.

By randomly assigning particular earthquake records to an equal number of individual batches of input properties and conducting a simulation, the seismic demand is computed for each discrete simulation. Figure 5.7 illustrates the linear least squares fit regression in lognormal space for the PSDMs of the portfolio of towers outlined in Section 5.2.1. The resulting computed coefficients, lognormal standard deviation and coefficient of determination are displayed within each plot. Taking the 88 m concrete tower in Figure 5.7(b) as an example, the coefficients are derived as $\ln(a) = 3.4364$ and $b = 1.0556$. The coefficient of determination, r^2, of 94.6% implies a relatively

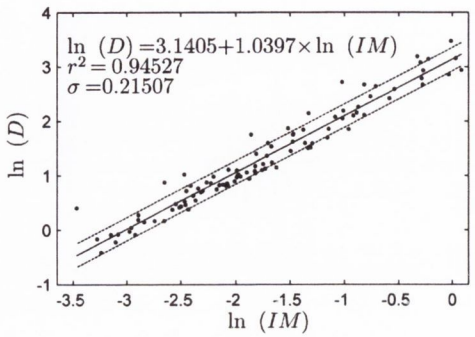

(a) 88 m Steel.

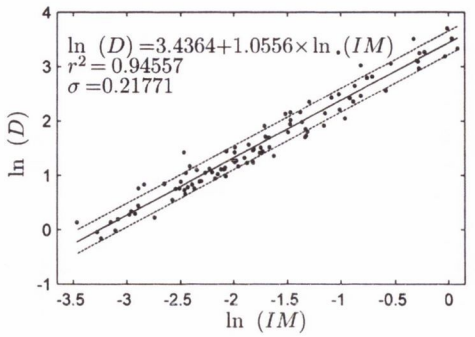

(b) 88 m Concrete.

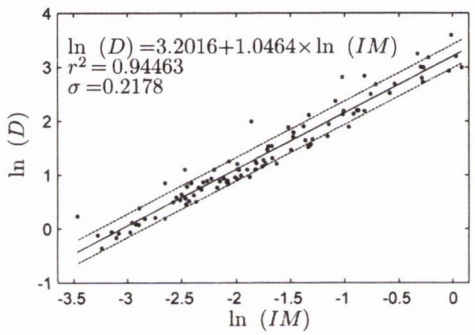

(c) 103 m Steel.

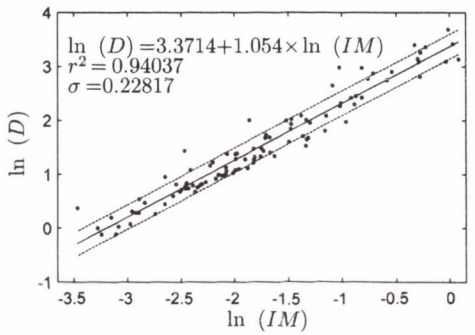

(d) 103 m Concrete.

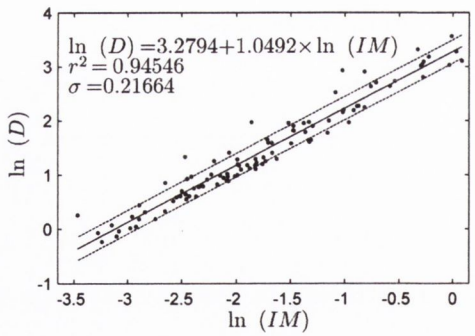

(e) 120 m Steel.

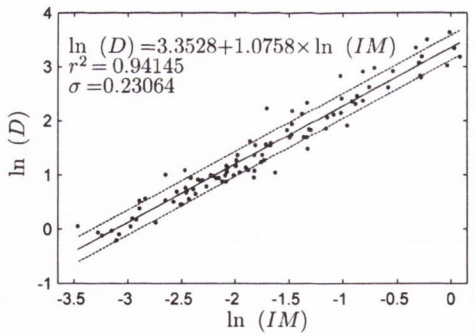

(f) 120 m Concrete.

Figure 5.7: Linear least squares fit regression in lognormal space for computed PSDMs of modelled of towers.

good fit to the data and the dispersion of 0.22 is considered low. The maximum dispersion computed for the 6 tower models was 0.23 as seen in Figure 5.7(f). Mackie and Stojadinović (2005) suggest that a dispersion of 0.3 is considered low and the corresponding model is, therefore, deemed appropriate for fragility curve development. It is particularly interesting to note the values of the linear regression coefficients, $\ln(a)$ and b, in each of the plots. Considering the steel towers in Figures 5.7(a), 5.7(c) and 5.7(e), it can be seen that the coefficients increase with increasing tower height. With regard to the intercept value, this increases by 0.061 between 88 m and 103 m heights and a further 0.078 between 103 m and 120 m. A similar trend is noticeable for the slope values with an increase of 0.007 between 88 m and 103 m and 0.003 between 103 m and 120 m. This trend is as expected, with the natural log of the median value for the demand increasing as the height increases, implying that a greater structural demand is put on the structures as their heights increase. On the other hand, considering the prestressed concrete towers in Figures 5.7(b), 5.7(d) and 5.7(f) the trend seems counter-intuitive with a reversal of the pattern noted for the steel towers. The intercept value decreases by 0.065 and 0.019 respectively over the two increases in height. A less explicit pattern is observed for the slope value with a decrease of 0.002 between 88 m and 103 m but it increases by 0.022 between 103 m and 120 m. This overall pattern implies that with increasing height, the demand placed on the tower structures is, in fact, decreasing, although to a lesser extent between 103 m and 120 m. This variation in the relationship between structural demand and height can be related to the natural frequencies of the different tower structures. Looking at the spectral characteristics of the suite of earthquakes outlined in Figure 5.5, it can be seen that the highest values of SDOF earthquake response lie between a time period of zero and two seconds. This corresponds with a natural frequency range in excess of 0.5 Hz. For a larger time period or lower natural frequency, the response is seen to consistently diminish. Figure 5.8 relates the values for the natural period of the six towers, derived from the natural frequency values defined in Table 5.1, to the mean response spectrum of an SDOF oscillator. Considering the 88 m steel tower, the first natural tower bending period is observed at 3.03 seconds and as the height increases to 103 m and 120 m the natural period is seen to decrease. This indicates,

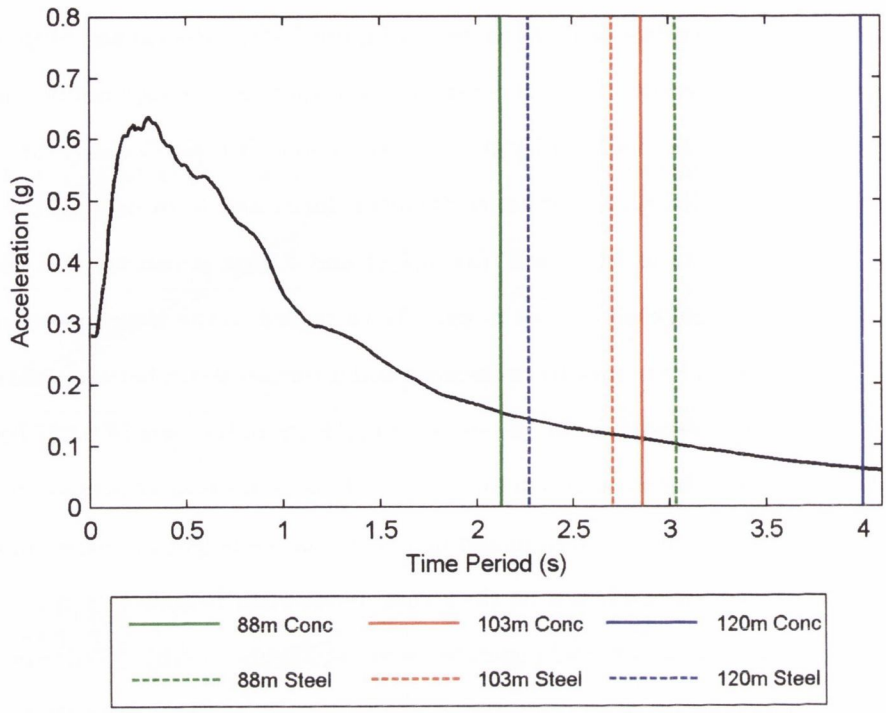

Figure 5.8: Mean earthquake spectrum and tower natural frequencies.

that with increasing height, the steel towers are tending to become stiffer. Relating the natural period values to the mean response spectrum of the suite of earthquakes it can be seen that with increasing height the natural bending period of the steel towers corresponds with a higher spectral response. For the case of the concrete towers, the opposite is true. Due to the fact that the concrete towers all have the properties of the 88 m tower, as the height increases, the bending stiffness reduces. This equates to a longer natural period with increasing height. While the natural period of the 88 m concrete tower corresponds with the greatest spectral response of the six towers, the 120 m tower exhibits the lowest spectral response with a natural period of 4.0 seconds, significantly longer than the next highest value of 3.03 seconds for the 88 m steel tower. Returning to the trend discussed for the linear regression coefficients in Figure 5.7, this is explained by the corresponding spectral responses of the towers for the mean spectrum of the suite of ground motions. The demand on the concrete towers is, somewhat counter-intuitively, decreasing with

increasing height due to the relationship of the tower natural period to the mean response spectrum of the suite of ground motions. Considering this effect for the suite of towers specified by Engström *et al.* (2010) and discussed in Appendix E.3, it is possible to assess the influence that the choice of specified towers has on the results of this chapter. These alternative concrete towers possess natural period values of 1.41 seconds, 1.82 seconds and 2.33 seconds at heights of 80 m, 100 m and 125 m respectively, while the steel towers relate to values of 2.5 seconds, 3.13 seconds and 3.85 seconds over the same range of heights. In both cases the natural period increases with increasing height, thus relating to a decreasing response akin to the studied concrete towers. The most notable factor to be considered, however, is the difference in the magnitudes of the natural periods. The effect of this will be further discussed later in the chapter.

5.2.5 Capacity Estimation

In estimating the capacity of the structure a number of appropriate functional limit-state capacities of wind turbine components were considered. Currently, in the operation of a wind turbine, a routine or emergency shut-down is triggered by either the detection of a wind speed beyond the cut-out wind speed or the occurrence of a fault situation. Dueñas Osorio and Basu (2008) highlighted the shortcomings of such an approach and suggested that acceleration based limit-states should be utilised instead. This would allow for the safe shut-down of the turbine before nacelle accelerations reach critical levels where damage to sensitive components could become an issue. As a lower-bound, a nacelle acceleration of $1\,m/s^2$ was investigated. Prowell *et al.* (2010) suggested this value as the point at which an emergency shut-down could be induced in the wind turbine system in order to avoid severe damage to sensitive equipment. It was found that each record in the suite of ground motions induced this minimum acceleration in all 6 towers. The limit-states employed in this study are based on levels of nacelle acceleration which impair the functionality of the wind turbine. Porter and Kiremidjian (2001) outlined the seismic vulnerability of various components present in buildings but which are also common in wind turbines. These include motors, generators, switchgear and electronic controls with

corresponding critical accelerations of 0.79 g, 0.87 g, 1.6 g and 3.5 g respectively. These acceleration thresholds will be utilised to define the limit-state capacities for the current study. Table 5.2 summarises the median acceleration and logarithmic standard deviation (dispersion) for each component limit-state.

Component	Motors	Generators	Switchgear	Electronic Controls
Acceleration Threshold (g)	0.79	0.87	1.6	3.5
Dispersion (β_C)	0.52	0.51	0.8	0.25

Table 5.2: Median and logarithmic standard deviation of acceleration limit-state values (Porter and Kiremidjian, 2001).

5.3 Fragility Analysis

The generation of fragility curves offers a performance based assessment of the various tower configurations when subjected to the suite of recorded ground motions. This ensures a general outline of the relative response characteristics for the towers to the seismicity of California.

Having quantified the seismic demand and seismic capacity for the particular structure or component in question, it is possible using Equation (5.5), to establish a fragility function. More appropriately, the calculated parameter values ($\ln(a)$, b, $\beta_{D|IM}$) from the PSDMs outlined in Section 5.2.4 along with capacity estimates for the acceleration limit-states may be used to estimate the likelihood of exceeding the proposed acceleration limit-state capacities by rearranging Equation (5.5) into the following form:

$$P\left[LS|IM\right] = \Phi\left(\frac{\ln\left(IM\right) - \frac{\ln(S_C)-\ln(a)}{b}}{\frac{\sqrt{\beta_{D|IM}^2+\beta_C^2}}{b}}\right) \tag{5.6}$$

where S_C is the proposed limit-state capacity and β_C is the associated dispersion. The fragility of the tower is subsequently modelled as a lognormal distribution as follows:

$$P\left[LS|IM\right] = \Phi\left(\frac{\ln\left(IM\right) - med_t}{\beta_t}\right) \tag{5.7}$$

where the median, $med_t = \frac{\ln(S_C)-\ln(a)}{b}$ and the dispersion, $\beta_t = \frac{\sqrt{\beta^2_{D|IM}+\beta^2_C}}{b}$. The fragility of the tower can then be assessed for each acceleration threshold specified in Table 5.2. The calculated results are presented in the following sections.

5.3.1 Standard Towers

Figure 5.9 illustrates the probabilities of LSE for each of the 3 sets of towers for the specified tower heights. Beginning with the 88 m tower, Figure 5.9(a), it is noticeable

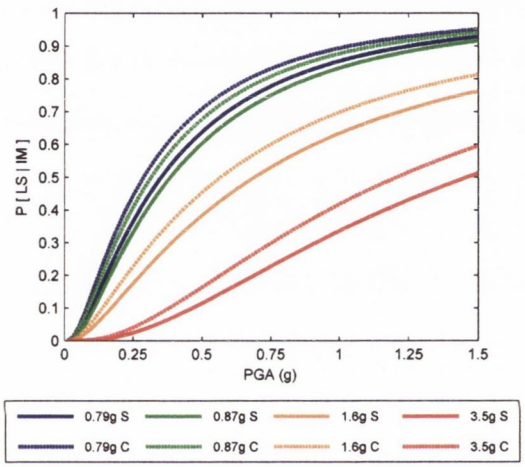

(a) 88 m Towers.

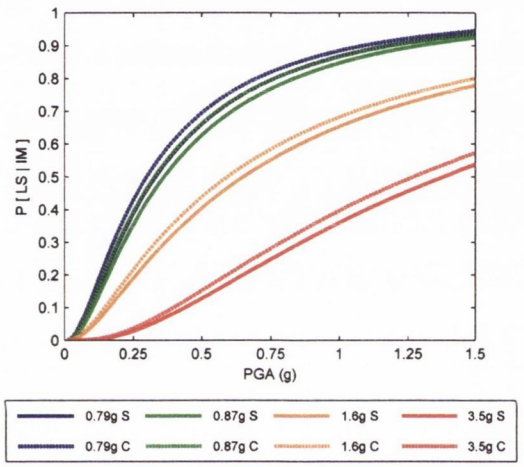

(b) 103 m Towers.

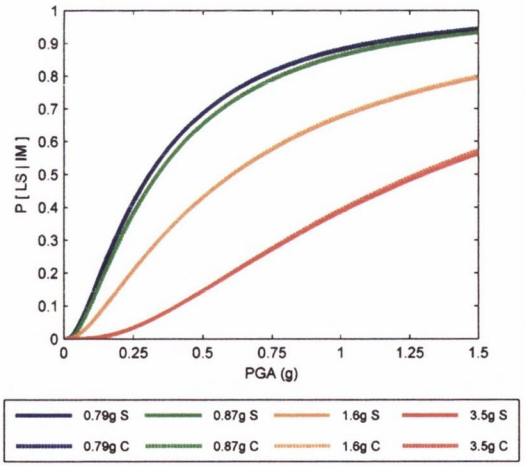

(c) 120 m Towers.

Figure 5.9: Seismic fragility curves for steel and concrete wind turbine towers.

in the plot that the dashed lines, which represent the concrete tower (C), exhibit higher probabilities of LSE than the solid lines, which represent the steel tower (S). Although the difference is not significant (a maximum difference in probability of LSE of 0.09), it implies that the steel design is more stable in an earthquake event and provides a reduced probability of exceeding the acceleration limit-states defined in Section 5.2.5 for a tower of this height. As the tower height increases to 103 m, as shown in Figure 5.9(b), the disparity between the tower performance decreases, although the concrete tower continues to exhibit higher probabilities of LSE. The steel tower remains the more advantageous solution in terms of increasing the reliability of sensitive components which are critical to the operation of the turbine. Figure 5.9(c) portrays the relative performance of the 120 m towers. It is evident that the probabilities of LSE are essentially equal. This indicates that at a height of 120 m there is minimal difference between the two tower designs when considering the vulnerability of the turbine components during seismic events. Overall, a trend is evident in the results which sees the probability of LSE increasing with height for the steel towers while the converse is true for the concrete towers. As with the variation in PSDM results, this can be explained by the differing trends in the change in tower natural frequency with height for the two materials. In assessing these results it is also essential to regard the decision in Section 5.2.1 to utilise the same properties as for the 88 m concrete tower in modelling the 103 m and 120 m towers. When compared to another set of similar, designed towers in Appendix E.3, a notable difference in the structural properties related to the natural period values, a property which is very relevant to seismic response. When assessed in the context of Figure 5.8, the values for the concrete towers are all below 2.33 seconds, thus relating to a more significant mean spectral response than the studied towers. Considering the steel towers, at the 80 m height the natural period is 2.5 seconds, compared to 3.03 seconds for the studied tower. This would imply a higher mean spectral response from the comparison tower. For the taller steel towers, however, the values are both above 3 seconds, with the 125 m tower possessing a value (3.85 seconds) quite close to that of the 120 m studied concrete tower (4.0 seconds). As a result, the 100 m and 125 m steel towers would be expected to exhibit a reduced response as compared to the similar

studied towers. Overall, the general trend that would be expected is for the concrete tower response to increase while the steel tower response decreases thus accentuating the difference in response outlined in the results presented in this chapter.

5.3.2 Long Term Effects in Prestressed Concrete Towers

Figure 5.10 displays the results of a second fragility analysis of the same suite of towers as discussed in Section 5.3.1, except with the consideration for the effects of creep and

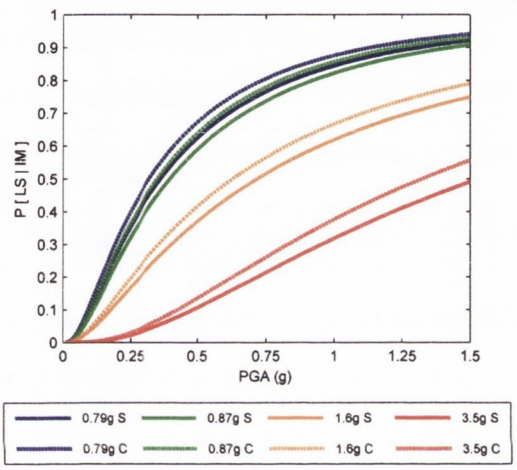

(a) 88 m Towers.

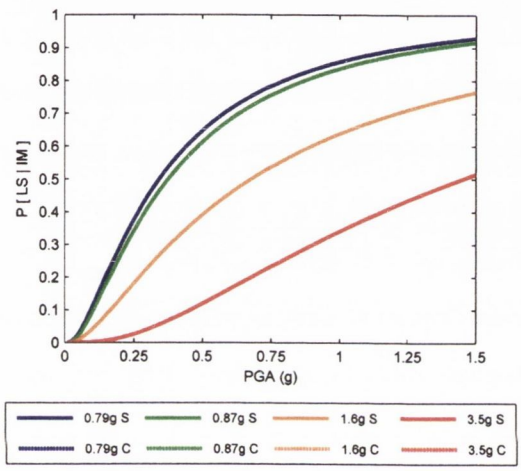

(b) 103 m Towers.

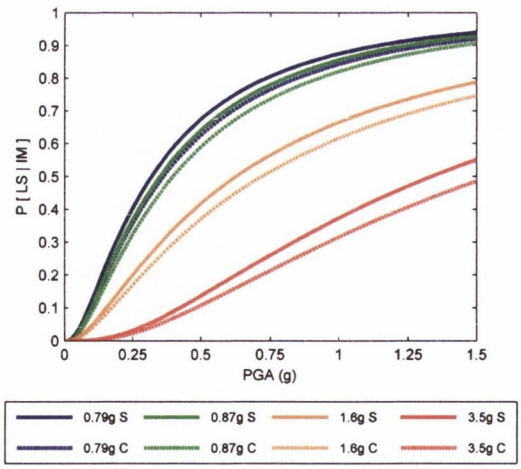

(c) 120 m Towers.

Figure 5.10: Seismic fragility curves for steel and concrete wind turbine towers incorporating long term effects in concrete.

shrinkage on the time-dependent representation of the modulus of elasticity in the concrete towers. In this instance, given that the bending stiffness of the concrete towers is reduced due to long term effects, it would be expected that the probability of LSE would therefore increase. However, this is shown not to be the case. Again, it is evident that little difference exists between the two tower designs for LSE although it is possible to separate the two designs in terms of relative performance. At 88 m the steel design can be seen to display lower probabilities of LSE. This is similar to the result for the standard concrete design outlined in Figure 5.9(a). Figure 5.10(b) shows that at 103 m there exists no difference in performance between the two tower designs. Comparing this to Figure 5.9(b) an improvement in performance is noticeable for the concrete tower configuration when long term effects are accounted for when considering a tower of 103 m in height. This fact is reiterated in Figure 5.10(c) where the concrete tower is seen to outperform the steel design when it was only capable of equalling the performance in Figure 5.9(c). Again, it seems counter-intuitive that by reducing the bending resistance of the concrete tower an improvement in performance may be achieved. This is, however, due to the position of the natural period of the towers relative to the mean response spectrum of the suite of earthquakes used in the study. As shown in Figure 5.8, structures with a higher natural period will experience a lower response to the earthquake ground motions. By reducing the bending stiffness of the towers, as was done in this analysis, the natural period of the structure is lengthened and therefore the mean response of the structure is also reduced. Despite the improved performance of the concrete towers in this instance, it is most likely that a stronger design with a shorter natural period, such as those detailed in Appendix E, would need to be employed for the 103 m and 120 m towers in order to satisfy serviceability limit-states.

5.3.3 The Effects of High Strain Rates on Concrete

The final analysis in this chapter addresses the effect of the rate of load application on the performance of the prestressed concrete towers. As discussed in Section 5.2.3, due to the high rates of load application associated with earthquake events, concrete structures can

behave with an instantaneous stiffness which is significantly greater than that observed under static loading conditions. Based on the evidence in Neville (1996), a 50 % increase in the modulus of elasticity for concrete was considered here. Intuitively, it would be expected that by increasing the bending stiffness of the tower, a reduction in the probability of LSE would be achieved. However, before consulting the simulated results illustrated in Figure 5.11, based on the findings of the previous analysis it is not difficult to envisage the effect

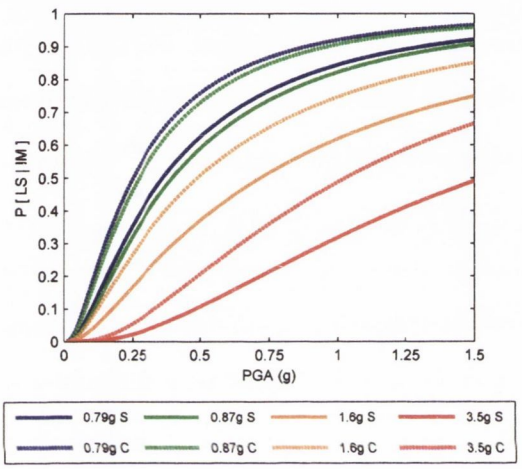

(a) 88 m Towers.

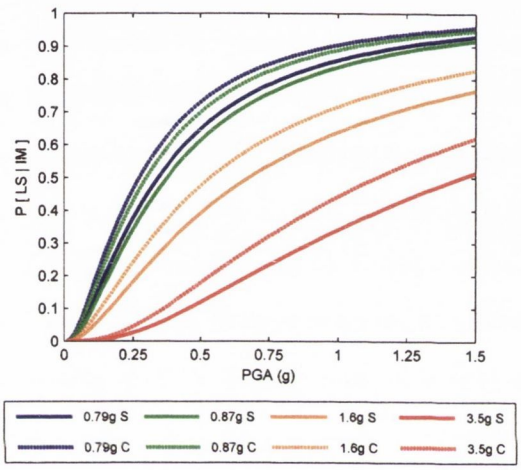

(b) 103 m Towers.

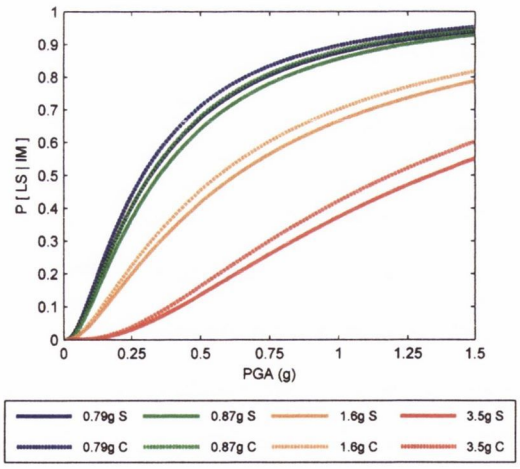

(c) 120 m Towers.

Figure 5.11: Seismic fragility curves for steel and concrete wind turbine towers incorporating the effects of high rates of load application for concrete towers.

this increase in bending stiffness will have on the results. By increasing the bending stiffness, the natural period of the structures are shortened and therefore, the towers will be susceptible to a higher mean response based on the mean response spectrum for the suite of earthquakes, illustrated in Figure 5.8.

Figure 5.11(a) displays the results for the 88 m steel and concrete towers. So far, from all of the results presented, this plot shows the greatest difference in performance observed in this study. A clear distinction exists between the concrete and steel towers, with the concrete tower exhibiting a higher probability, of up to 0.14, of LSE at a PGA of 0.5 g for the 1.6 g limit-state and 0.18 higher at 1.5 g PGA for the 3.5 g limit-state. As the height is increased to 103 m, Figure 5.11(b), the difference in performance is reduced to 0.9 at a PGA of 0.5 g for the 1.6 g limit-state and 0.11 at 1.5 g PGA for the 3.5 g limit-state. The improved performance of the steel tower is, once again, reduced in Figure 5.11(c) for the 120 m towers. Despite this, the steel tower continues to outperform the concrete tower. If another design, such as that specified by Engström *et al.* (2010), had been employed for the 103 m and 120 m prestressed concrete towers in this particular analysis, the natural period of the taller towers would have been further shortened and the resulting performance displayed in Figure 5.11(b) and 5.11(c) may closer resemble that of Figure 5.11(a).

5.4 Conclusion

With the growing prominence of wind turbines in seismic regions around the world as well as their increasing structural size in order to achieve greater efficiencies, there is an obvious requirement to improve the understanding of the seismic response of large scale multi-megawatt wind turbines. Also, as these turbines evolve, the possibility of employing alternative tower construction materials has become a reality with the use of prestressed concrete or hybrid tower configurations in place of the current industry standard steel option. This chapter set out to implement the capabilities of the structural model derived in Chapter 3 in order to quantify the relative performance of both steel and concrete

tower designs when subjected to seismic loading. In keeping with the analysis in Chapter 4, it was proposed to employ a probabilistic framework in the investigation of a series of 6 towers, 3 concrete and 3 steel for tower heights of 88 m, 103 m and 120 m. Fragility curves provided a means of relating the relative structural performance from a reliability perspective.

The two dimensional model derived in Chapter 3, and extended to cater for seismic loading, allowed for the simulation of two dimensional earthquake ground motions in combination with a specified wind loading. Turbulent wind loading was simulated for a mean hub-height speed of 11.4 m/s, the turbine's rated wind speed, and applied to the operating wind turbine throughout the simulations. Following an initial period allowed for the stabilisation of the dynamic system, recorded ground motion acceleration time-histories were subsequently applied to the operating wind turbine system and the resulting displacements and accelerations were analysed.

In order to generate the necessary fragility curves, probabilistic seismic demand analysis was performed on each of the towers. A suite of 100 recorded ground motions were utilised. These were representative of the seismicity of California, a region with a high density of wind turbine structures. By utilising peak ground acceleration as the seismic intensity measure a probabilistic seismic demand model was derived for each tower. This provided a mathematical relationship between the ground motion intensity measure and the structural response for each individual tower. The response variable chosen for the study was nacelle acceleration as this could be appropriately related to a series of acceleration based limit-states which define the ULS condition for various electronic and mechanical components located in the nacelle. This was shown to follow a power law relationship, which, when transformed into lognormal space, assumed a linear form. On undertaking a linear least squares fit regression of the data, a set of coefficients were established which quantified the relationship. Having specified values for the lognormally distributed capacity limit-states, the combination of the capacity and demand estimates was utilised in the formulation of the fragility curves.

With the aid of the individual demand models a series of fragility curves were generated

which outlined the probability of limit-state exceedance (LSE) for each individual tower with increasing ground motion intensity. This was carried out for three concrete tower conditions: standard towers, reduced stiffness due to long term effects, and increased stiffness due to the high rate of load application associated with earthquakes. The limit-states were based on a vulnerability study of components in buildings which are also common to wind turbines such as motors, generators, switchgear and electronic controls. For the case of the standard concrete towers it was shown that the steel design outperformed the concrete design at a height of 88 m. As the height increased, however, the gap was reduced with the two designs displaying similar performance at the 120 m height. When long term effects such as creep and shrinkage were considered a similar pattern was noted but the designs displayed equal performance at 103 m and the concrete tower outperformed the steel tower at 120 m. In a third analysis, the concrete towers were assumed to have a 50 % higher instantaneous modulus of elasticity based on evidence in the literature which suggests an increase in concrete strength at high rates of load application. The results of this analysis showed a distinct advantage for the steel towers across all heights and limit-states. These findings appear in one sense counter-intuitive given the expectation that a reduction in stiffness will relate to a decrease in performance and, conversely, an increase in stiffness will improve performance. Following an investigation of the results it was found that the most significant influence on the response values for the towers proved to be the value for the first natural bending frequency of the tower. Due to a lack of publicly available data on concrete wind turbine towers, the 103 m and 120 m prestressed concrete towers were implemented with the same base and top diameters, as well as concrete thickness, as the 88 m prestressed concrete tower. They were designed to be baseline estimates of the tower strength which in reality would be constructed from a stiffer design. It was shown, that due to the choice of concrete towers utilised in this study, the values for the first natural bending period were larger than in reality. While the steel towers showed a small decrease in natural period with increasing height, the concrete towers exhibited considerably larger values as the height increased. It was demonstrated that those structures with shorter natural period were susceptible to a larger mean response based on the

mean response spectrum for the suite of earthquake ground motions used in the study. This fact undoubtedly affected the outcome of this investigation. When consideration was given to a set of similar, designed towers, it was noted that the difference in response for the two tower materials would be further separated, with the steel towers exhibiting superior performance relative to the corresponding concrete towers. This conclusion is established from the significant difference in the natural period values for the two tower materials. While the prestressed concrete comparison towers possess noticeably smaller natural period values than the studied towers, this is not to say that every viable design must necessarily subscribe to such properties. Given that the 88 m concrete tower is a feasible design, with a natural period of 2.13 seconds and the comparison tower equates to a value of 1.41 seconds, it is clear that acceptable designs can be achieved for quite a range of natural period values. It is obvious, therefore, that it is essential to consider the operational environment and the local seismic risk when defining a particular wind turbine tower solution.

Aside from the quantitative outcomes of these analyses, this chapter provided a methodology for further investigation of wind turbine seismic performance with the application of probabilistic seismic demand analysis, a framework common to building and bridge structures but thus far unused in wind turbine applications. It also highlighted the considerable influence of the natural frequencies of the tower structures on the resulting responses and emphasises the benefit of structural control and damping systems for the protection of structures in seismically active regions. As a recommendation for future work, given the effect of the tower bending frequency on the seismic response, further investigation of tuned mass dampers and, more appropriately, active mass damper systems could prove highly beneficial to the future of wind turbine structures.

Chapter 6 -

Soil Structure Interaction

6.1 Introduction

The foundation of a wind turbine provides the sole link between the turbine structure and the underlying body of soil. It is, therefore, a crucial element of the structural design and must be detailed in a manner that ensures sufficient stability for the wind turbine components while at the same time satisfying cost, environmental and feasibility requirements. It is obvious that the form of the foundation is very much dependent on the underlying soil conditions as well as the surrounding environment. The contrasting requirements for both onshore and offshore foundation solutions has already been discussed in detail in Chapter 2. In keeping with the previous studies carried out, the focus of the current chapter will center on onshore foundations for large scale multi-megawatt wind turbines, for which the constraints of water depth and hydrodynamic loading are not an issue.

As noted in Section 2.6.3, in the analysis and design of wind turbine structures it is not uncommon for the connection between the structure and the underlying soil to be considered as a fully fixed support. This assumption has been proven to achieve acceptable results for certain stiff soil conditions (Harte *et al.*, 2012; Luco, 1986), and is considered a reasonable assumption in the initial design of a wind turbine structure (Hau, 2006). Despite these endorsements of a fixed support assumption in certain situations, it has without doubt been proven that SSI effects can have a significant impact on the dynamic response of a wind turbine structure. Most notably it has the influence of reducing the natural frequency of the structure and increasing the magnitude of maximum displacements (Andersen *et al.*, 2012; Bhattacharya and Adhikari, 2011; Murtagh *et al.*, 2005a).

In one particular study by He (2009) it was shown that the tower tip displacements of a wind turbine increased by 26% when SSI effects were included.

This study builds on the modelling procedure set out in Chapter 3 which sees the initial two dimensional model extended to cater for the additional DOFs introduced by the soil. This is achieved by introducing horizontal and rotational springs with specified static stiffness at the base of the tower. This is the most commonly used approach for modelling SSI in simulation tools for onshore wind turbines (Zaaijer, 2006). In fact, some tools neglect the horizontal spring and include the rotation spring only. A considerable assumption employed in this methodology is the choice of a static stiffness for the various springs. Soil is known to behave in an inherently non-linear fashion when subjected to variable loading and this is reflected in the various non-linear soil models which have been established in practice, including the Mohr-Coloumb (MC), Hardening Soil (HS) and Hardening Soil with small strain stiffness (HSS) models. Despite this, static stiffness values are common as part of SSI modelling for wind turbines (Zaaijer, 2006). DNV (2001) states for SSI models, that the dynamic stiffness may deviate from the static stiffness, in particular for the case of high frequent vibrations. However, for wind and wave loading of wind turbine foundations, for both onshore and offshore applications, the induced vibrations will be of such a nature that the static stiffnesses will be representative of the dynamic stiffnesses that are required in structural analysis. For the case of earthquake loading, however, frequency-dependent reductions of the static stiffnesses to get appropriate dynamic stiffnesses may be required and should be considered (DNV, 2002).

For the aforementioned reasons, the proposed study will focus solely on wind induced vibrations as any analysis of seismic responses would necessitate a frequency dependent soil stiffness model which is beyond the scope of this work. In the current chapter, the probabilistic approach of previous chapters will be extended to incorporate an analysis of SSI effects on both steel and concrete wind turbine towers. This investigation is carried out in collaboration with the Geotechnical Research Group (GRG) at University College Dublin (UCD) who operate an active test site for large scale deep and shallow foundations at Blessington, County Wicklow. The proposed investigation complements ongoing

research into the evaluation of the static and dynamic response of foundation solutions for offshore and onshore wind turbines. Utilising the soil properties of the test site, the GRG develop a 2D FE representation of the soil using a number of non-linear soil models.

The current investigation considers the 88 m steel and concrete towers defined in Section 4.2 in combination with the NREL 5 MW nacelle unit outlined in Section 3.5.1. An analysis of the maximum loads at the foundation/tower interface is carried out using the wind turbine design code FAST (Jonkman, 2012) for a series of primary load cases defined in BS EN 61400-1 (2005). An appropriately sized reinforced concrete spread footing is designed to cater for the maximum loading conditions for the concrete tower using the soil conditions of the test site. The process is repeated for the steel tower and a comparison of the resulting designs is established. For the purposes of the overall analysis, however, the foundation specified for the concrete tower is also applied to the steel tower in order to ensure an equal comparison. Combining the specified foundation, the calculated loads and the derived non-linear FE models, the required spring stiffnesses of the horizontal and rotational springs may be formulated. Similar to previous chapters, the structural input properties of the towers are subsequently modelled as random variables with specified PDF, mean and CoV which results in batches of input properties with statistically representative values. By carrying out simulations for each of the batches a statistical representation of the response is developed. Akin to previous chapters, this is illustrated through the use of fragility curves which relate the probability of exceeding a prescribed limit to the wind loading intensity. The response of both the nacelle and blades is analysed and compared to results for simulations not including SSI. A comparison is also drawn between the performance of the tubular steel and prestressed concrete towers in order to identify any possible differences in performance.

The purpose of this collaborative analysis between the author and the UCD GRG is for the production of a peer reviewed publication, detailing the relative influence of SSI on both tubular steel and prestressed concrete towers. From the author's perspective, the requirement was to implement an appropriate set of soil stiffness values, as part of the dynamic structural analysis, which would accurately capture the behaviour of a variable sup-

port condition at the base of the tower for a particular set of soil conditions. As part of this process, the tasks outlined throughout the remainder of this chapter were divided between the author and the researchers at UCD. Initially, the author carried out a detailed analysis of the ultimate loading conditions for both the prestressed concrete and tubular steel towers, as detailed in Section 6.3.1. This resulted in the calculation of critical loads at the base of the wind turbine tower which would be utilised in the foundation design. Using the soil properties of the UCD test site, the GRG designed and optimised a reinforced concrete slab foundation to cater for the critical loads which were previously established. This is discussed in Section 6.3.2. Utilising the proposed design, the GRG subsequently developed three different soil models as part of an FE analysis of the foundation and associated soil conditions. This produced a series of soil stiffness values representative of the variable support condition at the base of both the steel and concrete towers. The relevant details of this procedure are discussed in Sections 6.4 and 6.5. Implementing the calculated soil properties, Sections 6.6 and 6.7 describe the subsequent probabilistic analysis of the performance of both the steel and concrete towers, undertaken by the author. Further details of the implementation and outcomes of this study are provided in the following sections.

6.2 Test Site

The UCD GRG test site was chosen as a basis for the soil properties of a model of the SSI for the wind turbine. This particular site, which has been in operation for approximately 10 years, is an active test site for large scale deep and shallow foundations. The proposed analysis complements ongoing research into the evaluation of the static and dynamic response of wind turbine foundation solutions at the site. Thus far, thorough examinations of the soil properties have been undertaken (Gavin *et al.*, 2009; Gavin and O'Kelly, 2007; Gavin and Lehane, 2007), and a site specific HS model used in 2D PLAXIS FE analysis had previously been evaluated and calibrated by Tolooiyan and Gavin (2011). A summary of the site conditions can be found in Doherty *et al.* (2012) and a brief overview of the test site is provided in the current section.

The GRG site is located in a disused sand quarry in Blessington, County Wicklow, approximately 25 km southwest of Dublin. The site is composed of very dense sand with relative densities close to 100%. The sand has a constant volume friction angle of 36 ° with peak friction angles ranging between 36 ° and 54 °. The test site is in an over-consolidated state due to glacial action, ground water level changes, and recent sand extraction. The maximum pre-consolidation stress estimated from oedometer tests is approximately 800 kPa. The unit weight of the material calculated from sand replacement tests is $20\,kN/m^3$.

Extensive Cone Penetration Testing (CPT) has been performed at the site in association with model pile and footing tests. These tests reveal that the site has uniform and consistent soil properties throughout as reflected in Figure 6.1(a), where the multi-coloured lines represent various CPT tests across the site. Gavin *et al.* (2009) carried

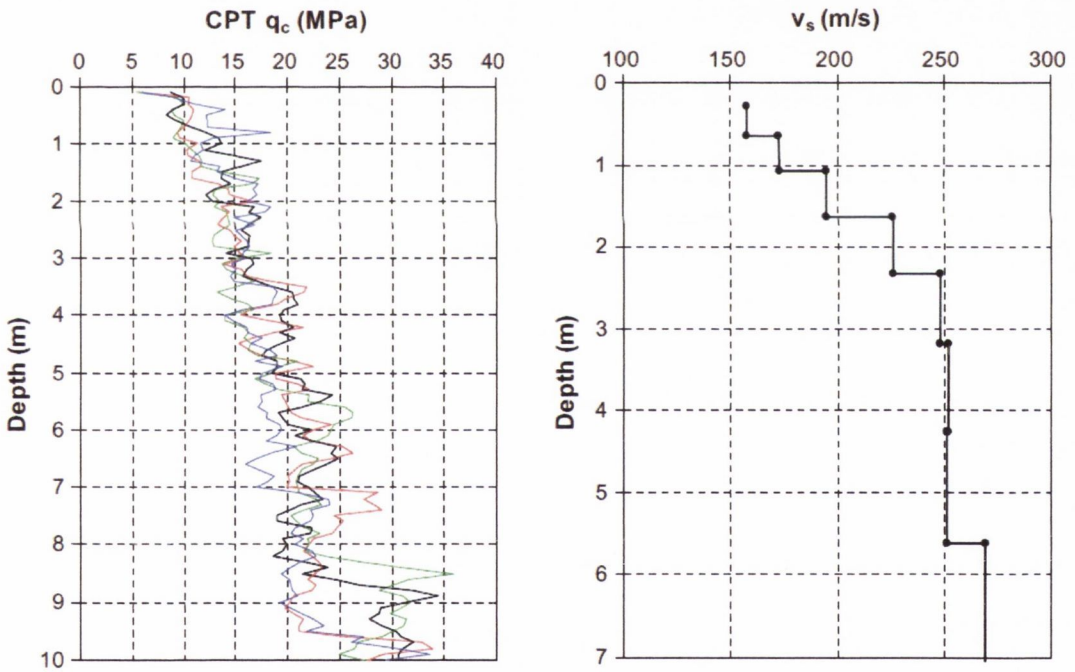

(a) CPT q_c profile.

(b) Shear wave velocity profile.

Figure 6.1: Soil testing results for dense sand at Blessington test site (Tolooiyan and Gavin, 2011).

out a range of plate loading tests which showed that the bearing capacity for the sand correlates well with the CPT q_c values. A value of 20% of the CPT q_c provides an accurate

estimate of the bearing capacity for a range of footing sizes for settlements of 10% of the foundation width. Soil stiffness values, Young's Modulus (E_0), and the initial small strain Shear Modulus (G_0), are also relatively high. The stiffness parameters were estimated from correlations with the shear wave velocity (v_s) measured using the Multi-Channel Analysis of Surface Waves (MASW) as depicted in Figure 6.1(b).

6.3 Foundation Design

Each of the loading components applied to a wind turbine system must be transferred through the structural system, into the foundation and subsequently into the underlying soil. These loads manifest themselves into forces and moments at the base of the tower as illustrated in Figure 6.2. As a result, the foundation must be designed to resist each

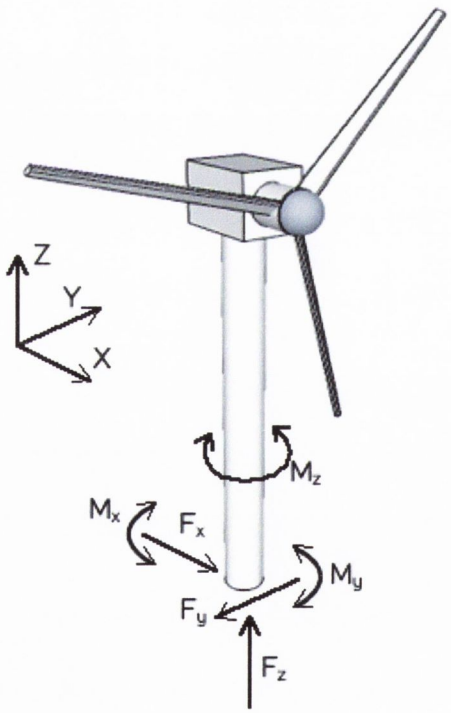

Figure 6.2: Outline of wind turbine foundation loads.

of these components. The governing criteria for wind turbine foundation design are rotational and horizontal stiffnesses. Wind turbine foundations must be adequately stiff

in order to avoid excessive motion at nacelle height. Bearing capacity and settlement issues are not as important because vertical loads for wind turbines are generally quite low (e.g. 50-75 kPa) and in most cases cause less than 25 mm of settlement in soils having adequate bearing capacity and stiffness (Tinjum and Christensen, 2010). Typical minimum values of the rotational and horizontal stiffnesses are 50 GNm/rad and 1000 MN/m respectively. However, in accordance with increasing wind turbine sizes and the related loading conditions these minimum acceptable values will need to be increased.

For the current study two tower configurations have been chosen to be investigated, namely an 88 m tubular steel tower and a prestressed concrete tower of equivalent height. The details of these towers have already been presented in Section 4.2. The steel tower is the equivalent land based tower specified for the NREL 5 MW baseline wind turbine (Jonkman *et al.*, 2009). This particular reference wind turbine is a well developed concept widely used in the literature. Whilst an associated foundation has not been prescribed, all of the necessary input properties are available for a detailed dynamic analysis using the verified wind turbine design code, FAST (Jonkman, 2012). This will allow accurate calculation of the ultimate and fatigue wind turbine design loads. The following section will describe the calculation of the force and moment components described in Figure 6.2.

6.3.1 Calculation of Critical Loads

In order to assess the loads to which the wind turbine will be subjected to throughout its lifetime, BS EN 61400-1 (2005) outlines a series of DLCs which encompass the majority of design situations relating to normal operation, start-up, shut-down, parked/idling states, fault situations, transportation, assembly, erection and maintenance conditions. The DLCs consider both extreme (ultimate) and fatigue loading situations expected over the lifetime of the machine. While the DLCs do not attempt to form an exhaustive list of the various combinations of operational states and external conditions, they do consider the cases of primary importance and are suggested as a minimum requirement for the verification of a wind turbine design.

For the case of the steel tower, an extensive loads analysis is provided for the wind

turbine system in Jonkman (2007). While this analysis relates to an offshore floating concept, a preliminary examination of the design loads is carried out for the onshore condition. For this preliminary loads analysis, it was not considered necessary to run all the DLCs prescribed by the design standards but instead to eliminate the fatigue-type DLCs and process only the anticipated ultimate loads. This omission follows from standard design practice for land-based and fixed-bottom sea-based wind turbines in which the structure is configured to survive ultimate loads before it is checked for fatigue. This is also relevant in the current instance where the design is confined to the foundation. While fatigue loads will often dictate the eventual design of specific wind turbine components such as the tower and blades, they have limited relevance in the foundation design.

Due to limitations with the control system of the particular turbine it was not deemed appropriate to include the DLCs concerning turbine start-up and shut-down. It was, however, possible to consider shut down in the case of a fault occurrence. Furthermore, DLCs relating to transport, assembly, maintenance and repair were not considered relevant to the foundation design. The remaining ultimate-type DLCs included cases for power production, power production with occurrence of fault, parked/idling and parked with a fault. Table 6.1 summarises the selected DLCs in conjunction with their associated safety factors which are relevant only to the foundation design. Each of the wind models specified for the DLCs are defined in BS EN 61400-1 (2005). They include the NTM, ETM, ECD, EWS, EOG and EWM. The specific wind models are defined in terms of the hub height wind speed, v_{hub}, which is assessed within the range of the wind turbine cut-in wind speed, v_{in}, the rated wind speed, v_r, and the cut-out wind speed, v_{out}. Each of the DLCs were simulated using the wind turbine design code FAST (Jonkman, 2012). This code utilises AeroDyn (Laino, 2012) to calculate the associated aerodynamic loads affecting the blade elements as well as the nacelle and tower. Full-field three-component turbulent wind velocity time-histories are developed with TurbSim (Kelley and Jonkman, 2012) employing the Kaimal spectrum (Kaimal *et al.*, 1972) and the specific non turbulent IEC (BS EN 61400-1, 2005) wind events are generated by IECWind (Buhl, 2012). For the power-production cases with and without faults, the quasi-steady BEM axial-induction

DLC	Model	Speed	Controls/Events	Load Factor
		Power Production		
1.1	NTM	$v_{in} < v_{hub} < v_{out}$	Normal operation	1.25×1.2
1.3	ETM	$v_{in} < v_{hub} < v_{out}$	Normal operation	1.35
1.4	ECD	$v_{hub} = v_r, v_r \pm 2\,m/s$	Normal operation $\pm\triangle$ wind direction	1.35
1.5	EWS	$v_{in} < v_{hub} < v_{out}$	Normal operation $\pm\triangle$ vert/horiz shear	1.35
		Power Production Plus Occurrence of Fault		
2.1	NTM	$v_{hub} = v_r, v_{out}$	Pitch runaway $\longrightarrow$ shut-down	1.35
2.3	EOG	$v_{hub} = v_r, v_r \pm 2\,m/s, v_{out}$	Loss of load $\longrightarrow$ shut-down	1.10
		Parked/Idling		
6.1	EWM	$v_{hub} = 0.95 \times v_{50}$	Yaw $= 0°, \pm 8°$	1.35
6.2	EWM	$v_{hub} = 0.95 \times v_{50}$	Loss of grid $\longrightarrow -180° <$ Yaw $< 180°$	1.10
6.3	EWM	$v_{hub} = 0.95 \times v_1$	Yaw $= 0°, \pm 20°$	1.35
		Parked/Idling Plus Occurrence of Fault		
7.1	EWM	$v_{hub} = 0.95 \times v_1$	Seized blade, Yaw $= 0°, \pm 8°$	1.10

Table 6.1: Summary of wind turbine design load cases used by (Jonkman, 2007).

model with the Beddoes-Leishman dynamic-stall model, as discussed in Section 2.3.4, was specified in AeroDyn.

Referring to the DLCs specified in Table 6.1, in the cases of those which necessitate a turbulent wind input, BS EN 61400-1 (2005) requires that the total period of load data shall be such that it ensures the statistical reliability of the estimate of the characteristic load. It states that at a minimum six 10-minute stochastic realisations (or a continuous 60 min period) shall be required for each mean, hub-height wind speed used in the simulations. The DLCs which involve fault conditions call for choosing faults with the worst consequences. Jonkman (2007) chose common design-driving faults based on experience with other land-based wind turbine loads analyses, which have also been used in this study. For DLC 2.1, a fault was simulated in the rotor-collective blade-pitch control system where one blade ignores its command and runs away to the minimum set point of 0° at the full pitch rate of $8°/s$. It was assumed that the turbine's protection system detects the fault in this situation by simulating a shut-down of the turbine. The shut-down is initiated after a 0.2 s delay (to account for the time it takes the protection system to detect the fault and take action) by feathering the other two blades at full pitch rate to the maximum pitch setting of 90°. For DLC 2.3, a fault was simulated where the load is lost, implying that the generator reaction torque is zero. In this situation, it was again assumed that the turbine's protection system detects the fault and shuts down the turbine by feathering all blades after a 0.2 s delay at full pitch rate to the maximum pitch setting. For DLC 7.1, the fault condition consisted of one blade being seized at the minimum set point (i.e. flat into the wind) while idling with the other two blades fully feathered.

On running each of the FAST dynamic simulations a significant database of result were produced. The response outputs were then analysed in order to identify the design driving loadcases. A summary of the DLCs relevant to the foundation design for the tubular steel tower are presented in Table 6.2 in the form of an extreme event table. For each load component corresponding to Figure 6.2 both the minimum and maximum values are identified along with the associated values for the other coinciding components. The design driving loads are highlighted in blue.

Load	**Type**	F_x (kN)	F_y (kN)	F_z (kN)	M_x (kNm)	M_y (kNm)	M_z (kNm)
F_x	Min	-413	57.1	-9.26E3	-4.42E3	-3.49E4	1.30E3
F_x	Max	1.81E3	-43.1	-9.38E3	9.04E3	1.53E5	1.49E3
F_y	Min	292	-465	-9.23E3	4.09E4	2.64E4	1.83E3
F_y	Max	379	442	-9.31E3	-2.77E4	2.78E4	-814
F_z	Min	406	-169	-1.05E4	2.15E4	3.82E4	9.41E3
F_z	Max	62.8	-296	-8.96E3	3.25E4	2.26E4	-6.36E3
M_x	Min	379	442	-9.31E3	-2.77E4	2.78E4	-814
M_x	Max	292	-465	-9.23E3	4.09E4	2.64E4	1.83E3
M_y	Min	-411	63.7	-9.26E3	-4.77E3	-3.53E4	1.58E3
M_y	Max	1.81E3	-43.1	-9.38E3	9.04E3	1.53E5	1.49E3
M_z	Min	534	17.1	-9.16E3	2.63E3	4.45E4	-1.23E4
M_z	Max	232	3.47	-9.41E3	4.90E3	3.02E4	1.20E4

Table 6.2: Critical load table for steel tower base (Jonkman, 2007).

Having identified the relevant loadcases for the tubular steel tower it was now necessary to establish an equivalent analysis of the concrete tower. The FAST design code requires a set of predefined modeshapes for the flexible elements (i.e. tower and blades) for input into the model. These were already established for the tubular steel tower but for the case of the prestressed concrete tower it was necessary to compute the required values. The modeshapes are specified in the form of a sixth order polynomial. In order to establish the relevant modeshapes for the concrete tower an associated program called BModes (Bir, 2012) is employed. BModes is a validated finite-element code that provides dynamically coupled modes for a beam. The beam can be a rotor blade, rotating or non-rotating, or a tower. Both the blade and the tower can have a tip attachment modelled as a rigid body with mass, six moments of inertia, and a mass centroid that may be offset from the blade or tower axis. Examples of tip attachments are aerodynamic brakes for blades and nacelle-rotor sub-assemblies for towers. The 88 m concrete tower was specified as an input for the code along with the relevant properties of the 5 MW turbine and nacelle unit which it supports. The modeshapes output from the program could subsequently be implemented in the FAST code. The same analysis process undertaken for the tubular steel tower was repeated for the prestressed concrete tower configuration with all of the turbine and external parameters kept the same. Each of the DLCs specified in Table

6.1 were analysed and the design driving loadcases were once again identified. Table 6.3 presents an overall summary of the design relevant load values for the concrete tower.

Load	**Type**	F_x (kN)	F_y (kN)	F_z (kN)	M_x (kNm)	M_y (kNm)	M_z (kNm)
F_x	Min	-694	35.4	-1.72E4	-1.76E3	-5.38E4	517
F_x	Max	1.58E3	320	-1.71E4	-3.11E4	1.55E5	1.15E3
F_y	Min	4	-640	-1.73E4	5.16E4	3.67E3	2.87E3
F_y	Max	186	548	-1.73E4	-3.40E4	-1.09E4	-1.47E3
F_z	Min	239	-40	-1.76E4	8.56E3	2.03E4	9.41E3
F_z	Max	224	61	-1.68E4	8.66E3	2.56E4	-8.40E3
M_x	Min	-637	523	-1.64E4	-3.93E4	-4.54E4	-2.42E3
M_x	Max	17	-546	-1.72E4	5.38E4	-4.74E3	2.91E3
M_y	Min	-694	35.4	-1.69E4	-1.76E3	-5.38E4	517
M_y	Max	1.58E3	320	-1.71E4	-3.11E4	1.55E5	1.15E3
M_z	Min	16	74	-1.69E4	-25	-9.36E3	-1.66E4
M_z	Max	586	-21	-1.75E4	5.70E3	5.77E4	1.59E4

Table 6.3: Critical load table for concrete tower base.

The specified critical loads will be subsequently utilised in the design of the reinforced concrete slab foundation. The sizing and modelling procedures for the resulting design are detailed in the following sections.

6.3.2 Sizing the Foundation

Allowable deformation limits and stiffness values are most frequently set out by the wind turbine manufacturers. However, DNV (2002) also presents a set of general guidelines. These offer guidance for calculating bearing capacity, sliding resistance, overturning resistance and horizontal, vertical and rotational stiffness values. The effective area method is suggested for the prediction of foundation response under combined vertical and moment loading. The current study employs this method for initial sizing of the foundations. An FE design program, PLAXIS 2D, is subsequently used to assess the foundation response under a range of loading conditions.

Effective Area Approach

In the effective area approach outlined in DNV (2002), a combined moment and vertical load may be modelled as an eccentrically applied load. When the resultant load is applied eccentrically to one axis of symmetry the effective area of the foundation, A_{eff}, may be defined as:

$$A_{eff} = \left(1 - 2\frac{e}{b}\right) A \tag{6.1}$$

where A is the foundation area (m^2), b is the foundation width (m) and the eccentricity e, also measured in metres is defined as the moment applied (M) divided by the total vertical load (F_z). The vertical load includes the tower load (V_T) and the gravitational load from the foundation (V_F). The total effective bearing capacity of the foundation for the combined loading is then calculated as:

$$Q_{eff} = q \times A_{eff} \tag{6.2}$$

where q is the bearing resistance of the soil which is in this case taken as 20 % of the average q_c value within the zone of influence of the foundation. Based on the findings of Gavin *et al.* (2009), a value of 3.1 MPa is chosen. If this capacity exceeds the imposed loading by a recommended factor of safety then the foundation is deemed safe. Given the stiff over-consolidated sand and the high bearing capacity present at the GRG test site, a relatively high eccentricity/width (e/b) ratio of 0.405 was chosen for the concrete design loading conditions to ensure that moderate displacements would occur and that the foundation design would not be overly conservative. A numerical solver was subsequently employed to form an optimum foundation with minimum volume that would have an e/b ratio of 0.405, subject to the concrete loading conditions. The results of this procedure are presented in Table 6.4. Sensible sizing constraints were imposed such that the depth of foundation (d) would be within the range of 2-3 m and the foundation width would be within the range of 10-20 m. A 14 m square, 2 m deep foundation satisfied these requirements. This is an acceptable design when compared to the foundation requirements of other large turbines of

Tower Material	Foundation Size	M (MNm)	V_F (MN)	V_T (MN)	F_z (MN)	e (m)	e/b $(-)$	A_{eff} $(\%)$	A_{eff} (m^2)	q (MPa)	Q_{eff} (MN)	Q_{eff}/F_z $(-)$
Concrete	$14\,m$	155.3	9.8	17.6	27.4	5.67	0.405	19	37.3	3.1	115.6	4.2
Steel	$14\,m$	153.0	9.8	9.4	19.5	7.85	0.56	0	0	3.1	0	-
Steel	$15.83\,m$	153.0	12.5	9.4	21.9	6.98	0.441	11.8	29.6	3.1	91.8	4.2

Table 6.4: Results from the effective area approach.

this size (ENERCON, 2010b) Considering Table 6.4 for the concrete tower solution, when the maximum moment is applied the ultimate bearing resistance of the soil is greater than the imposed loads by a factor of 4.2. The benefits of the higher vertical load for the concrete tower is clear using this approach. The greater total vertical load facilitates a reduction in the eccentricity of the load and thereby increases the effective area of the foundation and foundation resistance. The foundation for the steel tower would have to be increased in size to a 15.83 m square foundation in order to get an equivalent factor of safety against failure under combined loading, incurring a greater cost as a consequence. Since the purpose of this analysis is to assess the relative performance of the steel and concrete tower solutions for a 5 MW wind turbine, the 14 m square foundation was also specified for the tubular steel tower.

6.4 Foundation Modelling

A plane strain model is implemented for the FE analysis using PLAXIS 2D (2011). PLAXIS 2D is an FE program specialising in geotechnical applications. The proposed two dimensional FE model provides an accurate framework for predicting the response of the soil foundation interaction. A three dimensional FE analyses would provide a more rigorous assessment of the soil mass and loading conditions but would require significantly greater computational and time resources. As outlined in Section 6.3, the governing criteria for wind turbine foundation design are the horizontal and rotational stiffness values. The foundation must be capable of resisting the maximum horizontal force and moment loading without undergoing excessive horizontal displacement or rotation. From an analysis of the extreme events table, Table 6.2, it can be seen that the maximum moment (M_y) occurs when the horizontal load (F_x) is also at its maximum value. At the same time F_y, M_x and M_z are all relatively low in comparison to their respective maximum values. The two dimensional FE model is most effective in modelling F_x, M_y and F_z if the model geometry is aligned with the x direction. Hence, in the context of rotational and horizontal stability for the current study, the dominant loading conditions on the foundation

are F_x, the wind loading in the x direction, M_y, the moment created as a result of the F_x and F_z, the vertical loading primarily due to the weight of the tower and associated turbine components. The wind forces acting perpendicular to the x axis are relatively small and it is assumed that the resultant strain in the perpendicular direction is close to zero.

As part of the input to PLAXIS 2D a 1 m wide section of the wind turbine foundation, equivalent to 7% of the foundation width, along with the surrounding soil is represented in a plain strain model as illustrated in Figure 6.3. In order to simplify the analysis,

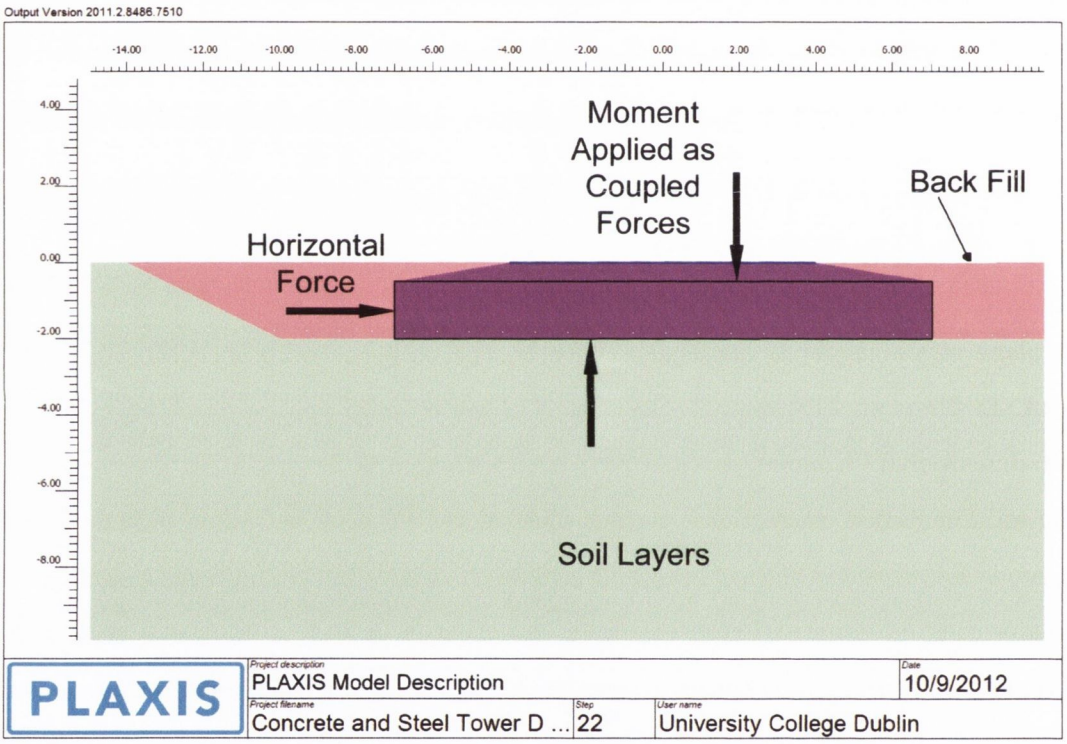

Figure 6.3: Outline of PLAXIS FE foundation model (Quilligan *et al.*, 2012a).

the wind turbine foundation is assumed to behave as a rigid body, thus allowing loading to spread uniformly along the width of the foundation perpendicular to the direction of loading. Consequently 7% of the resultant loads and moments will act through the 1 m wide 14 m long strip. The vertical tower load, V_T, is applied to the top of the foundation as a uniformly disturbed load (UDL), the moment is applied as a coupled

force about the centre point of the tower base and the wind load F_x is applied as a UDL to the side of the foundation as depicted in Figure 6.3. To simulate foundation-soil interaction, interface elements are applied at the foundation-soil boundary. These enable relative displacement (slipping/gapping) between the foundation and soil. An interface reduction factor (R_{inter}) is also applied. This influences both the stiffness and strength properties at the interface and it determines when relative displacements occur between the foundation and the soil. In accordance with concrete-sand interface values (Gómez *et al.*, 2003), an R_{inter} value of 0.8 was selected for the foundation-soil interface.

6.4.1 Soil Properties

For the proposed analysis, the Blessington sand (Bs) is modelled using three different soil models which are commonly used in foundation design. These include a MC, HS and HSS models. The relevant parameters for each of the soil models are presented in Table 6.5 and explained in the relevant sections which follow. The combination of the three different soil

Parameter	**Units**	**MC**	**MC**	**HS**	**HSS**
Soil Type		*Fill*	*Bs*	*Bs*	*Bs*
Unit Weight γ_b	(kN/m^3)	20	20	20	20
E_{50}^{ref}	(kPa)	-	-	44,000	44,000
E_{ur}^{ref}	(kPa)	-	-	155,000	155,000
E_{oed}^{ref}	(kPa)	-	-	25,000	25,000
E	(kPa)	30,000	varies	-	-
G_0^{ref}	(kPa)	-	-	-	136,000
$\gamma_{0.7}$		-	-	-	0.008
Cohesion	(kPa)	0	0	0	0
Ultimate Friction Angle	(°)	42.4	42.4	42.4	42.4
Ultimate Dilatancy Angle	(°)	6.6	6.6	6.6	6.6
Poisson's Ratio		0.2	0.2	0.2	0.2
R_f		-	-	0.8	0.8
P_{ref}	(kPa)	-	-	100	100

Table 6.5: Breakdown of Blessington sand properties (Tolooiyan and Gavin, 2011).

models ensures that a broad range of possible soil behaviour is captured. The relevance of the MC model relates to the relatively small magnitudes of strains which occur in the soil

around the foundation. Within this small strain range the soil is assumed to behave with linear elastic stiffness close to its initial small strain stiffness E_0, with plastic straining occurring once the deviatoric stress exceeds a limiting value. The HS model captures the non-linear stress-strain response and the HSS model behaves similarly except with higher stiffnesses in the very small strain range. The relevant attributes of each soil model are presented in the following sections with a more extensive description available in PLAXIS (2011).

Mohr-Coulomb

The main features of the MC model are illustrated in Figure 6.4. The soil strain is completely reversible when the current stress level is within the yield limit. Once the stress level exceeds the yield stress irreversible plastic straining occurs. The PLAXIS 2D (2011) MC model requires five input parameters. Two of them define the soil elastic behaviour;

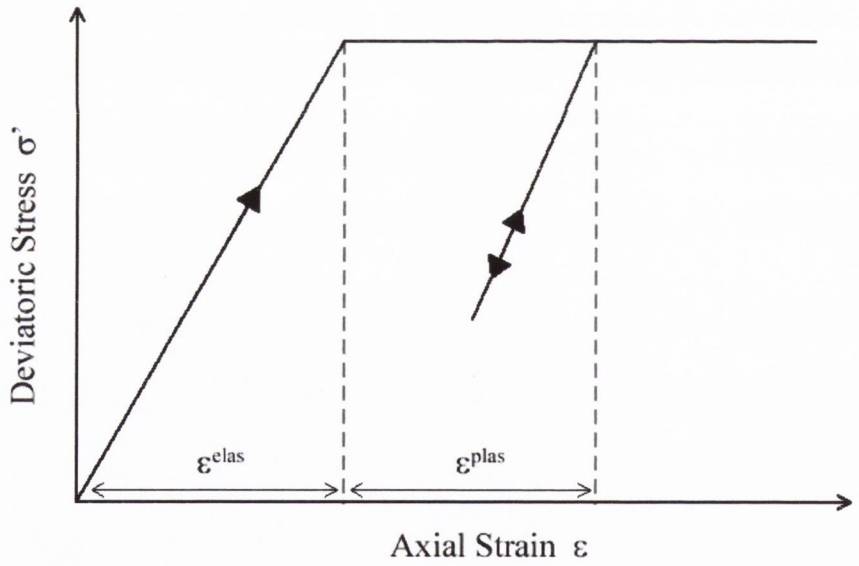

Figure 6.4: Deviatoric stress versus axial strain for Mohr-Coulomb model (PLAXIS, 2011).

Young's modulus (E) and Poisson's Ratio (ν). The other three parameters define the soil plasticity; Friction Angle (ϕ), Dilatancy Angle (ψ) and Cohesion (c). The soil stiffness is independent of the mean stress level. The MC model is recommended for use as a first

analysis of a problem due to its efficient computation capabilities as a result of the linear stiffness.

For full scale use, a number of limitations exist for this model. Soils do not tend to behave in a linear elastic-plastic fashion as stiffness is dependent on both stress and strain. Specifying one single stiffness parameter is only accurate for a specific set of stress and strain values. However, if a value of E is chosen that is consistent with the stress and strain values in the soil during loading, then the soil models accuracy may be improved. This is achieved through rigorous analysis of the soil properties and by comparison with additional soil models, including HS and HSS.

In order to accurately represent the variation of Young's modulus with depth below ground level in the current study, eight soil layers were defined. These soil layers are unevenly spaced as there is a greater variation of soil properties closer to the surface at the GRG test site (Tolooiyan and Gavin, 2011). A conservative estimate of 0.3 % was made for the maximum strain levels which would be generated and according to Gavin *et al.* (2009) this yielded a soil stiffness of 85 % of the initial Young's Modulus (E_0). E_0 values were obtained from the shear wave profile in Figure 6.1(b) and Equation (6.3).

$$E_0 = G_0 \left(2 \left(1 + \nu\right)\right) \tag{6.3}$$

where G_0 is given by:

$$G_0 = \gamma_B . \nu_s^2 \tag{6.4}$$

and γ_b is the bulk unit weight of the soil.

Hardening Soil

HS is an advanced soil model used for the simulation of non-linear soil behaviour. Similar to the MC model, limiting states of stress are described by means of the Friction Angle (ϕ), Dilatancy Angle (ψ) and Cohesion (c). The non-linear stiffness is defined by three input stiffness parameters; E_{50} represents the stiffness measured in a tri-axial compression test when the shear stress (τ) is 50% of the maximum shear stress (τ_{max}), E_{ur} is

the tri-axial unloading stiffness, and E_{oed} is the tangent stiffness modulus for primary loading. These stiffness values are stress dependant and are defined for a reference stress (P_{ref}) of 100 kPa. Another key element of this model is that it captures the hyperbolic stress-strain relationship of soil for primary loading as depicted in Figure 6.5 where the deviatoric stress (σ') is plotted against axial strain. As σ' approaches its ultimate value (q_f), the soil stiffness significantly reduces. q_a is an asymptote to the stress strain curve with the failure ratio R_f defined as q_a/q_f.

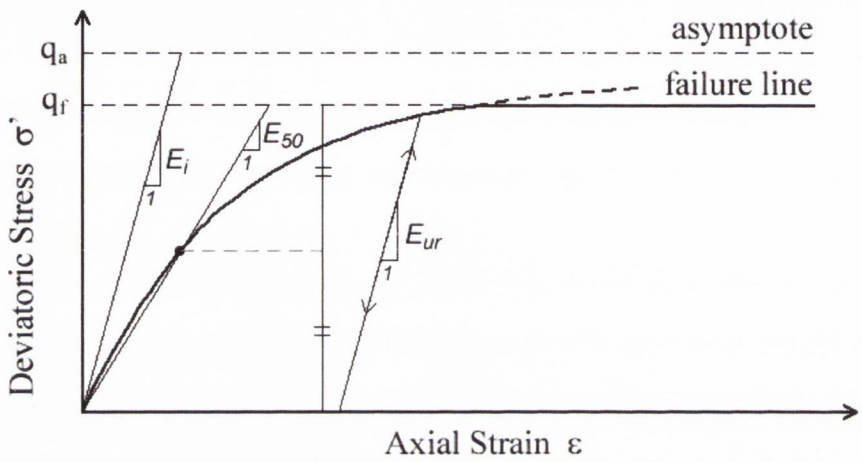

Figure 6.5: Deviatoric stress versus axial strain for Hardening Soil model (PLAXIS, 2011).

Hardening Soil With Small Strain Stiffness (HSS)

The HSS model is a modification for the Hardening Soil model that accounts for increased stiffness at small strains (PLAXIS, 2011). At low strain levels the soil exhibits higher stiffness values which vary non-linearly with strain level. The model is described with the same soil parameters as the HS model and two additional parameters. G_0^{ref} is the small strain shear modulus and $\gamma_{0.7}$ is the strain level at which the shear modulus has reduced to 70 % of the small strain shear modulus. As reflected by the name, the advantages of this soil model are most apparent at small strains which highlights its relevance in the current study. Figure 6.6 illustrates the soil stiffness versus strain level relationship, along with the strain ranges for typical structures and testing equipment. In the current investigation,

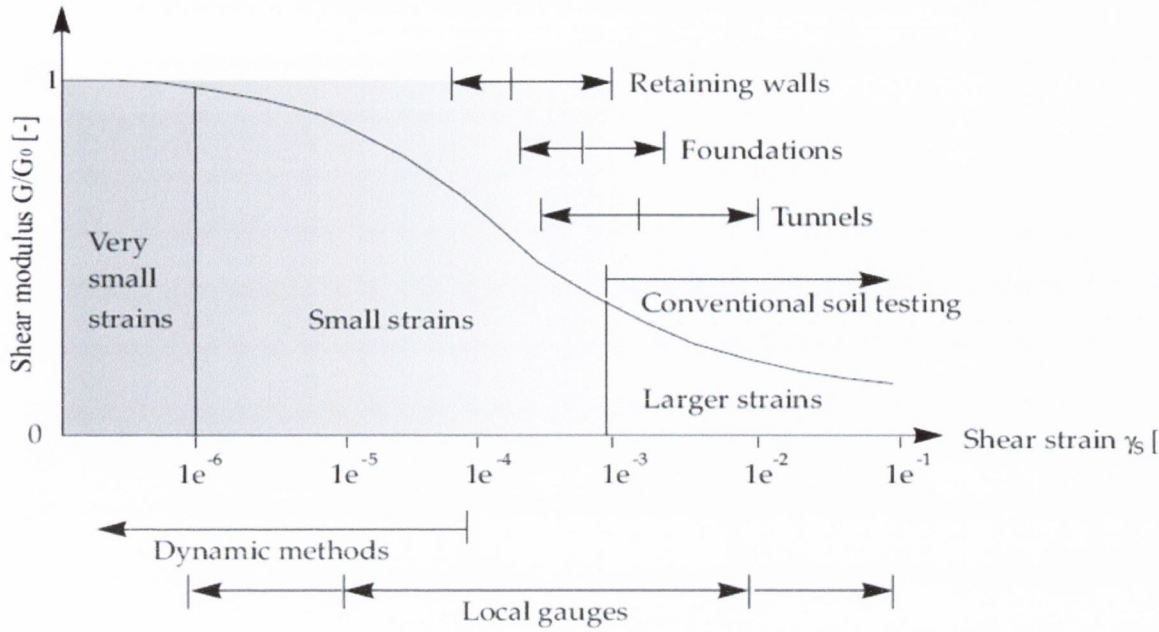

Figure 6.6: Shear modulus strain response and strain range of typical structures and testing methods (PLAXIS, 2011).

the maximum recorded strain was 8.8×10^{-4} which is within the indicated small strain range in Figure 6.6. This highlights the relevance of a small strain model to the current study.

6.4.2 Mesh Generation

Following specification of the model geometry, standard fixities were applied. Automatically assigned horizontal fixities were added at both the left and right boundary and total fixities were introduced at the bottom boundary. The boundary conditions offer a realistic representation of the soil behaviour if the model extends well beyond the studied geometry. In order to minimize boundary effects a distance of $7b$ (where b is the width of the foundation) was established between the edge of the foundation and the outer boundaries as per standard procedure. This value is shown to be sufficient through a plot of the resultant vertical stresses throughout the model. Figure 6.7 verifies that minimal effects are experienced at the boundaries and that boundary effects will not influence the results. An automatic mesh generation function was then employed to formulate an unstructured

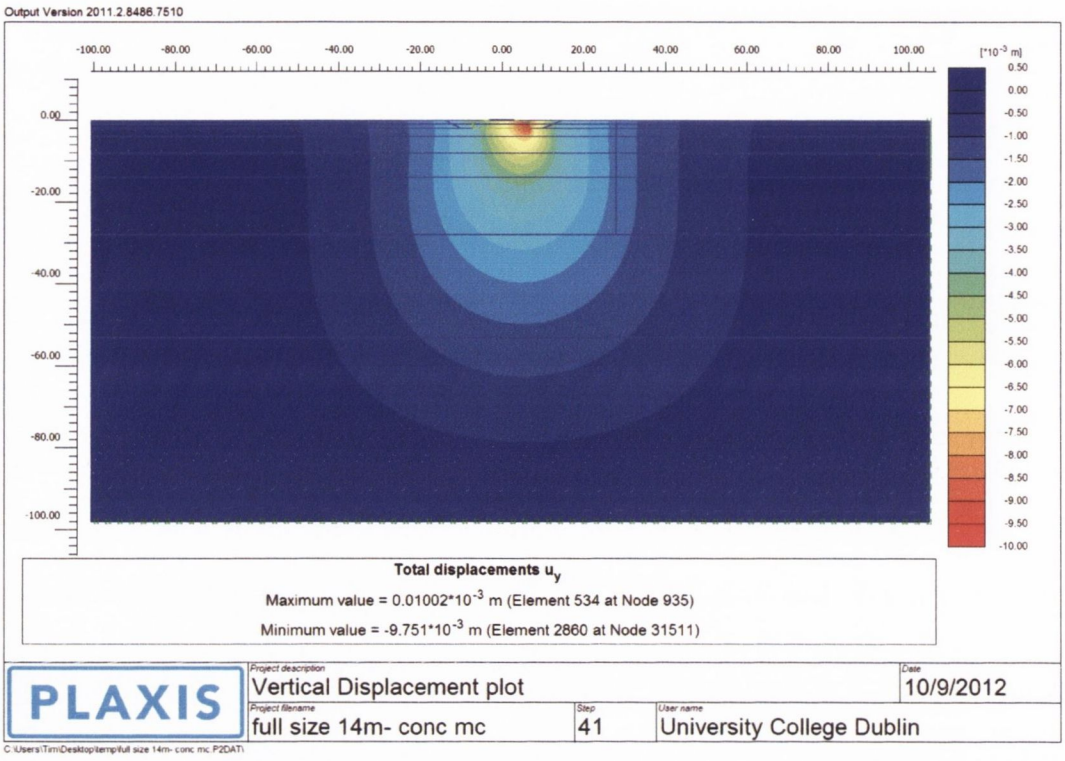

Figure 6.7: Vertical displacement distribution throughout the foundation model (Quilligan *et al.*, 2012a).

mesh of triangular elements. The soil element consisted of a fourth order polynomial element with 15 nodes which offered the highest accuracy compared to other soil elements. Refinement of the mesh was subsequently carried out in order to minimise sensitivity to mesh variation and ensure an optimal resolution in the vicinity of the foundation where the greatest strain effects are recorded. Figure 6.8 illustrates the resulting mesh connectivity plot for the wind turbine foundation which was used for all analyses of the steel and concrete towers.

6.5 Calculation of Soil Parameters

Having refined the FE model, a series of six calculations were undertaken. These included calculations for both of the towers using each of the three soil models outlined previously. PLAXIS 2D (2011) divides each of the calculations into phases which separate the found-

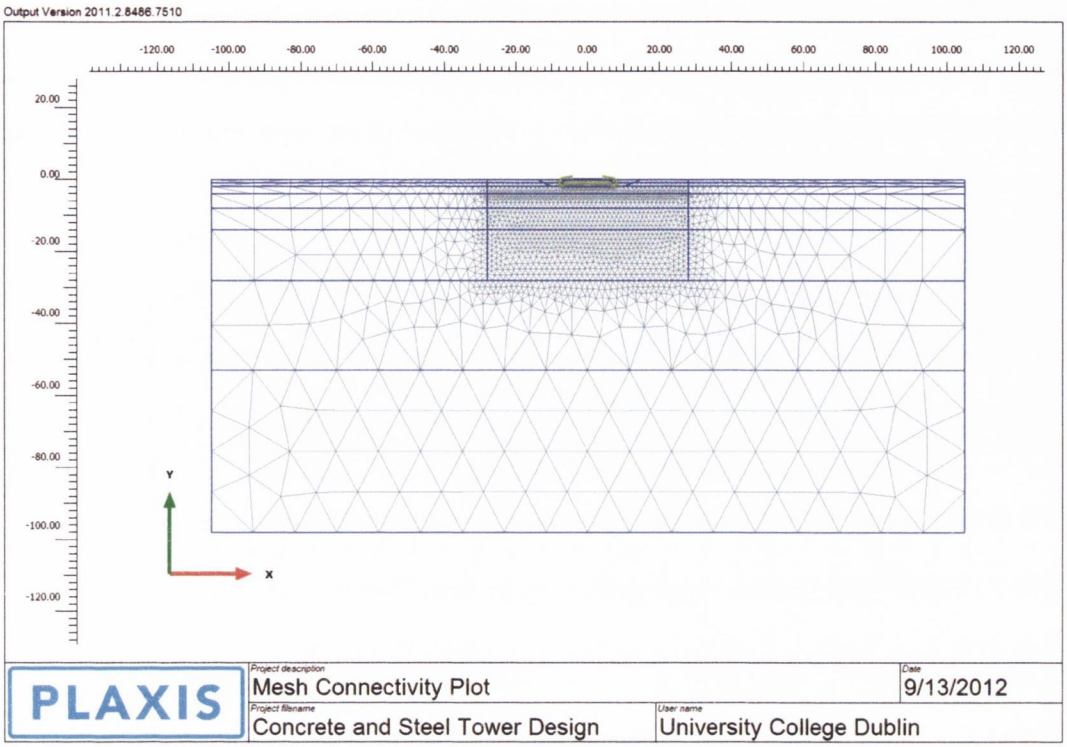

Figure 6.8: Outline of PLAXIS FE mesh connectivity (Quilligan *et al.*, 2012a).

ation loading into relevant sequences. These include the construction of the foundation, the installation of the tower, and the operation of the wind turbine in both normal and extreme conditions. As previously outlined, the purpose of the soil modelling procedures and calculations is to establish representative horizontal and rotational soil stiffness values for implementation in the extended two dimensional structural model derived in Section 3.3.1. The determination of these values is described in the following sections.

6.5.1 Data Analysis and Determination of Spring Stiffness Values

Rotational Stiffness

In order to calculate the rotational stiffness of the foundation for the two tower configurations and the various soil models, an assessment of the vertical displacements of the nodes at the centre, RHS and LHS of the base of the foundation was carried out. Differential settlements between the two edges of the foundation were obtained from these values and

converted into a rotation angle measured in degrees. It was subsequently possible to generate plots of applied moment versus rotation such as that shown in Figure 6.9 for the steel tower and HS model. The plot illustrates the initial maximum and minimum loading and

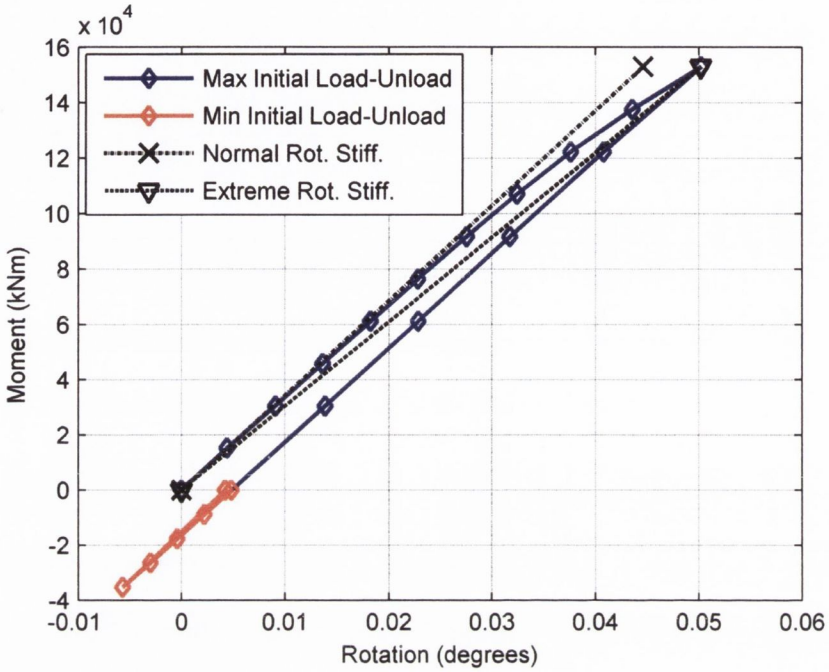

Figure 6.9: Foundation moment vs. rotation response for steel tower with HS model (Quilligan *et al.*, 2012a).

unloading sequences. It is evident that the foundation exhibits a linear elastic moment rotation response for first time loading up to a limiting moment value of approximately 90×10^3 kNm, after which the stiffness is reduced. On first-time loading to the maximum value, the foundation is less stiff than for subsequent load cycles at which point it follows the unloading path. The extreme rotational spring stiffness was calculated by dividing the maximum rotation by the maximum applied moment while the normal spring stiffness was established by dividing the maximum recoverable rotation by the maximum moment. The response of the foundation using the calculated normal and extreme linear elastic spring stiffness values is also depicted in Figure 6.9. The normal stiffness represents an initial loading up to 90×10^3 kNm, or subsequent reloading of a system which has previously reached its maximum load. The extreme stiffness represents an initial loading of the

foundation up to the maximum load or further loading of the system beyond the maximum load. For the case of the steel tower, the maximum base moment calculated under normal operational conditions was 71×10^3 kNm. This implies that for normal operating conditions, whether the foundation has previously been loaded to the maximum value or not, the foundation stiffness can be represented by the normal stiffness value.

Horizontal Stiffness

In order to assess the horizontal spring stiffnesses, graphs of horizontal force versus displacement were also created. Figure 6.10 demonstrates the horizontal force-displacement behaviour for the foundation of the steel tower using the HS model. Akin to the moment

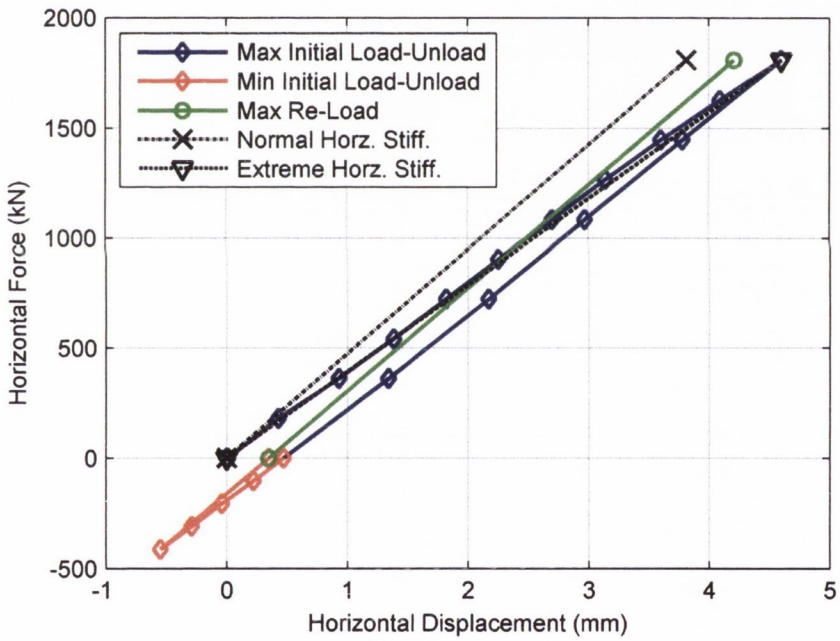

Figure 6.10: Foundation horizontal force vs. displacement response for steel tower with HS model (Quilligan *et al.*, 2012a).

rotation response, the foundation has a lower horizontal stiffness when it is initially loaded to the maximum value. Once unloaded, subsequent reloading exhibits a stiffer response as shown by the green line. The normal and extreme horizontal spring stiffnesses were calculated in the same manner as for the rotational stiffnesses and the stiffness response

behaviour of the foundation using these values is also illustrated in Figure 6.10. In this instance, any initial loading beyond 200 kN must be related to the extreme stiffness value. However, once the maximum loading has been achieved, any further loading within the range of the maximum load will follow the green reload line which is represented by the normal stiffness value.

Vertical Stiffness

Figure 6.11 presents a vertical displacement response for nodes at the LHS and RHS of the foundation, as well as a central node on the base of the foundation for each of the phases of a calculation. Following the construction phases, the initial loading of the found-

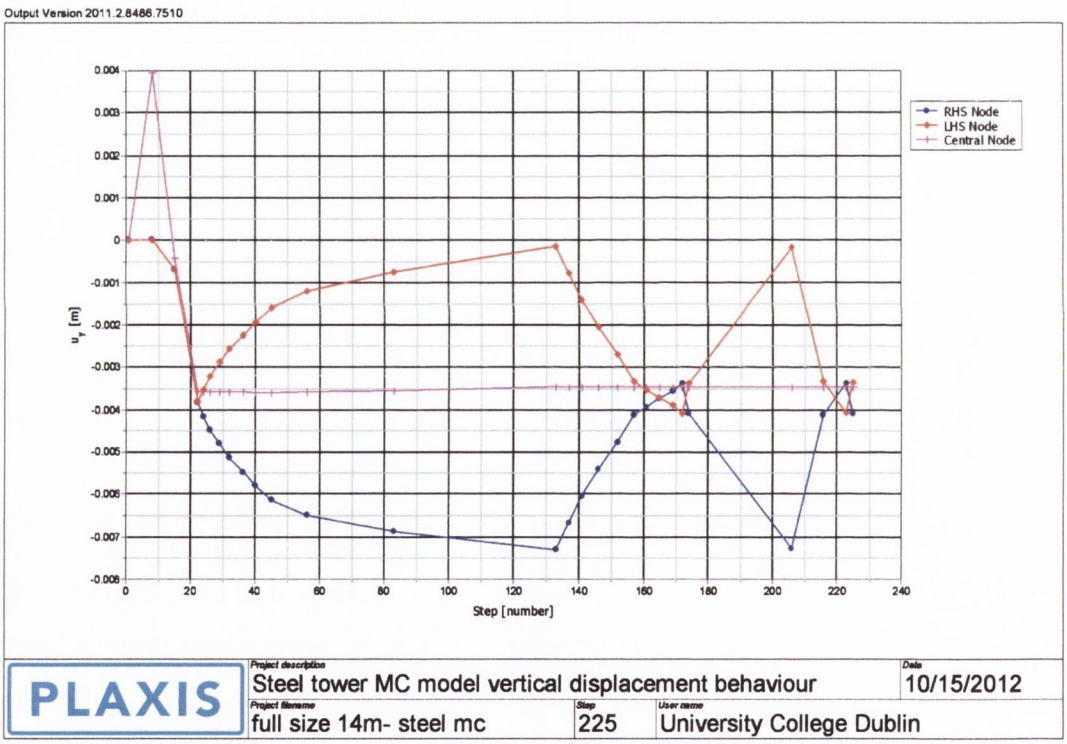

Figure 6.11: Graph of output vertical displacement vs. step number for steel tower and MC model) (Quilligan *et al.*, 2012a).

ation commences at step number 22 on the graph. After this point the response of the aforementioned nodes is illustrated for each of the loading and unloading phases. While the RHS and LHS nodes exhibit noticeable displacement responses, it is evident that the

central node remains stable throughout these sequences. It was therefore decided that the calculation of vertical spring stiffness values was not required and hence, the foundation is assumed to be fixed in the vertical direction.

6.5.2 Soil Model Evaluation

The values for the horizontal and rotational spring stiffnesses for both tower configurations and the three soil models were obtained using the procedures outlined in the preceding sections. The calculated values are presented in Table 6.6. Similar values are achieved

Parameter	Units	Tower	Load Case	MC	HS	HSS
Rotational Stiffness	(GNm/rad)	Steel	(N)	339	196	399
	(GNm/rad)	Steel	(E)	299	175	357
	(GNm/rad)	Concrete	(N)	346	210	427
	(GNm/rad)	Concrete	(E)	334	196	402
Horizontal Stiffness	(MN/m)	Steel	(N)	839	476	953
	(MN/m)	Steel	(E)	747	393	827
	(MN/m)	Concrete	(N)	735	424	851
	(MN/m)	Concrete	(E)	704	374	778

Table 6.6: Spring stiffness values for Blessington sand (Quilligan *et al.*, 2012a).

for both the MC and HSS models, while the HS spring stiffness values are slightly lower. This suggests that the MC model can be accurately implemented if an appropriate value of Young's Modulus is chosen. As per Figure 6.6, the soil strains activated below the wind turbine foundation are predominantly in the small strain range. The foundation response is less stiff when the soil is modelled with the HS model as this model does not exhibit higher soil stiffness values in the small strain range. Therefore, following the foundation analysis, the recommended spring stiffness values are those obtained using the MC and HSS models while those established from the HS model may prove less accurate. It should also be noted that, while each of the rotational stiffness values calculated in Table 6.6 are above the recommended minimum value of $50\,GNm/rad$ proposed by (Tinjum and Christensen, 2010), the horizontal stiffness values are all below the recommended minimum value of $1000\,MN/m$.

Concrete Tower Evaluation

In geotechnical terms the concrete tower solution offers a more favourable design for the 5 MW wind turbine on a number of aspects. Firstly, during the initial design stage, it was shown that a 13% larger foundation area would be required for the tubular steel tower solution in order to maintain the same factor of safety against failure in bearing as the prestressed concrete tower. As evident in Table 6.7, the differential settlements and horizontal displacements were also reduced using the concrete configuration. Finally, for the concrete solution, the full foundation area remained in compression during all phases of loading, implying that no uplift was occurring. For the case of the steel tower it was found that the compressed area was only 85 % during extreme loading.

Parameter	Units	Tower	Load Case	MC	HS	HSS
Differential Settlement	(mm/m)	Steel	(E)	0.60	0.88	0.50
	(mm/m)	Concrete	(E)	0.47	0.79	0.45
Horizontal Displacement	(mm)	Steel	(E)	2.42	4.60	2.19
	(mm)	Concrete	(E)	2.25	4.23	2.03
Initial Vertical Displacement	(mm)	Steel	(N)	3.75	8.46	3.80
	(mm)	Concrete	(N)	6.30	17.77	6.49
Contact Area	(%)	Steel	(E)	85	85	85
	(%)	Concrete	(E)	100	100	100

Table 6.7: Computed foundation displacements (Quilligan *et al.*, 2012a).

On investigating the horizontal spring stiffness values detailed in Table 6.6 it is evident that higher values are achieved for the steel tower. This does not, however, equate with an overall stiffer response. Results of a decoupled analysis for the HS model reveal that the moment loading has a significant effect on the total horizontal displacement. This is not reflected in how the horizontal stiffness value is calculated (i.e. the total horizontal load is divided by the total displacement), which leads to the steel tower having a higher horizontal stiffness value. If, instead, the horizontal load is applied as a percentage of the maximum horizontal load for each tower solution then the concrete tower will have a stiffer response each time. This is illustrated in Table 6.8, where the displacement at 100 % of maximum combined vertical, horizontal and moment load is less for the prestressed concrete tower.

The superior geotechnical performance of the prestressed concrete tower configuration

Tower	Horiz. Load (mm)	Moment effect (mm)	Total Horiz. Disp. (mm)
Steel	1.8	+2.8	4.6
Concrete	1.58	+2.65	4.23

Table 6.8: Decoupled foundation displacements for horizontal loading only, moment loading only and combined horizontal and moment loading, utilising the HS model (Quilligan *et al.*, 2012a).

is a direct result of the increased vertical loading due to the larger self weight of the concrete tower. This additional loading creates a more uniform soil bearing response beneath the foundation and, in turn, helps to minimise differential settlements and improves the rotational stability of the foundation. A similar effect is also induced for the horizontal stability of the foundation.

6.6 Model Implementation

Thus far, the benefits of a prestressed concrete tower system have been highlighted in the context of its influence on the foundation design, where superior stability and a more structurally efficient solution can be achieved in comparison to the foundation necessary for a traditional tubular steel tower. The objective of this study, however, is to investigate the relative comparison of wind turbine structural performance, considering both the tower and blades, for the two tower configurations when SSI is included in the model. This is achieved by employing the foundation design specified in Section 6.3.2 along with its associated horizontal and rotational stiffness values as part of probabilistic based analysis of the structural performance achieved by the specified towers.

6.6.1 Outline of Analysis

The steel and concrete towers implemented in the study are each 88 m in height. Supporting the NREL 5 MW baseline wind turbine, this facilitates a hub height of 90 m. The turbine has already been thoroughly discussed in Section 3.5.1 with the relevant properties specified in Table 3.1 and further details provided in Appendix C. An extensive description of the tubular steel and prestressed concrete towers has also been provided in Section 4.2,

with further details specified in Appendix E. The probabilistic framework of the study is facilitated by modelling the tower structural properties and environmental inputs as stochastic variables. The structural properties such as the material modulus of elasticity (E), density (ρ), material thickness (t), and the environmental variables such as air density (ρ_{air}) are each given a specified PDF with a corresponding mean and CoV. These values have been previously defined in Table 4.4. Utilising the Monte Carlo method, batches of input variables are generated with the appropriate statistical variation. Each batch is subsequently implemented in a dynamic simulation in the derived model over a range of 12 wind speeds from 5 m/s to 25 m/s (within the operational range of the turbine), thus generating structural responses such as displacements, velocities and accelerations. The output time-histories provide the necessary information to facilitate a statistical representation of the response. Similar to each of the previous investigations this is illustrated with the use of fragility curves which effectively relate the probability of a structure exceeding a prescribed limit-state to the magnitude of the applied loading. In this instance, the maximum nacelle and blade-tip displacements are related to the mean hub-height wind speed. A displacement based limit-state is prescribed based on the maximum response. For the case of nacelle response, this is equivalent to the smallest maximum nacelle displacement for either the steel or concrete tower (whichever is the lesser) at the maximum mean hub-height wind speed (25 m/s, the wind turbine cut-out wind speed). Similarly, for the blade response, it is the smallest maximum blade-tip displacement for either tower at the cut-out wind speed which defines the limit-state.

6.6.2 Foundation Input Properties

In relation to the model input properties relevant to the foundation design, namely, the horizontal and rotational stiffness values, it is necessary to choose the most appropriate values for the particular analysis being carried out. With respect to the various soil models (MC, HS, HSS), the structural response will be simulated using all three models, therefore, facilitating a comparison of the soil models as well as a more robust analysis of the wind turbine structural performance. Another aspect of the soil modelling framework is deciding

whether to use the normal or extreme stiffness values. For the case of rotational stiffness, it was shown in Figure 6.9 that, for a steel tower under initial loading, the moment rotation follows a linear-elastic relationship up to a limiting value of approximately 90×10^3 kNm. This is considerably in excess of the maximum base moment recorded for the tower during normal operation (71×10^3 kNm). This trend held for each of the tower types and soil models employed in the study and considering that the simulations are each carried out within the normal operational range of the turbine, it is, therefore, a justifiable assumption to choose the normal stiffness value for the rotational stiffness. In the case of the horizontal stiffness, Figure 6.10, this distinction is not quite as well defined. A linear response is only reliable on initial loading up to approximately 200 kN. The maximum horizontal tower base load recorded during normal operation was 830 kN, far in excess of the region of linear response. Therefore, if the turbine systems are to be considered previously unloaded before the analysis takes place, it would be necessary to utilise the extreme stiffness value. In order to standardise the problem for each of the tower configurations and soil models it was decided that each of the towers will be assumed to have achieved its maximum load previous to the initiation of the analysis. As a result, any further loading up to and including the maximum load will follow the reloading path which has a representative stiffness value equal to the normal stiffness value. This justifies the use of the normal stiffness values, as detailed in Table 6.6, for both rotational as well as horizontal stiffness for each of the tower configurations and soil models. The results of the proposed analysis are presented and discussed in the following sections.

6.6.3 Long Term Effects on Concrete Strength

The effects of creep and shrinkage on the long term strength of prestressed concrete structures has already been extensively discussed in Section 4.2.5, and applied in analyses in both Chapter 4 and Chapter 5. Both of these effects have the ability to induce tensile stresses which may lead to cracking of the concrete and, consequently, affect the bending stiffness of the structure. By using Equation (4.2), in conjunction with a conservative estimate for the creep coefficient, it was shown that the long term modulus of elasticity

could be estimated as half of its initial value following a 28 day curing period. Given the mean value specified in Table 4.4, an adjusted modulus of elasticity of 13 MPa was established as appropriate. Accounting for the effects of shrinkage and creep in this manner, a series of simulations will be undertaken in this analysis to provide comparison to the standard results.

6.7 Results

In producing the results for this investigation, simulations were carried out for both the steel and concrete towers at each of the 12 mean hub-height wind speeds using all three soil structural models as well as an additional simulation employing the fixed support assumption at the base of the tower. Initially a comparison is made between the results for each of the three soil models and fixed support case. Subsequently, the maximum nacelle and blade responses for both tower configurations are compared in order to quantify any relative difference in performance between the two tower solutions when SSI is incorporated in the study.

6.7.1 Comparison of SSI Effects With Fixed Support Assumption

In the first instance of this investigation, the three soil models (MC, HS, HSS) are compared with the fixed support assumption ("No Soil") for both the steel and concrete towers. Figure 6.12 presents the median values for the maximum nacelle and blade displacements as well as a set of corresponding fragility curves for the steel tower. For the case of the nacelle displacements, Figure 6.12(a), the values are seen to vary within the range of 0.069 m and 0.157 m. Immediately, a distinct trend is obvious across each of the soil models. It is noticeable that at the lower mean hub-height wind speeds, each of the four displacement curves are quite close, but as the wind speed is increased, corresponding with an increase in loading, the lines are seen to diverge. This is possibly a result of increased rotation of the foundation with increasing wind speed. Beyond the rated wind speed (which is highlighted in the plot at 11.4 m/s), it appears that, with increasing mean hub-height

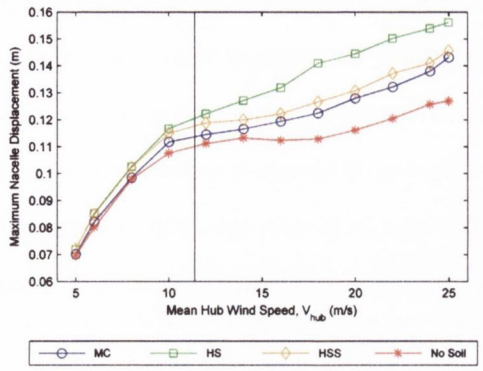

(a) Nacelle displacements.

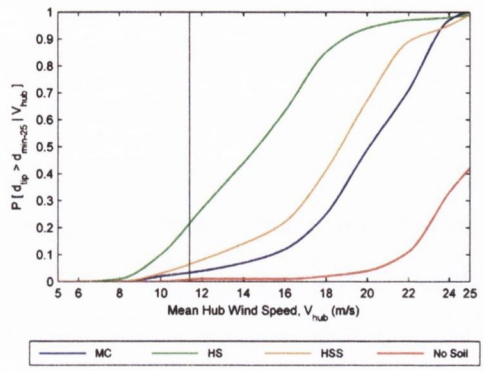

(b) Nacelle fragility curves.

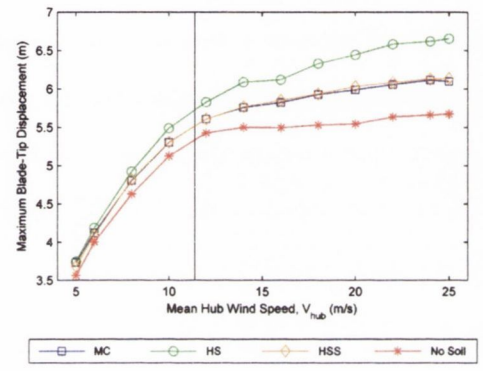

(c) Blade displacements.

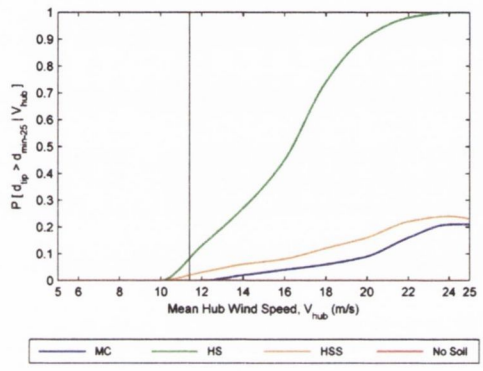

(d) Blade fragility curves.

Figure 6.12: Median of maximum nacelle and blade-tip displacements as well as associated fragility curves for an 88 m steel tower using MC, HSS and HS soil models.

wind speed, the displacements for each of the soil models increases with a power-law relationship. An interesting trend is also observed below the rated wind speed, where the displacements noticeably drop off very rapidly, and the soil models appear to converge. This may be a consequence of the aerodynamic efficiency of the turbine across its range of wind speeds. Referring to Table C.3 in Appendix C, it is shown that once the rated wind speed is exceeded, the blades are pitched, or twisted, in order to optimise the efficiency of the blades relative to the wind inflow velocity and therefore maintain the rated level of power generation. Below the rated speed, as in this case, the option of pitching the blades is not available and control is achieved by reducing the rotor speed of the turbine. As information was not available in relation to matching the rotor speed to the wind inflow

velocity, it was decided for this study that the rotor speed would remain constant at the rated value of 12.1 rpm. This fact may have contributed to the noticeable reduction in nacelle displacement below the rated wind speed. In comparing the maximum values for each of the models, the outcome is as expected. The lowest displacements are exhibited by the "No soil" model, which due to its assumption of a fixed support at the tower base, would be expected to represent a stiffer structure and therefore lower maximum displacements. The largest displacements are recorded for the HS model. In an assessment of the foundation performance in Section 6.5.2, this was identified as the least reliable of the three models, given the particular soil properties at the test site. Both the MC and HSS models were identified as being the most reliable soil models in this instance, given the occurrence of small strain values and the proximity of the stiffness values for the two models. This is also reflected in Figure 6.12(a), where both models are seen to produce similar displacement values across the entire range of wind speeds, with the MC model exhibiting moderately lower displacement values.

Based on the maximum nacelle displacement values, it is possible to generate fragility curves in order to further analyse the comparative performance of the various models. Figure 6.12(b) presents such a set of fragility curves for the nacelle displacements with the steel tower. The limit-state is calculated from the smallest maximum nacelle displacement at the 25 m/s wind speed. A similar pattern is evident as was observed in Figure 6.12(a) with the "No Soil" model displaying the least probability of LSE across the range of wind speeds while the HS model stands out above the rest of the cases. Once again, the MC and HSS models exhibit similar performance across the range of wind speeds with the MC model displaying a lower probability of LSE. At the cut-out wind speed (25 m/s) the "No Soil" model is shown to have a probability of LSE of 0.42, while the MC model has a probability of 1.0 and the HS and HSS models display a probability of 0.98. Figures 6.12(c) and 6.12(d) present the same analysis for the blade-tip displacement response. In Figure 6.12(c) a similar pattern is evident as for the nacelle vibrations. At lower wind speeds the three soil models and "No Soil" case produce similar values. As the wind speed increases the displacements increase rapidly up until the rated wind speed, after which point a more

gradual increase in displacements is noticeable. The reason for this has been previously attributed to the power control mechanisms in the turbine. Also, in comparing the four cases, it is seen that the "No Soil" case produces the lowest displacements, the MC and HSS models show almost equivalent response, while the HS model results in the largest blade-tip displacements. The fragility curves presented in Figure 6.12(d) appear more dramatic than those in Figure 6.12(b), although similar patterns are evident. According to Figure 6.12(c), the median values of the maximum blade-tip displacements for the "No Soil" and HS models at the cut-out wind speed, differ by 1 m in magnitude. This is reflected in Figure 6.12(b) where at no wind speed does the "No Soil" model exceed the limit-state set by the HS model. The MC and HSS models are, once again, shown to exhibit similar performance, although in this case, at the cut-out wind speed, the MC model has a probability of LSE of 0.21, the HSS model equates to a probability of 0.23, while the HS model exhibits a probability of 1.0.

In order to highlight the difference in wind turbine response with and without SSI, Figure 6.13 details the percentage difference in response relative to the "No Soil" case for both the nacelle and blades. Considering the nacelle displacements in Figure 6.13(a),

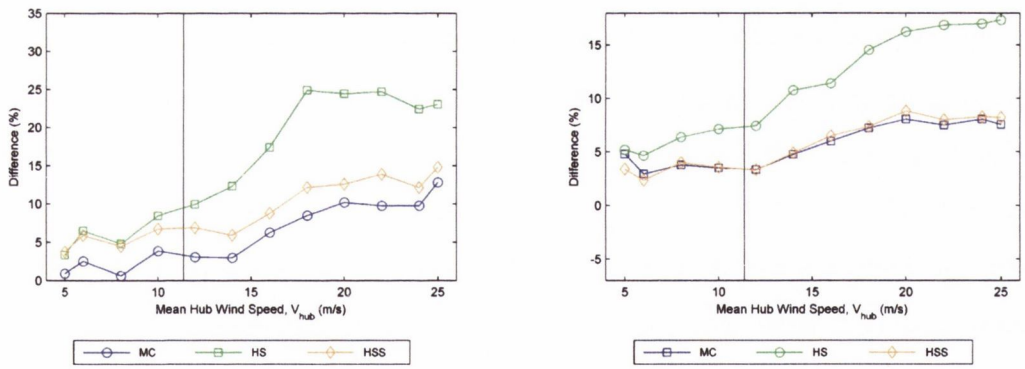

(a) Nacelle displacements.

(b) Blade displacements.

Figure 6.13: Percentage difference in maximum response between "No Soil" case and SSI models for steel tower.

although the trend appears non-linear, the percentage difference is seen to increase with increasing wind speed. The MC model observes the lowest deviation from the "No Soil"

condition, with a 2 % difference at the cut-in wind speed and a 13 % difference at the cut-out wind speed. The HSS model follows a similar trend, although with a larger percentage difference, varying from 4 % to 15 % for the cut-in and cut-out wind speeds respectively. The HS model gives the largest difference in response. It follows the values of the HSS model up to the 10 m/s wind speed but records a maximum difference in response of 25 % at the 18 m/s wind speed. Looking at the blade response, a similar trend is evident in Figure 6.13(b), although the percentage difference in response is less with maximum differences of 8 % and 17 % recorded for the HSS and HS models respectively. These values highlight the importance of considering SSI in predicting the response of a wind turbine system. With up to a possible 25 % difference in nacelle response and 17 % difference in blade-tip response, it is evident that SSI contributes significantly to the wind turbine dynamics.

A similar comparison of the three soil models and the "No Soil" condition is presented for the concrete tower in Figure 6.14. While similar patterns are noticeable within Figure 6.14(a), they are not as clearly defined as was evident for the steel tower. On initial viewing the most striking aspect of this plot is the range of displacements which the concrete tower experiences. Across the series of wind speeds and soil models, the concrete tower nacelle displacements vary between 0.03 m and 0.083 m as compared to values of 0.069 m and 0.157 m for the steel tower. There is also less definition between the soil models, particularly at lower mean hub-height wind speeds where the three models exhibit similar values up to a mean wind speed of 13 m/s, after which the models tend to diverge. Despite this, similar trends are noticeable yet again. The "No Soil" condition yields significantly lower displacements across all wind speeds (15 % lower than MC model at 25 m/s) and, beyond a wind speed of 13 m/s, the HS model shows higher displacements than the other models. The MC and HSS models are also seen to behave similarly, with the MC model yielding lower displacements beyond the 14 m/s wind speed. The power-law relationship for increasing wind speeds is also observed, although in this instance it is less defined. The lack of definition in the pattern of response for the concrete tower is a direct result of the greater variability of the concrete modulus of elasticity quoted in Table 4.4. The CoV of

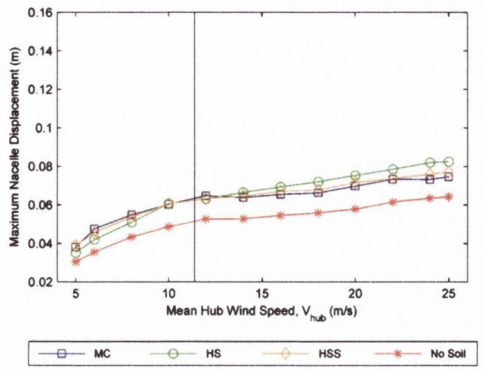

(a) Nacelle displacements.

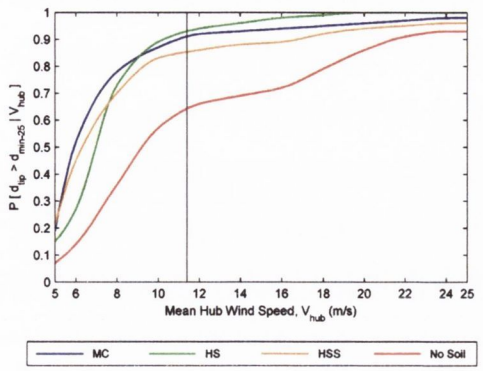

(b) Nacelle fragility curves.

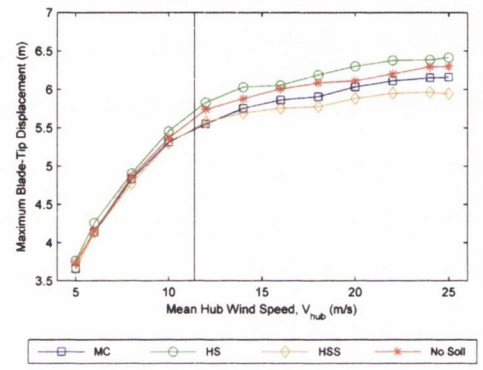

(c) Blade displacements.

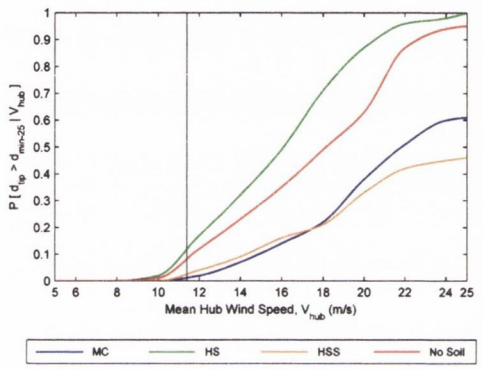

(d) Blade fragility curves.

Figure 6.14: Median of maximum nacelle and blade-tip displacements as well as associated fragility curves for an 88 m concrete tower using MC, HSS and HS soil models.

the concrete modulus of elasticity is 23 %, which compares to 3 % for steel. Considering the fragility curves illustrated in Figure 6.14(b), there is less deviation in performance between the three soil models and "No Soil' model, than was observed for the steel tower in Figure 6.12(b). While the fixed base tower model exhibits a difference in probability of LSE to the best performing soil model of 0.3 at the 8 m/s wind speed, this is reduced to 0.03 at the 25 m/s wind speed. However, the "No Soil" model remains the best performing model across the entire range of wind speeds. The HS soil model gives the lowest probability of LSE compared to the other soil models at lower wind speeds while the HSS model performs best beyond a mean hub-height wind speed of 7 m/s. Overall, it is more difficult to separate the performance of the various soil models for the concrete tower. Despite

this, the magnitudes of displacements are significantly lower than for the steel tower.

The performance of the various soil models in terms of the blade-tip displacement response is also assessed in Figures 6.14(c) and 6.14(d). While similar trends in displacement response are present, this case proves unusual in that the MC and HSS models show improved displacement response in terms of both median response and the probability of LSE. For the steel tower, the introduction of SSI was shown to noticeably reduce performance. For the concrete tower, the MC and HSS models are shown to outperform the "No Soil" condition. Figure 6.14(c) shows noticeably less divergence in the median blade-tip response than Figure 6.12(c) with increasing wind speed. These differences may be attributed to the greater variability in the concrete tower strength and the higher natural frequency of the concrete tower for the "No Soil" condition. Referring to Table 5.1, the natural frequency of the 88 m steel tower is 0.33 Hz as compared to 0.47 Hz for the concrete tower for the "No Soil" condition. The value of 0.47 Hz is significantly closer to the blade natural frequency of 0.79 Hz than the steel tower and may be responsible for the greater blade-tip response in the case of the concrete tower. In Section 4.6 it was shown that the steel tower exhibited considerably lower blade-tip displacements than the concrete tower at the 88 m tower height. As the stiffness and natural frequency of the concrete tower was reduced by increasing the height to 103 m, the maximum blade-tip displacements are reduced. This was shown in Figure 4.11. In this particular investigation, the concrete tower stiffness is reduced by incorporating SSI and, in the case of the MC and HSS soil models, this has the effect of reducing the blade-tip displacement response relative to the "No Soil" condition.

Similar to the plots of the percentage difference in wind turbine response with and without SSI presented for the steel tower in Figure 6.13, Figure 6.15 details the percentage difference in response relative to the "No Soil" case for both the nacelle and blades when a prestressed concrete tower is employed. On initial observation, the most noticeable trait in the plots is the difference in values when compared to the steel tower in Figure 6.13. Considering the nacelle response, Figure 6.15(a), the minimum difference in response is 10 % which compares to 1 % for the steel tower. Although the magnitude of the nacelle

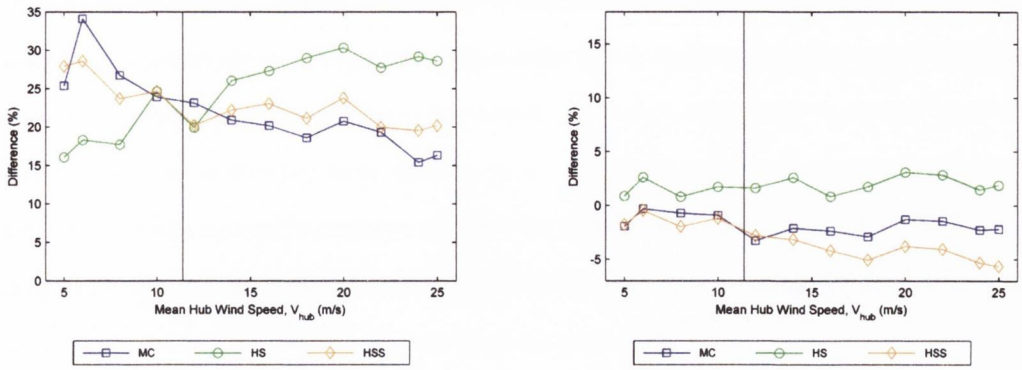

(a) Nacelle displacements.

(b) Blade displacements.

Figure 6.15: Percentage difference in maximum response between "No Soil" case and SSI models for concrete tower.

response is lower for the concrete tower, the inclusion of SSI has a more significant effect on the response. Another noticeable trend is that for the MC and HS models, the difference in response appears to be decreasing with increasing wind speed. This is to be expected, given that the maximum displacement values for the various soil models in Figure 6.14(a) did not appear to diverge with increasing wind speed, akin to the steel tower. The MC model shows a 25 % and a 16 % difference in response at the cut-in and cut-out wind speeds respectively. Again, the HSS model observes a similar trend while the HS model appears to increase with increasing wind speed. For the blade response in Figure 6.15(b), the maximum difference is 3 %. The most notable trait in this plot is the fact that the MC and HSS models shown a reduction in response when compared to the fixed support case. This effect has already been attributed to the proximity of the concrete tower natural frequency to the flapwise blade natural frequency for the fixed support case. Similar to Figure 6.15(a), the blade-tip response appears to decrease with increasing wind speed for the MC and HSS models. The HS model exhibits a more constant difference, varying minimally between 0 and 3 %.

6.7.2 Comparison of Steel and Concrete Tower Response

Already, from the comparison of relative displacement levels in Figures 6.12 and 6.14 it is obvious that there exists a noticeable difference in the performance for the steel and

concrete towers over the entire range of wind speeds and considering each of the soil models. What is as, if not more, significant is the effect of neglecting SSI on the predicted response of the wind turbine. This difference is further illustrated in Figure 6.16 which compares the median values for the maximum nacelle displacements of the two towers according to the soil model utilised as well as outlining reference displacement values for the "No Soil" case, indicated by "NS Steel" and "NS Concrete". Also included in the plots is the nacelle

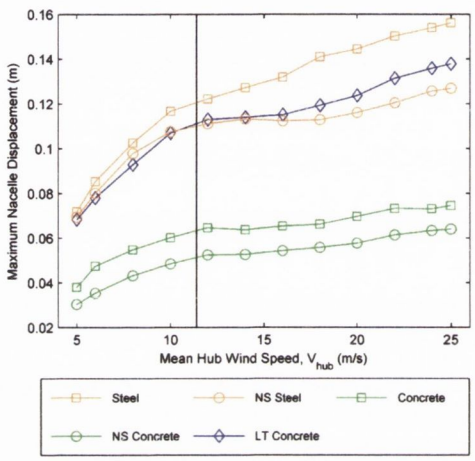

(a) MC model.

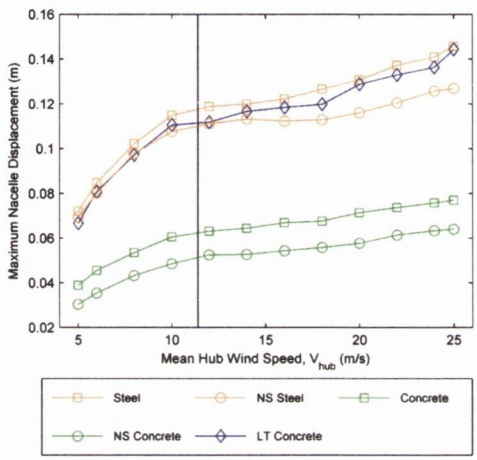

(b) HSS model.

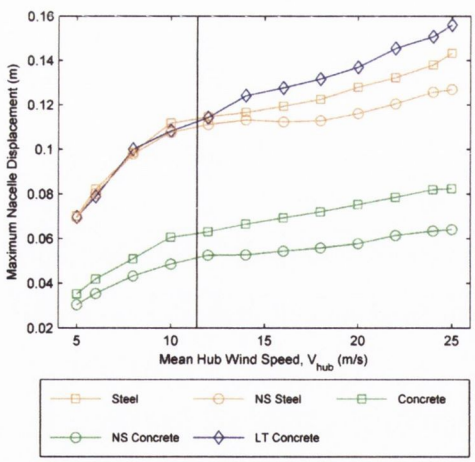

(c) HS model.

Figure 6.16: Median of maximum nacelle displacements for MC, HSS and HS soil models.

displacement response for a concrete tower incorporating long term effects, as outlined in Section 6.6.3. The difference in performance between the two towers for each of the soil

models is distinctly obvious in all three figures. To quantify this, Figure 6.17 outlines the percentage increase in nacelle response for the steel tower when compared to the concrete tower for each of the soil models. The average difference across the range of wind speeds is

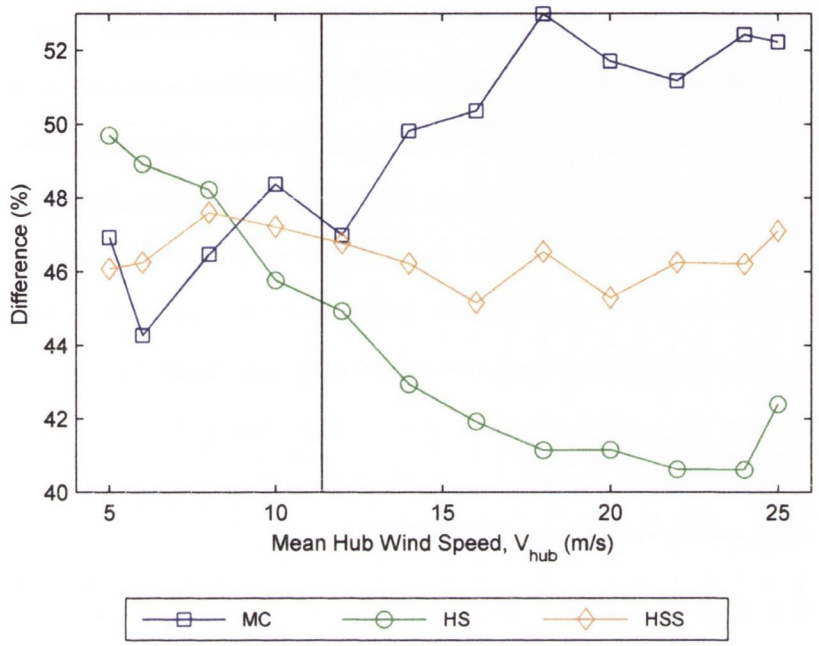

Figure 6.17: Percentage difference in nacelle response for the steel and concrete towers for each soil model.

50 % for the MC model, 46 % for the HSS model and 44 % for the HS model. The difference is also seen to increase with increasing wind speed for the MC model, remain constant, close to 46 % for the HSS model and decrease with increasing wind speed for the HS model.

In order to represent the difference in performance through a statistical representation of the likelihood of LSE, it is necessary to specify a limit-state which relates to the performance of both structures. Due to the considerable difference in the magnitude of nacelle displacements for the two towers, it was not possible to relate their performance in this sense. Across all wind speeds and for each soil model, the concrete tower outperformed the steel tower on a scale not identifiable with fragility curves. As an alternative, it was found to be possible to relate the performance of the steel tower to that of a prestressed concrete tower which has taken account for long term effects such as creep and shrinkage.

As per Section 6.6.3, a reduced value for the modulus of elasticity of concrete was applied to the prestressed concrete tower design to allow for long term effects. Also included in Figure 6.16 are the median values for the maximum displacements of the reduced strength prestressed concrete tower, "LT Concrete". These are shown to be significantly larger than the displacement values for the standard concrete tower, although they still remain lower than the steel tower response for both the MC and HSS soil models. For the HS model, shown in Figure 6.16(c), the long term concrete tower demonstrates an equivalent response to the steel tower up to the 12 m/s wind speed but beyond this speed exhibits a larger response, up to 10 % greater than the steel tower. When the "No Soil" condition is compared to the standard tower response for both tower types, a noticeable increase in displacements can be identified with the inclusion of SSI. Considering the steel tower response for both the MC and HSS soil models, it is shown that the steel tower has lower displacements than the "LT Concrete" tower. By including SSI, this pushes the maximum displacement response beyond that of the "LT Concrete" tower. For the case of the HS model, a similar effect is evident, although the median response values remain below that of the "LT Concrete" tower.

Figure 6.18 presents a set of fragility curves which illustrate the respective probabilities of LSE for both the steel and long term prestressed concrete towers for each of the three soil models. As with the median values for the maximum displacements in Figure 6.16, the MC and HSS models show similar results, whereas the HS model deviates somewhat from this pattern. In Figures 6.18(a) and 6.18(b) the steel tower is shown to outperform the concrete tower at lower wind speeds while the concrete tower exhibits superior performance at higher wind speeds. This can be explained by the greater variability of the concrete modulus of elasticity, resulting in a portion of the concrete towers possessing considerably lower bending stiffness values than the mean value. For the MC model, the steel tower has a probability of LSE of 0.21 at the 10 m/s mean hub-height wind speed, compared to 0.31 for the long term concrete tower. At the cut-out wind speed the relative probabilities are 0.71 for the concrete tower and 1.0 for the steel tower. A similar pattern is evident for the HSS model depicted in Figure 6.18(b). A noticeable trend in the two

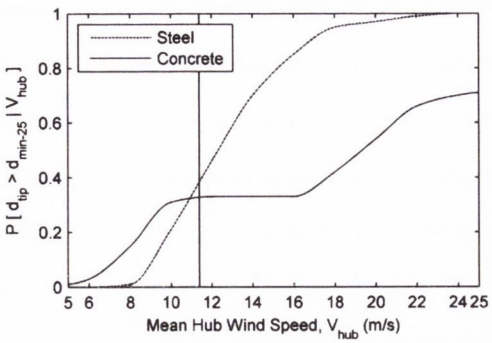

(a) MC model.

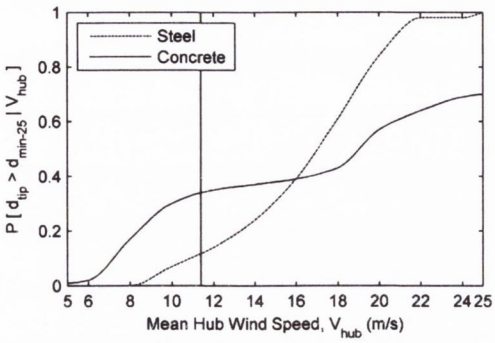

(b) HSS model.

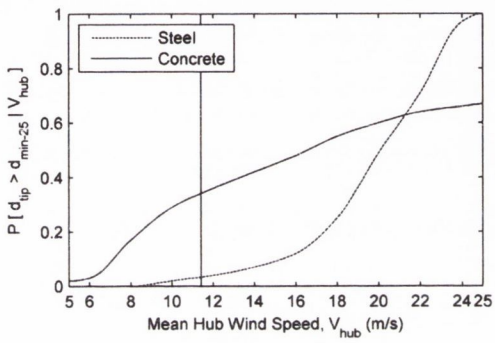

(c) HS model.

Figure 6.18: Fragility curves for nacelle displacements for MC, HSS and HS soil models.

plots is the formation of a step in both of the fragility curves for the concrete tower. This can be directly linked to both the higher variability of the concrete tower strength and the relatively slow increase in median displacements for the reduced strength concrete tower between wind speeds of 10 and 18 m/s, as seen in Figures 6.16(a) and Figure 6.16(b). At the lower wind speeds the displacements increase rapidly and due to the high variability of the concrete strength, a small proportion of the concrete towers, which are significantly less stiff, exceed the limit-state. Between wind speeds of 10 and 18 m/s, the maximum displacements do not increase significantly due to the pitching of the blades, as discussed in Section 6.7.1 and therefore, the probability of LSE does not increase greatly. Figure 6.18(c) quantifies the probability of LSE for the HS model. In this case the concrete tower exhibits a higher probability of LSE up to a mean hub-height wind speed of 21 m/s with respective probabilities of LSE of 0.03 and 0.35 for the steel and concrete towers at the

rated wind speed. Beyond the 21 m/s speed the concrete tower outperforms the steel tower and at the cut-out wind speed the probability of LSE is 1.0 for the steel tower and 0.67 for the concrete tower. It should be noted that in all cases highlighted in Figure 6.18, the concrete tower in question is based on a conservative estimate of concrete strength following the onset of long term effects as discussed in Section 6.6.3.

6.7.3 Comparison of Blade Response for Steel and Concrete Towers

The previous section has shown that ignoring SSI has significant implications for the predicted response. It also showed that the concrete tower outperforms the steel tower in terms of nacelle displacement response. In fact, the difference was so great that the relative performance could not be compared by means of fragility curves. A comparison of the steel tower with a conservatively prescribed concrete tower incorporating long term effects showed that the two towers exhibited similar response with the concrete tower outperforming the steel tower at higher wind speeds. This section compares the blade-tip displacement response for both a steel and concrete tower, as well as a concrete tower incorporating long term effects. Figure 6.19 presents the median values for the maximum blade-tip displacements for the three towers and the three soil models incorporated in the study. Not considering the "NS Steel" and "NS Concrete" towers, for both the MC and HSS models (Figures 6.19(a) and 6.19(b)), the reduced strength concrete tower, "LT Concrete", demonstrates the largest blade-tip displacements across the range of wind speeds. For the MC model, the steel and concrete towers exhibit an almost equivalent blade response, whereas for the HSS model, the concrete tower exhibits the smallest blade-tip displacements. For the HS model, illustrated in Figure 6.19(c), the three towers are seen to give almost equal blade response, except beyond the mean hub-height wind speed of 16 m/s, the steel tower exhibits larger displacements than the other two towers. A clear trend is evident across each of the plots with the displacements increasing rapidly up to the rated wind speed, after which point the rate of increase is significantly reduced. This has previously been explained as being a direct consequence of the pitching control mechanism of the blades beyond the rated wind speed. The range of displacements for

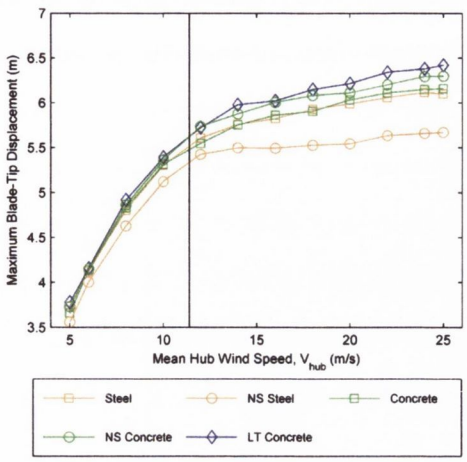

(a) MC model.

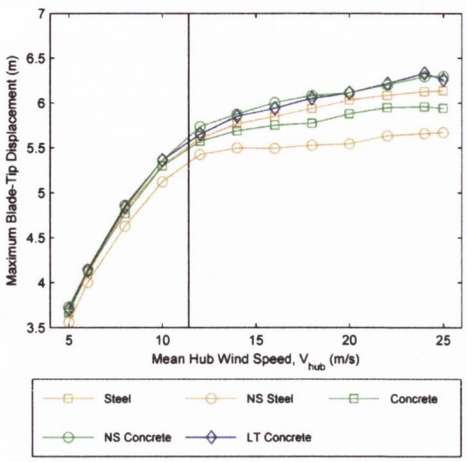

(b) HSS model.

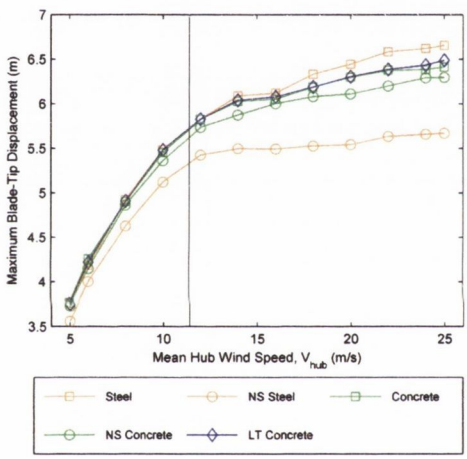

(c) HS model.

Figure 6.19: Median of maximum blade-tip displacements for MC, HSS and HS soil models.

the three models is also quite similar, varying between 3.6 m and 6.7 m. When the "No Soil" case is taken into account for both towers, the effects of SSI again become obvious. For each of the soil models, the inclusion of SSI effects is seen to noticeably increase the magnitude of the displacements across the whole range of wind speeds for the steel tower. For the concrete tower, the same trend is seen in the HS model but for the MC and HSS models, a reduction in blade displacement response is observed. This result has already been discussed in relation to Figure 6.14.

Akin to Figure 6.17, Figure 6.20 outlines the percentage increase (or decrease) in blade-

tip response for the steel tower when compared to the concrete tower for each of the soil models. In this case the percentage difference is noticeably smaller than for the compar-

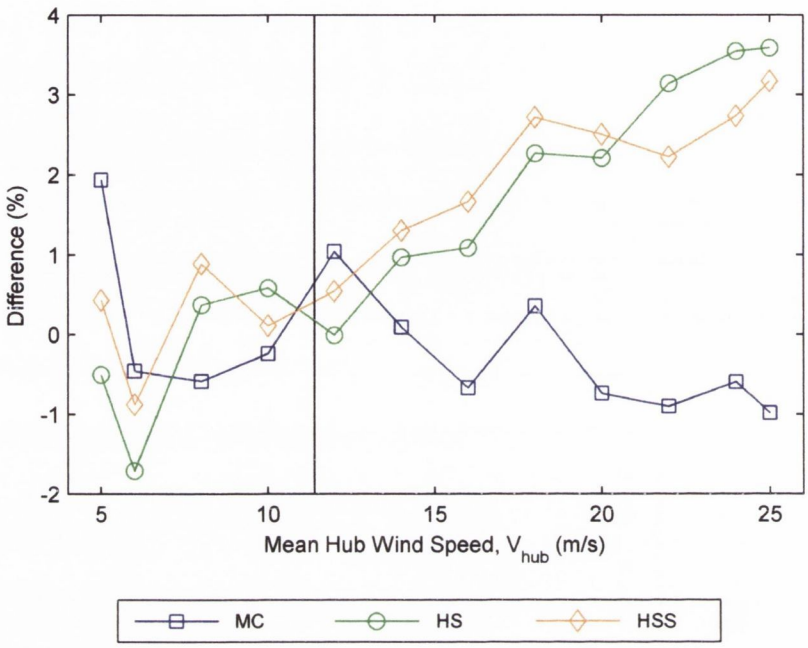

Figure 6.20: Percentage difference in blade-tip response for the steel and concrete towers for each soil model.

ison of nacelle response. It is evident that the HS and HSS models relate to an increase in the percentage difference with increasing wind speed with respective values of - 0.5 % and 0.5 % at the cut-in wind speed, comparing to values of 3.6 % and 3.1 % at the cut-out wind speed. In contrast, the MC model shows a decreasing difference in response with increasing with speed, having a value at the cut-in speed of 2 %, corresponding to a value of - 1 % at the cut-out speed.

Figure 6.21 presents a set of fragility curves representing the probability of LSE for the blade-tip displacements for all three towers using each of the soil models. Akin to the median displacement response illustrated in Figure 6.19, no significant differences exist between the blade-tip displacement response for the three towers for any of the soil models considered. For the MC model, the steel and concrete towers show almost equivalent probabilities of LSE across the range of wind speeds. The "LT Concrete" tower exhibits

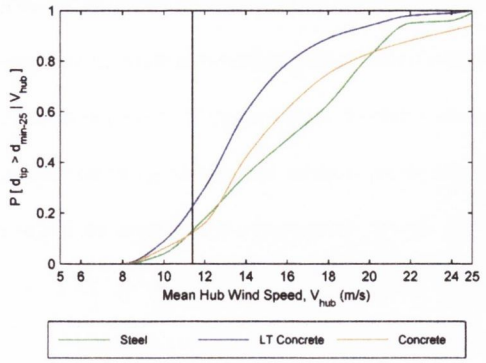

(a) MC model.

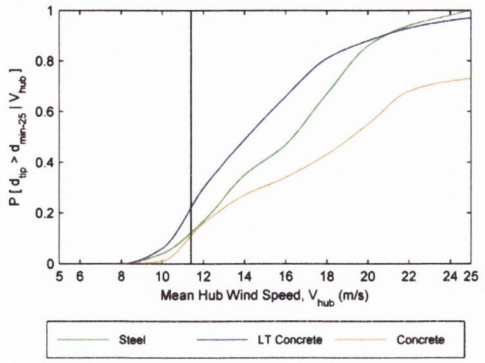

(b) HSS model.

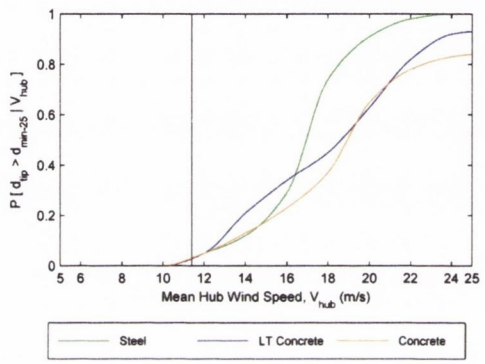

(c) HS model.

Figure 6.21: Fragility curves for blade-tip displacements for MC, HSS and HS soil models.

the highest probability of LSE for all wind speeds, although the difference is not particularly large. The greatest difference occurs at a mean hub-height wind speed of 18 m/s, where the steel tower gives a probability of LSE of 0.63, whereas the "LT Concrete" tower corresponds to a probability of 0.89. A greater difference in performance is evident for the HSS model where the standard concrete tower exhibits a noticeably lower probability of LSE than the steel and "LT Concrete" towers. This highlights the importance of considering long term effects in concrete. At the mean hub-height wind speed of 18 m/s the concrete tower has a probability of LSE of 0.43 while the steel tower corresponds to a probability of 0.67 and the "LT Concrete" tower 0.81. At the cut-out wind speed the steel tower equates to a probability of 1.0, the "LT Concrete" tower 0.97 and the concrete tower 0.73. For the HS model, the probabilities are, once again, quite closely related,

with the steel tower exhibiting a higher probability of LSE above the 16 m/s wind speed. Referring to the two soil models identified as the most accurate for the current investigation (MC and HSS), it is seen that the "LT Concrete" tower corresponds to consistently higher probabilities of LSE. The concrete and steel towers share a similar performance, although, according to the HSS model, the concrete tower offers an advantage at higher wind speeds.

6.8 Conclusion

Thus far, the investigations carried out as part of this thesis have assumed a fixed support at the base of the wind turbine tower. As the purpose of the studies has primarily been a comparison of performance between two tower designs, a detailed soil structure interaction model has not been seen as a necessity for the analysis. It has also been shown in the literature that a fixed base assumption can, in many instances, accurately represent the structural response and is generally seen as a good first approximation in general turbine design. Despite this, other studies have proven the often significant influence of soil structure interaction (SSI) for particular soil types. Also, when considering the vast difference in structural mass between the steel and concrete towers utilised in this thesis, it may prove interesting to assess any differential effects to the respective responses as a result of considering SSI. Therefore, the current chapter set out to compare the relative structural performance of wind turbines employing both tubular steel and prestressed concrete tower solutions with the inclusion of SSI as part of the modelling framework.

Initially, two towers were specified for a height of 88 m utilising both prestressed concrete and tubular steel designs. A standard 5 MW wind turbine was also identified to be supported by the two towers. An initial analysis of the DLCs was carried out using the verified wind turbine design code, FAST, in order to establish the critical loads present at the tower base. This analysis was carried out for both the steel and concrete towers as per the requirements of the International Electrotechnical Commission (IEC) design standards. In coordination with the UCD Geotechnical Research Group a design was

established for a reinforced concrete slab foundation for a wind turbine exhibiting the established critical loads in the environment of an active geotechnical test site at Blessington, County Wicklow. The test site consisted of a very dense sand in a highly over-consolidated state. Utilising the well documented soil properties, along with the established foundation design, a series of soil models were developed in order to accurately capture the soil response under the prescribed loading conditions. These facilitated the establishment of both horizontal and rotational soil stiffness values which could be input into the structural dynamic model derived in Chapter 3.

From a geotechnical perspective, the concrete tower solution offers a more favourable design for the 5 MW wind turbine considered in the study. Firstly, during the initial design stage, it was shown that a 13 % larger foundation area would be required for the tubular steel tower solution in order to have the same factor of safety against failure as the prestressed concrete tower. Differential settlements and horizontal displacements were shown to be reduced by employing the concrete configuration. Also, for each of the soil models outlined in the study, the full foundation area for the concrete tower remained in compression during all phases of loading, implying that no uplift was occurring. This was not the case for the steel tower which had only 85 % of the foundation area in compression during extreme loading. The greater rotational and horizontal stability of the foundation in the case of the concrete tower was attributed to the increased vertical loading due to the larger self weight of the concrete tower. This additional loading created a more uniform soil bearing response beneath the foundation, thus, minimising differential settlements and improving horizontal and rotational stability.

Having established the foundation design along with its associated stiffness properties for the two tower configurations, the next step was to implement a probabilistic based comparison of the structural performance of the tower configurations under operational wind loading conditions. This was facilitated by establishing batches of stochastic variables using the Monte Carlo method, as per each of the previous studies, and matching them with the foundation stiffness parameters for each of the soil models. Subsequently, simulations were undertaken for each batch of data and upon completion the response of the wind

turbine systems were analysed, allowing a comparison of the relative tower performance for each of the soil models to be produced. It was also possible to compare the relative response of the various soil models to the fixed based assumption. Initially, the median values of the maximum nacelle and blade-tip displacements were plotted. A statistical breakdown of the relative performance was also illustrated using fragility curves which relate the probability of exceeding a prescribed limit-state to the specified loading magnitude, mean hub-height wind speed in this instance. A displacement based limit-state was chosen based on the maximum nacelle and blade-tip displacements.

In an analysis of the soil models it was highlighted that the most reliable models for assessment of the soil response were the Mohr-Coulomb (MC) and Hardening Soil With Small Strain Stiffness (HSS) models, given the prevalence of small strains for the particular soil type and the similarity of the soil stiffness values produced by the two models. This was reflected in a comparison of the nacelle and blade responses for each of the soil models as well as the fixed support assumption, "No Soil". In relation to the steel tower, for both the nacelle and blade-tip response, the "No Soil" condition corresponded to the lowest median values for the maximum displacements as well as exhibiting the lowest probability of limit-state exceedance (LSE) of all four SSI cases. Conversely, the Hardening Soil (HS) model exhibited the highest median displacement values as well as the greatest probability of LSE across the entire range of wind speeds. The MC and HSS models, as expected, behaved similarly for both the nacelle and blade-tip responses, with the HSS model relating to a marginally higher response. When the response of the soil models was compared to the "No Soil" case it was shown that an increase in response of between 1 and 25 % was achieved for the nacelle response and up to 17 % for the blade response through the inclusion of SSI. The difference in response was also shown to increase with increasing wind speed. An equivalent analysis was also carried out for the concrete tower and produced similar findings. In this case, however, for the nacelle response it was found that it was more difficult to differentiate the tower response for each of the soil models. This was attributed to the greater variability of the concrete strength specified, as compared to the steel strength with respective CoV values for the modulus of elasticity of 23 %, and 3 %. It

was also noted that the range of displacements produced by the concrete tower (0.03 m and 0.083 m) was significantly lower than for the steel tower (0.069 m and 0.157 m) across the entire range of wind speeds. Considering the blade response, a similar trend was noticeable except for the unusual result that the MC and HSS models show improved displacement response in terms of both median response and the probability of LSE over the "No Soil" condition. This was explained by the proximity of the concrete tower natural frequency to the blade natural frequency in the "No Soil" condition, a situation which was eliminated by the introduction of SSI effects. Aside from this, the HS model exhibited the largest response in terms of median displacements as well as probabilities of LSE while the MC and HSS models demonstrated similar responses. In calculating the percentage difference in response relative to the "No Soil" case, it was shown that the nacelle response had a much larger relative increase in response compared to the steel tower, with a minimum increase in response of 10 %. An interesting factor in both the nacelle and blade response was the fact that the difference in response relative to a fixed based tower decreased with increasing wind speed.

In order to quantify the relative performance of the steel and concrete towers, a comparison of the respective displacement responses was also undertaken. A plot of the median values for the maximum nacelle displacements illustrated the significant difference in the magnitude of displacements for the two tower configurations. This equated to an average difference across the range of wind speeds of 50 % for the MC model, 46 % for the HSS model and 44 % for the HS model. A plot of the median displacement response of a concrete tower ("LT Concrete") with reduced stiffness due to the incorporation of long term effects was also included. Although this tower was conservatively configured, the response appeared much more closely related to that of the steel tower. Response values for a fixed base steel and concrete tower were also plotted. These showed the significant increase in nacelle response when SSI was taken into account. In an effort to compare the relative response of the steel and concrete towers through the use of fragility curves, the relative displacement values proved too dissimilar to achieve this. However, it was possible to compare the steel and "LT Concrete" towers. Once again, the MC and HSS models

demonstrated similar results with the steel tower exhibiting lower probabilities of LSE at lower wind speeds while the "LT Concrete" tower proved superior at higher wind speeds. A common trend was evident in the formation of a step in both of the fragility curves for the concrete tower for the MC and HSS models. This was linked to both the higher variability of the concrete tower strength and the relatively slow increase in median displacements for the reduced strength concrete tower between wind speeds of 10 and 18 m/s due to the blade pitching mechanism. The HS model illustrated a better performing steel tower up to a wind speed of 21 m/s, after which the concrete tower exhibited a lower probability of LSE. At the cut-out wind speed, the concrete tower had a probability of LSE of 0.7 which compared to a probability of 1.0 for the steel tower.

The blade displacement response for the three towers and three soil models was also assessed. A clear trend was evident across each of the plots with the displacements increasing rapidly up to the rated wind speed, after which point the rate of increase was significantly reduced. This was previously outlined as a consequence of the pitching control mechanism of the blades beyond the rated wind speed. The range of displacements for the three models was also seen to be quite similar. While no significant difference in displacement response was evident between each of the towers and soil models, it was noticeable for both the MC and HSS models that the "LT Concrete" tower corresponded with the largest median displacement response. For the MC model the steel and concrete towers exhibited an almost equivalent response while the steel tower demonstrated larger displacements with the HSS model. In the HS model the response of the three towers was identical up to a wind speed of 14 m/s, after which point the steel tower exhibited a larger response. Response values for the "No Soil" case were also plotted for both the steel and concrete tower. The steel tower showed a significant increase in response for each of the soil models when SSI was accounted for. The concrete tower, on the other hand, showed a decrease in the magnitude of displacement response for both the MC and HSS models. A comparison of the performance was also carried out using fragility curves. Similar to the median displacement response, no significant difference in performance was identified. Considering the MC and HSS models, the two soil models identified as the

most reliable for the modelled soil type, the "LT Concrete" tower displayed a consistently higher probability of LSE. The steel and concrete towers exhibited a similar response for the MC model, while the concrete tower gave improved performance at higher wind speeds for the HSS model. The HS model showed the least distinction between the three models, while the steel tower resulted in a greater probability of LSE at higher wind speeds.

Overall, this study highlighted the necessity to consider SSI in predicting the response of large scale multi-megawatt wind turbines as well as the relevance of the MC and HSS soil models to the current analysis. It outlined the significant improvement in foundation design efficiency achievable by utilising a prestressed concrete tower solution as well as the comparatively lower magnitudes of displacement response exhibited by a prestressed concrete tower. When long term effects in concrete were considered, in a conservative manner, the difference in performance was seen to be reduced although the concrete tower remained the more efficient design at higher wind speeds. Due to the extent of the difference in displacement response between the steel and standard concrete tower, the use of high strength concrete was not considered in this study. Detailing a high strength concrete, as was considered in Chapter 4 would have further accentuated the superior performance of the prestressed concrete solution. In terms of blade response, there were no significant differences identified between the steel and concrete towers. Despite this, it was shown that the "LT Concrete" tower resulted in a higher probability of LSE while the standard concrete tower offered the lowest probability of LSE at higher wind speeds for two of the three models. It should be noted that in the current study, the damping effects of soil on the structural response were not considered. These have been known, for certain soil types, to reduce wind turbine vibration response. An investigation of the comparative effects of soil damping on both tubular steel and prestressed concrete towers may prove insightful as a theme for future work. The current study also only considered a single soil type, that of the Blessington sand at the test site. A comparison of the relative effects of varying soil types on the different tower configurations may also prove interesting in future analysis. This would also necessitate an assessment of different foundation types, which, in itself, would prove an interesting undertaking for future work.

Chapter 7 -

Conclusions

7.1 Introduction and Review of Objectives

Given the growing constraints on fossil fuel resources and the emergence of renewable energy concepts as viable alternatives for energy generation, this thesis identified a limitation to the progression of wind turbine design beyond the current state of the art. This was established from an extensive review of the literature, carried out in Chapter 2. Aside from hydroelectric power generation, wind energy is the most advanced renewable energy concept. In order to improve efficiency and become more competitive relative to the more traditional energy generation techniques, wind turbines must become larger, stretching further into the multi-megawatt domain and, as a consequence, be supported on taller and stronger tower structures. This poses a problem for wind turbine designers due to the limitations faced by the current, industry standard, tubular steel tower designs. As heights of 85 to 90 m are exceeded, the tubular steel design faces manufacturing problems, transport issues, as well as an inability to perform to the required standard when supporting the increasingly large turbines. Based on a detailed assessment of the literature it was shown that, in order for wind turbines to progress, alternative tower solutions must be sought. It was also noted that, to date, limited effort has been expended in the investigation of the relative benefits of these alternative designs.

The focus of this thesis was on assessing the structural performance of prestressed concrete and tubular steel tower designs for heights in the range of 88-120 m. This height range was chosen as it is representative of current state of the art multi-megawatt wind turbines and is at the upper range of the capabilities of tubular steel towers. A probabilistic

representation of the relative performance of both tower configurations was derived for a series of loading requirements and measured responses with the aim of quantifying the performance in terms of structural reliability. The more detailed aspects of this analysis are reflected in the objectives set out in Section 1.2. These may be summarised as follows:

1. Initially, it was desired to undertake a thorough investigation of the literature in order to identify the most appropriate dynamic modelling techniques relevant to wind turbine systems. Based on the findings of this investigation, a one dimensional dynamic model was to be developed which could effectively capture both flapwise blade vibration, longitudinal tower motion as well as the coupling effects between the tower and blades. This model was required to embody both accuracy and computational efficiency in order to facilitate the detailed investigations to come.

2. The first investigation of wind turbine tower performance entailed the determination of the structural response of both tubular steel and prestressed concrete towers under normal operating conditions for basic, one dimensional response. This was achieved through the application of the one dimensional model previously established through Objective 1. The relevant details in the undertaking of this analysis and the resulting outcomes are further discussed in Section 7.2.1.

3. In an effort to extend the relevance of the study the next objective required the development of a more sophisticated structural model which captured the complex dynamic interactions within a two dimensional framework. The aforementioned one dimensional model was to be further extended to incorporate edgewise blade vibrations, lateral tower motion, nacelle tilt, roll and yaw as well as rotor shaft rotation. Again, this model was required to achieve accurate results with adequate computational efficiency and this was to be proven through a verification against a licensed wind turbine design program.

4. In a continuation of the analysis of the structural performance of the two tower construction materials, further objectives saw the implementation of the two dimensional model while subjecting the structures to various loading conditions. In the

first instance, seismic loading of the wind turbine structures was to be considered due to its increasing relevance to wind turbine design. This would be accomplished by implementing a probabilistic modelling technique, probabilistic seismic demand analysis, a procedure which has not previously been adopted in the literature, and offers a tool for future seismic investigations of wind turbine systems. The implementation of this investigation and the findings which ensued are further discussed in Section 7.2.2.

5. While, thus far, the focus has been on the effect of the tower construction material on the associated tower response, in another instance the effect of the tower configuration on the dynamic response of the blades was addressed. Having not previously been addressed in the literature, this was a relevant issue given the detrimental effects of excessive vibration on wind turbine blades. Comparison was made between the two chosen tower configurations in the context of the recorded blade vibration response for a series of wind turbines with varying height. A more detailed discussion of the implementation and outcomes of this analysis is provided in Section 7.2.3.

6. The final objective set out for this thesis called for the extension of the aforementioned two dimensional model to account for the effects of soil structure interaction (SSI). Given the considerable difference in structural mass between tubular steel and prestressed concrete tower designs, it was proposed that the effect of SSI may not be consistent for the two designs. By extending the two dimensional model to account for a variable support condition at the tower base, the response of the two 88 m towers could be measured under wind loading for a specified set of soil parameters. This would improve the realistic nature of the results and offer the possibility of highlighting relative differences in tower performance due to SSI effects. The details of this study are discussed in greater detail in Section 7.2.4.

7.2 Summary of Work and Fulfilment of Objectives

Chapter 2 outlined a detailed review of the literature carried out by the author. This had the aim of identifying trends in the wind turbine industry, establishing the requirements of state of the art concepts and designs as well as addressing the various modelling techniques and analysis methods necessary for an investigation of wind turbine structural performance, tower performance in particular. Based on the findings of this review, it was possible to identify gaps in the literature and, therefore, appropriately define the aforementioned objectives of this thesis. Throughout this review, particular attention was paid to assessing the various modelling techniques employed in quantifying the dynamic response of wind turbines subjected to various structural loading conditions. The requirements for accurately modelling turbulent wind loading as well as seismic loading were also addressed.

Based on the findings of the aforementioned literature review, Chapter 3 detailed the derivation of a number of wind turbine structural dynamic models which would facilitate the subsequent investigations of the tubular steel and prestressed concrete tower performance. In line with a number of previous studies identified in the literature, the initial model was formulated with the capability of efficiently capturing the one dimensional response of a wind turbine system. This required an approximation of the flapwise blade vibration as well as longitudinal tower motion. As the majority of the wind loading acts in a single direction for normal operational conditions, and the most significant components of the tower and blade response coincide with the direction of loading, a one dimensional dynamic model is accepted as a good approximation of wind turbine structural response. Given the nature of the studies to be conducted, this offered a useful starting point for the assessment of relative tower performance. Having achieved Objective 1, this model offered the necessary tools to undertake the initial study of tower performance called for in Objective 2. The implementation of this study is detailed in the following section.

7.2.1 One Dimensional Tower Comparison

In line with Objective 2, the first part of Chapter 4 set out to assess the one dimensional structural performance of tubular steel and prestressed concrete wind turbine towers, for heights ranging from 88 m to 120 m. Utilising the one dimensional model established from Objective 1, a suite of towers were investigated to determine the structural responses under varying conditions of turbulent wind loading. In all cases a representative 5 MW wind turbine was supported by the towers while in an operational state. A probabilistic representation of the tower structural properties as well as the environmental conditions was employed in the classification of the study parameters. This allowed for the generation of batches of statistically representative model input values using the Monte Carlo method. Simulations were conducted for each batch of variables and the resulting responses were illustrated with the use of fragility curves, a method of characterising the reliability of a structure, or structural component, for a prescribed limit-state or limit-states. Maximum nacelle displacements were utilised in determining the structural performance of the towers and consequently, the limit-states were defined relative to these values. As part of this study additional concrete towers were specified to incorporate both a conservatively modelled reduced strength concrete due to long term effects, as well as a high strength concrete which would likely be employed in a structure of this type. The findings of this study are discussed in Section 7.3.

7.2.2 Probabilistic Seismic Demand Analysis

The development of the investigation outlined Chapter 5 saw the fulfilment of Objectives 3 and 4. Initially, the one dimensional model derived as part of Objective 1 was extended to facilitate an approximation of two dimensional wind turbine dynamic response. This included additional DOFs to account for edgewise blade vibration, lateral tower motion, nacelle tilt, roll and yaw as well as rotor shaft rotation. The developed model provided an efficient and accurate solution for representing the two dimensional motion of a wind turbine system and the validity of the results were subsequently verified through a comparison of the output natural frequencies and computed displacement time histories with

a licensed wind turbine design program.

Utilising the two dimensional model derived as part of Objective 3, the remainder of the chapter detailed an analysis of the performance of both steel and concrete tower designs when subjected to seismic loading. Once again a series of tubular steel and prestresssed concrete towers were considered at heights of 88 m, 103 m and 120 m in combination with the NREL 5 MW wind turbine. The structural input properties of the towers were modelled as random variables with specified PDF, mean and CoV. Additional concrete towers were also specified to include a reduced concrete strength due to long term effects as well as a higher strength concrete due to the effects of a high rate of loading which is synonymous with earthquake events. In order to generate the necessary fragility curves, probabilistic seismic demand analysis was performed on each of the towers. A suite of 100 recorded ground motions were utilised. These were representative of the seismicity of California, a region with a high density of wind turbine structures. By utilising peak ground acceleration as the seismic intensity measure a probabilistic seismic demand model was derived for each tower. This provided a mathematical relationship between the ground motion intensity measure and the structural response for each individual tower. The response variable chosen for the study was nacelle acceleration as this could be appropriately related to a series of acceleration based limit-states which define the ULS condition for various electronic and mechanical components located in the nacelle. Having specified values for the lognormally distributed capacity limit-states, a combination of the capacity and demand estimates was utilised in the formulation of the fragility curves. The results of this investigation are summarised in Section 7.3.

7.2.3 Tower Comparison With Blade Fragilities

In another application of the two dimensional dynamic structural model, Objective 5 was also addressed in Chapter 4 with an investigation of the influence of the choice of tower construction material on the dynamic response of the wind turbine blades. In a continuation of the previous studies, both prestressed concrete and tubular steel towers were considered at heights of 88 m, 103 m and 120 m where the structural input properties

were modelled as stochastic variables with specified PDF, mean and CoV. In all cases the standard NREL 5 MW wind turbine was supported by the towers. Turbulent wind loading was simulated for a series of mean hub-height wind speeds varying from 16 m/s to 25 m/s and the resulting dynamic response of the blades was assessed. A limit-state was chosen based on the resultant blade-tip displacement and this was employed in the generation of fragility curves to facilitate an assessment of the blade response associated with the tubular steel and prestressed concrete towers. The outcomes of this analysis are highlighted in Section 7.3.

7.2.4 Soil Structure Interraction

The final objective of this thesis involved the consideration of SSI on the overall response of the wind turbine system in the context of a comparison of tubular steel and prestressed concrete wind turbine towers. This was achieved through an analysis conducted in Chapter 6. In this case both a prestressed concrete and tubular steel tower design were specified for a height of 88 m. Utilising the verified wind turbine design code FAST, a detailed analysis of the ultimate loading conditions of the turbines was conducted in accordance with the International Electrotechnical Commission (IEC) design standards. In collaboration with the UCD Geotechnical Research Group, an appropriate foundation design was established based on the computed critical loads at the base of the towers and the extensively analysed soil conditions at the UCD geotechnical research test site. In order to guarantee an equal comparison of performance, the same foundation was considered for both towers despite the requirement for a larger foundation to achieve the same factor of safety for the steel tower. Utilising three industry standard soil models, a two dimensional FE model was established for the foundation and soil conditions considered. This facilitated the computation of soil stiffness values for both the tubular steel and prestressed concrete wind turbine towers for each of the three soil models. Having derived the soil stiffness values, these were combined with batches of statistically representative tower structural input properties as per each of the previous studies. Simulations were undertaken for each of the batches and the resulting responses were analysed. In this instance both

nacelle and blade response was considered, with limit-states identified based on maximum nacelle and blade-tip displacement. Utilising plots of maximum displacement values as well as fragility curves, comparisons were established between the three soil models and the fixed support assumption for each of the towers. A comparison was subsequently drawn between the performance of the steel and concrete towers for each of the soil models as well as the fixed support assumption at the base of the tower, considering both the nacelle and blade-tip response. An additional analysis was also undertaken for a prestressed concrete tower incorporating a conservative assumption of the long term effects on the strength of the concrete. The results achieved for this tower design were also included in the aforementioned comparison. The findings of this investigation are detailed in the next section.

7.3 Summary of Findings and Recommendations for Future Work

Each of the investigations carried out as part of this thesis, and summarised in the previous sections, had the objective of determining various structural responses for both the tubular steel and prestressed concrete tower designs subjected to a series of different loading conditions. This section summarises the findings of these investigations.

In the first instance, the one dimensional response of prestressed concrete and tubular steel tower configurations was determined at heights of 88 m, 103 m and 120 m. For the case of prestressed concrete, simulations were undertaken for a standard strength, a reduced strength and a high strength concrete tower. At the time the study was undertaken, due to a lack of publicly available material detailing the properties and dimensions of prestressed concrete towers at heights beyond 88 m, it was decided to use the same tower diameters and concrete thickness for the taller towers as for the 88 m tower. The influence of this assumption on the results was addressed in the discussion in the context of Appendix E.3, which provides a comparison to more recently identified, designed towers. For the case of the standard strength concrete, at all heights it was seen that the prestressed

concrete noticeably outperformed the steel towers which exhibited significantly higher probabilities of limit-state exceedance (LSE). When a conservative model of long term effects in prestressed concrete was implemented for a 120 m tall tower, it was observed that the steel and concrete tower showed minimal difference in performance with steel exhibiting superior results at lower wind speeds but a reversal of performance being observed at higher wind speeds. As a high strength concrete would likely be used in such structures, a 120 m tall tower was configured with such a property. This was observed to induce a distinct improvement over regular strength concrete and, therefore, the steel option as would be expected. The inclusion of long term effects in the simulation reduced this improvement but the prestressed concrete tower remained significantly ahead of the steel option in terms of reduced probability of LSE. Another important factor was the consideration of the results in the context of the assumptions made in defining the properties of the prestressed concrete towers. From the analyses undertaken in Appendix E.3, it was shown that the 103 m and 120 m studied towers offered lower resistance to wind excitation than equivalent, designed examples which were most likely specified with high strength concrete. This validated the assumption that the choice of prestressed concrete towers offered a baseline comparison to more realistic designs in terms of resistance to wind excitation. An interesting undertaking identified for future work would be to consider the effects of creep and shrinkage on prestressed concrete structures in a more detailed manner. It was suggested that a conservative estimate of the creep coefficient was chosen in this investigation. By varying the creep coefficient based on external conditions and structural specifications, a variation of resulting long term concrete strengths may be achievable.

In a second study, the structural response of prestressed concrete and tubular steel towers was determined at the three heights once more, except in this case the towers were subjected to seismic loading. Again, a reduced strength concrete was also considered as well as the effects of high frequency loading on concrete strength. For the case of the standard concrete towers it was shown that the steel design outperformed the concrete design at a height of 88 m. As the height increased, however, the gap was reduced with the two designs displaying equal performance at the 120 m height. When long term effects

such as creep and shrinkage were considered a similar pattern was noted but the designs displayed equal performance at 103 m and the concrete tower outperformed the steel tower at 120 m. In a third analysis, the concrete towers were assumed to have a 50 % higher instantaneous modulus of elasticity based on evidence in the literature which suggested an increase in concrete strength at high rates of load application. The results of this analysis showed a distinct advantage for the steel towers across all heights and limit-states. These findings appeared somewhat counter-intuitive given the expectation that a reduction in strength would relate to a decrease in performance and, conversely, an increase in strength will improve performance. Following an investigation of the results it was found that the most significant influence on the response values for the towers proved to be the value for the first natural bending frequency of the towers. As the 103 m and 120 m prestressed concrete towers were designed to be a lower-bound of the realistic tower strength, it was shown that the values for the period of first natural bending were larger than in reality. While the steel towers showed a small decrease in natural period with increasing height, the concrete towers exhibited considerably larger values as the height increased. It was demonstrated that those structures with shorter natural period were susceptible to a larger mean response based on the mean response spectrum for the suite of earthquake ground motions used in the study. This fact undoubtedly affected the outcome of this investigation. When consideration was given to the designed towers, detailed in Appendix E.3, it was suggested that the tubular steel designs would show further improvement over the corresponding prestressed concrete towers. This was due to the significantly higher natural frequency values for the concrete towers as well as the decreasing frequency profile identified for both materials with increasing height. Overall, the most significant finding of this investigation was the influence of tower natural frequency on the resulting seismic response. This highlighted the importance of considering the tower natural frequency value when designing such structures. Given this fact, an interesting topic identified for future work was the investigation of tuned mass dampers and, more appropriately, active mass damper systems which could prove highly beneficial to the future of wind turbine structures in regions susceptible to seismic activity.

When the influence of the tower construction material on the magnitude of wind turbine blade vibrations was investigated, it was shown that the choice of tower construction material does in fact have an influence on the resulting blade response. In the context of the specific steel and prestressed concrete towers specified in this investigation, it was shown that at lower heights the steel towers exhibited more favourable performance in terms of the magnitude of the blade-tip displacements and the frequency of LSE. As the hub-height was increased the relative advantage of the steel option was seen to diminish with minimal difference in performance across the range of wind speeds for the 120 m towers. In this case the steel tower outperformed the prestressed concrete by 6 % at the 18 m/s wind speed while a reversal in performance was observed beyond 19 m/s with the concrete tower showing superior performance for the greater wind speeds. An explanation for the reducing difference in performance with increasing height was identified based on the differing trends in natural frequency values over the height range (i.e. increasing values for steel, decreasing values for concrete). On reviewing another suite of similar towers, it was seen that both the steel and concrete towers exhibited decreasing natural frequency values with increasing height. This would most likely serve to increase the advantage of the steel towers. Also, the natural frequencies of the concrete towers were seen to be noticeably higher than the studied towers, thus coming closer to the blade natural frequencies and increasing the blade response. What was shown by this particular investigation was that by altering the tower construction material, the dynamic response of the wind turbine blades can be affected, although this is primarily due to the resulting natural frequencies of the towers. This is a useful finding given the requirement to minimise blade vibrations in order to increase their reliability and, as a consequence, their expected design life.

The final investigation undertaken in this thesis focussed on the effect of SSI on the dynamic response of the prestressed concrete and tubular steel designs for an 88 m tall tower. Firstly, during the initial design stage, it was shown that the foundation area for the tubular steel tower solution would be required to be designed 13 % larger than the foundation area for the prestressed concrete tower in order to have the same factor of safety against failure. Differential settlements and horizontal displacements were shown to be

reduced by employing the concrete configuration. Also, for each of the soil models outlined in the study, the full foundation area for the concrete tower remained in compression during all phases of loading, implying that no uplift was occurring. This was not the case for the steel tower which had only 85 % of the foundation area in compression during extreme loading. These relative advantages were attributed to the increased vertical loading due to the larger self weight of the concrete tower. In comparing the three soil models, based on the soil properties at the test site, the Mohr-Coulomb (MC) and Hardening Soil With Small Strain Stiffness (HSS) models were identified as the most reliable in representing the soil behaviour. This was reflected in a comparison of the tower and blade response for the various soil models for both the steel and concrete towers where the MC and HSS models were shown to exhibit similar performance in all cases. When compared to a fixed support assumption at the base of the tower it was evident that the response incorporating SSI significantly increased vibration magnitudes with the exception of the blade response for the prestressed concrete tower. In this case the MC and HSS models related to a reduced response. This was attributed to the proximity of the first natural bending frequency of this particular tower to the blade natural frequency. When the relative responses of the tubular steel and prestressed concrete tower designs were compared it was seen that the concrete configuration offered a significant advantage over the steel tower in terms of maximum nacelle displacements. The difference in performance was so extensive that it could not be quantified with fragility curves. When a reduced strength concrete tower was prescribed to model the effects of creep and shrinkage, it was shown to have less of an advantage over the steel tower. In terms of maximum displacements the reduced strength prestressed concrete tower corresponded to lower displacement magnitudes for the MC and HSS models. When the probability of LSE was investigated the steel tower exhibited an advantage over the reduced strength concrete tower at lower wind speeds while this was seen to be reversed at higher wind speeds, above 10 m/s for the MC model, 16 m/s for the HSS model and 20 m/s for the Hardening Soil (HS) model. When blade response was addressed, the difference in performance was not quite as accentuated as it was for the nacelle response. Despite this, for each of the soil models implemented,

the reduced strength concrete tower related to larger magnitude blade-tip displacements as well as a higher probability of LSE. The steel and standard concrete towers exhibited an almost equivalent response for the MC model, with the steel tower exhibiting superior performance for wind speeds between 13 m/s and 20 m/s and the concrete tower exhibiting improved performance above 20 m/s. For the HSS model, the standard concrete tower gave improved performance at wind speeds above 12 m/s. In conducting this study the effects of soil damping, which for certain soil types may reduce vibration magnitudes for both the tower and blades, was not considered. In considering possibilities for future work in this area it would prove interesting to investigate any relative differences in the effects of soil damping on each of the towers. While only a single soil type (Bs) was considered in this case, another interesting undertaking would be to consider any relative differences in tower performance for a range of different soil types. An investigation such as this would necessitate the consideration of different foundation solutions, which, in itself, would be an worthwhile consideration for future work.

Overall, the findings of the investigations undertaken in this thesis gave a variation of results for the relative performance of tubular steel and prestressed concrete wind turbine towers:

- For the one dimensional response under normal wind loading, the concrete tower showed a significant advantage over the steel option.

- When seismic loading was considered the steel tower outperformed the concrete tower, although the first natural bending frequency of the towers was shown to have a significant effect on these results.

- In consideration of the influence of tower construction material on the blade response it was seen that the steel towers outperformed the concrete option at lower heights. As the height was increased the advantage was seen to diminish with a resulting equivalent blade response at the tallest height of 120 m. When a similar set of designed towers were considered, it was suggested, based on the natural frequency values, that the steel towers would exhibit further improved performance across all

heights.

- Finally, when SSI was introduced, its effect on the overall response of the wind turbine system was shown to be significant. The considerable advantage of utilising a prestressed concrete tower design was also highlighted with a more efficient foundation design and significantly lower nacelle displacements.

In each of the studies, variations of the concrete strength were also implemented to take into account long term effects on prestressed concrete, high strength concrete specifications, as well as the influence of the rate of load application on the resulting instantaneous strength of concrete. In review of the findings of this thesis, a number of opportunities for future work have been identified:

- To consider the effects of creep and shrinkage on prestressed concrete structures in a more detailed manner for each of the relevant studies.
- Given the effect of the tower bending frequency on the seismic response, further investigation of tuned mass dampers and, more appropriately, active mass damper systems could prove highly beneficial to the future of wind turbine structures.
- In reference to the incorporation of SSI, it would prove interesting to investigate any relative differences in the effects of soil damping on each of the towers.
- Given that only a single soil type was considered in this thesis, a worthwhile undertaking would be to consider any relative differences in tower performance for a range of different soil types. This could be extended to cater for an investigation of different foundation solutions.
- Another aspect common to each of the investigations carried out which was not considered, was the differences in damping properties between steel and concrete. Concrete is known to possess advantageous damping properties and an investigation of the resulting effect on the response of the prestressed concrete towers would be a beneficial undertaking for further work.

References

Abramovich, H. and Rosen, A. (1988). "Model of the aeroelastic behavior of Darrieus wind turbine blades," *Wind Engineering*, 12(3), 149 – 164.

ADAMS (2012). "Multibody Dynamics Simulator," URL `http://www.mscsoftware.com/Products/CAE-Tools/Adams.aspx`, (Accessed: July 24, 2012).

Agarwal, P. and Manuel, L. (2011). "Incorporating irregular nonlinear waves in coupled simulation and reliability studies of offshore wind turbines," *Applied Ocean Research*, 33(3), 215 – 227.

AlHamaydeh, M. and Hussain, S. (2011). "Optimized frequency-based foundation design for wind turbine towers utilizing soil-structure interaction," *Journal of the Franklin Institute*, 348(7), 1470 – 1487.

Andersen, L., Vahdatirad, M., Sichani, M. and Sørensen, J. (2012). "Natural frequencies of wind turbines on monopile foundations in clayey soils-A probabilistic approach," *Computers and Geotechnics*, 43, 1 – 11.

Andersen, L., Vahdatirad, M. and Sørensen, J. (2011). "Reliability-based assessment of the natural frequency of an offshore wind turbine founded on a monopile," in: *Proceedings of the 13th International Conference on Civil, Structural and Environmental Engineering Computing, 2011*, Chania, Crete, Greece.

Arasu, P. V., Sagayaraj, D. and Gowrishankar, J. (2011). "Seismic Analysis of a Wind Turbine Steel Tower," in: *Altair - 2011 HyperWorks Technology Conference.*

Arrigan, J., Pakrashi, V., Basu, B. and Nagarajaiah, S. (2011). "Control of flapwise vibrations in wind turbine blades using semi-active tuned mass dampers," *Structural Control and Health Monitoring*, 18(8), 840–851.

ATC (1985). "Earthquake damage evaluation data for California," Tech. Rep. ATC-13, Applied Technology Council.

ATC (1991). "Seismic vulnerability and impact of disruption of lifelines in the conterminous United States," Tech. Rep. ATC-25, Applied Technology Council.

ATS (2012). "Advanced Tower Systems," URL `http://www.advancedtowers.com/company/`, (Accessed: July 28, 2012).

Baban, S. M. and Parry, T. (2001). "Developing and applying a GIS-assisted approach to locating wind farms in the UK," *Renewable Energy*, 24(1), 59 – 71.

Barltrop, N., Adams, A., Hallam, G. and Limited, M. T. D. (1991). *Dynamics of fixed marine structures*, MTD Ltd. publication, Butterworth-Heinemann.

Barthebnie, R., Larsen, G., Pryor, S., Jørgensen, H., Bergstrom, H., Schlez, W., Rados, K., Lange, B., Vlund, P., Neckelmann, S., Mogensen, S., Schepers, G., Hegberg, T., Folkerts, L. and Magnusson, M. (2004). "ENDOW (Efficient Development of Offshore Wind Farms): Modelling wake and boundary layer interactions," *Wind Energy*, 7(3), 225 – 245.

Basoz, N., Kiremidjian, A., King, S. A. and Law, K. H. (1999). "Statistical analysis of bridge damage data from the 1994 Northridge, CA, earthquake," *Earthquake Spectra,*, 15(1), 25–54.

Basoz, N. and Kiremidjian, A. S. (1999). "Development of empirical fragility curves for bridges," in: *Proceedings of the 1999 5th U.S. Conference on Lifeline Earthquake Engineering: Optimazing Post-Earthquake Lifeline System Reliability*, vol. 16, p. 693–702.

Baumgart, A. (2002). "A mathematical model for wind turbine blades," *Journal of Sound and Vibration*, 251(1), 1–12.

Bažant, Z. and Cedolin, L. (1987). "Discussion of "Free Vibration Behavior of Prestressed Beams" by K. Kanaka Raju and G. Venkateswara Rao (February, 1986, Vol. 112, No. 2)," *Journal of Structural Engineering*, 113(9), 2087–2087.

Baxevanou, C., Chaviaropoulos, P., Voutsinas, S. and Vlachos, N. (2008). "Evaluation study of a Navier-Stokes CFD aeroelastic model of wind turbine airfoils in classical flutter," *Journal of Wind Engineering and Industrial Aerodynamics*, 96(8-9), 1425 – 1443.

Bazeos, N., Hatzigeorgiou, G. D., Hondros, I. D., Karamaneas, H., Karabalis, D. L. and Beskos, D. E. (2002). "Static, seismic and stability analyses of a prototype wind turbine steel tower," *Engineering Structures*, 24(8), 1015–1025.

Behr, R. and Worrell, C. (1998). "Limit states for architectural glass under simulated seismic loadings," in: *Proceedings of Seminar on Seismic Design, Retrofit, and Performance of Nonstructural Components*, ATC-29-1, Applied Technology Council, Redwood City, CA, pp. 229–240.

Betz, A. (1926). *Wind-energie und ihre ausnutzung durch windmühlen*, Vandenhoeck.

Bhattacharya, S. and Adhikari, S. (2011). "Experimental validation of soil-structure interaction of offshore wind turbines," *Soil Dynamics and Earthquake Engineering*, 31(5-6), 805 – 816.

Bir, G. (2012). "BModes," URL `http://wind.nrel.gov/designcodes/preprocessors/bmodes/`, (Last modified: June 28, 2012; Accessed July 28, 2012).

BLADED (2012). "Wind Turbine Design Software," Garrad Hassan and Partners Ltd, URL `http://www.gl-garradhassan.com/en/software/GHBladed.php`, (Accessed: July 24, 2012).

Bond, L. and Clayton, B. (1989). "Non-destructive testing and condition monitoring of wind turbine blades," *Wind Engineering*, 13(1), 19 – 29.

Bowen, B. M. (2008). "Analysis of turbulence profiles from three tall towers: departure from similarity theory in near-neutral and stable conditions," *The Open Atmospheric Science Journal*, 2(1), 106–116.

Bramwell, A., Done, G. and Balmford, D. (2001). *Bramwell's helicopter dynamics*, American Institute of Aeronautics and Astronautics.

Brand, A. (2007). "Modelling the effect of wind farming on mesoscale flow-Part 1: flow model," *Journal of Physics: Conference Series*, 75(1), 012043 (13 pp.).

Breton, S.-P. and Moe, G. (2009). "Status, plans and technologies for offshore wind turbines in Europe and North America," *Renewable Energy*, 34(3), 646 – 654.

BS 8110-2 (1985). "Structural Use of Concrete — Part 2: Code of Practice for Special Circumstances," British Standards Institution.

BS EN 206-1 (2000). "Concrete — Part 1: Specification, Performance, Production and Conformity," British Standards Institution.

BS EN 61400-1 (2005). "Wind Turbines — Part 1: Design Requirements." British Standards Institution.

BS EN 61400-3 (2009). "Wind Turbines — Part 3: Design Requirements for Offshore Wind Turbines," British Standards Institution.

Buhl, M. (2012). "IECWind," URL `http://wind.nrel.gov/designcodes/preprocessors/iecwind/`, (Last modified: October 08, 2012; Accessed October 08, 2012).

Buhl Jr., M. L. and Manjock, A. (2006). "A comparison of wind turbine aeroelastic codes used for certification," in: *Collection of Technical Papers - 44th AIAA Aerospace Sciences Meeting*, vol. 13, Reno, NV, United states, pp. 9456 – 9469.

Burton, T., Jenkins, N., Sharpe, D. and Bossanyi, E. (2011). *Wind Energy Handbook*, Wiley.

Businger, J. A., Wyngaard, J. C., Izumi, Y. and Bradley, E. F. (1971). "Flux profile relationships in the atmospheric surface layer," *Journal of the Atmospheric Sciences*, 28, 181–189.

Byrne, B. and Houlsby, G. (2003). "Foundations for offshore wind turbines," *Philosophical Transactions of the Royal Society London, Series A (Mathematical, Physical and Engineering Sciences)*, 361(1813), 2909 – 30.

Byrne, B., Houlsby, G., Martin, C. and Fish, P. (2002). "Suction caisson foundations for offshore wind turbines," *Wind Engineering*, 26(3), 145 – 55.

Chakrabarti, S. K., Halkyard, J. and Capanoglu, C. (2005). *Handbook of Offshore Engineering*, vol. 1, chap. 1, Elsevier, pp. 1–38.

Chan, T. and Yung, T. (2000). "A theoretical study of force identification using prestressed concrete bridges," *Engineering Structures*, 22(11), 1529 – 1537.

Chattot, J. J. (2008). "Tower shadow modelization with helicoidal vortex method," *Computers and Fluids*, 37(5), 499 – 504.

Chaviaropoulos, P., Sørensen, N., Hansen, M., Nikolaou, I., Aggelis, K., Johansen, J., Gaunaa, M., Hambraus, T., Von Geyr, H., Hirsch, C., Shun, K., Voutsinas, S., Tzabiras, G., Perivolaris, Y. and Dyrmose, S. (2003). "Viscous and aeroelastic effects on wind turbine blades. The VISCEL project. Part II: Aeroelastic stability investigations," *Wind Energy*, 6(4), 387 – 403.

Chella, M. A., Tørum, A. and Myrhaug, D. (2012). "An overview of wave impact forces on offshore wind turbine substructures," *Energy Procedia*, 20(0), 217 – 226.

Chen, X. B., Li, J. and Chen, J. Y. (2009). "Wind-induced response analysis of a wind turbine tower including the blade-tower coupling effect," *Journal of Zhejiang University - Science A*, 10(11), 1573–1580.

Chen, Z. and Zhong, S. (1988). "Application of energy methods in aeroelastic stability analysis for wind turbine blades," *Wind Engineering*, 12(2), 140 – 146.

Clausen, N. E., Bjerregaard, E., Madsen, B. T., Morthorst, P. E. and Sørensen, P. (2004). "Offshore wind energy and industrial development in the Republic of Ireland," Tech. rep., Risø National Laboratory on behalf of Sustainable Energy Ireland.

Cleary, B., Duffy, A. and O'Connor, A. (2012). "Using Life Cycle Assessment to Compare Wind Energy Infrastructure," in: *International Symposium on Life Cycle Assessment and Construction*, Nantes, France.

Clough, R. W. and Penzien, J. (1993). *Dynamics of Structures*, second edn., McGraw-Hill, Singapore.

Cluley, N. and Shepherd, R. (1996). "Analysis of concrete cable-stayed bridges for creep, shrinkage and relaxation effects," *Computers & Structures*, 58(2), 337 – 350.

Colwell, S. and Basu, B. (2009). "Tuned liquid column dampers in offshore wind turbines for structural control," *Engineering Structures*, 31(2), 358–368.

Connell, J. R. (1982). "The spectrum of wind speed fluctuations encountered by a rotating blade of a wind energy conversion system," *Solar Energy*, 29(5), 363–375.

Cornell, C., Jalayer, F., Hamburger, R. and Foutch, D. (2002). "Probabilistic basis for 2000 SAC federal emergency management agency steel moment frame guidelines," *Journal of Structural Engineering*, 128(4), 526–533.

Dall'Asta, A. and Dezi, L. (1996). "Discussion of "Prestress Force Effect on Vibration Frequency of Concrete Bridges" by M. Saiidi, B. Douglas, and S. Feng," *Journal of Structural Engineering*, 122(4), 458–458.

Dall'Asta, A. and Leoni, G. (1999). "Vibrations of Beams Prestressed by Internal Frictionless Cables," *Journal of Sound and Vibration*, 222(1), 1 – 18.

de Vries, E. (2009). "New vertical-axis offshore concept aims high," Windstatus Newsletter.

Dehm, J. (2007). "160 m self-supporting lattice tower for a wind energy conversion system. The highest wind energy system in the world," *Stahlbau*, 76(4), 213 – 221.

Deák, G. (1996). "Discussion of "Prestress Force Effect on Vibration Frequency of Concrete Bridges", by M. Saiidi, B. Douglas, and S. Feng," *Journal of Structural Engineering*, 122(4), 458–459.

Dempsey, N. (2008). "Irish Road Traffic (Construction and use of Vehicles) (Amendment) Regulations," Office of the Attorney General, S.I. No. 366.

DNV (2001). "Guidline for the Design of Wind Turbines," Tech. Rep. DNV/Risø, Det Norske Veritas, Copenhagen and Wind Energy Department, Risø National Laboratory.

DNV (2002). "Guidline for the Design of Wind Turbines, Second Edition," Tech. Rep. DNV/Risø, Det Norske Veritas, Copenhagen and Wind Energy Department, Risø National Laboratory.

DNV-OS-J101 (2010). "Design of Offshore Wind Turbine Structures," DNV.

DoELG (2006). *Wind Energy Development Guidelines*, Department for the Environment, Heritage and Local Government.

Doherty, P., Kirwan, L., Gavin, K., Igoe, D., Tyrrell, S., Ward, D. and O'Kelly, B. (2012). "Soil properties at the UCD geotechnical research site at Blessington," in: *Proceedings of Bridge and Concrete Research in Ireland Conference*, C. Caprani and A. O'Connor, eds., pp. 499–504.

DOWNWIND (2012). "EU Funded (FP6)," URL `http://ec.europa.eu/research/energy/eu/projects/index_en.cfm?researcharea=wind`, (Accessed: July 17, 2012).

Dueñas Osorio, L. and Basu, B. (2008). "Unavailability of wind turbines due to wind-induced accelerations," *Engineering Structures*, 30(4), 885–893.

Dutta, A. and Mander, J. (1998). "Seismic fragility analysis of highway bridges," Center-to-Center Project Workshop on Earthquake Engineering Frontiers in Transportation Systems, International Center for Disaster-Mitigation Engineering (INCEDE).

Eidinger, J. and Goettel, K. (1998). "The benefits and costs of seismic retrofits of non-structural components for hospitals, essential facilities, and schools," in: *Proceedings of Seminar on Seismic Design, Retrofit, and Performance on Nonstructural Components*, ATC-29-1, Applied Technology Council, Redwood City, CA, pp. 491–504.

Elgaard, M., Mathiesen, B. and Papsø, B. (1988). "Offshore windfarm wind turbines of 200-300 kW with separate foundations," *Journal of Wind Engineering and Industrial Aerodynamics*, 27(1-3), 359 – 371.

Ellingwood, B. R., Celik, O. C. and Kinali, K. (2007). "Fragility assessment of building structural systems in Mid-America," *Earthquake Engineering & Structural Dynamics*, 36(13), 1935–1952.

Elnashai, A., Borzi, B. and Vlachos, S. (2004). "Deformation-based vulnerability functions for RC bridges," *Structural Engineering and Mechanics*, 17(2), 215 – 244.

ENERCON (2007). "World's most powerful wind turbine installed near Emden," Windblatt Magazine for wind energy; Issue 04.

ENERCON (2010a). "E-126 turns into 7.5 MW turbine," Windblatt Magazine for wind energy; Issue 01.

ENERCON (2010b). "First wind farm delivered by E-Ship 1," Windblatt Magazine for wind energy; Issue 03.

ENERCON (2012). "ENERCON GMBH," URL `http://www.enercon.de/en-en/`, (Accessed: July 29, 2012).

Energiministeriet, D. (1986). *Wind energy: research and technological development in Denmark*, Danish Ministry of Energy.

Engström, S., Lyrner, T., Hassanzadeh, M., Stalin, T. and Johansson, J. (2010). "Tall Towers for Large Wind Turbines," Tech. Rep. 10:48, Elforsk, Electricity and Power Production.

Ferguson, M. E. (1998). "Opti-OWECS, Final Report, Vol. 4: A typical design solution for an offshore wind energy conversion system," Tech. Rep. OPTI-OWECS, Institute for Wind Energy, Delft University of Technology.

Frederick, G. and Savino, J. (1986). "Summary of tower designs for large horizontal axis wind turbines," Tech. Rep. NASA-TM-87166, National Aeronautics and Space Administration.

Frick, S., Huenges, E., Jorde, K., Jung, R., Kabus, F., Kaltschmitt, M., Kehl, K., Laing, D., Lewandowski, I., Ortmanns, W., Rau, U., Sanner, B., Sauer, D. U., Schneider, S., Schröder, G., Seibt, P., Skiba, M., Streicher, W., Weinrebe, G. and Wiese, A. (2007). *Renewable Energy: Technology, Economics and Environment*, Springer.

Friedmann, P. P. (1980). "Aeroelastic stability and response analysis of large horizontal-axis wind turbines," *Journal of Wind Engineering and Industrial Aerodynamics*, 5(3-4), 373 – 401.

Ganander, H. (2003). "The Use of a Code-Generating System for the Derivation of the Equations for Wind Turbine Dynamics," *Wind Energy*, 6(4), 333 – 345.

Garrad, A. (1983). "Dynamics of wind turbines," *Physical Science, Measurement and Instrumentation, Management and Education - Reviews, IEE Proceedings A*, 130(9), 523 –530.

Garside, A. J. and Kyles, B. (1984). "Installation and operation of a wind turbine on the island of Tristan Da Cunha," in: *Pergamon Press*, Inverness, Scotland, pp. 145 – 154.

Gavin, K., Adekunte, A. and O'Kelly, B. (2009). "A field investigation of vertical footing response on sand," in: *Proceedings of the ICE - Geotechnical Engineering*, vol. 162 of *01*, p. 257 –267.

Gavin, K. and Lehane, B. (2007). "Base load - displacement response of piles in sand," *Canadian Geotechnical Journal*, 44(9), 1053–1063.

Gavin, K. and O'Kelly, B. (2007). "Effect of friction fatigue on pile capacity in dense sand," *Journal of Geotechnical and Geoenvironmental Engineering*, 133(1), 63–71.

Ghali, A. and Neville, A. M. (1997). *Structural Analysis: A Unified Classical and Matrix Approach*, 4 edn., E & FN Spon.

Gill, A. E. and Fraser, R. (2002). "Challenges in the design of an offshore wind turbine foundation for arctic conditions," in: *Proceedings of the International Conference on Offshore Mechanics and Arctic Engineering*, vol. 4, Oslo, Norway, pp. 507 – 515.

Gjerse, N. F. (2005). "Design of monopile foundations for large offshore wind turbines - Experiences from the first projects offshore the British coast," in: *Proceedings of the 7th European Conference on Numerical Methods in Geotechnical Engineering*, Seoul, Republic of Korea, pp. 433 – 440.

Gómez, J., Filz, G. and Ebeling, R. (2003). "Extended hyperbolic model for sand-to-concrete interfaces," *Journal of Geotechnical and Geoenvironmental Engineering*, 129(11), 993–1000.

Goodman Jr., F. and Vachon, W. (1982). "United States electric utility activities in wind power," in: *Fourth International Symposium onWind Energy Systems*, Stockholm, Sweden, pp. 305 – 321.

Gsänger, S. and Pitteloud, J. D. (2012). "2011 Report," The World Wind Energy Association, URL `www.WWindEA.org`.

Gualtieri, G. and Secci, S. (2011). "Wind shear coefficients, roughness length and energy yield over coastal locations in Southern Italy," *Renewable Energy*, 36(3), 1081 – 1094.

Haggett, C. (2011). "Understanding public responses to offshore wind power," *Energy Policy*, 39(2), 503 – 510.

Hamed, E. and Frostig, Y. (2006). "Natural frequencies of bonded and unbonded prestressed beams - prestress force effects," *Journal of Sound and Vibration*, 295(1-2), 28–39.

Hand, M., Simms, D., Fingersh, L., Jager, D., Cotrell, J., Schreck, S. and Larwood, S. (2001). "Unsteady aerodynamics experiment phase VI: wind tunnel test configurations and available data campaigns," Tech. Rep. NREL/TP-500-29955, National Renewable Laboratory, Golden, CO.

Hänler, M., Ritschel, U. and Warnke, I. (2006). "Systematic modelling of wind turbine dynamics and earthquake loads on wind turbines," in: *European Wind Energy Conference and Exhibition, Athens, Greece*, pp. 1–6.

Hansen, M. (2007). "Aeroelastic instability problems for wind turbines," *Wind Energy*, 10(6), 551 – 577.

Hansen, M., Gaunaa, M. and Madsen, H. (2004). "A Beddoes-Leishman type dynamic stall model in state-space and indicial formulations," Tech. Rep. Risø-R-1354(EN), Technical University of Denmark.

Hansen, M. H. (2003). "Improved modal dynamics of wind turbines to avoid stall-induced vibrations," *Wind Energy*, 6(2), 179–195.

Hansen, M. O. L. (2008). *Aerodynamics of Wind Turbines*, second edn., Earthscan, 8–12 Camden High Street, London, NW1 0JH, UK.

Hansen, M. O. L., Sørensen, J. N., Voutsinas, S., Sørensen, N. and Madsen, H. A. (2006). "State of the art in wind turbine aerodynamics and aeroelasticity," *Progress in Aerospace Sciences*, 42(4), 285–330.

Hansen, S. and Larsen, G. (2003). "Wind shear extremes at possible offshore wind turbine locations," *Wind Engineering*, 27(5), 339 – 49.

Harte, M., Basu, B. and Nielsen, S. (2012). "Dynamic Analysis of Wind turbines Including Soil-Structure Interaction," *Engineering Structures*, 45(0), 509 – 518.

Harte, R. and Van Zijl, G. P. A. G. (2007). "Structural stability of concrete wind turbines and solar chimney towers exposed to dynamic wind action," *Journal of Wind Engineering and Industrial Aerodynamics*, 95(9-11), 1079–1096.

Hau, E. (2006). *Wind Turbines: Fundamentals, Technologies, Applications, Economics*, 2 edn., Springer, Berlin.

HAWC2 (2012). "Wind Turbine Design Code," URL `http://www.risoe.dtu.dk/sitecore/content/Risoe_dk/Home/HAWC2.aspx`, (Accessed: July 24, 2012).

He, G. (2009). "Seismic response analysis of wind turbine tower systems considering soil-structure interaction," *Jixie Gongcheng Xuebao/Journal of Mechanical Engineering*, 45(7), 87 – 94.

He, G.-L., Zhou, Y. and Li, J. (2009). "Seismic analysis of wind turbine system," *Gongcheng Lixue/Engineering Mechanics*, 26(7), 72 – 77, integrated modelling;Physical stochastic model;Seismic analysis;Soil-structure interaction;Wind turbine system;.

Henderson, A., Nielsen, F. G., Andersen, M., Argyriadis, K., Butterfield, S., Fonseca, T., N.and Kuroiwa, Le Boulluec, M., Liao, S. J., Turnock, S. and Waegter, J. (2006). "Ocean wind and wave energy utilization," in: *Report from Specialist committee V.4 to the 16th ISSC*, vol. 3, Southhampton, pp. 253 – 271.

Henderson, A. R. and Zaaijer, M. B. (2002). "Hydrodynamic loading of compact structures and the effect on foundation design," in: *International Conference on Marine Renewable Energy - Conference Proceedings*, Newcastle upon Tyne, United kingdom, pp. 183 – 190.

Higson, H., Griffiths, R., Jones, C. and Hall, D. (1994). "Concentration measurements around an isolated building: A comparison between wind tunnel and field data," *Atmospheric Environment*, 28(11), 1827 – 1836.

Hodges, D. H. and Patil, M. (2000). "Multi-flexible-body analysis for application to wind-turbine control design," in: *Proceedings of the 19th Wind Energy Symposium*, AIAA-2000-0030, Reno, Nevada.

Holierhoek, J. G. (2008). "Aeroelasticity of large wind turbines," Ph.D. thesis, Delft University of Technology, Delft.

Houlsby, G., Kelly, R., Huxtable, J. and Byrne, B. (2005). "Field trials of suction caissons in clay for offshore wind turbine foundations," *Geotechnique*, 55(4), 287 – 96.

Hwang, H. and Jaw, J. (1990). "Probabilistic damage analysis of structures," *Journal of Structural Engineering*, 116(7), 1992–2007.

Hwang, H., Jernigan, J. B. and Lin, Y.-W. (2000). "Evaluation of seismic damage to Memphis bridges and highway systems," *Journal of Bridge Engineering*, 5(4), 322 – 330.

Hydro-Québec (1984). *4-MW Vertical-axis Aerogenerator*, Hydro-Québec.

HYPERWIND (2012). "EU Funded (FP7)," URL `http://ec.europa.eu/research/energy/eu/projects/index_en.cfm?researcharea=wind`, (Accessed: July 17, 2012).

IEA (2010). "Electricity Information," International Energy Agency, URL `www.iea.org`.

Ishii, H. and Ishihara, T. (2010). "Numerical study of maximum wind load on wind turbine towers under operating conditions," in: *Proceedings of the Fifth International Symposium on Computational Wind Engineering (CWE2010)*, Chapel Hill, North Carolina, USA.

Jain, S. K. and Goel, S. C. (1996). "Discussion of "Prestress Force Effect on Vibration Frequency of Concrete Bridges" by M. Saiidi, B. Douglas, and S. Feng," *Journal of Structural Engineering*, 122(4), 459–460.

Janetzke, D. C. and Kaza, K. R. (1983). "Whirl flutter analysis of a horizontal-axis wind turbine with a two-bladed teetering rotor," *Solar Energy*, 31(2), 173 – 182.

Jensen, J. J., Olsen, A. S. and Mansour, A. E. (2011). "Extreme wave and wind response predictions," *Ocean Engineering*, 38(17-18), 2244 – 2253.

Jernigan, J. and Hwang, H. (2002). "Development of bridge fragility curves," in: *Proceedings of Seventh U.S. National Conference on Earthquake Engineering*, EERI, Boston, MA.

Jin, M. and Astaneh, A. (1998). "Study of Seismc Resistance of Desktop Computers," in: *Proceedings of seminar on seismic design, retrofit, and performance of nonstructural components*, ATC-29-1, Applied Technology Council, Redwood City CA, pp. 379–392.

Jonkman, J. (2012). "NWTC Design Codes: FAST (Fatigue, Aerodynamics, Structures, and Turbulence)," URL `http://wind.nrel.gov/designcodes/simulators/fast/`, (Last modified: March 08, 2012; Accessed: July 17, 2012).

Jonkman, J. and Buhl, M. (2005). "FAST User's Guide," Tech. Rep. NREL/EL-500-38230, National Renewable Energy Laboratory, Golden, Colorado, USA.

Jonkman, J., Butterfield, S., Musial, W. and Scott, G. (2009). "Definition of a 5 MW reference wind turbine for offshore system development," Tech. Rep. NREL/TP-500-38060, National Renewable Energy Laboratory, Golden, Colorado, USA.

Jonkman, J. M. (2007). "Dynamics modeling and loads analysis of an offshore floating wind turbine," Tech. Rep. NREL/TP-500-41958, National Renewable Energy Laboratory, 1617 Cole Boulevard, Golden, Colorado.

Kaimal, J. C., Wyngaard, J. C., Izumi, Y. and Coté, O. R. (1972). "Spectral characteristics of surface layer turbulence," *Quarterly Journal of the Royal Meteorological Society*, 98, 563–589.

Karim, K. R. and Yamazaki, F. (2003). "A simplified method of constructing fragility curves for highway bridges," *Earthquake Engineering and Structural Dynamics*, 32(10), 1603 – 1626.

Kelley, N. and Jonkman, B. (2012). "NWTC Computer-Aided Engineering Tools: TurbSim," URL `http://wind.nrel.gov/designcodes/preprocessors/turbsim/`, (Last modified: August 06, 2012; Accessed: September 12, 2012).

Kühn, M., Cockerill, T., Harland, L., Harrison, R., Schöntag, C., van Bussel, G. and Vugts, J. (1997). "Opti-OWECS Final Report Vol. 2: Methods assisting the design of offshore wind energy conversion systems," Tech. Rep. OPTI-OWECS, Institute for Wind Energy, Delft University of Technology.

Kim, C. R. Y. C. H., JT; Yun (2004). "Identification of Prestress-Loss in PSC Beams Using Modal Information," *Structural Engineering and Mechanics*, 17, 467 – 482.

Kim, H., Lee, S. and Lee, S. (2011). "Influence of blade-tower interaction in upwind-type horizontal axis wind turbines on aerodynamics," *Journal of Mechanical Science and Technology*, 25(5), 1351 – 1360.

King, E., Pilla, F. and Mahon, J. (2012). "Assessing noise from wind farm developments in Ireland: A consideration of critical wind speeds and turbine choice," *Energy Policy*, 41(0), 548 – 560.

Kjellin, J., Bülow, F., Eriksson, S., Deglaire, P., Leijon, M. and Bernhoff, H. (2011). "Power coefficient measurement on a 12 kW straight bladed vertical axis wind turbine," *Renewable Energy*, 36(11), 3050 – 3053.

Kong, C., Bang, J. and Sugiyama, Y. (2005). "Structural investigation of composite wind turbine blade considering various load cases and fatigue life," *Energy*, 30(11-12), 2101–2114.

Kong, F. and Evans, R. (1987). *Reinforced and Prestressed Concrete*, 3 edn., Spon Press, Cambridge.

Krogh, L., Lyngs, J. and Steenfelt, J. (2011). "Gravity based foundations for the Red Sand 2 offshore wind farm, Denmark," in: *Frontiers in Offshore Geotechnics II - Proceedings of the 2nd International Symposium on Frontiers in Offshore Geotechnics*, Perth, WA, Australia, pp. 587 – 592.

Kunnath, S. K., Larson, L. and Miranda, E. (2006). "Modelling considerations in probabilistic performance-based seismic evaluation: Case study of the I-880 viaduct," *Earthquake Engineering and Structural Dynamics*, 35(1), 57 – 75.

Laino, D. J. (2012). "NWTC Design Codes: AeroDyn," URL `http://wind.nrel.gov/designcodes/simulators/aerodyn/`, (Last modified: June 28, 2012; Accessed: September 12, 2012).

Lanzafame, R. and Messina, M. (2010). "Horizontal axis wind turbine working at maximum power coefficient continuously," *Renewable Energy*, 35(1), 301 – 306.

Larsson, A.-K. (1994). "Environmental impact from an offshore plant," *Wind Engineering*, 18(5), 213 – 218.

Lavassas, I., Nikolaidis, G., Zervas, P., Efthimiou, E., Doudoumis, I. N. and Baniotopoulos, C. C. (2003). "Analysis and design of the prototype of a steel 1-MW wind turbine tower," *Engineering Structures*, 25(8), 1097–1106.

Layton, J. (2012). "Modern Wind Power Technology," How Stuff Works, URL `http://science.howstuffworks.com/environmental/green-science/wind-power2.htm`, (Accessed: July 23, 2012).

Lee, D., Hodges, D. H. and Patil, M. J. (2002). "Multi-flexible-body dynamic analysis of horizontal axis wind turbines," *Wind Energy*, 5(4), 281–300.

Leishman, J. and Beddoes, T. (1989). "A semi-empirical model for dynamic stall," *Journal of the American Helicopter Society*, 34(3), 3–17.

Luco, J. E. (1986). "Soil-structure interaction effects on the seismic response of tall chimneys," *Soil Dynamics and Earthquake Engineering*, 5(3), 170 – 177.

Ma, H. and Chen, L. (2010). "Static and dynamic analysis modeling for offshore wind turbine foundation structures," in: *Proceedings of the 9th (2010) ISOPE Pacific/Asia Offshore Mechanics Symposium, PACOMS-2010*, Busan, Republic of Korea,, pp. 57 – 60.

Maalawi, K. Y. and Negm, H. M. (2002). "Optimal frequency design of wind turbine blades," *Journal of Wind Engineering and Industrial Aerodynamics*, 90(8), 961–986.

Mackie, K. and Stojadinović, B. (2001). "Probabilistic seismic demand model for California highway bridges," *Journal of Bridge Engineering*, 6(6), 468–481.

Mackie, K. and Stojadinović, B. (2003). "Seismic demands for performance-based design of bridges," Tech. Rep. PEER2003/16, Pacific Earthquake Engineering Research Center.

Mackie, K. and Stojadinović, B. (2004). "Fragility curves for reinforced concrete highway overpass bridges," in: *Thirteenth World Conference on Earthquake Engineering*, Vancouver, BC, Canada.

Mackie, K. R. and Stojadinović, B. (2005). "Comparison of incremental dynamic, cloud, and stripe methods for computing probabilistic seismic demand models," in: *Proceedings of the 2005 Structures Congress and Exposition*, vol. 171, ASCE, New York, pp. 1835–1845.

Madsen, P. H. and Frandsen, S. (1984). "Wind-induced failure of wind turbines," *Engineering Structures*, 6(4), 281–287.

Mander, J. and Basoz, N. (1999). "Seismic fragility curve theory for highway bridges," in: *Proceedings of the 5th U.S. Conference on Lifeline Earthquake Engineering*, W. M. Elliott, ed., Seattle, Washington.

Mann, J. (1998). "Wind field simulation," *Probabilistic Engineering Mechanics*, 13(4), 269–282.

Marino, E., Borri, C. and Lugni, C. (2011a). "Influence of wind-waves energy transfer on the impulsive hydrodynamic loads acting on offshore wind turbines," *Journal of Wind Engineering and Industrial Aerodynamics*, 99(6-7), 767 – 775.

Marino, E., Borri, C. and Peil, U. (2011b). "A fully nonlinear wave model to account for breaking wave impact loads on offshore wind turbines," *Journal of Wind Engineering and Industrial Aerodynamics*, 99(4), 483 – 490.

Márquez, F. P. G., Tobias, A. M., Pérez, J. M. P. and Papaelias, M. (2012). "Condition monitoring of wind turbines: techniques and methods," *Renewable Energy*, 46, 169 – 178.

Math Works (2010). "Matlab R2010b," The Math Works, Inc.

Matsumiya, H., Kobayashi, T., Ishida, A. and Tanaka, A. (1990). "The research and development of wind turbine generator systems in Japan," in: *Proceedings of European Community Wind Energy Conference*, Bedford, UK, pp. 55 – 60.

Mayfield, B. (1982). *Creep and shrinkage in concrete structures*, Wiley, Chichester.

Mazloom, M. (2008). "Estimating long-term creep and shrinkage of high-strength concrete," *Cement and Concrete Composites*, 30(4), 316 – 326.

Melchers, R. (1987). *Structural reliability: analysis and prediction*, Ellis Horwood series in civil engineering, Ellis Horwood.

Mikitarenko, M. A. and Perelmuter, A. V. (1998). "Safe fatigue life of steel towers under the action of wind vibrations," *Journal of Wind Engineering and Industrial Aerodynamics*, 74-76, 1091–1100.

Moghaddasi, M., Cubrinovski, M., Chase, J., Pampanin, S. and Carr, A. (2011). "Effects of Soil-Foundation-Structure Interaction on Seismic Structural Response Via Robust Monte Carlo Simulation," *Engineering Structures*, 33(4), 1338 – 1347.

Murtagh, P., Basu, B. and Broderick, B. (2005a). "Response of wind turbines including soil-structure interaction," in: *Proceedings of the Tenth International Conference on Civil, Structural and Environmental Engineering Computing*, Rome, Italy.

Murtagh, P. J., Basu, B. and Broderick, B. M. (2004a). "Mode acceleration approach for rotating wind turbine blades," in: *Proceedings of the Institution of Mechanical Engineers – Part K – Journal of Multi-body Dynamics*, vol. 218, pp. 159–167.

Murtagh, P. J., Basu, B. and Broderick, B. M. (2004b). "Simple models for natural frequencies and mode shapes of towers supporting utilities," *Computers & Structures*, 82(20-21), 1745–1750.

Murtagh, P. J., Basu, B. and Broderick, B. M. (2004c). "Wind force time-history generation by discrete fourier transform (DFT)," in: *Multi-body Dynamics; Monitoring and Simulation Techniques*, H. Rahnejat and S. Rothberg, eds., vol. 3, Professional Engineering Publishing, pp. 147–154.

Murtagh, P. J., Basu, B. and Broderick, B. M. (2005b). "Along-wind response of a wind turbine tower with blade coupling subjected to rotationally sampled wind loading," *Engineering Structures*, 27(8), 1209–1219.

Murtagh, P. J., Ghosh, A., Basu, B. and Broderick, B. M. (2008). "Passive control of wind turbine vibrations including blade/tower interaction and rotationally sampled turbulence," *Wind Energy*, 11(4), 305–317.

Naguleswaran, S. (1994). "Lateral vibration of a centrifugally tensioned uniform euler-bernoulli beam," *Journal of Sound and Vibration*, 176(5), 613–624.

Naguleswaran, S. (1997). "Out-of-plane vibration of a uniform euler-bernoulli beam attached to the inside of a rotating rim," *Journal of Sound and Vibration*, 200(1), 63–81.

NASA (1979). "MOD-2 wind turbine system concept and preliminary design report. Volume 2: Detailed report," Tech. Rep. NASA CR–159609, Boeing Engineering and Construction.

Negm, H. M. and Maalawi, K. Y. (2000). "Structural design optimization of wind turbine towers," *Computers & Structures*, 74(6), 649–666.

Neilsen, P. (1990). "Study on the next generation of large wind turbines. III. Site and installation costs. Operation and maintenance costs," in: *Proceedings of European Community Wind Energy Conference*, Bedford, UK, pp. 438 – 42.

Neville, A. M. (1996). *Properties of Concrete*, fourth edn., John Wiley & Sons.

Nielsen, F., Andersen, M., Argyriadis, K., Butterfield, S., Fonseca, T., N.and Kuroiwa, Le Boulluec, M., Liao, S.-J., Turnock, S. and Waegter, J. (2006). "Ocean wind and wave energy utilization," in: *Report from Specialist committee V.4 to the 16th ISSC*, vol. 1, Southampton, pp. 1–35.

Nielsen, J. J. and Sørensen, J. D. (2011). "On risk-based operation and maintenance of offshore wind turbine components," *Reliability Engineering & System Safety*, 96(1), 218 – 229.

Nigam, N. and Jennings, P. (1968). "Digital calculation of response spectra from strong motion earthquake records," Tech. rep., California Institute of Technology.

Nigam, N. and Narayanan, S. (1994). *Applications of Random Vibrations*, Springer-Verlag, Delhi.

Noguchi, T., Tomosawa, F., Nemati, K. M., Chiaia, B. M. and Fantilli, A. P. (2009). "A practical equation for elastic modulus of concrete," *American Concrete Institute - Structural Journal*, 106(5), 690–696.

Novak, M. and Hifnawy, L. E. (1983). "Damping of structures due to soil-structure interaction," *Journal of Wind Engineering and Industrial Aerodynamics*, 11(1-3), 295 – 306.

Novak, M. and Hifnawy, L. E. (1988). "Structural Response to Wind With Soil-Structure Interaction," *Journal of Wind Engineering and Industrial Aerodynamics*, 28(1-3), 329 – 338.

Nuta, E., Christopoulos, C. and Packer, J. (2011). "Methodology for seismic risk assessment for tubular steel wind turbine towers: application to Canadian seismic environment," *Canadian Journal of Civil Engineering*, 38(3), 293 – 304.

O'Connor, A. and Enevoldsen, I. (2008). "Probability based modelling and assessment of an existing post-tensioned concrete slab bridge," *Engineering Structures*, 30(5), 1408 – 1416.

ORECCA (2012). "EU Funded (FP7)," URL `http://ec.europa.eu/research/energy/eu/projects/index_en.cfm?researcharea=wind`, (Accessed: July 24, 2012).

OTDS (2012). "Overhead Transmission Distribution Systems Ltd," URL `http://www.otds.co.uk/lattice-towers.php`, (Accessed: July 29, 2012).

Øye, S. (1991). "Dynamic stall, simulated as a time lag of separation," in: *Proceedings of the Fourth IEA Symposium on the Aerodynamics of Wind Turbines*, K. McAnulty, ed., no. 118 in ETSU-N.

Ozgumus, O. and Kaya, M. (2006). "Flapwise bending vibration analysis of double tapered rotating Euler-Bernoulli beam by using the differential transform method," *Meccanica*, 41(6), 661–670.

Padgett, J., Nielson, B. and DesRoches, R. (2008). "Selection of optimal intensity measures in probabilistic seismic demand models of highway bridge portfolios," *Earthquake Engineering and Structural Dynamics*, 37(5), 711–725.

Padgett, J. E. (2007). "Seismic vulnerability assessment of retrofitted bridges using probabilistic methods," Phd dissertation, School of Civil and Environmental Engineering, Georgia Institute of Technology.

Padgett, J. E. and DesRoches, R. (2008). "Methodology for the development of analytical fragility curves for retrofitted bridges," *Earthquake Engineering and Structural Dynamics*, 37(8), 1157 – 1174.

Paredes, J. A., Barbat, A. H. and Oller, S. (2011). "A compression-tension concrete damage model, applied to a wind turbine reinforced concrete tower," *Engineering Structures*, 33(12), 3559 – 3569.

Passon, P. and Kühn, M. (2005). "State-of-the-art and development needs of simulation codes for offshore wind turbines," in: *Copenhagen Offshore Wind 2005 Conference and Expedition Proceedings*, Copenhagen, Denmark.

Pedersen, R., Nielsen, S. and Thoft-Christensen, P. (2012). "Stochastic analysis of the influence of tower shadow on fatigue life of wind turbine blade," *Structural Safety*, 35, 63 – 71.

PEER (2012). "The PEER Strong Motion Database," URL `http://peer.berkeley.edu/peer_ground_motion_database`, (Accessed: September 29, 2012).

Peters, D. A. and He, C. J. (1991). "Correlation of measured induced velocities with a finite-state wake model," *Journal of the American Helicopter Society*, 36(3), 59 – 70.

Petrov, A. A. (1998). "Dynamic response and life prediction of steel structures under wind loading," *Journal of Wind Engineering and Industrial Aerodynamics*, 74-76, 1057–1065.

Pieraccini, M., Parrini, F., Fratini, M., Atzeni, C. and Spinelli, P. (2008). "In-service testing of wind turbine towers using a microwave sensor," *Renewable Energy*, 33(1), 13 – 21.

PLAXIS (2011). *PLAXIS Material Models Manual*, PLAXIS bv, The Netherlands.

PLAXIS 2D (2011). "PLAXIS 2D 2011 - Geotechnical Engineering Software," Plaxis bv, URL `http://www.plaxis.nl/`, (Accessed: September 6, 2012).

Polyzois, D. J., Raftoyiannis, I. G. and Ungkurapinan, N. (2009). "Static and dynamic characteristics of multi-cell jointed GFRP wind turbine towers," *Composite Structures*, 90(1), 34–42.

Porter, K. A. and Kiremidjian, A. S. (2001). "Assembly-based vulnerability of buildings and its uses in seismic performance evaluation and risk-management decision-making," Tech. Rep. 139, Earthquake Engineering Research Center, Stanford, CA.

Prowell, I., Elgamal, A., Jonkman, J. and Uang, C.-M. (2010). "Estimation of seismic load demand for a wind turbine in the time domain," in: *European Wind Energy Conference (EWEC 2010), Warsaw, Poland*, pp. 1–7.

Prowell, I., Veletzos, M., Elgamal, A. and Restrepo, J. (2009). "Experimental and numerical seismic response of a 65 kW wind turbine," *Journal of Earthquake Engineering*, 13(8), 1172–1190.

Puthoff, R. L., Collins, J. L. and Wolf, R. A. (1980). "Installation and checkout of the DOE/NASA MOD-1 2000 kW wind turbine generator." *AIAA Paper*, 249 – 260.

Qu, W., Chen, Z. and Xu, Y. (2001). "Dynamic analysis of wind-excited truss tower with friction dampers," *Computers & Structures*, 79(32), 2817 – 31.

Quarton, D. C. (1998). "The evolution of wind turbine design analysis–a twenty year progress review," *Wind Energy*, 1(S1), 5–24.

Quilligan, A., O'Connor, A., Hennessey, T., Doherty, P. and Gavin, K. (2012a). "Effect of soil structure interaction on wind turbine tower response for Blessington sand," (In Draft).

Quilligan, A., O'Connor, A. and Pakrashi, V. (2012b). "Fragility Analysis of Steel and Concrete Wind Turbine Towers," *Engineering Structures*, 36, 270–282.

Raju, K. and Rao, G. (1986). "Free Vibration Behavior of Prestressed Beams," *Journal of Structural Engineering*, 112(2), 433–437.

Randolph, M. F. (1981). "The response of flexible piles to lateral loading," *Géotechnique*, 31(2), 247–59.

Rehman, S. and Al-Abbadi, N. M. (2005). "Wind shear coefficients and their effect on energy production," *Energy Conversion and Management*, 46(15 - 16), 2578 – 2591.

Reid, S. and Qin, C. (1990). "Comparison of concrete creep strains due to bending and axial compression," in: *National Conference Publication - Institution of Engineers*, Adelaide, Australia, pp. 255 – 258.

Repetto, M. P. and Solari, G. (2010). "Wind-induced fatigue collapse of real slender structures," *Engineering Structures*, 32(12), 3888 – 3898.

Richards, G., Noble, B. and Belcher, K. (2012). "Barriers to renewable energy development: A case study of large-scale wind energy in Saskatchewan, Canada," *Energy Policy*, 42, 691 – 698.

Rihal, S. (1982). "Behavior of nonstructural building partitions during earthquakes," in: *Proceedings of the Seventh Symposium on Earthquake Engineering*, Department of Earthquake Engineering, University of Roorke, India, pp. 267–277.

Ritschel, U., Warnke, I. and Kirchner, J. (2003). "Wind turbines and earthquakes," in: *World Wind Energy Conference, Cape Town, South Africa*, pp. 1–8.

Rodríguez, J., Martí, J. and Martínez, F. (2010). "Post-cracking behavior of a wind turbine concrete tower," in: *Proceedings of SIMULIA Customer Conference*, Providence, Rhode Island, pp. 632–646.

SAC (2012). "SAC Joint Venture Steel Project Phase 2," URL `http://nisee.berkeley.edu/data/strong_motion/sacsteel/ground_motions.html`, (Accessed: September 19, 2012).

Saiidi, M., Douglas, B. and Feng, S. (1994). "Prestress Force Effect on Vibration Frequency of Concrete Bridges," *Journal of Structural Engineering*, 120(7), 2233–2241.

Sambar, H., Pavelic, V. and Warner, R. (1980). "Computer simulation and design of the control system for a wind turbine generator," *Transactions of the ASME. Journal of Mechanical Design*, 102(1), 14 – 18.

Schepers, J. and Snel, H. (1995). "Dynamic inflow: yawed conditions and partial span pitch control," Tech. Rep. ECN-C-95-056, CEC JOULE II.

Seidel, M. (2003). "Experiences with two of the world's largest wind turbine towers," in: *Proceedings of the 2003 European Wind Energy Conference and Exhibition*, GE Wind Energy GmbH, Madrid.

Seidel, M. (2007). "Jacket substructures for the REpower 5 MW wind turbine," in: *Conference Proceedings European Offshore Wind 2007*, Berlin.

Seidel, R. (1978). "Power oscillations of a 100 kW wind turbine generator," in: *Proceedings of the 25th Annual Cleveland Electronics Conference*, New York, NY, USA, pp. 112 – 13.

Sesto, E. and Casale, C. (1998). "Exploitation of wind as an energy source to meet the world's electricity demand," *Journal of Wind Engineering and Industrial Aerodynamics*, 74-76, 375 – 387.

Shafieezadeh, A., Ramanathan, K., Padgett, J. E. and DesRoches, R. (2011). "Fractional order intensity measures for probabilistic seismic demand modeling applied to highway bridges," *Earthquake Engineering & Structural Dynamics*, 41(3), 391–409.

Shen, P., Fang, H. and Xia, X. (2009). "Effect of concrete creep and shrinkage on tall hybrid structures and its countermeasures," *Frontiers of Architecture and Civil Engineering in China*, 3(2), 234 – 9.

Shinozuka, M., Feng, M., Kim, H. and Kim, S. (2000a). "Nonlinear static procedure for fragility curve development," *Journal of Engineering Mechanics*, 126(12), 1287–1295.

Shinozuka, M., Feng, M. Q., Dong, X., Uzawa, T. and Ueda, T. (2000b). "Damage assessment of a highway network under scenario earthquakes for emergency response decision support," in: *Proceedings of SPIE - The International Society for Optical Engineering*, vol. 3988, Society of Photo-Optical Instrumentation Engineers, Newport Beach, CA, USA., p. 264–275.

Shinozuka, M., Feng, M. Q., Kim, H., Uzawa, T. and Ueda, T. (2003). "Statistical analysis of fragility curves," Tech. Rep. MCEER-03-0002, Multidisciplinary Center for Earthquake Engineering Research.

Shome, N. (1999). "Probabilistic seismic demand analysis of nonlinear structures," PhD dissertation, Department of Civil and Environmental Engineering, Stanford University, Stanford, CA.

Silva, M. A., Brasil, R. M. and Arora, J. S. (2008). "Formulations for the optimal design of RC wind turbine towers," in: *Proceedings of the International Conference on Engineering Optimization - EngOpt 2008*, Rio de Janeiro, Brazil.

Simiu, E. and Scanlan, R. H. (1996). *Wind Effects on Structures: Fundamentals and Applications to Design*, 3 edn., John Wiley & Sons, New York.

Singh, A. (2007). "Concrete construction for wind energy towers," *Indian Concrete Journal*, 81(8), 43 – 49.

Snel, H. and Schepers, J. (1995). "Joint investigation of dynamic inflow effects and implementation of an engineering method," Tech. Rep. ECN-C–94-107, CEC JOULE I.

Soria, E., Avia, F., Matas, A. and Guisado, J. (1990). "Operation and maintenance experiences and test results from the AWEC-60 project [wind power]," in: *Proceedings of European Community Wind Energy Conference*, Bedford, UK, pp. 467 – 71.

Staino, A., Basu, B. and Nielsen, S. (2012). "Actuator control of edgewise vibrations in wind turbine blades," *Journal of Sound and Vibration*, 331(6), 1233 – 1256.

Stevenson, W., O'Donnell, I. and Wilson, A. (1989). "250 kW wind turbine generator-Orkney utility experience of operation and maintenance," in: *Proceedings of European Wind Energy Conference and Exhibition EWEC '89*, London, UK, pp. 636 – 9.

STRABAG (2009). "The base of power: Strabag offshore wind serial system," STRABAG Offshore Wind GmbH.

Suh, S. H., Roh, H. W., Kim, H. R., Lee, K. Y. and Kim, K. S. (1997). "Application of computational techniques for studies of wind pressure coefficients around an odd-geometrical building," *Journal of Wind Engineering and Industrial Aerodynamics*, 67-68, 659 – 670.

Swartz, R., Lynch, J., Zerbst, S., Sweetman, B. and Rolfes, R. (2010). "Structural monitoring of wind turbines using wireless sensor networks," *Smart Structures and Systems*, 6(3), 183 – 96.

Theodorsen, T. (1935). "General theory of aerodynamic instability and the mechanism of flutter," Tech. Rep. 496, NACA.

Thomsen, J. H., Forsberg, T. and Robert Bittner, P. (2007). "Offshore wind turbine foundations - The COWI experience," in: *Proceedings of the 26th International Conference on Offshore Mechanics and Arctic Engineering*, vol. 5, San Diego, CA, United states, pp. 533 – 540.

Thomsen, K. and Sørensen, P. (1999). "Fatigue loads for wind turbines operating in wakes," *Journal of Wind Engineering and Industrial Aerodynamics*, 80(1-2), 121 – 136.

Tinjum, J. M. and Christensen, R. W. (2010). *Wind energy systems: optimising design and construction for safe and reliable operations*, chap. 2, Woodhead Publishing Ltd, United Kingdom, pp. 28–45.

Toft, H. S. and Sørensen, J. D. (2011). "Reliability-based design of wind turbine blades," *Structural Safety*, 33(6), 333 – 342.

Tolooiyan, A. and Gavin, K. (2011). "Modelling the cone penetration test in sand using cavity expansion and arbitrary Lagrangian Eulerian finite element methods," *Computers and Geotechnics*, 38(4), 482 – 490.

Tricklebank, A. H., Halberstadt, P. H., Magee, B. J. and Bromage, A. (2007). "Concrete towers for onshore and offshore wind farms," Tech. rep., The Concrete Centre.

Troen, I. and Petersen, E. L. (1989). "European wind atlas," Risø National Laboratory.

Tse, F. S., Morse, I. E. and Hinkle, R. T. (1978). *Mechanical Vibrations: Theory and Applications*, Allyn and Bacon.

Ula, A. (1987). "Modelling and performance simulation of a large wind turbine generator," in: *Proceedings of the IASTED International Symposium Applied Simulation and Modelling - ASM '87*, Anaheim, CA, USA, pp. 221 – 5.

UN (1998). "Kyoto Protocol to the United Nations Framework Convention on Climate Change," United Nations, URL `www.unfccc.int`.

Van Buren, E. (2011). "Effect of foundation modelling methodology on the dynamic response of offshore wind turbine support structures," in: *Proceedings of the International Conference on Offshore Mechanics and Arctic Engineering - OMAE*, vol. 5, Rotterdam, Netherlands, pp. 501 – 510.

van der Tempel, J. and Molenaar, D. (2002). "Wind turbine structural dynamics-A review of the principles for modern power generation, onshore and offshore," *Wind Engineering*, 26(4), 211 – 22.

Veers, P. (1988). "Three-dimensional wind simulation," Tech. Rep. SAND88–0152, Distribution UC–261, Applied Mechanics Division IV, Sandia National Laboratories, Albuquerque, New Mexico.

Veers, P. S., Ashwill, T. D., Sutherland, H. J., Laird, D. L., Lobitz, D. W., Griffin, D. A., Mandell, J. F., Musial, W. D., Jackson, K., Zuteck, M., Miravete, A., Tsai, S. W. and Richmond, J. L. (2003). "Trends in the design, manufacture and evaluation of wind turbine blades," *Wind Energy*, 6(3), 245 – 259.

Vestas (2004). "General Specification, V90 - 3 MW," Vestas Wind Systems, URL `http://www.vestas.com/`.

Vestas (2005). "General Specification, V90 - 1.8/2 MW (Optispeed Wind Turbine)," Vestas Wind Systems, URL `http://www.vestas.com/`.

Virlogeux, M. (2006). "Der viadukt aber das tarntal bei Millau - ton den ersten entwurfsgedanken bis zur fertigstellung," *Bautechnik*, 83(2), 85–107.

Vrouwenvelder, T. (1997). "The JCSS probabilistic model code," *Structural Safety*, 19(3), 245–251.

Wang, J., Qin, D. and Lim, T. C. (2010). "Dynamic analysis of horizontal axis wind turbine by thin-walled beam theory," *Journal of Sound and Vibration*, 329(17), 3565–3586.

WINDPOWER (2012). "Estimating mean wind speed," URL `http://www.wind-power-program.com/windestimates.htm`, (Accessed: July 31, 2012).

Witcher, D. (2005). "Seismic analysis of wind turbines in the time domain," *Wind Energy*, 8(1), 81 – 91.

Wolf, J. and Deeks, A. (2004). *Foundation Vibration Analysis: A Strength-of-materials Approach*, Elsevier.

WWEA (2011). "Half-year Report 2011," The World Wind Energy Association, URL `http://www.wwindea.org`.

Yamazaki, F., Hamada, T., Motoyama, H. and Yamauchi, H. (1999). "Earthquake damage assessment of expressway bridges in Japan," *Technical Council on Lifeline Earthquake Engineering Monograph*, 16, 361–370.

Yang, W. W., Chang, T. Y. P. and Chang, C. C. (1997). "An efficient wind field simulation technique for bridges," *Journal of Wind Engineering and Industrial Aerodynamics*, 67-68, 697–708.

Younsi, R., El-Batanony, I., Tritsch, J. B., Naji, H. and Landjerit, B. (2001). "Dynamic study of a wind turbine blade with horizontal axis," *European Journal of Mechanics - A/Solids*, 20(2), 241–252.

Yuncheng, C., Yuyue, C. and Peichao, W. (1988). "Design of GRP composite wind turbine blades," *Wind Engineering*, 12(2), 125 – 133.

Zaaijer, M. (2006). "Foundation modelling to assess dynamic behaviour of offshore wind turbines," *Applied Ocean Research*, 28(1), 45 – 57.

Zaaijer, M. (2009). "Review of knowledge development for the design of offshore wind energy technology," *Wind Energy*, 12(5), 411 – 30.

Zaaijer, M., Herman, S., Fish, P., Veldkamp, D. and Topper, T. (2002). "Suction bucket foundation - feasibility and pre-design for the 6 MW DOWEC," Tech. rep., Dutch Offshore Wind Energy Converter project.

Zayed, T., Sharifi, M. R., Baciu, S. and Amer, M. (2008). "Slip-form application to concrete structures," *Journal of Construction Engineering and Management*, 134(3), 157 – 168.

Zeng, Q. and Han, D. (2011). "Selection of concrete creep analytical models for modern prestressed bridges," *Applied Mechanics and Materials*, 90-93, 1023 – 1026.

Zhang, M., Li, H., Li, P. and James Hu, S.-L. (2010). "Fundamental structural frequency analysis for jacket-type offshore wind turbine," in: *Proceedings of the International Offshore and Polar Engineering Conference*, vol. 1, Beijing, China, pp. 665 – 671.

Zhang, P. and Huang, S. (2011). "Review of aeroelasticity for wind turbine: Current status, research focus and future perspectives," *Frontiers in Energy*, 5(4), 419–434.

Zhang, Y. and Li, R. (2007). "Natural frequency of full-prestressed concrete beam," *Transactions of Tianjin University*, 13(5), 354–359.

Zhao, X. and Maißer, P. (2006). "Seismic response analysis of wind turbine towers including soil-structure interaction," *Proceedings of the Institution of Mechanical Engineers, Part K: Journal of Multi-body Dynamics*, 220(1), 53–61.

Zhao, X. and Weiss, G. (2011). "Suppression of the vibrations of wind turbine towers," *IMA Journal of Mathematical Control and Information*, 28(3), 377 – 89.

Appendix A - Stiffness Matrix Generation Using Virtual Work Method

The stiffness matrices for the tower and blade elements, related to the nodal mass matrices, are obtained by first establishing the flexibility matrix and utilising the relationship:

$$[K] = [F]^{-1} \tag{A.1}$$

where $[K]$ is the stiffness matrix and $[F]$ is the flexibility matrix. The flexibility matrix is a measure of the nodal displacement at each of the specified nodes caused by a unit force at a particular node. For prismatic members, the coefficients can be calculated for each of the nodes according to the procedure outlined in Figure A.1. According to Ghali and

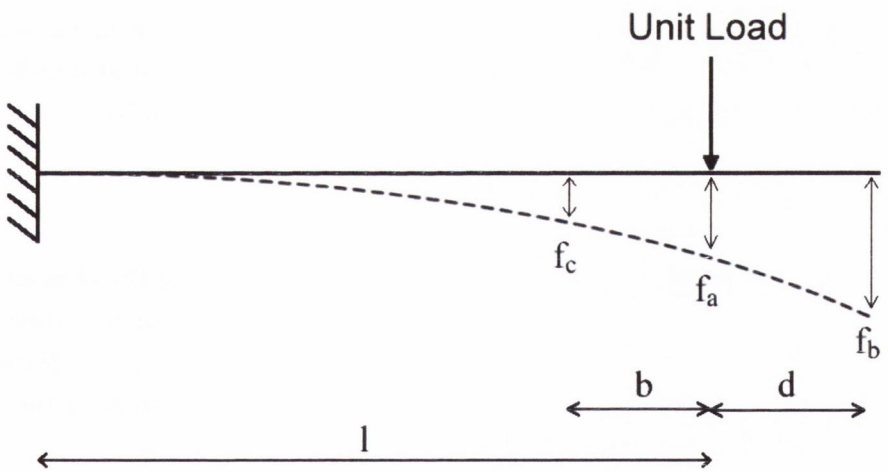

Figure A.1: Flexibility coefficients for prismatic members.

Neville (1997) the displacement (flexibility matrix coefficients) at nodes 'a', 'b' and 'c', due to a unit load at node 'a' may be calculated by:

$$f_a = \frac{l^3}{3EI} \tag{A.2}$$

$$f_b = f_a + \frac{dl^2}{2EI} \tag{A.3}$$

$$f_c = \frac{l^3}{3EI}\left(1 - \frac{3b}{2l} + \frac{b^3}{2l^3}\right) \tag{A.4}$$

where EI is the bending stiffness of the prismatic member. By systematically applying a unit load at each of the specified nodes along the member and calculating the resultant displacements for each of the nodes, the flexibility matrix becomes:

$$[F] = \begin{bmatrix} \delta_{11} & \delta_{12} & \cdots & \delta_{1N} \\ \delta_{21} & \delta_{22} & \cdots & \delta_{2N} \\ \vdots & \vdots & \ddots & \vdots \\ \delta_{N1} & \delta_{N2} & \cdots & \delta_{NN} \end{bmatrix} \tag{A.5}$$

where δ_{ij} represents the displacement at node i due to a unit load at node j, up to a total number of N nodes. By subsequently calling on the relationship described by Equation (A.1), the stiffness matrix may be established.

It has been stated that the aforementioned procedure only applies if the members in question are prismatic in nature. The difficulty faced in the current thesis is that the members in question are non-prismatic, both tower and blade elements. This fact calls for an extension of the procedure to account for a variable bending stiffness (EI) along the length of the member. This can be accounted for with the aid of virtual work. Ghali and Neville (1997) states that for any external load, the displacement at a node j along a non-prismatic member when considering only bending may be given by:

$$D_i = \int \frac{M_{ui}(x)M(x)}{EI(x)} dl \tag{A.6}$$

where $EI(x)$ is the variable bending stiffness at any point x along the element, $M(x)$ is the moment due to the external load and $M_{ui}(x)$ is the internal moment caused by a unit virtual load applied at the coordinate i where the displacement is required. If the external loading is also a unit load applied at coordinate j for the calculation of the flexibility coefficients in bending, Equation (A.6) becomes:

$$\delta_{ij} = \int \frac{M_{ui}(x)M_{uj}(x)}{EI(x)} dl \tag{A.7}$$

Referring, once more, to the procedure outlined in Figure A.1, the displacements at nodes 'a', 'b' and 'c' due to a unit load at 'a' may be calculated as:

$$f_a = \int \frac{M_{ua}^2(x)}{EI(x)} dl \tag{A.8}$$

$$f_b = \int \frac{M_{ub}(x)M_{ua}(x)}{EI(x)}dl \tag{A.9}$$

$$f_c = \int \frac{M_{uc}(x)M_{ua}(x)}{EI(x)}dl \tag{A.10}$$

Integrating along the length of the member for each of the specified nodes provides for the establishment of the flexibility matrix in the form of Equation (A.5).

Appendix B - Presentation of Mass and Stiffness Matrices for One Dimensional Model

The generalised mass matrix for the one dimensional system may be outlined as follows:

$$M = \begin{bmatrix} M_b & 0 & 0 & M_{bt} \\ 0 & M_b & 0 & M_{bt} \\ 0 & 0 & M_b & M_{bt} \\ M_{tb} & M_{tb} & M_{tb} & M_t \end{bmatrix} \tag{B.1}$$

where, considering two flapwise modes for each of the blades (which are assumed to be identical):

$$M_b = \begin{bmatrix} \int_0^R m_b(z)\phi_{b,1}^2(z)dz & 0 \\ 0 & \int_0^R m_b(z)\phi_{b,2}^2(z)dz \end{bmatrix} \tag{B.2}$$

For the case of the tower, considering three longitudinal modes:

$$M_t = \begin{bmatrix} M_{t,11} & M_{t,12} & M_{t,13} \\ M_{t,21} & M_{t,22} & M_{t,23} \\ M_{t,31} & M_{t,32} & M_{t,33} \end{bmatrix} \tag{B.3}$$

where the diagonal terms:

$$M_{t,ii} = M_{nac} \times \phi_{t,i}^2(H) + \int_0^H M_t(Z) \times \phi_{t,i}^2(Z)dZ + 3\phi_{t,i}^2(H) \int_0^R m_b(z)dz \tag{B.4}$$

and the off-diagonal terms:

$$M_{t,ij} = M_{t,ji} = M_{nac} \times \phi_{t,i}(H)\phi_{t,j}(H) + 3\phi_{t,i}(H)\phi_{t,j}(H) \int_0^R m_b(z)dz \tag{B.5}$$

Coupling of the tower and blade motion is facilitated through the off-diagonal terms, M_{bt} and M_{tb}, in Equation B.1. For the blade and tower matrices outlined in Equations B.2

and B.3, these may be represented as follows:

$$M_{tb} = [M_{bt}]^T = \begin{bmatrix} \phi_{t,1}(H)\int_0^R m_b(z)\phi_{b,1}(z)dz & \phi_{t,1}(H)\int_0^R m_b(z)\phi_{b,2}(z)dz \\ \phi_{t,2}(H)\int_0^R m_b(z)\phi_{b,1}(z)dz & \phi_{t,2}(H)\int_0^R m_b(z)\phi_{b,2}(z)dz \\ \phi_{t,3}(H)\int_0^R m_b(z)\phi_{b,1}(z)dz & \phi_{t,3}(H)\int_0^R m_b(z)\phi_{b,2}(z)dz \end{bmatrix} \tag{B.6}$$

The corresponding generalised stiffness matrix for the one dimensional system can be represented by:

$$K = \begin{bmatrix} K_b & 0 & 0 & 0 \\ 0 & K_b & 0 & 0 \\ 0 & 0 & K_b & 0 \\ 0 & 0 & 0 & K_t \end{bmatrix} \tag{B.7}$$

where:

$$K_b = \begin{bmatrix} K_{b,11} & 0 \\ 0 & K_{b,22} \end{bmatrix} \tag{B.8}$$

with:

$$\begin{aligned} K_{b,ii} = &\int_0^R EI_b(z)\left(\frac{d^2}{dz^2}\phi_{b,i}(z)\right)^2 dz \\ &+ \frac{1}{2}\Omega^2\left(\int_0^R m_b(z)\times(R^2-z^2)\times\left(\frac{d}{dz}\phi_{b,i}(z)\right)^2 dz\right) \end{aligned} \tag{B.9}$$

and:

$$K_t = \begin{bmatrix} K_{t,11} & 0 & 0 \\ 0 & K_{t,22} & 0 \\ 0 & 0 & K_{t,33} \end{bmatrix} \tag{B.10}$$

with:

$$K_{t,ii} = \int_0^H EI_t(Z)\left(\frac{d^2}{dZ^2}\phi_{t,i}(Z)\right)^2 dZ \tag{B.11}$$

The solution vector of the time-varying terms for the system modelled by the preceding matrix derivation may be described as follows:

$$[u(t)]^T = \{q_{b1,1}(t), q_{b1,2}(t), q_{b2,1}(t), q_{b2,2}(t), q_{b3,1}(t), q_{b3,2}(t), q_{t1}(t), q_{t2}(t), q_{t3}(t)\} \tag{B.12}$$

Appendix C - Definition of Test Turbine

In addition to the general properties for the NREL baseline reference wind turbine listed in Section 3.5.1, Jonkman *et al.* (2009) provides a detailed description of the structural and aerodynamic properties of the blade aerofoils. Table C.1 contains additional blade structural properties used in the wind turbine model. The "Radius" column outlines the distance of each point on the blade from the rotor centre, "BlFract" represents the fractional distance of each node from the root of the blade, "StrTwst" denotes the structural angle of twist for the aerofoil section relative to the plane of rotation, "BMassDen" is the mass density of the blade at each particular node, "FlpStiff" is the structural stiffness of the blade in the flapwise direction, "EI", of each blade at each particular node and "EdgStiff" specifies the edgewise structural stiffness. Values for these parameters are specified a 49 discrete points along the blade length, thus giving a detailed description of the complex blade structural properties.

Radius	**BlFract**	**StrTwst**	**BMassDen**	**FlpStiff**	**EdgStiff**
(m)	$(-)$	$(°)$	(kg/m)	(Nm^2)	(Nm^2)
1.50	0.00000	13.308	709.7315	18.11E+09	18.11E+09
1.70	0.00325	13.308	709.7315	18.11E+09	18.11E+09
2.70	0.01951	13.308	808.4427	19.43E+09	19.56E+09
3.70	0.03577	13.308	774.1413	17.46E+09	19.49E+09
4.70	0.05203	13.308	773.6103	15.29E+09	19.79E+09
5.70	0.06829	13.308	619.3716	10.78E+09	14.86E+09
6.70	0.08455	13.308	470.6994	7.23E+09	10.22E+09
7.70	0.10081	13.308	443.2890	6.31E+09	9.14E+09
8.70	0.11707	13.308	418.8109	5.53E+09	8.06E+09
9.70	0.13335	13.308	399.3923	4.98E+09	6.88E+09
10.70	0.14959	13.308	417.7833	4.94E+09	7.01E+09
11.70	0.16585	13.308	445.6589	4.69E+09	7.17E+09
12.70	0.18211	13.181	435.7269	3.95E+09	7.27E+09
13.70	0.19837	12.848	424.6105	3.39E+09	7.08E+09

Table C.1: Distributed blade structural properties (Jonkman *et al.*, 2009).

Radius (m)	**BlFract** ($-$)	**StrTwst** ($°$)	**BMassDen** (kg/m)	**FlpStiff** (Nm^2)	**EdgStiff** (Nm^2)
14.70	0.21465	12.192	398.7212	2.93E+09	6.24E+09
15.70	0.23089	11.561	368.8260	2.57E+09	5.05E+09
16.70	0.24715	11.072	365.3293	2.39E+09	4.95E+09
17.70	0.26341	10.792	362.2570	2.27E+09	4.81E+09
19.70	0.29595	10.232	354.7251	2.05E+09	4.50E+09
21.70	0.32846	9.672	344.9730	1.83E+09	4.24E+09
23.70	0.36098	9.110	336.5955	1.59E+09	3.99E+09
25.70	0.39350	8.534	328.0549	1.36E+09	3.75E+09
27.70	0.42602	7.932	308.1031	1.10E+09	3.45E+09
29.70	0.45855	7.321	300.1438	8.76E+08	3.14E+09
31.70	0.49106	6.711	275.2882	6.81E+08	2.73E+09
33.70	0.52358	6.122	264.6925	5.35E+08	2.55E+09
35.70	0.55610	5.546	252.6280	4.09E+08	2.33E+09
37.70	0.58862	4.971	230.6461	3.15E+08	1.83E+09
39.70	0.62115	4.401	209.3783	2.37E+08	1.58E+09
41.70	0.65366	3.834	187.5418	1.76E+08	1.32E+09
43.70	0.68618	3.332	172.5827	1.26E+08	1.18E+09
45.70	0.71870	2.890	161.4151	1.07E+08	1.02E+09
47.70	0.75122	2.503	145.2371	9.09E+07	7.98E+08
49.70	0.78376	2.116	135.4316	7.63E+07	7.09E+08
51.70	0.81626	1.730	112.1295	6.11E+07	5.19E+08
53.70	0.84878	1.342	103.2565	4.95E+07	4.54E+08
55.70	0.88130	0.954	94.3416	3.94E+07	3.95E+08
56.70	0.89756	0.760	86.7659	3.47E+07	3.53E+08
57.70	0.91382	0.574	76.2130	3.04E+07	3.04E+08
58.70	0.93008	0.404	71.8915	2.65E+07	2.81E+08
59.20	0.93821	0.319	69.2697	2.38E+07	2.61E+08
59.70	0.94636	0.253	62.0317	1.96E+07	1.59E+08
60.20	0.95447	0.216	58.4503	1.60E+07	1.38E+08
60.70	0.96260	0.178	54.8647	1.28E+07	1.19E+08
61.20	0.97073	0.140	51.3418	1.01E+07	1.01E+08
61.70	0.97886	0.101	47.8963	7.55E+06	8.51E+07
62.20	0.98699	0.062	43.5591	4.60E+06	6.43E+07
62.70	0.99512	0.023	11.9725	2.50E+05	6.61E+06
63.00	1.00000	0.000	10.7871	1.70E+05	5.01E+06

Table C.1: (continued...)

Table C.2 contains additional blade aerodynamic properties used in the wind turbine model. The "Node" column outlines the number of each node along the blade, "RNodes" represents the distance of each node along the blade from the rotor centre, "DRNodes" is the length of blade associated with each particular node and "Chord" is the chord length at each particular node. The final column, "Aerofoil Table", relates to the relevant aerofoil table which details the Lift and Drag coefficients for the particular aerofoil element as a function of the blade angle of attack. The properties of these aerofoil tables are listed in Jonkman *et al.* (2009).

Node (−)	**RNodes** (m)	**AeroTwst** (m)	**DRNodes** (m)	**Chord**	**Aerofoil Table**
1	2.8667	13.308	2.733	3.542	Cylinder1.dat
2	5.6000	13.308	2.733	3.854	Cylinder1.dat
3	8.3333	13.308	2.733	4.167	Cylinder2.dat
4	11.7500	13.308	4.1000	4.557	DU40_A17.dat
5	15.8500	11.480	4.1000	4.652	DU35_A17.dat
6	19.9500	10.162	4.1000	4.458	DU35_A17.dat
7	24.0500	9.011	4.1000	4.249	DU30_A17.dat
8	28.1500	7.795	4.1000	4.007	DU25_A17.dat
9	32.2500	6.544	4.1000	3.748	DU25_A17.dat
10	36.3500	5.361	4.1000	3.502	DU21_A17.dat
11	40.4500	4.188	4.1000	3.256	DU21_A17.dat
12	44.5500	3.125	4.1000	3.010	NACA64_A17.dat
13	48.6500	2.319	4.1000	2.764	NACA64_A17.dat
14	52.7500	1.526	4.1000	2.518	NACA64_A17.dat
15	56.1667	0.863	2.7333	2.313	NACA64_A17.dat
16	58.9000	0.370	2.7333	2.086	NACA64_A17.dat
17	61.6333	0.106	2.7333	1.419	NACA64_A17.dat

Table C.2: Distributed blade aerodynamic properties (Jonkman *et al.*, 2009).

Table C.3 highlights the rotor collective blade pitch properties for the turbine with increasing wind speed beyond the rated wind speed of 11.4 m/s and at the rated rotor speed of 12.1 rpm. Once the rated wind speed is passed, the blades are set to pitch in order to control the loading applied to the blades and, therefore, the power output of the generator.

Wind Speed (m/s)	**Rotor Speed** (rpm)	**Pitch Angle** $(°)$
11.4 - Rated	12.1	0.00
12.0	12.1	3.83
13.0	12.1	6.60
14.0	12.1	8.70
15.0	12.1	10.45
16.0	12.1	12.06
17.0	12.1	13.54
18.0	12.1	14.92
19.0	12.1	16.23
20.0	12.1	17.47
21.0	12.1	18.70
22.0	12.1	19.94
23.0	12.1	21.18
24.0	12.1	22.35
25.0	12.1	23.47

Table C.3: Rotor collective blade pitch properties as a function of wind speed (Jonkman *et al.*, 2009).

Appendix D - Peer Reviewed Publications

Journal Papers

- Quilligan, A., O'Connor, A.J. and Pakrashi, V (2012), "Fragility Analysis of Steel and Concrete Wind Turbine Towers," Engineering Structures, 36, 270-282. http://dx.doi.org/10.1016/j.engstruct.2011.12.013

- Quilligan, A. and O'Connor, A.J. (2012), "Earthquake Response of Steel and Concrete Wind Turbine Towers Employing Probabilistic Seismic Demand Analysis," Structural Safety, (Under Review).

- Quilligan, A. and O'Connor, A.J. (2012), "The Influence of Tower Construction Material on Wind Turbine Blade Dynamic Response," Wind Energy, (Under Review).

Conference Papers

- Quilligan, A. and O'Connor, A.J. (2012), "Generating Dynamic Time History Responses for Concrete Wind Turbine Towers," in: *Proceedings of the Bridge and Concrete Research in Ireland Conference, BCRI 2012*, Dublin, September 6th - 7th.

- Quilligan, A. and O'Connor, A.J. (2012), "Comparison of Wind Turbine Models Subjected to Wind and Earthquake Loading," in: *Proceedings of the 53rd Structures, Structural Dynamics and Materials Conference 2012*, Honolulu, Hawaii, April 23rd - 26th.

- Quilligan, A. and O'Connor, A.J. (2010), "Feasibility of Concrete Wind Turbine Towers," in: *Proceedings of the Bridge and Concrete Research in Ireland Conference, BCRI 2010*, Cork, September 2nd - 3rd.

- Quilligan, A. and O'Connor, A.J. (2010), "Optimisation of Concrete Wind-Turbine Towers," TCD-UCD Engineering Innovation Research Workshop, Dublin, November 27th.

- Quilligan, A. and O'Connor, A.J. (2010), "Optimisation of Concrete Wind-Turbine Towers," Globe Forum Dublin 2010 in The Convention Centre Dublin, November 17^{th} - 18^{th}, (poster).

Appendix E - Tower Properties

E.1 Steel Towers

88 m Steel Tower

Table E.1 presents the distributed mass and stiffness properties of the NREL baseline 5 MW wind turbine equivalent on-shore tower, as Specified by Jonkman *et al.* (2009). Note that 'Elevation' signifies the the vertical elevation above the tower base, 'Ht_Fract' represents the fractional height of each particular node, 'Mass_Den' is the mass density of the tower at the particular node and 'FA_Stiff' stands for the forward-aft (flapwise direction for blades) stiffness of the tower at the particular node and 'SS_Stiff' corresponds to the edgewise blade stiffness.

Elevation (m)	**Ht_Fract** $(-)$	**Mass_Den** (kg/m)	**FA_Stiff** (Nm^2)	**SS_Stiff** (Nm^2)
0.00	0.0	5575	614E+09	614E+09
8.76	0.1	5274	535E+09	535E+09
17.52	0.2	4973	463E+09	463E+09
26.28	0.3	4673	399E+09	399E+09
35.04	0.4	4372	342E+09	342E+09
43.80	0.5	4071	291E+09	291E+09
52.56	0.6	3770	246E+0	246E+099
61.32	0.7	3469	206E+09	206E+09
70.08	0.8	3169	172E+09	172E+09
78.84	0.9	2868	142E+09	142E+09
87.60	1.0	2567	116E+09	116E+09

Table E.1: Distributed properties of equivalent onshore tower for NREL 5 MW baseline wind turbine (Jonkman *et al.*, 2009)

103 m Steel Tower

The total mass of the components supported by the standard 103 m tower is 112 metric tonnes for the Vestas 3 MW turbine Vestas (2005). This represents 32 % of the mass of the 5 MW baseline turbine specified for this study. The top and bottom diameters of the tower are, therefore, scaled up by 68 % to give the values specified in Table 4.1. The base steel thickness is estimated as the thickness of the 88 m tower (0.035 m) scaled up by a factor of 18 % which represents the increase in height. The distributed properties used to model the 103 m steel tower are presented in Table E.2.

Elevation (m)	**Ht_Fract** $(-)$	**Mass_Den** (kg/m)	**FA_Stiff** (Nm^2)	**SS_Stiff** (Nm^2)
0.00	0.0	7838	1.24E+12	1.24E+12
10.30	0.1	7311	1.13E+12	1.13E+12
20.60	0.2	6784	1.02E+12	1.02E+12
30.90	0.3	6257	9.04E+11	9.04E+11
41.20	0.4	5730	7.91E+11	7.91E+11
51.50	0.5	5202	6.79E+11	6.79E+11
61.80	0.6	4675	5.67E+11	5.67E+11
72.10	0.7	4148	4.54E+11	4.54E+11
82.40	0.8	3621	3.42E+11	3.42E+11
92.70	0.9	3094	2.30E+11	2.30E+11
103.0	1.0	2567	1.17E+11	1.17E+11

Table E.2: Distributed properties of scaled 103 m steel tower.

120 m Steel Tower

No tower has been found in literature against which to model the 120 m steel tower. As a result, the properties of this tower are estimated from scaling the 103 m Vestas tower and the 88 m NREL tower. The change in hub-height elevation from the 103 m tower represents a 17 % increase in tower height. The base diameter and steel thickness are consequently increased by 17 %. The distributed properties used to model the 120 m steel tower are presented in Table E.3.

Elevation (m)	**Ht_Fract** $(-)$	**Mass_Den** (kg/m)	**FA_Stiff** (Nm^2)	**SS_Stiff** (Nm^2)
0.00	0.0	10744	2.33E+12	2.33E+12
12.0	0.1	9926	2.11E+12	2.11E+12
24.0	0.2	9108	1.89E+12	1.89E+12
36.0	0.3	8290	1.67E+12	1.67E+12
48.0	0.4	7473	1.45E+12	1.45E+12
60.0	0.5	6655	1.22E+12	1.22E+12
72.0	0.6	5838	1.00E+12	1.00E+12
84.0	0.7	5020	7.81E+11	7.81E+11
96.0	0.8	4202	5.60E+11	5.60E+11
108.0	0.9	3385	3.39E+11	3.39E+11
120.0	1.0	2567	1.17E+11	1.17E+11

Table E.3: Distributed properties of scaled 120 m steel tower.

E.2 Concrete Towers

The properties of the 88 m concrete tower are established from a typical tower of this height. No literature could be found detailing the properties and dimensions of concrete towers in the range of 100 m to 120 m. It was, therefore, decided to use the same properties for the taller towers as for the 88 m tower, except for the height. The diameters and concrete thickness of the taller towers would obviously be greater in reality but these towers will provide a lower-bound with which to compare the steel counterparts. The distributed properties used to model the three concrete towers are presented in Tables E.4-E.6.

Elevation (m)	**Ht_Fract** ($-$)	**Mass_Den** (kg/m)	**FA_Stiff** (Nm^2)	**SS_Stiff** (Nm^2)
0.00	0.0	15682	1.38E+12	1.38E+12
8.76	0.1	14990	1.27E+12	1.27E+12
17.52	0.2	14297	1.15E+12	1.15E+12
26.28	0.3	13604	1.04E+12	1.04E+12
35.04	0.4	12912	9.26E+11	9.26E+11
43.80	0.5	12219	8.12E+11	8.12E+11
52.56	0.6	11526	6.98E+11	6.98E+11
61.32	0.7	10833	5.84E+11	5.84E+11
70.08	0.8	10141	4.69E+11	4.69E+11
78.84	0.9	9448	3.55E+11	3.55E+11
87.60	1.0	8755	2.41E+11	2.41E+11

Table E.4: Distributed properties of 88 m concrete tower.

Elevation (m)	**Ht_Fract** ($-$)	**Mass_Den** (kg/m)	**FA_Stiff** (Nm^2)	**SS_Stiff** (Nm^2)
0.00	0.0	15682	1.38E+12	1.38E+12
10.30	0.1	14990	1.27E+12	1.27E+12
20.60	0.2	14297	1.15E+12	1.15E+12
30.90	0.3	13604	1.04E+12	1.04E+12
41.20	0.4	12912	9.26E+11	9.26E+11
51.50	0.5	12219	8.12E+11	8.12E+11
61.80	0.6	11526	6.98E+11	6.98E+11
72.10	0.7	10833	5.84E+11	5.84E+11
82.40	0.8	10141	4.69E+11	4.69E+11
92.70	0.9	9448	3.55E+11	3.55E+11
103.0	1.0	8755	2.41E+11	2.41E+11

Table E.5: Distributed properties of 103 m concrete tower.

Elevation (m)	**Ht_Fract** $(-)$	**Mass_Den** (kg/m)	**FA_Stiff** (Nm^2)	**SS_Stiff** (Nm^2)
0.00	0.0	15682	1.38E+12	1.38E+12
12.0	0.1	14990	1.27E+12	1.27E+12
24.0	0.2	14297	1.15E+12	1.15E+12
36.0	0.3	13604	1.04E+12	1.04E+12
48.0	0.4	12912	9.26E+11	9.26E+11
60.0	0.5	12219	8.12E+11	8.12E+11
72.0	0.6	11526	6.98E+11	6.98E+11
84.0	0.7	10833	5.84E+11	5.84E+11
96.0	0.8	10141	4.69E+11	4.69E+11
108.0	0.9	9448	3.55E+11	3.55E+11
120.0	1.0	8755	2.41E+11	2.41E+11

Table E.6: Distributed properties of 120 m concrete tower.

E.3 Tower Validation

In defining the towers listed above, it was stated that at the time of undertaking of this research, minimal information could be sourced on the properties of wind turbine towers of the size considered. As a result, a number of assumptions were made. Scaling was employed for the steel towers and, as prestressed concrete towers at heights of 103 and 120 m could not be validated against operational towers, it was decided to use the same dimensions as for the 88 m tower, the height excepted. This methodology was employed on the basis that the concrete towers offered a baseline to the actual towers which would be used in reality. The comparisons drawn between the steel and concrete towers could then be interpreted in the context of how the towers were established, and conclusions as to how this may affect the results could be formed. Having completed the analyses presented in this thesis, a suite of similar towers were encountered. These were established by Engström *et al.* (2010) as part of a study to establish the economy of different tower designs for tall towers in forested areas in Sweden. This appendix compares the structural performance of the suite of steel and concrete towers utilised throughout this thesis to the set of similar towers detailed in Engström *et al.* (2010). This will facilitate the establishment of arguments as to how the performance of the studied towers could change.

The study by Engström *et al.* (2010) looks at a variety of wind turbine tower designs. These include welded tubular steel towers, tubular steel with bolted friction joints (FJS), prestressed concrete (PC) towers, a hybrid design incorporating prestressed concrete and welded tubular steel, steel lattice towers and timber towers. Two turbines were considered to be supported by the towers. These included the same 5 MW turbine, as specified by the NREL, which was employed in this thesis (Jonkman *et al.*, 2009), as well as a 3 MW turbine which was scaled down from the 5 MW turbine. Tower heights of 80 m, 100 m,

125 m, 150 m and 175 m were examined. The critical load cases were established based on the requirements of BS EN 61400-1 (2005) using the Vidyn model, developed by Ganander (2003). A "rough" design was then carried out for each of the tower materials, hub heights and turbine sizes. This facilitated an estimation of the cost of each tower solution for the variety of situations (hub heights and turbine sizes) considered. The established properties for the towers relevant to this thesis are presented in Table E.7. It should be noted that, for the welded tubular steel design, heights beyond 100 m were not feasible due to the exceedance of the base diameter of the 4.5 m threshold, thus disqualifying a tower from being transported by road. Therefore, only the steel friction jointed solution is considered. Also, in the case of the timber and steel lattice towers, these designs were found to be unsuitable for the case of the 5 MW turbine. For the purposes of this appendix, comparison is drawn between the studied steel towers and the friction jointed steel towers presented by Engström *et al.* (2010). This is also provided in the case of the prestressed concrete towers. The corresponding property values for the studied towers are shown in brackets beside the tower to which they will be compared. An immediate difference noticeable in

Tower Material	Height (m)	Top/Base Ø (m)	Weight (tonnes)	Natural Frequency (Hz)
FJS	80 (87.6)	3.8/5.8 (3.87/6)	285 (357)	0.4 (0.33)
FJS	100 (103)	3.8/6.4 (3.87/7.2)	401 (536)	0.32 (0.37)
FJS	125 (120)	3.8/7.0 (3.87/8.43)	566 (799)	0.26 (0.44)
PC	80 (87.6)	3.8/7.8 (4.8/8.2)	948 (1054)	0.71 (0.47)
PC	100 (103)	3.8/8.8 (4.8/8.2)	1286 (1259)	0.55 (0.35)
PC	125 (120)	3.8/10.1 (4.8/8.2)	1768 (1466)	0.43 (0.25)

Table E.7: Calculated properties of towers established by Engström *et al.* (2010).

the tower properties is the tower heights. The smaller towers differ by 7.6 m, the middle towers by 3 m and the taller towers by 5 m. Despite this, the towers are deemed close enough in height in order to establish a comparison. In addressing the top diameters of the towers, the steel towers are quite close, with only 70 mm of difference, while the concrete towers differ by 1 m. In considering the tower base diameters, the studied steel towers equate to larger values, with the difference in magnitude increasing with increasing height. Despite this, the largest difference, which occurs with the 120 m and 125 m towers, equates to only 17 %. For the prestressed concrete towers, a mere 5 % difference exists for the 80 m and 88 m towers, with the 88 m tower being the larger. As the base diameter is kept the same across the range of heights for the studied towers, the comparable towers possess larger base diameters at the taller heights. The tower masses for the steel towers are considerably larger for the studied towers while the prestressed concrete towers exhibit closely similar values for all except the 120/125 m towers, where the studied tower is 21 % smaller. The final comparison is drawn between the natural frequencies for the towers.

A considerable difference is seen for the steel towers where the studied towers increase in value with increasing height, while the opposite occurs with the comparison towers. While the values for the prestressed concrete towers both decrease with increasing height, the studied towers possess considerably lower values than the comparison towers.

In order to assess the effect of the difference in tower properties on the resulting dynamic response, a series of simulations have been undertaken and the results are presented through both output time histories as well as fragility curves. The time-histories were generated, using the dynamic model described in Section 3.2, through simulations at the turbine cut-out wind speed (25 m/s) with the turbine in an operational state. The fragility curves were subsequently formed using the same procedure as was adopted in Section 4.3. The first of these comparisons is for the 80 m and 88 m steel towers. The results are presented in Figure E.1. Immediately, upon assessment of the time history response of the two towers in Figure E.1(a), it is noticeable that the two towers produce a very similar response. While there exist an almost 8 m (9 %) difference in the tower heights, the taller tower is 19 % heavier, thus giving rise to the similar response. When the corresponding fragility curve is consulted, Figure E.1(b), again the two towers are seen to produce similar results. The difference in the probability of limit state exceedance varies between 2 % and a maximum of 8 %.

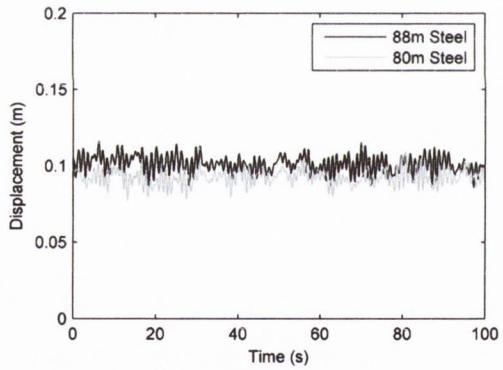

(a) Typical time history response at cut-out wind speed.

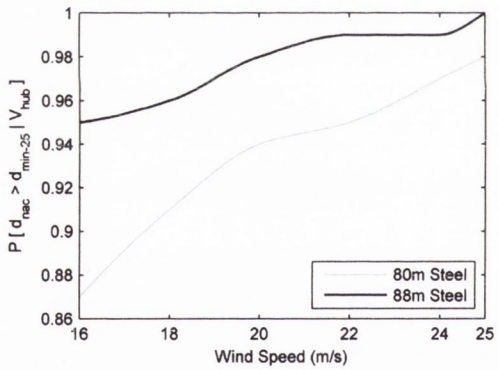

(b) Comparative tower fragilities.

Figure E.1: Comparison of modelled 88 m steel tower with 80 m verified tower.

The 80 m and 88 m prestressed concrete towers are compared in Figure E.2. For the case of the concrete towers, the values of the concrete strength nor the concrete thickness chosen in the design by Engström *et al.* (2010) were not specified. Therefore, in order to get a sense of the comparison, two concrete strengths are specified. A medium strength concrete with a compressive cube strength of $30\,N/mm^2$ is estimated to have a mean modulus of elasticity of 26 GPa while a high strength concrete ($f_{cu} = 60N/mm^2$) is assigned a mean modulus of elasticity of 32 GPa (Kong and Evans, 1987). However, it is possible, based on

the properties presented in the study, to estimate the concrete strength and wall thickness which were employed using reverse engineering. Using a five DOF lumped mass model and not including the nacelle mass on top, a close approximation of the published natural frequencies could be achieved using a modulus of elasticity of 32 GPa and a wall thickness of 275 mm. Despite this, the exact methods of determining the tower frequencies are not described, so results are plotted for both strengths in order to assess the range of possible results expected from the towers specified by Engström *et al.* (2010). The studied towers are assigned a modulus of elasticity of 26 GPa. In Figure E.2(a) the response time histories are plotted for the studied tower, "88m Conc", as well as the comparison tower for both concrete strengths, "80 Conc-26" and "80m Conc-32". Similar to the steel towers in Figure E.1, the concrete towers show very closely related simulation responses. Despite the height difference, the response of the studied tower lies directly between the two comparison towers. This emphasises that, for the range of concrete strengths which would be most likely utilised for such a structure, the studied tower behaves very closely to the comparison towers. This is further backed up by the fragility curves presented in Figure E.2(b). Both the studied tower and the higher strength comparison tower (the most probable design) exhibit almost identical probabilities of limit-state exceedance. The lower strength concrete tower relates to higher probabilities but similarity still exists, with the difference in probabilities varying between 7 % and a maximum of 25 %.

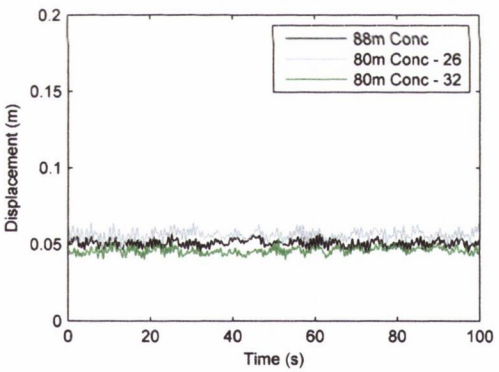

(a) Typical time history response at cut-out wind speed.

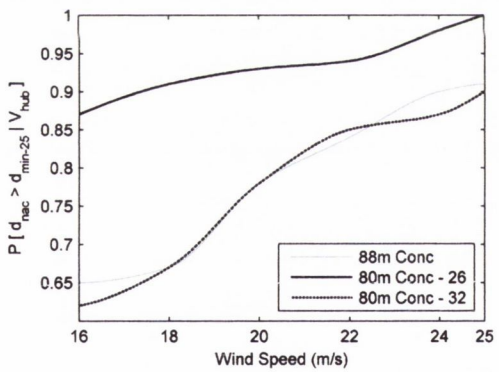

(b) Comparative tower fragilities.

Figure E.2: Comparison of modelled 88 m concrete tower with 80 m verified tower.

Figure E.3 offers a comparison between the 100 m and 103 m steel towers. In this instance the studied tower, which is 3 m taller, relates to a more stable design with lower response values as well as probabilities of limit state exceedance. While the natural frequencies of the two towers are quite close, the studied tower is somewhat heavier, giving rise to the difference in response.

The 100 m and 103 m prestressed concrete towers are compared in Figure E.4. Once

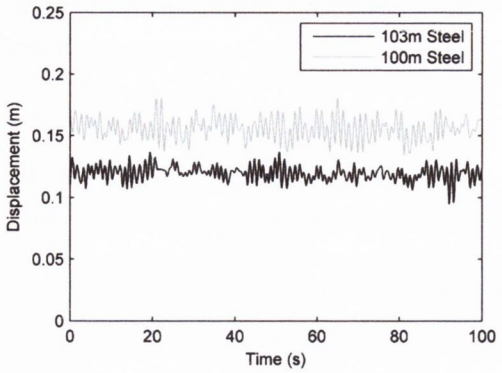

(a) Typical time history response at cut-out wind speed.

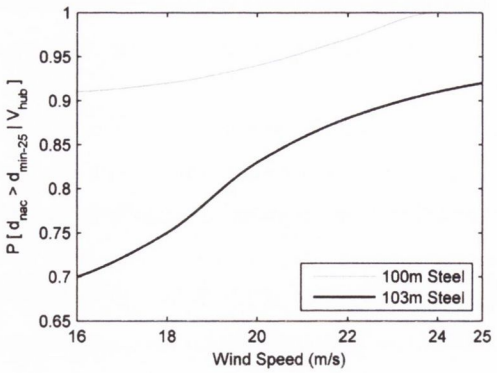

(b) Comparative tower fragilities.

Figure E.3: Comparison of modelled 103 m steel tower with 100 m verified tower.

again two concrete strengths are specified. In a similar fashion to Figure E.2(a), the time history response for the studied tower lies between that of the two comparison towers and the responses are seen to be quite close in magnitude. For the fragility curves in Figure E.4(b) the studied tower is seen to exhibit almost identical values as for the lower strength concrete tower. The higher strength tower offers further improved results but the difference is limited to between 4 % and a maximum of 20 %. Despite the difference in natural frequency values, the two towers have very similar masses and again, it can be said that the towers offer quite similar responses to wind excitation with the studied tower being between the two comparison towers. Also, it should be noted that the studied tower offers a baseline with which to compare other prestressed concrete towers under wind excitation.

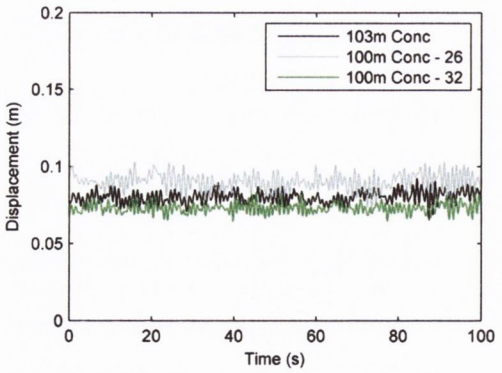

(a) Typical time history response at cut-out wind speed.

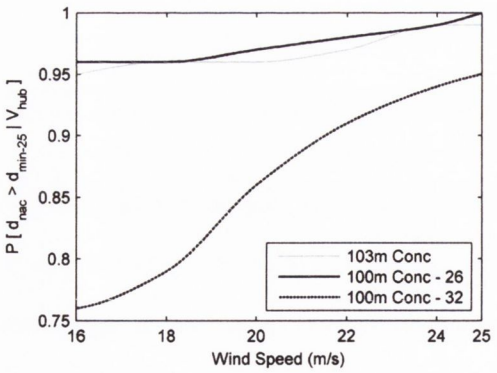

(b) Comparative tower fragilities.

Figure E.4: Comparison of modelled 103 m concrete tower with 100 m verified tower.

The 120 m and 125 m steel towers are compared in Figure E.5. Although the height difference is only 5 m (4 %), in this case the towers are significantly different in both natural frequency as well as mass. This is reflected in the results with the time history being significantly larger for the comparison tower. This is further highlighted in the fragility curve, Figure E.5(b), with the studied tower displaying a much higher resistance to wind excitation and a correspondingly lower range of probabilities of limit-state exceedance.

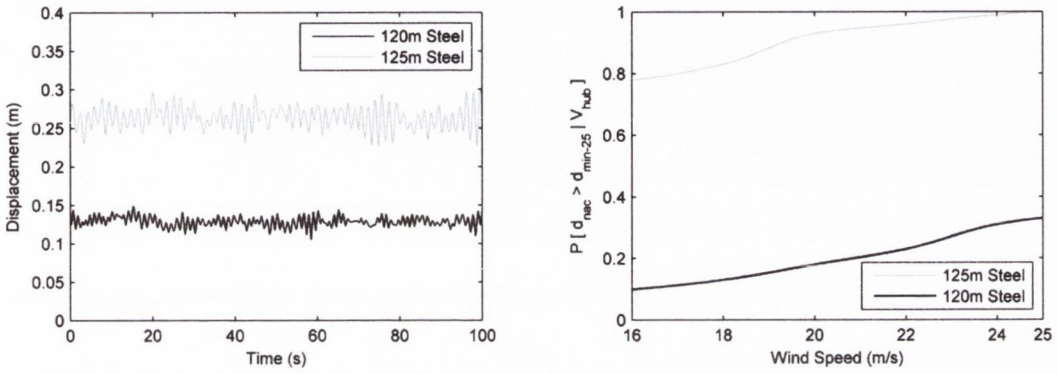

(a) Typical time history response at cut-out wind speed.

(b) Comparative tower fragilities.

Figure E.5: Comparison of modelled 120 m steel tower with 125 m verified tower.

The final comparison is established between the 120 m and 125 m prestressed concrete towers. The results are presented in Figure E.6. As with the results for the previous concrete towers, the response of the studied tower once again lies between the two comparison towers. While the comparison towers are somewhat heavier and the natural frequency higher, the studied tower outperforms the medium strength concrete example while the higher strength concrete tower significantly outperforms the the other two in terms of probabilities of limit-state exceedance. Given the likelihood of the higher strength concrete being employed in the design, this, once again reflects the choice of the studied prestressed concrete tower to reflect a baseline of the likely response.

Overall, it can be shown from this appendix that the assumptions made as to the sizing of both the steel and concrete towers as part of this study are viable and that the results formed in the thesis may be interpreted in the context of these assumptions. For the steel towers, both solutions are almost identical at the 80/88 m height. At 100/103 m the studied tower offers a more stable solution and better resistance to wind excitation while this advantage is seen to extend at the 120/125 m height where the studied tower significantly outperforms the comparison tower. This reflects a conservative design approach for the studied steel towers which may be taken into account when interpreting the results of any analysis carried out. In terms of the concrete towers, again almost identical behaviour is recorded at the 80/88 m height. The studied tower lies between the values for the two

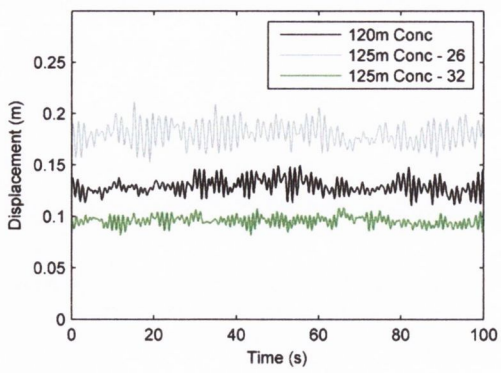

(a) Typical time history response at cut-out wind speed.

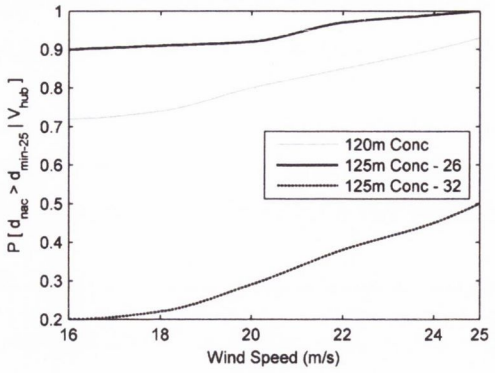

(b) Comparative tower fragilities.

Figure E.6: Comparison of modelled 120 m concrete tower with 125 m verified tower.

concrete strengths at 100/103 m with a closer proximity to the lower strength concrete tower. Finally, at the 120/125 m height the spacing of the results is increased but the same pattern is noticeable with the studied tower between the two comparison towers, although with a closer relation to the lower strength concrete tower. Given that the choice of the higher strength concrete is most likely for the comparison towers, the results of this appendix show that the studied prestressed concrete towers may be viewed as baseline designs for estimating the response of more realistic towers subjected to wind excitation. This fact will be considered when interpreting any results presented throughout this thesis.

A final factor which may have an impact on results, which must be noted at this point, is the difference in the values for the natural frequencies. For the steel towers, the natural frequencies of the studied towers increases from 0.33 Hz to 0.44 Hz with the increase in height while the opposite is true for the comparison towers with decreasing profile from 0.4 Hz to 0.26 Hz. In the case of the concrete towers, although both towers both show a decreasing profile of natural frequency values, the magnitude of the natural frequencies are considerably larger for the comparison towers. While the variation in the results can be clearly seen for the case of wind excitation, as shown by Figures E.1 to E.6, the affect of the difference in natural frequency may have a more significant impact when other loading scenarios are considered. In particular, structural response to earthquake excitation has been shown to be considerably affected by natural frequency values. Therefore, the results produced from the investigations undertaken as part of this thesis will each be discussed in the context of these factors and the findings of this appendix.